

# **Agricultural Land Use Mapping in West Africa Using Multi-sensor Satellite Imagery**

## **Kartierung landwirtschaftlicher Landnutzung unter Verwendung multi-sensoraler Satellitendaten**

**Dissertation zur Erlangung des  
naturwissenschaftlichen Doktorgrades  
der Julius-Maximilians-Universität Würzburg**



**vorgelegt von**

**Gerald Forkuor**

**aus**

**Kumasi, Ghana**

**Würzburg, 2014**

Eingereicht am: .....25/09/2014.....

Mitglieder der Promotionskommission: Prof. Dr. Christopher Conrad; Prof. Dr. Jürgen Rauh

Vorsitzender:....Prof. Dr. Barbara Hahn.....

Gutachter 1: Prof. Dr. Christopher Conrad

Gutachter 2: Prof. Dr. Heiko Paeth

Tag des Promotionskolloquiums:.....14/01/2015.....

Doktorurkunde ausgehändigt am:.....

Dedicated to my wife, Elfrida, and our three lovely

Kids: Brain, Lizette and James

## Abstract

Rapid population growth in West Africa has led to expansion in croplands due to the need to grow more food to meet the rising food demand of the burgeoning population. These expansions negatively impact the sub-region's ecosystem, with implications for water and soil quality, biodiversity and climate. In order to appropriately monitor the changes in croplands and assess its impact on the ecosystem and other environmental processes, accurate and up-to-date information on agricultural land use is required. But agricultural land use mapping (i.e. mapping the spatial distribution of crops and croplands) in West Africa has been challenging due to the unavailability of adequate satellite images (as a result of excessive cloud cover), small agricultural fields and a heterogeneous landscape. This study, therefore, investigated the possibilities of improving agricultural land use mapping by utilizing optical satellite images with higher spatial and temporal resolution as well as images from Synthetic Aperture Radar (SAR) systems which are near-independent of weather conditions. The study was conducted at both watershed and regional scales.

At watershed scale, classification of different crop types in three watersheds in Ghana, Burkina Faso and Benin was conducted using multi-temporal: (1) only optical images (RapidEye) and (2) optical plus dual polarimetric (VV/VH) SAR images (TerraSAR-X). In addition, inter-annual or short term (2-3 years) changes in cropland area in the past ten years were investigated using historical Landsat images. Results obtained indicate that the use of only optical images to map different crop types in West Africa can achieve moderate classification accuracies (57% to 71%). Overlaps between the cropping calendars of most crops types and certain inter-croppings pose a challenge to optical images in achieving an adequate separation between those crop classes. Integration of SAR images, however, can improve classification accuracies by between 8 and 15%, depending on the number of available images and their acquisition dates. The sensitivity of SAR systems to different crop canopy architectures and land surface characteristics improved the separation between certain crop types. The VV polarization of TerraSAR-X was found to better discrimination between crop types than the VH. Images acquired between August and October were found to be very useful for crop mapping in the sub-region due to structural differences in some crop types during this period.

At the regional scale, inter-annual or short term changes in cropland area in the Sudanian Savanna agro-ecological zone in West Africa were assessed by upscaling historical cropland information derived at the watershed scale (using Landsat imagery) unto a coarse spatial resolution, but geographically large, satellite imagery (MODIS) using regression based modeling. The possibility of using such regional scale cropland information to improve government-derived agricultural statistics was investigated by comparing extracted cropland area from the fractional cover maps with district-level agricultural statistics from Ghana. The accuracy of the fractional cover maps (MAE between 14.2% and 19.1%) indicate that the heterogeneous agricultural landscape of West Africa can be suitably represented at the regional or continental scales by estimating fractional cropland cover on low resolution. Analysis of the results revealed that cropland area in the Sudanian Savanna zone has experienced inter-annual or short term fluctuations in the past ten years due to a variety of factors including climate factors (e.g. floods and droughts), declining soil fertility, population increases and agricultural policies such as fertilizer subsidies. Comparison of extracted cropland area from the fractional cover maps with government's agricultural statistics (MoFA) for seventeen districts (second administrative units) in Ghana revealed high inconsistencies in the government statistics,

and highlighted the potential of satellite derived cropland information at regional scales to improve national/sub-national agricultural statistics in West Africa.

The results obtained in this study is promising for West Africa, considering the recent launch of optical (Landsat 8) and SAR sensors (Sentinel-1) that will provide free data for crop mapping in the sub-region. This will improve chances of obtaining adequate satellite images acquired during the cropping season for agricultural land use mapping and bolster opportunities of operationalizing agricultural land use mapping in West Africa. This can benefit a wide range of biophysical and economic models and improve decision making based on their results.

## Zusammenfassung

Das schnelle Bevölkerungswachstum im Westen Afrikas hat, durch das erhöhte Bedürfnis nach Lebensmitteln der expandierenden Bevölkerung, zu einer steigenden Lebensmittelnachfrage und damit zur Ausweitung von Ackerland geführt. Diese Expansionen haben negative Einflüsse auf das Ökosystem der Subregion, die Konsequenzen für Wasser- und Bodenqualität, sowie für Biodiversität und das Klima nach sich ziehen. Um die Veränderungen der Ackerflächen überwachen und die Folgen für das Ökosystem und anderer Umweltprozesse richtig abschätzen zu können, werden genaue und aktuelle Informationen über die landwirtschaftliche Nutzung benötigt. Das Kartographieren landwirtschaftlicher Flächennutzung (z.B. das Abbilden der räumlichen Verteilung von Feldfrüchten und Ackerflächen) in Westafrika wurde durch die mangelhafte Verfügbarkeit geeigneter Satellitendaten (durch das Auftreten massiver Wolkenbedeckung), der geringen Größe der landwirtschaftlichen Flächen, sowie der heterogenen Landschaft, erschwert. Aus diesen Gründen untersucht diese Studie das Potential landwirtschaftlich genutzte Flächen, durch die Nutzung von optischen Satellitensystemen mit höherer geometrischer und temporaler Auflösung und Aufnahmen des Synthetic Aperture Radar (SAR) als ein nahezu wetterunabhängiges System, aufzunehmen. Diese Studie wurde sowohl auf der Skala von Wassereinzugsgebieten als auch von Regionen erstellt (Agrarökologische Zone in der sudanesischen Savanne).

Auf der Skala der Wassereinzugsgebiete wurden Klassifikationen verschiedener Feldfrüchte in drei Einzugsgebieten in Ghana, Burkina Faso und Benin, mithilfe multitemporaler Abbildungen, bestehend aus entweder (1) nur optischer Abbildungen (Rapideye) oder (2) optischer und dual polarimetric (VV/VH) SAR Aufnahmen (TerraSAR-X), durchgeführt. Zusätzlich wurden interannuelle oder kurzzeitige (2-3 Jahre) Veränderungen in der Ausdehnung von Ackerflächen über die vergangenen zehn Jahre hinweg mittels historischer Landsataufnahmen untersucht. Die Ergebnisse zeigen, dass das Kartographieren verschiedener Feldfrüchte in Westafrika durch nur optische Abbildungen eine moderate Klassifikationsgenauigkeit von 57% bis 71% wiedergibt. Überlappungen zwischen dem Anbauplan der meisten Feldfrüchte und dem Zwischenfruchtanbau stellen eine Herausforderung für optische Abbildungen dar, um eine angemessene Unterscheidung der Feldfrüchte zu erreichen. Die Hinzunahme von SAR Aufnahmen kann die Klassifikationsgenauigkeit, abhängig von der Anzahl verfügbarer Szenen und deren Aufnahmedatum, jedoch um 8% bis 15% erhöhen. Die Empfindlichkeit der SAR Systeme gegenüber unterschiedlichem Aufbau der Fläche von Feldfrüchten und der Charakteristika der Landoberfläche verbesserten die Trennbarkeit unterschiedlicher Feldfrüchte. Wie sich herausstellte hat die VV Polarisation von TerraSAR-X eine bessere Trennung der Feldfrüchte bewirkt als die VH Polarisation. Außerdem zeigt sich, dass Aufnahmen zwischen August und Oktober sehr nützlich zur Abbildung von Feldfrüchten in der Subregion sind, da in dieser Zeit strukturelle Unterschiede einiger Feldfrüchte beobachtet werden können.

Auf regionalem Maßstab wurden interannuelle oder kurzzeitige Veränderungen der Ackerflächen in der agrarökologischen Zone der sudanesischen Savanne in Westafrika durch das hochskalieren historischer Informationen zu den Ackerflächen auf der Skala der Wassereinzugsgebiete (aus Landsat Aufnahmen) auf eine gröbere Auflösung, aber geographisch weite Satellitenszene (MODIS), unter Zuhilfenahme eines auf Regression basierenden Modells, berechnet. Die Möglichkeit regionalskalierte Informationen zu Ackerflächen zu nutzen um staatlich erstellte landwirtschaftliche Statistiken zu verbessern wurde untersucht, indem die extrahierte Fläche der Äcker aus

fraktionierten Karten zur Landbedeckung mit landwirtschaftlichen Statistiken auf Distrikt-Level miteinander verglichen werden. Die Genauigkeit der fraktionierten Landbedeckungskarten (Mean Absolute Error zwischen 14,2% und 19,1%) weist darauf hin, dass die heterogene Agrarlandschaft Westafrikas auf einem regionalen oder kontinentalen Maßstab, durch die Abschätzung fraktionierter Ackerflächen aus gering aufgelösten Satellitendaten, angemessen repräsentiert werden kann. Die Analyse der Ergebnisse zeigt, dass die Ackerflächen der Agrarökologischen Zone der sudanesischen Savanne interannuelle oder kurzzeitige Schwankungen in den vergangenen zehn Jahren unterlegen waren. Diese Schwankungen ergeben sich durch bestimmte Faktoren wie: klimatische Faktoren (z.B. Überschwemmungen oder Dürren), sinkende Bodenfruchtbarkeit, Bevölkerungswachstum und landwirtschaftliche Politik wie der Subvention von Düngemitteln. Der Vergleich von fraktionierter Landbedeckungskarten mit staatlich erstellten landwirtschaftlichen Statistiken (MoFA) in 17 Distrikten in Ghana ergaben große Unregelmäßigkeiten in den staatlichen Statistiken und zeigten das Potential von aus Satellitendaten abgeleiteten Informationen zu Ackerflächen auf regionalem Maßstab um nationale oder subnationale landwirtschaftliche Statistiken in Westafrika zu verbessern.

Angesichts der baldigen Starts der optischen (Landsat 8) und SAR (Sentinel-1) Sensoren, die frei zugängliche Daten für die Kartierung von Feldfrüchten in der Subregion liefern werden, sind die Ergebnisse, die in dieser Studie gewonnen wurden, vielversprechend für Westafrika. Dadurch steigen die Chancen, dass adäquate Satellitenszenen für das Abbilden landwirtschaftlicher Landnutzung während der Anbauzeitraums bezogen und operationalisiert werden können. Dies hat zur Folge, dass ein breites Spektrum biophysikalischer und ökonomischer Modelle davon profitieren und die Entscheidungsfindung durch die Ergebnisse optimiert wird.

## Acknowledgements

I would like to thank the Almighty God for His abundant grace and mercies showered on me and my family during the last three years. He has been my sole source of strength throughout this period.

I am extremely grateful to my principal supervisor, Prof. Dr. Christopher Conrad, whose guidance, suggestions, comments, constructive criticism and wealth of experience in Remote Sensing significantly shaped this thesis in the right direction. I'm grateful to him for his time and patience in supervising my PhD study.

I would also like to thank Prof. Dr. Heiko Paeth, my second supervisor, for his invaluable comments and suggestions which improved the overall quality of this study. Special thanks also go to Dr. Michael Thiel and Dr. Tobias Landmann, who served as my mentors at different stages of my PhD study. I enjoyed working with you on and off the field, and your time, patience and guidance are greatly appreciated. Michael, thanks for having time to read through most of my thesis and providing critical comments.

My sincere thanks go to all my former and present colleagues at the Department of Remote Sensing, University of Wuerzburg. I would like to say a big thank you to all of you for the great friendship you extended to me and the assistance (academic and social) you provided me during my time at the department. Worth mentioning here are Tobias Landmann and Julian Zeidler, who were selfless in helping me settle into the German system. I would also like to thank Fabian Löw and Benjamin Leutner for the invaluable comments they gave on some aspects of my thesis, as well as Mattia Rossi for kindly translating the abstract from English to German.

I am grateful to the German Federal Ministry of Education and Research (BMBF) for providing financial assistance for this study through the West African Science Service Center for Climate Change and Adapted Land Use (WASCAL) project. Special thanks also goes to the RapidEye and TerraSAR-X science teams of the German Aerospace Center (DLR) who graciously provided the high spatial resolution satellite imagery used in this study. I also acknowledge Ghana's Ministry of Food and Agriculture for providing the agricultural statistics used in this study.

The staff and management of the WASCAL competency center in Ouagadougou, Burkina Faso were of immense help to me during my field surveys in 2012 and 2013. I would like to particularly thank Dr. Boubacar Barry, who gave me the necessary logistical support and advice during my field visits. Thanks also go to Dr. Sylvestre Da, Dr. Nadine Worou and Mr. Aaron Aduna, who gave me the necessary support and directions during my stay in the WASCAL focal watersheds. I would like to also acknowledge Evence Zoungrana, Igor Bado, Marcel Somande, Issa Zongo, Sessouma Moussa and Daid Kwesi Orchard who assisted me in diverse ways during my field visits.

Finally, I'm grateful to my family and friends who supported me in prayers and by way of encouragement.



## List of Figures

Figure 3. 1 Map showing the geographical locations of the watersheds as well as the extent of the regional scale analysis.....	25
Figure 3. 2 Deviation of annual rainfall at Dano meteorological station from a 40-year mean.....	27
Figure 3. 3 Comparison between annual rainfall totals in Dano and Bolgatanga met stations in Burkina Faso and Ghana respectively.....	27
Figure 3. 4 Average monthly rainfall and temperature in Bolgatanga, Ghana from 1977 to 2004.....	28
Figure 4. 1 Processing steps undertaken to correct SLC-off Landsat ETM+ data using previously acquired Landsat TM or SLC-on ETM+ images.....	38
Figure 4. 2 Comparison of a SLC-off Landsat image with a corresponding gap-filled image for the Landsat tile: path 196 and row 052 (Dano watershed). ....	38
Figure 4. 3 Comparison of a SLC-off Landsat image with a corresponding gap-filled image for the Landsat tile: path 194 and row 052 (Vea watershed).....	39
Figure 4. 4 Comparison of raw and fitted NDVI data (using the Savitzky-Golay adaptive filter) for the year 2012 .....	43
Figure 4. 5 Comparison between (a) a raw TSX image (b) a corresponding image filtered with the Lee adaptive filter (window size of 7x7) and (c) a non-local means filtered image (similarity window of 9x9 and search window of 21x21). ....	47
Figure 4. 6 Spatial distribution of crop fields surveyed during the 2013 field campaign .....	49
Figure 5. 1 Overview of the different scales of analysis conducted in the study .....	51
Figure 5. 2 Phenological profiles of some LULC classes in the Vea watershed. Each profile represents the mean signature of a field.....	57
Figure 5. 3 Cropping calendar for major crops in the focal watersheds based on the 2013 field survey results.....	60
Figure 5. 4 Phenological profiles of same crops ploughed at different periods of the cropping season and different crops ploughed at similar periods in the cropping season. Each profile represents the mean signature of a field.....	61
Figure 5. 5 Example of (1) same crops ploughed and planted at different periods of the cropping season and (2) effect of intercropping. Top left: a cotton field ploughed and planted in June and at early vegetative stage as of early July; top right: a cotton field ploughed as of early July. Bottom left: a rice only field; bottom right: a yam field intercropped with yam in the “gullies”.....	62
Figure 5. 6 Feature space plots of the main crop classes in Vea. The images used in each plot demonstrate their ability to better discriminate a certain crop type.....	63
Figure 5. 7 Schematic of the main processing steps in the sequential masking approach adopted to classify crops and crop groups in the focal watersheds. ....	65
Figure 5. 8 Geographical extents of Landsat images analyzed for the Dano and Vea watersheds .....	66
Figure 5. 9 Feature space plots of the five LULC classes considered in the Landsat scale classification. ....	68
Figure 5. 10 Schematic representation of the main processes involved in upscaling Landsat level results onto MODIS resolution .....	69
Figure 5. 11 Extent of Landsat and MODIS data in the upscaling analysis .....	70

Figure 6. 1 Comparison of a pan-sharpened Quickbird image (0.6 m resolution) acquired on 13th November 2013 with the RapidEye cropmask derived by classifying the June, October and November RE images of Dassari.....	75
Figure 6. 2 Spatial distribution of the four main LULC classes in the Vea watershed. Crop classification was subsequently conducted on only the cropland areas. ....	77
Figure 6. 3 Spatial distribution of the four main LULC classes in the Dano watershed. Crop classification was subsequently conducted on only the cropland areas.....	77
Figure 6. 4 Spatial distribution of the four main LULC classes in the Dassari watershed. Crop classification was subsequently conducted on only the cropland areas.....	78
Figure 6. 5 Classification of all possible permutation of available imagery in the Vea watershed. The number of classifications performed at each round of permutations is provided in parenthesis on the x-axis .....	79
Figure 6. 6 Classification of all possible permutation of available imagery in the Dano watershed. The number of classifications performed at each round of permutations is provided in parenthesis on the x-axis .....	80
Figure 6. 7 Classification of all possible permutation of available imagery in the Dassari watershed. The number of classifications performed at each round of permutations is provided in parenthesis on the x-axis .....	81
Figure 6. 8 Spatial distribution of crop types in the Vea watershed. Each detailed look is approximately 2km by 2km .....	91
Figure 6. 9 Spatial distribution of crop types in the Dano watershed. Each detailed look is approximately 2km by 2km .....	91
Figure 6. 10 Spatial distribution of crop types in the Dassari watershed. Each detailed look is approximately 2km by 2km .....	92
Figure 6. 11 Left: Harvested sorghum field in the Dano watershed with the sorghum stalks cut down and ready to be transported; right: A harvested groundnut field in the Vea watershed. The plants have been uprooted and transported home, leaving on a mixture of bare patches and grasses.....	94
Figure 6. 12 Annual cropland area in the Vea (a) and Dano (b) watersheds between 2002 and 2013 and relationship with total annual rainfall. Blue bars represent annual cropland area while red line represents total annual rainfall .....	95
Figure 6. 13 Changes in the major LULC classes in the Dano watershed between 2007 and 2008. Low cropland coverage in 2007 is believed to be as a result of floods that year. ....	97
Figure 6. 14 Comparison of modeled cropland cover maps at MODIS scale with corresponding Landsat classification .....	99
Figure 6. 15 Regional scale cropland distribution maps between 2002 and 2013 .....	101
Figure 6. 16 Comparison of fractional cropland cover for the 2011 with the MODIS V051 LULC product of 2011 developed by the MODIS land team.....	102
Figure 6. 17 Changes in cropland area in the Sudanian Savanna agro-ecological zone in West Africa between 2002 and 2013 .....	103
Figure 6. 18 Districts (2nd administrative unit) of Ghana used in the plausibility analysis.....	104
Figure 6. 19 Comparison between cropland area derived from the MODIS fractional cover and official cropped area statistics from Ghana's agricultural ministry for seventeen districts in northern Ghana. Cropland area is expressed as the percentage of the district area.....	105

Figure 6. 20 Comparison of Landsat, MODIS and MoFA cropland area estimates for five districts in northern Ghana.....	107
Figure 7. 1 Demonstration of the effects of per-pixel classification in Dassari (left) and Dano (right). Emphasis on red circles.....	110
Figure 7. 2 Suitability of the watershed's landscape for segmentation .....	110
Figure 7. 3 Feature space plot of yam and rice fields in the Dassari watershed using the July VV and VH TSX intensities. Each point represents the average values in a field .....	114
Figure 7. 4 Potential of the TSX image acquired in August (left) and September (right) to separate the cotton from other crop classes in the Dano watershed. Each point represents the mean values in each field.....	116
Figure 7. 5 Potential of the TSX image acquired in September to separate maize from legume fields in the Veve watershed. Each point represents field means. ....	117
Figure 7. 6 (a) Feature space plot of the maize and cereals classes in the Dassari watershed using the VV and VH intensities of the July TSX image; (b) same plot as (a) for the August TSX image. Each point represents class means. ....	119
Figure 7. 7 Comparison of Landsat derived (reference) cropland estimate with estimates from the 2002 fractional cover map for five districts .....	128

## List of Tables

Table 4. 1 Available RapidEye data for the three watersheds and their acquisition dates .....	34
Table 4. 2 RapidEye spectral indices extracted for each available time-step.....	35
Table 4. 3 Landsat time-series available for the Dano watershed. Only images with a cloud cover of less than twenty percent were considered for download (Path 196, row 052) .....	36
Table 4. 4 Landsat time-series available for Vea. Only images with a cloud cover of less than twenty percent were considered for download (path 194, row 052) .....	36
Table 4. 5 Spectral Indices extracted for each available Landsat time-step in Tables 4.3-4.4 .....	40
Table 4. 6 Numbers and corresponding first date of the composite periods of the MODIS product MOD13Q1 .....	41
Table 4. 7 Acquisition dates of the TerraSAR-X imagery analyzed in the study. Multiple acquisitions were made per month in 11 days interval (indicated by curly brackets) to cover the spatial extent of the respective watersheds .....	44
Table 4. 8 Periods of field campaigns in the three watersheds in 2013. Arrows indicate the start and end of each campaign.....	48
Table 4. 9 Number of fields (crops only) surveyed in each of the watersheds during the field campaigns .....	48
Table 5. 1 Land use and land cover classes considered in the derivation of a crop mask for the focal watersheds.....	56
Table 5. 2 Training and validation samples used in the general land use/land cover mapping in the respective watersheds. Water samples for Dassari are relatively few due to fewer water bodies in this watershed.....	59
Table 5. 3 Training and validation samples used in crop classification in the focal watershed .....	59
Table 5. 4 Name and description of classes considered in the Landsat historical analysis .....	66
Table 5. 5 Experiments to determine optimal parameters for the development of random forest regression tree models .....	71
Table 6. 1 Results of the permutation of all possible combinations of available optical images in the Vea watershed for the derivation of a crop mask. ....	73
Table 6. 2 Results of the permutation of all possible combinations of available optical images in the Dano watershed for the derivation of a crop mask.....	74
Table 6. 3 Results of the permutation of all possible combinations of available optical images in the Dassari watershed for the derivation of a crop mask.....	74
Table 6. 4 Area statistics of the four main LULC classes in the study watershed.....	76
Table 6. 5 The best image combination used to separate different crop classes in the Vea watershed .....	83
Table 6. 6 The best image combination used to separate different crop classes in the Dano watershed .....	83
Table 6. 7 The best image combination used to separate different crop classes in the Dassari watershed .....	83
Table 6. 8 Summary results of the sequential masking and one-time classification performed with and without SAR data. ....	84
Table 6. 9 McNemar’s test results based on a comparison of the sequential masking and one-time classifications for the study watersheds.....	85
Table 6. 10 Confusion matrix for the sequential masking classification in Vea with optical+SAR .....	85

Table 6. 11 Confusion matrix for the sequential masking classification in Dano with optical+SAR .....	85
Table 6. 12 Confusion matrix for the sequential masking classification in Dassari with optical+SAR..	86
Table 6. 13 Comparison of classwise accuracies derived for the Vea watershed using based on the one-time classification and sequential masking classification .....	86
Table 6. 14 Comparison of classwise accuracies derived for the Dano watershed using based on the one-time classification and sequential masking classification. ....	86
Table 6. 15 Comparison of classwise accuracies derived for the Dassari watershed using based on the one-time classification and sequential masking classification .....	87
Table 6. 16 Crop area statistics derived from the crop classification results at watershed scale .....	89
Table 6. 17 Overall and classwise accuracies achieved for the historical Landsat classifications conducted in the Dano watershed.....	93
Table 6. 18 Overall and classwise accuracies achieved for the historical Landsat classifications conducted in the Vea watershed .....	93
Table 6. 19 Changes in general LULC classes in the Vea watershed between 2002 and 2013.....	96
Table 6. 20 Changes in general LULC classes in the Dano watershed between 2002 and 2013 .....	96
Table 6. 21 Accuracy estimates derived from the validation of the modeled fractional cover maps..	97

## Table of Contents

Abstract.....	IV
Zusammenfassung .....	VI
Acknowledgements.....	VIII
List of Figures .....	IX
List of Tables .....	XII
1. Introduction .....	1
1.1. Background .....	1
1.2. Problem statement .....	4
1.3. Objectives of the study .....	5
1.4. Thesis outline .....	6
2. State of the Art.....	7
2.1. Definitions and concepts .....	7
2.2. Crop mapping in West Africa .....	8
2.3. Data and scale issues .....	10
2.3.1. Spatial and temporal resolution .....	10
2.3.2. Integration of multi-sensor data .....	12
2.3.3. Ancillary data .....	14
2.4. Classification methods .....	16
2.4.1. Supervised versus unsupervised classification .....	16
2.4.2. Parametric versus non-parametric classifiers.....	17
2.5. Classification approaches.....	19
2.5.1. Pixel-based classification .....	19
2.5.2. Sub-pixel based classification .....	20
2.5.3. Object-based classification .....	22
2.5.4. Per-field classification .....	22
3. Study Area .....	24
3.1. Geographical location .....	24
3.2. Biophysical characteristics .....	26
3.2.1. Climate .....	26
3.2.2. Topography, Geology and Soils.....	29
3.3. Socio-economic characteristics.....	30
3.3.1. Demography.....	30
3.3.2. Livelihoods and income .....	30

3.3.3. Land tenure and security .....	31
3.4. Cropping system .....	32
4. Data and Pre-processing .....	34
4.1 Optical satellite images .....	34
4.1.1. RapidEye.....	34
4.1.2. Landsat.....	35
4.1.3. Moderate Resolution Image Spectrometer (MODIS) .....	40
4.2. Synthetic Aperture Radar(SAR) data.....	43
4.2.1. TerraSAR-X .....	43
4.2.2. Filtering of the SAR data .....	46
4.3. Ancillary data .....	47
4.3.1. Field and reference data .....	47
4.3.2. Agricultural census data.....	49
4.3.3. Climate data .....	50
5. Methodology.....	51
5.1. Random Forests (RF) .....	52
5.2. Classification accuracy .....	54
5.3. Crop mapping at watershed scale .....	55
5.3.1. Derivation of a crop mask .....	55
5.3.2 Crop classification at watershed scale .....	59
5.4 Mapping cropland area at watershed scale.....	65
5.5 Mapping cropland area at regional scale (Sudanian Savanna) .....	68
6. Results.....	73
6.1 Crop mapping at watershed scale.....	73
6.1.1 Derivation of a crop mask .....	73
6.1.2 Crop mapping.....	78
6.2 Cropland mapping at watershed scale .....	92
6.2.1 Classification accuracies.....	92
6.2.2. Watershed-scale cropland dynamics between 2002 and 2013.....	95
6.2.3. Spatial distribution of land use and land cover classes .....	96
6.3 Upscaling of watershed cropland information unto regional scale.....	97
6.3.1 Spatial distribution of croplands at regional scale.....	98
6.3.2 Plausibility analysis.....	103
7. Discussion of Results.....	108

7.1 Crop mapping at watershed scale.....	108
7.1.1 Challenges in crop mapping .....	108
7.1.2 Advantages of sequential masking classification.....	111
7.1.3 Crop separability .....	112
7.2 Cropland dynamics at watershed scale between 2002 and 2013 .....	119
7.3 Regional scale cropland dynamics .....	123
7.3.1 Accuracy of fractional cover maps.....	124
7.3.2 Spatial distribution of croplands in the Sudanian Savanna zone.....	125
7.3.3 Plausibility analysis.....	126
8. Conclusions and Outlook .....	129
8.1 Spatial resolution, field size and landscape heterogeneity .....	130
8.2 Crop classification .....	130
8.3 Crop classification using only optical imagery .....	130
8.4 Crop classification using optical and SAR data.....	131
8.5 Best temporal window(s) for cropland and crop mapping.....	131
8.6 Spatial distribution of cropland and crops at watershed scale.....	132
8.7 Cropland dynamics at watershed scale between 2002 and 2013 .....	132
8.8 Upscaling watershed cropland information to regional scale .....	133
8.9 Improving agricultural statistics with regional scale cropland maps.....	133
8.10 The way forward for crop mapping in West Africa.....	134
References .....	137
Appendices.....	165



### 1. Introduction

#### 1.1. Background

Land use and Land cover changes (LULCC) are among the most significant human modifications to the earth's terrestrial surface (Lambin *et al.* 2001). Land cover refers to the natural and man-made coverings on the earth's surface such as vegetation, soil and water; while land use is considered as the exploitation of the earth's biophysical attributes by humans for a particular purpose (Giri 2012). Although LULCC is an ancient phenomenon, research conducted in the past decades has revealed unprecedented rates of LULC changes, primarily driven by technological development and high human population growth (Lambin and Meyfroidt 2011). These changes are in turn having a negative impact on ecosystem and environmental processes at local, regional and global scales, threatening the capacity of the earth's ecosystems to provide the required goods and services (Giri 2012).

Agricultural land use (exploitation of natural landscapes for agricultural purposes) is the most pervasive of all land uses in the world today (Ramankutty *et al.* 2008). Large amounts of natural vegetation (tropical forest/woodlands and savannas/grasses) have been cleared over the years for agricultural purposes in response to increasing population and the need to produce more food (Lambin and Meyfroidt 2011). For example, Mayaux *et al.* (2005) reported that about 5-10 million hectares of forest are transformed into agricultural land annually. Ramankutty and Foley (1999) estimated that since 1850, about 6 million km<sup>2</sup> of tropical forest/woodland and 4.7 million km<sup>2</sup> of savannas/grasses/steppes have been converted for agricultural use. Recent estimates indicate that global agricultural land (i.e. croplands and pastures) accounts for between 33 and 40 % of the earth's terrestrial surface (Ramankutty and Foley 1998, Foley *et al.* 2005, Ramankutty *et al.* 2008, Thenkabail *et al.* 2010) while the remainder is occupied by cities, deserts, reserves and other land uses that are unsuitable for agriculture (Ellis *et al.* 2010).

In recent decades, however, expansion of agricultural land has taken place mainly in tropical regions, primarily at the expense of tropical forest, while other regions (e.g. temperate zones) have experienced minimal expansion or a decrease (Foley *et al.* 2011). Studies have shown that expansion in agricultural land area in tropical regions (especially developing countries) in the 1980s and 1990s was mainly responsible for the global trend, increasing by as much as 629 million ha, while developed countries lost 335 million ha (Gibbs *et al.* 2010). In Sub-Saharan Africa (SSA), FAO (2004) estimated that agricultural lands increased from 120 million ha in 1961 to 162 million ha in 2000, representing a percentage increase of 35 % over a 40 year period. These increases have occurred at the expense of forests, grasses and shrublands. For example, Gibbs *et al.* (2010) found that about 60% of new agricultural land in Africa between 1980 and 2000 was derived from intact forest while 35% was from disturbed forest. In East Africa and other sub-regions where there's little or no forest, shrublands were converted for agricultural purposes. Brink and Eva (2009) also reported that 58 % of new agricultural areas in Africa between 1975 and 2000 were derived from forest.

## Introduction

---

Numerous studies conducted at local, national and regional scales in West Africa (WA) have noted similar trends. Results from a land cover change analysis conducted over the whole of WA between 1975 and 1990 indicate a decline in the annual rate of change of “dense tree cover” (-0.95 %), “other wooded land” (-0.37 %), “tree cover mosaic” (-0.05 %), while “other vegetation types” (including agricultural land) recorded a positive annual rate of change of 0.7% (Vittek *et al.* 2014). Brinkmann *et al.* (2012) reported that between 1990 and 2009, the proportion of cultivated land in woody savannas surrounding four cities in WA (Kano, Niamey, Bobo-Dioulasso, Sikasso) increased by 35 %. In a local level study, Wood *et al.* (2004) noted that agricultural land in South-central Senegal increased by about 128 % between 1973 and 1999 mainly at the cost of upland woodland and riparian forest. A related study conducted at the national level between 1965 and 2000, however, revealed a moderate increase in agricultural land from 17 to 21 % between the periods, although differences at local level were noted (Tappan *et al.* 2004). Paré *et al.* (2008) explored the LULCC in Southern Burkina Faso between 1984 and 2002. They reported that cropland areas experienced a positive annual rate of change of 3.8 % over the study period, while forest, grazing land and gallery forest experienced a negative annual rate of 0.4, 0.9 and 1.6 % respectively. Cropland was found to have increased by between 7 and 14% in some villages at the expense of forest cover which reduced from 78 to 48 % within the same period. Forkuor and Cofie (2011) also noted that 14% of evergreen forest was converted to agricultural land in Freetown, Sierra Leone, between 1986 and 2000. Considering that global trends in cropland areas is projected to increase by between 69 and 180 million ha by 2050 (Alexandratos and Bruinsma 2012), tropical regions in the developing world such as West Africa are expected to account for a greater proportion of this change (Foley *et al.* 2011).

This rapid expansion in agricultural lands, however, has adverse effects on the environment, and is currently considered as the main driver of many environmental threats facing the world today (Ramankutty *et al.* 2008, Foley *et al.* 2011). For example, the release of carbon dioxide into the atmosphere as a result of deforestation alters land surface albedo, evapotranspiration and cloud cover, which in turn induces climate change and variability (Giri 2012). It is estimated that deforestation contributes 12 percent of the total anthropogenic carbon dioxide (CO<sub>2</sub>) emissions annually (Friedlingstein *et al.* 2010). Valentini *et al.* (2014) revealed that between 1990 and 2009, West Africa recorded the largest carbon emissions in SSA, accounting for 107 Tg C yr<sup>-1</sup> out of a total of 320 ± 50 Tg C yr<sup>-1</sup>, owing to the high deforestation rates. Consequently, WA is considered to be one of the most vulnerable regions to climate change (Boko *et al.* 2007, Sylla *et al.* 2010). Increasing habitat and biodiversity loss in the region has also been linked to cropland expansion into forest areas (Øygard *et al.* 1999, Norris *et al.* 2010, Heubes *et al.* 2013). LULC changes are further responsible for increasing land degradation and declining soil fertility (Tolba and El-Kholy 1992, Braimoh and Vlek 2004, Bationo *et al.* 2007, Biro *et al.* 2013). Other negative impacts include reduction in soil organic carbon (SOC) stocks (Murty *et al.* 2002, Bationo *et al.* 2007), decline in surface and groundwater quality (Gordon *et al.* 2010, Bossa *et al.* 2012) and loss of aquatic ecosystems and marine fisheries (Gordon *et al.* 2010, Power 2010, Foley *et al.* 2011).

## Introduction

---

These negative consequences notwithstanding, expansion in agricultural land use provides essential ecosystem services to West Africans and the world at large (Power 2010). Prominent among these services is the provision of food for the ever increasing population in WA. Estimates show that WA has experienced high population growth in the past few decades and is currently among the high population growth rate regions in the world, with an annual sustained rate exceeding 2% (Ezeh *et al.* 2012). It is projected that the region's population will increase from 290 million in 2008 to about 500 million in 2050 (ECOWAP 2008). These increases have been found to have strong links to the rapid expansion in croplands (Raynaut 2001, Ouedraogo *et al.* 2010). Besides the provision of food, agriculture is the main source of livelihood for the majority of West Africans, providing employment for an estimated 60% of the populace (ECOWAP 2008). Agriculture also contributes greatly to the economies of most countries as well the whole sub-region (African Development Bank 2011). Between 2000 and 2004, the agricultural sector accounted for 1.2% out of a total of 3.9% regional annual Gross Domestic Product (GDP) growth rate (International Food Policy Research Institute 2006). In Ghana, the agricultural sector contributed 38% of the country's annual GDP in 2008 (ISSER 2008). These benefits, coupled with the need to cultivate more food to feed the burgeoning population means that expansion of agricultural lands in the sub-region will continue. In this regard, it is essential to take steps to ensure minimal repercussions from the negative environmental consequences outlined above.

An important first step to ensuring a balance between cropland expansion and environmental degradation is the accurate mapping of croplands as well as crop types on a regular basis (Wood *et al.* 2000, Bauer *et al.* 2003, Donner and Kucharik 2003). Agricultural land use mapping (mapping spatial distribution of crops or crop mapping) can benefit a wide range of biophysical and economic models that assesses the impacts of agriculture on the environment and vice versa. For example, simulation models that integrate climate and crop data to assess climate change impacts on crop yields have become popular in recent years (Jones and Thornton 2003, Thornton *et al.* 2009, Jalloh *et al.* 2013, Sultan *et al.* 2013). However, most of these studies lack explicit information on the spatial distribution of crops under investigation (Jalloh *et al.* 2013, Sultan *et al.* 2013), or rely on approximations to identify the possible location of crops in the study area (Jones and Thornton 2003, Thornton *et al.* 2009). Additionally, the scale of maps used is often too coarse to allow applicability in local level analysis. In this regard, the provision and utilization of accurate and up-to-date agricultural land use maps can assist in better identifying priority areas (due to spatial and temporal variation in crop response to CC) and improve targeting of policy interventions. Updated agricultural land use information can also help in monitoring changes in cropping systems and patterns and gauge farmer's reaction to climate change. Furthermore, hydrological models (Li *et al.* 2007), decision support systems (Laudien *et al.* 2010) and early warning systems (Hutchinson 1991, Genesio *et al.* 2011) can benefit from improved agricultural land use products.

Remotely Sensed (RS) data have, over the years, provided useful information for agricultural land use mapping. RS have an advantage over traditional surveying methods in that large areas can be mapped in a relatively short period with lesser financial demand. Additionally, periodic acquisition of

RS data enables analysis to be conducted at regular intervals, which aids in identifying changes. For many years, data from various optical sensors (Landsat, SPOT, MODIS, etc.) have been analyzed at different scales to produce agricultural land use maps (De Wit and Clevers 2004, Turker and Arikan 2005, Conrad *et al.* 2011, Foerster *et al.* 2012).

### 1.2. Problem statement

Although crop mapping has actively been undertaken in other parts of the world (e.g. US, Europe, Asia, etc.), very little has been done in West Africa. This can be attributed to two main challenges. First, agriculture in the region is mainly practiced at subsistence level (Bayala *et al.* 2012), which leads to small agricultural fields that typically have an area of less than 2 ha (Igue *et al.* 2000). This, coupled with sub-canopy cultivation (Wood *et al.* 2004), intercropping (Dixon *et al.* 2001) and cultivation around hamlets (Laube 2007), results in a highly fragmented landscape. Consequently, crop mapping using medium resolution RS data such as Landsat, which has been found to be the most frequently used RS data in Africa (Roy *et al.* 2010), leads to high spectral heterogeneity and poor results (Smith *et al.* 2003, Husak *et al.* 2008). The second challenge has to do with the number of images (temporal sequence) that are available for crop mapping in WA. Owing to the dependence of agriculture on rainfall, the cropping season coincides with the main rainfall season, during which high cloud cover hinder optical systems from acquiring cloud free images. This means that images of key phenological periods are often not available for analysis, resulting in difficulty in discriminating different crop types. As a result, numerous LULCC studies conducted in the region (Tappan *et al.* 2004, Wood *et al.* 2004, Cord *et al.* 2010, Ruelland *et al.* 2010) have had to lump crop types into a single thematic class (agricultural lands or cropland). Other studies that used multi-temporal data acquired during the cropping season (e.g. Turner and Congalton (1998)) concentrated on mapping single crops. Although high temporal RS data such as the Moderate Resolution Imaging Spectrometer (MODIS) exist, and has been proven useful in crop mapping in other parts of the world (Wardlow and Egbert 2008, Conrad *et al.* 2011, Redo and Millington 2011), its usefulness in WA is limited by a low spatial resolution (250 m), which cannot adequately represent the fragmented landscape of the region.

RS data with both high spatial and temporal resolution is, therefore, required to improve agricultural land use mapping in West Africa (Wellens *et al.* 2013, Forkuor *et al.* 2014). Advances in space technology have led to the launch of satellites with high spatial resolution, large swath width or coverage area and near-daily revisit times. Examples are RapidEye and SPOT 6/7, which have spatial resolutions of 5 m and 1.5 m and revisit times of 5.5 days and a day respectively. These sensors provide a better chance of identifying the typically small farm plots in WA, while the probability of obtaining cloud free images during the cropping season is increased.

Recent studies have identified the integrative use of optical and Synthetic Aperture Radar (SAR) imagery for crop mapping as a viable solution to the problem of cloud cover in optical imagery (Gauthier *et al.* 1998, Ban 2003, Blaes *et al.* 2005, McNairn *et al.* 2009, Sheoran and Haack 2013, Forkuor *et al.* 2014, Hong *et al.* 2014). SAR systems, unlike optical sensors that rely on an external

source of energy, have their own source of energy. They emit short burst radio waves and receive the reflected echoes from objects on the earth's surface. The longer wavelengths of radio waves enable transmitted signals to penetrate clouds and other atmospheric conditions that inhibit optical sensors from acquiring clear images (Henderson *et al.* 2002). Radar systems are, therefore, highly reliable in terms of data provision, and can provide imagery during periods that optical sensors fail. Whereas backscatter intensities recorded by radar systems are largely a function of the size, shape, orientation and the dielectric constant of the scatterer (Haack 2007), optical systems measure the biophysical properties (e.g. canopy moisture, leaf area and level of greenness of vegetation) of the reflecting feature. These differences in imaging and information content leads to complementarity of radar and optical systems (GERSTL 1990). This complementarity has been proven by numerous studies. For example, McNairn *et al.* (2009) tested the integration of Landsat TM and SAR data (Radarsat, ENVISAT ASAR) for five regions in Canada. They concluded that in the absence of a good time-series of optical imagery, integration of two SAR images and a single optical image is sufficient to deliver operational accuracies (>85 % overall accuracy). Rosenthal and Blanchard (1984) and Brisco *et al.* (1989) noted an increase of 20% and 25% respectively in overall accuracy when radar and optical imagery were integrated in crop mapping. Other studies also found relatively lower percentage increases (between 5 and 8%) when the two data sources were combined in a crop mapping exercise (Brisco and Brown 1995, Gauthier *et al.* 1998, Ban 2003, Blaes *et al.* 2005, Sheoran and Haack 2013).

### 1.3. Objectives of the study

The study is being conducted within the framework of the West African Science Service Center on Climate Change and Adapted Land use (WASCAL - [www.wascal.org](http://www.wascal.org)), which has been set up in West Africa to, among other things, develop effective adaptation and mitigation measures that enhance the resilience of human and environmental systems to climate change and increased variability. WASCAL focuses on the Sudanian Savanna agro-ecological zone of West Africa, and conducts primary research activities in three focal watersheds located in Burkina Faso, Ghana and Benin. This study is, therefore, conducted at two spatial scales. The first is the watershed scale in which the focal watersheds are the unit of analysis while the second is a regional scale where a broader region within the Sudanian Savanna zone is investigated.

The overall goal of this study is to investigate how the use of higher spatial and temporal resolution optical and radar imagery can improve agricultural land use mapping in the Sudannian Savanna zone of West Africa. In addition, inter-annual or short term (2-3 years) changes in cropland over the last ten years (2002 to 2013) are investigated using moderate resolution imagery. The specific objectives of the study are:

1. To ascertain whether the use of finer spatial and temporal resolution optical imagery (RapidEye) improves the detection of the typically small agricultural fields and different crop types in the WASCAL focal watersheds.

2. To determine the contribution of SAR imagery (TSX), when used together with optical data, in improving the detection of different crop types in the WASCAL focal watersheds.
3. To determine the inter-annual or short term (2-3 years) changes in croplands (extensification or shrinkage) in the focal watersheds in the last ten years using moderate resolution satellite imagery (Landsat).
4. To investigate the possibility of upscaling the cropland information derived at the watershed level using moderate resolution imagery (Landsat) in (3) above unto a low spatial resolution imagery (MODIS) in order to gain an understanding of the changes in cropland area at the regional scale (i.e. the Sudanian Savanna zone).
5. To test whether regional scale cropland area maps such as developed in (4) above can improve national/sub-national government-derived agricultural statistics in West Africa.

### **1.4. Thesis outline**

The remainder of this thesis comprises of chapters 2 through to 8. Chapter 2 presents a review of the state-of-the-art in remote sensing (RS) based agricultural land use mapping. Pertinent issues about the satellite data and methods used for agricultural land use mapping are reviewed in the light of recent research. The biophysical and socio-economic characteristics of the study areas are given in chapter 3. In chapter 4, the satellite imagery and other ancillary data used in this study are described. Chapter 5 deals with the methodology employed to achieve the objectives of the study. Results are presented in chapter 6 while discussions of the results are presented in chapter 7. Conclusions and recommendations for future work are provided in chapter 8.

### 2. State of the Art

This chapter presents a review of the state-of-the-art in remote sensing (RS) based agricultural land use mapping. It has been divided into five sections. The first section provides the definition and explanation of the major terminologies used in agricultural land use mapping. Section two reviews agricultural land use mapping efforts in West Africa and outlines the challenges such efforts have faced so far. In section three, pertinent issues (spatial and temporal resolution) about the satellite data used for agricultural land use mapping are reviewed, while the usefulness of integrating data other than satellite imagery (ancillary) is discussed in the light of recent research. Finally, a review of the different methodologies and approaches used to process satellite images into agricultural land use maps is present in sections four and five.

#### 2.1. Definitions and concepts

This section explains the major terminologies that are used in the context of earth observation based land use mapping. It is intended to assist non-remote sensing readers to better understand the concepts and theories described in this document.

**Agricultural land use** refers to the use of a piece of land exclusively for agricultural purposes. This includes land dedicated to crop cultivation as well as pasture/forage land for livestock rearing. This study, however, focuses on crop cultivation. Thus, the mention of agricultural land use in this document will refer to land dedicated to crop cultivation.

**Crop mapping** refers to the identification and mapping of different crop types on a piece of land through field surveys, remote sensing approaches, or a combination of both. Since agricultural land use has been defined in this document as land dedicated to crop cultivation, agricultural land use mapping will be used interchangeably with crop mapping in this document.

**Cropping system** refers to the pattern of crops or the temporal sequence in which crops are cultivated on a piece of land and the management techniques used on that piece of land over a fixed period (one year or the length of a cropping season). Examples of cropping systems include mono-cropping, inter-cropping, sequential cropping and strip cropping.

**Phenology** is the scientific study of the recurrence of annual biological events in animal and plant life such as flowering, breeding and migration that are influenced by climatic conditions. Crop phenological stages include flowering, leaf development, maturity, senescence and harvesting.

**Temporal resolution** refers to the frequency at which an imaging sensor acquires images over the same geographical area (also known as revisit period). Sensors that acquire images at a higher frequency or have a short revisit period (e.g. hours to days) are termed high temporal resolution while those with a revisit period of weeks or months are known as low temporal resolution sensors.

**Spatial resolution** refers to the size of the smallest object on the ground that can be resolved by an imaging system. High spatial resolution images have a small pixel size (i.e. the smallest resolvable

object), which means fine details are seen and smaller objects can be distinguished on them. On the other hand, low spatial resolution images have a large pixel size on which only coarse features can be observed.

**Optical Imaging Systems** refer to satellites that rely on the sun's illumination for imaging features on the earth's surface. Consequently, they are unable to make acquisitions at night. Additionally, images acquired in bad weather conditions (e.g. cloudy weather) are of little use for mapping. Examples of such satellites are the range of Landsat sensors - <http://landsat.usgs.gov/>, SPOT - <http://www.astrium-geo.com/en/143-spot-satellite-imagery> and RapidEye - <http://blackbridge.com/rapideye/>. Images from such sensors are referred to as optical images.

**Radar (Radio Detection and Ranging) Imaging Systems** are systems that have their own source of illumination and can, therefore, acquire images at any time during the day and in all weather conditions. Examples are RadarSat, ENVISAT and TerraSAR-X.

### 2.2. Crop mapping in West Africa

Agriculture (crop cultivation) is the main source of livelihood in West Africa and as such, regular monitoring of croplands is essential for efficient planning and sustainable development. Traditionally, crop mapping in the sub-region has been undertaken by the agricultural ministries in the respective countries. Representative crop types are sampled and mapped with prismatic compass and a tape at an administrative level (provincial or district) by trained staff. Recently, some ministries (e.g. Ghana's Ministry of Food and Agriculture) have introduced the use of handheld GPS devices in their mapping exercises. The sampled and mapped fields are aggregated to provincial/district level as production, yield and cropped area figures using statistical approaches. The limitation of this method, however, is that the spatial pattern of different crop types within the surveyed unit is not revealed.

RS-based mapping in West Africa is recent. Although the acquisition of aerial photographs and other high spatial resolution data such as Corona and Argon images dates back to the 1950s and 1960s, analysis of these images to reveal land use and land cover (LULC) types were not reported until the late 1980s or later. National mapping agencies only analyzed acquired aerial photographs using photogrammetric methods to produce topographical maps. In Ghana, for instance, the first set of topographical maps was produced in 1974 from aerial photographs acquired in 1969 and 1972 (MLGRD 2012). The launch of Landsat-1 in 1972 (and subsequently SPOT in 1986 and Landsat 4 in 1982)(Chander *et al.* 2009) provided a unique opportunity for analysis to be conducted to reveal LULC changes occurring at varying scales in the sub-region. In addition, the declassification of America's space-based intelligence national reconnaissance missions of Corona, Argon and Lanyard in 1995 (Clinton 1995) was a major breakthrough for historical LULC analysis to be conducted in data poor regions like West Africa (Tappan *et al.* 2000). Since then, numerous LULC change studies have been conducted.



Initial studies focused on historical changes, especially concerning agricultural land and natural vegetation, between the 1960s and 1990s. Aerial photographs, Corona and Argon images, and data from the early Landsat missions were important source of data for these analyses. For example, Stancioff *et al.* 1986 reported the production of a LULC map of Senegal through the interpretation and analyses of aerial photographs, multi-temporal Landsat data and extensive field data collected between 1982 and 1985. Gilruth *et al.* (1990) analyzed historical aerial photographs acquired in 1953 and 1989 and Landsat Multi Spectral Scanner (MSS) imagery of 1973 and 1985 to assess and map changes in agricultural land use in three neighboring catchments in central Guinea. Tappan *et al.* (2000) studied the LULC changes that have occurred in central Senegal between 1963 and 1992 using data from the Argon, Corona and Landsat Thematic Mapper (TM).

Increased availability of remotely sensed data, especially after the launch of Aster and Landsat Enhanced TM (ETM) in 1999, enabled an extension of LULC analysis into the late 1990s and 2000s. For example Braimoh (2009), Paré *et al.* (2008), Wardell *et al.* (2003), Duadze (2004), Wood *et al.* (2004), Forkuor and Cofie (2011), Ruelland *et al.* (2010) and Brinkmann *et al.* (2012) used improved temporal (i.e. annual) data to conducted LULC changes between the 1970s and 2000s. Other studies also analyzed Aster images to reveal LULC types (Cord *et al.* 2010). The free Landsat data distribution policy implemented by the United States Geological Survey (USGS) in 2008 further boosted mapping efforts in the sub-region, as all Landsat data became freely available to the scientific community for analysis. Roy *et al.* (2010), however, noted that this free data policy has not fully benefited RS-based research in Africa due to the continent's poor internet connectivity (ITU 2007).

Efforts have also been made by the USGS and some WA institutions to improve LULC mapping at the sub-regional level. For instance, the Earth Resources Observation Systems (EROS) Data Center of the USGS in collaboration with AGRHYMET (Centre Regional de Formation et d'Application en Agrométéorologie et Hydrologie Opérationnelle) in Niamey, Niger have been spearheading LULC change mapping in twelve WA countries (Benin, Burkina Faso, Chad, the Gambia, Ghana, Guinea, Guinea-Bissau, Mali, Mauritania, Niger, Senegal, Togo). The aim is to characterize land change trends between the 1960s, '80s and 2000s as well as better understand the biophysical and socio-economic forces driving these changes (Tappan and Cushing 2008, <http://lca.usgs.gov/lca/africalulc/>).

High temporal but poor spatial resolution imagery (e.g. MODIS and AVHRR) have also been used to map LULC in West Africa. This has mostly been in the form of global LULC products (e.g. GLC2000 (Mayaux *et al.* 2004), GLOBCOVER (Arino *et al.* 2008), MODIS V05/MCD12Q1 (Friedl *et al.* 2010)) that have been used extensively in various national and sub-regional analyses. Studies have, however, shown that these products are inconsistent especially in providing information on cropland extent and distribution (Hannerz and Lotsch 2008, Fritz *et al.* 2010). Recently, Vintrou *et al.* (2012) used time-series MODIS data (MOD13Q1) acquired in 2007 to map cultivated lands in the fragmented rural landscapes of Mali. Visual interpretation of Landsat imagery aided in the MODIS classification. Validation against global LULC products (GLC2000 Africa, GLOBCOVER, MODIS V05 and ECOCLIMAP-

II) using high spatial resolution SPOT (2.5 m) classifications revealed their approach produced better results and further confirmed inconsistencies in the global products.

A common disadvantage of all the studies reviewed above is that they deal with general LULC where different crop types are lumped into a single thematic class – for instance “agricultural land” or “cropland”. This is partly due to the fact that most studies used single date images for the different years analyzed. Additionally, most images used were acquired either at the end of the cropping season or in the dry season when minimal cloud cover allows for clear images to be taken by optical sensors. Consequently, previous studies have provided little or no information on the spatial distribution of different crop types in WA. Studies that have utilized multi-temporal data acquired within a calendar year only concentrated on single crops. For example Turner and Congalton (1998) used three SPOT-X images acquired in the cropping season of 1988 (June, July and September) to map the spatial distribution of rice fields in the inland Niger Delta of Mali. They developed a stepwise classification approach to overcome the problem of spectral heterogeneity on small field sizes that normally characterize West African landscapes.

The recent launch of high spatial resolution optical and SAR satellites with a shorter revisit time is expected to improve chances of obtaining multi-temporal images acquired during the cropping season and thereby improve mapping of the spatial distribution of crop types in West Africa.

### **2.3. Data and scale issues**

#### **2.3.1. Spatial and temporal resolution**

At the core of all crop mapping exercises is the ability to adequately identify (separate) the different crop types in the area under consideration. To this end, the type of data to be used is critical, and may impact the results to a significant extent (Moody and Woodcock 1994). Two properties that are essential to be considered in this regard are the temporal and spatial resolutions of the input imagery. The spatial resolution of the image being used must be high enough to identify/capture the typical plot sizes in the study area (Turner *et al.* 1995), while the temporal resolution must be sufficient to discriminate the crop classes under consideration based on their phenological profiles (Murakami *et al.* 2001, Wardlow *et al.* 2007).

High temporal resolution images (e.g. MODIS and AVHRR), which have an hourly to daily global coverage and are available free of charge, have been noted to be appropriate for crop mapping (Justice *et al.* 1985, Jakubauskas *et al.* 2002, Townshend and Justice 2002, Fritz *et al.* 2008, Conrad *et al.* 2011, Redo and Millington 2011). This is primarily due to changes in the spectral reflectance factors of different crops during their growing season, resulting in distinct phenological cycles for different crops. This property enables high temporal images to detect the distinct phenological signals of specific crops, which subsequently leads to a better separation between classes (Wardlow *et al.* 2006, 2007). In regions where agricultural fields are reasonably large (e.g. average of 32.4 ha in US Great Plains - Wardlow *et al.* 2007), high temporal resolution images such as MODIS, which has a coarse spatial resolution (250 m), have been found to possess sufficient spatial, temporal and

spectral resolution to discriminate major crop types and their management practices (Wardlow *et al.* 2007, Wardlow and Egbert 2008).

But same cannot be said about smallholder-dominant agricultural regions where typical farm sizes are far less than a MODIS or AVHRR pixel. The use of such high temporal resolution images for crop mapping in such regions leads to the problem of mixed pixels, where the signal from multiple land cover types could be encoded in one pixel (Smith *et al.* 2003, Jung *et al.* 2006, Husak *et al.* 2008). The severity of such problems is dependent on factors such as landscape heterogeneity (mean patch size and proportion of each cover type, or spatial aggregation pattern), spatial resolution of imagery being used and the scale of analysis (i.e. local or regional) (Moody and Woodcock 1994). Thus, although high temporal resolution images can adequately capture the distinct phenological cycles of various crops, their coarse spatial resolution limits their use in fragmented and heterogeneous landscapes where field sizes are smaller than the spatial resolution of the images.

A number of solutions exist to overcome this problem. The first and most viable one is the use of high spatial resolution imagery (e.g. Landsat, SPOT/HRV, RapidEye, QuickBird, etc.) which can adequately capture the typical small plot sizes in heterogeneous landscapes (Murakami *et al.* 2001, Turker and Arikan 2005, Conrad *et al.* 2010, 2014). However, these data sources have a number of challenges which sometimes inhibit accurate crop classification. First, the relatively long revisit period of most of these sensors results in a poor image temporal sequence. Consequently, images for certain critical crop growth stages could be unavailable for analysis. Secondly, cloud cover during the cropping season (especially in rainfed-dominant agricultural regions) prevents these sensors from acquiring sufficient images required for accurate crop classification (Marshall *et al.* 1994, Brisco and Brown 1995). But even if a good temporal sequence can be obtained, their acquisition could be costly, especially when the area being investigated is large and the imagery is from a commercial sensor (e.g. SPOT, RapidEye, etc). In other words, the acquisition of image data with high spatial and temporal resolution for accurate crop mapping comes with a high financial burden. In this regard, recent studies have conducted investigations to determine the optimum number of acquisitions and the most suitable temporal windows (i.e. best period within the cropping season to acquire images) for accurate discrimination of crop classes (Odenweller and Johnson 1984, Dawbin and Evans 1988, Jewell 1989). For example Conrad *et al.* (2014) in a study in West-Uzbekistan analyzed nine RE time-steps which spanned the entire irrigation period of a 230,000 ha irrigated agricultural landscape. They concluded that five, out of the nine, time-steps (temporal windows) acquired at distinctive stages in the irrigation period was enough to achieve the same classification accuracies (85%) attained by using all the nine. Turner and Congalton (1998) concluded that two, out of three analyzed SPOT scenes, were sufficient to map the spatial distribution of rice fields in the inland Niger Delta of Mali. In a separate study in the Saga Plains of Japan, Murakami *et al.* (2001) analyzed nine SPOT/HRV scenes acquired in eight separate months in 1997 for crop discrimination. They noted that four scenes acquired at distinct phenological stages (April, June, July, September) were able to classify the cropping systems almost as well as when all scenes were combined. These results can aid

in cost reduction in terms of data acquisition and provide essential information for planning future crop mapping and operationalization efforts.

In large area crop mapping (e.g. regional or sub-regional scales), the acquisition of high spatial and temporal resolution images may be too costly and economically imprudent. This is mainly due to the relatively small footprint of most high resolution satellites, and the need to mosaic multiple scenes to cover a large area (Ozdogan 2010). Thus even if the most suitable temporal window for accurate crop mapping has been determined, acquisition of multiple scenes for just a time-step could still be financially burdensome. In such cases, sub-pixel classification of high temporal but low spatial resolution images (e.g. MODIS and AVHRR) has been undertaken (Adams *et al.* 1986). Sub-pixel classification can overcome the problem of mixed pixels in heterogeneous landscapes. Unlike hard classifiers that assign a single class to each pixel, these approaches estimate the fractional proportion of each cover type within a “coarse” pixel. Further details on sub-pixel classification have been given in Section 2.5.2.

### **2.3.2. Integration of multi-sensor data**

Multi-sensor data has been used to overcome the challenge of obtaining sufficient high spatial and temporal images for accurate crop mapping. In these approaches, data from multiple sensors are combined to improve classification accuracy (McNairn *et al.* 2009, Conrad *et al.* 2010, Forkuor *et al.* 2013, Waske 2014, Wu *et al.* 2014). Owing to differences in imaging characteristics and orbiting patterns of different sensors, it is possible to obtain multiple images acquired at different times by different sensors that adequately provide the temporal sequence needed for accurate crop mapping. Additionally, the different image characteristics of multiple sensors can be fused to reveal detailed information (e.g. spatial and temporal) which is not obtainable on either of the images (Dong *et al.* 2009). Multi-sensor integration studies can be categorized into three main groups: (1) Integration of multiple optical images, (2) optical and synthetic aperture radar (SAR) images and more recently (3) multi-frequency radar images.

#### **Optical-optical integration**

Most studies in this category combined multi-resolution (spatial and temporal) data to improve crop classification. Watts *et al.* (2011), for example, combined MODIS and Landsat data using the Spatial and Temporal Adaptive Reflectance Fusion Model (STARFM) and produced synthetic 30 m Landsat-like high temporal resolution data for mapping no-till and minimal tillage conservation classes in north-central Montana. STARFM basically allows the generation of multi-temporal synthetic Landsat data based on a spatially weighted relationship between the reflectance of previously acquired Landsat and MODIS data (Gao *et al.* 2006, Hilker *et al.* 2009). Their study revealed that the STARFM-generated synthetic Landsat time-series produced comparable results (or sometimes better) to the MODIS time-series. They concluded that the approach can improve mapping heterogeneous landscapes where the mixed pixel problem often leads to degraded results. Similarly, Thenkabail and Wu (2012) and Wu *et al.* (2014) noted that the integration of Landsat and MODIS data improves mapping of croplands due to the combination of the spatial and temporal characteristics of the two

data sources. The relatively high spatial resolution of Landsat also aided Lobell and Asner (2004) to accurately determine end member spectra with which they performed temporal unmixing of MODIS data to derive fractional crop cover. In other studies (e.g. Conrad *et al.* 2010), the derivation of field vector boundaries from very high resolution data (SPOT 2.5 m) were integrated with a per-pixel classification based on an ASTER image (15 m) to improve the detection of crop types in the Khorezm region of Uzbekistan. Forkuor *et al.* (2013) combined multi-temporal Landsat and a single-date RE image to map crop groups in northern Ghana, West Africa. They noted that the combined use of the multi-sensor data produced better results than when each sensor data was used separately.

### **Optical-SAR integration**

Integration of data from optical and SAR sensors have become popular in recent years primarily due to the independence of radar systems to weather and other environmental conditions that have for years prevented optical systems from acquiring sufficient multi-temporal data for accurate mapping. Unlike optical sensors, SAR systems can reliably acquire adequate multi-temporal data needed for crop mapping. Integration of data from the two sources, therefore, ensure a complete image coverage of the cropping season, allowing for important crop growth stages to be identified and analyzed. Additionally, differences in their imaging mode and information content permit a synergistic use of the two data sources to improve classification accuracies (GERSTL 1990, Sheoran and Haack 2013). Although classification of multi-temporal SAR images have consistently achieved lower accuracies compared to optical data, their contribution to improving classification accuracies in multi-sensor approaches has been highlighted by numerous studies. Blaes *et al.* (2005), for instance, classified crops in Belgium by integrating three optical images (SPOT and Landsat) acquired during early, mid and late season, and fifteen radar images (ERS and RadarSat) acquired throughout the cropping season. They found that the greater the number of SAR images used in the classification, the higher the overall accuracy. Their results showed that three to five SAR images could replace the late season optical image and still achieve comparable accuracies. Brisco and Brown (1995) also noted that certain crop classes (grain and alfalfa) could be discriminated better when a single date optical data is integrated with multi-date SAR data acquired during the cropping season. Similarly, McNairn *et al.* (2009) concluded that in the absence of a good time-series of optical imagery, integration of two SAR images and a single optical image is sufficient to deliver operational accuracies (>85 % overall accuracy) in large area crop mapping.

### **Multi-frequency SAR integration**

Recent advances in space technology have resulted in a surge in the launch of spaceborne SAR systems. Since 1995, a number of radar systems, each operating at a different frequency within the microwave portion of the electromagnetic spectrum, have been launched. These include Earth Resources Satellite (ERS-2), RADARSAT 1 and 2 (C-band, 5.4GHz), ALOS PALSAR (L-band, 1.27GHz), TerraSAR-X (X-band, 9.6GHz) and the soon to be launched Sentinel-1 satellites. Another rapid

development in radar systems is the increasing provision of multiple (dual or quad) polarization data which provide additional information (e.g. crop structure and condition) not obtainable on single polarization data. These developments have generated much research interest in exploiting multi-frequency, multi-polarization SAR data for improving crop classification (Chen *et al.* 1996, Ferrazzoli *et al.* 1997, Skriver 2012). Several studies have noted that classification accuracies improved when multi-temporal, multi-frequency polarimetric SAR data were used synergistically in crop mapping. For example, Shang *et al.* (2009), integrated single, dual and quad polarimetric data from multi-frequency SAR data (ENVISAT ASAR, RADARSAT 1 & 2, ALOS PALSAR, TerraSAR-X) to map major crop types in two separate sites in Canada. They found that integrating multi-frequency SAR data increased classification accuracy by between 3 and 18% depending on the image combination. They concluded that overall accuracies of up to 85% or greater is attainable when multi-temporal multi-frequency SAR data alone is used in crop classification. In a related study in the North China Plain, Jia *et al.* (2012) found that the integration of multi-temporal ENVISAT ASAR and TerraSAR-X data produced a better overall accuracy than either of the two. Both studies agree that in the absence of optical imagery (due to persistent cloud cover), multi-frequency SAR data can achieve satisfactory results in crop mapping

### 2.3.3. Ancillary data

Multi-date satellite imagery is required for accurate crop classification (Jewell 1989). However, the complexity of cropping systems, different management practices and regional variations in climate often lead to inaccurate results when classification is limited to only spectral information (Jensen 1996, Wardlow *et al.* 2007, Peña-Barragán *et al.* 2011). Integration of ancillary data in the classification process has been noted to improve accuracy and the quality of remote sensing derived products (Hutchinson 1982, Foody 1995, Ozdogan and Gutman 2008). Ancillary data are spatial and/or non-spatial information that can aid the classifier to make better decisions to improve classification accuracy. In crop mapping, this may include: (1) knowledge of the cropping system and phenological properties of crops (Wardlow *et al.* 2007, Conrad *et al.* 2011), (2) cultivation and management practices (Turner and Congalton 1998), (3) agricultural statistics and field/parcel boundaries (De Wit and Clevers 2004) and (4) GIS layers of environmental properties such as soil, rainfall and transportation network (Kontoes *et al.* 1993, Cohen and Shoshany 2002, 2005). Various approaches for incorporating ancillary data in the classification process have been outlined by Jensen (1996) and include: geographical stratification (e.g. De Wit and Clevers 2004, Wardlow and Egbert 2008), classifier operators (e.g. Gong and Howarth 1990, Cohen and Shoshany 2002) and post-classification sorting (e.g. McNairn *et al.* 2009). Results of different crop mapping exercises that incorporated ancillary data have confirmed their usefulness in improving classification accuracy by resolving common problems encountered in crop classification.

In classifying the major crop types in the US Great Plains with 16-day MODIS metrics, Wardlow *et al.* 2007 used their knowledge of the phenological response of the crops and differences in environmental conditions (e.g. precipitation) and management practices (e.g. region-specific planting dates) to overcome potential classification errors due to intra-class regional variations

expressed in the MODIS data across the study area. They successfully mapped the major crops as well as the different management practices in the region.

De Wit and Clevers (2004), in a crop mapping exercise in the Netherlands, developed a per-field classification methodology in which they used their knowledge of the phenological behavior of different crops to first group (cluster) fields with similar phenologies before conducting separate per-pixel classifications on each cluster. Eventual integration of a field boundary database in the methodology improved the accuracy of crop discrimination compared to previous exercises in the same country.

Conrad *et al.* (2011) derived temporal segments from 8-day 250 m MODIS NDVI time-series based on the phenological patterns of major irrigated crops in the Khorezm region in Uzbekistan. They found that classification of these temporal segments achieved better accuracy (6-7%) than when the original annual time-series were used. Development of the temporal segments based on the phenological behavior of crops ensured that intra-annual temporal differences in crop phenology, which can be caused by varying management practices, is accounted for; hence the improved accuracy. Sakamoto *et al.* (2005) also utilized information on crop phenology and cultivation practices to accurately discriminate crop classes in Japan.

Based on their knowledge of cultivation and management practices, Turner and Congalton (1998) implemented a hybrid classification system (unsupervised classification, stratification and then supervised classification) which accurately accounted for the high spectral heterogeneity of ploughed rice fields and non-ploughed fields in the inland Niger Delta of Mali. They noted the suitability of the approach to mapping land use in spectrally heterogeneous regions.

Other studies improved crop discrimination by integrating geographic data and satellite imagery in knowledge based systems (Tailor *et al.* 1986). Cohen and Shoshany (2002) introduced an integrative knowledge-based approach in which they combined multi-temporal Landsat data, environmental properties (soil type and precipitation) and expert agricultural knowledge to discriminate eight crop types in a highly fragmented and heterogeneous region in Israel. An initial unsupervised classification of the multi-temporal imagery into clusters was followed by the application of "split and merge" rules which were developed through comprehensive learning of relationships between crop types, imagery properties and other data including agricultural knowledge, soil types and annual precipitation. The inclusion of the soil and precipitation layers was found to improve the separation between certain crop types, culminating in an average crop recognition accuracy exceeding 85%. In a follow-up study, Cohen and Shoshany (2005) integrated satellite data, soil and precipitation layers in a Knowledge-based system (KBSs) that utilizes the Dempster-Shafer Theory of Evidence to map seven crops in Israel. Compared to an unsupervised classification, the KBS approach was found to be superior, especially in discriminating crops in heterogeneous regions. Similarly, other studies have reported improvements in classification accuracy when ancillary information in the form of geographic data was integrated with satellite imagery (Kontoes *et al.* 1993).

### 2.4. Classification methods

#### 2.4.1. Supervised versus unsupervised classification

The aim of image classification is to (semi)-automatically label all pixels in an image into different themes or classes (Lillesand *et al.* 2004). This may be done by analyzing the spectral or temporal pattern of the pixels or a combination of the above mentioned properties. Broadly, image classification can be achieved through two approaches – unsupervised and supervised methods.

In unsupervised classification, statistical approaches are applied to image pixels to automatically identify distinct spectral classes (clusters) in an image data. The approach requires the operator to specify the number of clusters to be generated, and then the classifier automatically aggregates the image pixels into the required clusters by minimizing some predefined error function (Tso and Mather 2009). The final LULC type of each cluster can then be determined by the analyst by comparing the classified image with ground reference data. K-means is the most widely used unsupervised classification algorithm in the field of remote sensing (Mather 2004). Another algorithm is the Iterative Self Organizing Data Analysis (ISODATA) technique (Jensen 1996).

In supervised classification, the analyst guides the classification procedure by specifying representative sample sites (also known as reference data) for each of a predefined class (Lillesand *et al.* 2004). In the case of crop mapping, for instance, this will be representative fields of the type of crops intended to be classified. The reference data is usually divided into training for training a classifier and testing data for assessing the accuracy of the classification results. Homogeneous cover types (or pure pixels) are usually selected as reference data for accurate classification (Townshend 1981, Tso and Mather 2009). The training data is used together with the appropriate supervised classification method to automatically label all pixels or objects in the image as belonging to one of the representative classes.

Compared to unsupervised classification, many researchers prefer supervised classification as it has been reported to generally give more accurate results (Tso and Mather, 2009). However, unsupervised approaches sometimes have an advantage over supervised approaches in that an analyst conducting supervised classification may be unable to generate training data for all representative cover types due to financial, accessibility or constraints due to the size of the study area; whereas an unsupervised classification algorithm, when properly set up, can identify all possible classes in the study area (Lillesand *et al.* 2004). This is particularly true in highly fragmented and heterogeneous, where the mixture of small patches of different cover types often leads to misclassifications.

In order to utilize the benefits of both methods (supervised/unsupervised), some crop mapping studies combined the two approaches to improve overall classification accuracy (Turner and Congalton 1998, Cohen and Shoshany 2002, Gumma *et al.* 2014). Generally, an unsupervised classification was first conducted to reveal a large number of spectral clusters which were later merged using a supervised approach to produce the final classification (decision rules). Other studies



also used unsupervised classification to identify broad classes (due to lack of suitable training data), after which supervised classification was conducted on each of the broad classes identified (Wardlow and Egbert 2008).

### **2.4.2. Parametric versus non-parametric classifiers**

Supervised classification algorithms can be categorized into two broad groups - parametric and non-parametric classifiers. Parametric classifiers are based on statistical theory. Statistical parameters (e.g. mean, variance) are extracted from the training data and used together with the appropriate classification method to automatically classify the whole image. Examples of classifiers in this category are parallelepiped (PP), minimum distance (MD) and maximum likelihood classifiers (MLC) (Tso and Mather 2009). At the core of all these classifiers is the assumption that the spectral signatures of elements within a spectral class are normally distributed. This assumption, however, does not fit all practical applications (or real conditions), leading to failure of these approaches to produce good results in complex landscapes with classes of high variance (Hansen *et al.* 1996). Despite these limitations, the MLC is one of the most widely used classifiers in remote sensing (Wang 1990, Hansen *et al.* 1996), and has also been applied in crop mapping in recent years (Foerster *et al.* 2012).

Non-parametric classifiers overcome the statistical assumptions of parametric methods and have been noted by several studies to consistently produce high classification accuracies than their parametric counterparts (Hansen *et al.* 1996, Friedl and Brodley 1997, Murthy *et al.* 2003, Pal and Mather 2003, Mondal *et al.* 2012). Frequently used classifiers in this category include artificial neural networks (ANN), support vector machines (SVM) and decision trees (DT).

ANNs are learning algorithms that learn about regularities in a training dataset and then use this information to construct rules that can be extended to unknown data or the whole image (Tso and Mather 2009). Like other supervised classification algorithms, the performance of ANNs is, to a very large extent, dependent on how well it has been trained. A variety of ANN architectures exist (Lippmann 1987), but the most frequently used in remote sensing is a group of networks called the multi-layer perceptron neural network with back-error propagation (Paola and Schowengerdt 1995, Atkinson and Tatnall 1997). ANNs have proven superior to parametric methods (e.g. MLC) (Paola and Schowengerdt 1995, Frizzelle and Moody 2001), but their performance against other non-parametric methods (especially SVM) showed either a comparable (Dixon and Candade 2007) or lower performance (Huang *et al.* 2002, Watanachaturaporn *et al.* 2008). Notable disadvantages of ANNs include their implementation and computational complexity (Huang *et al.* 2002, Budreski *et al.* 2007), reliance on large training samples and proneness to overfitting when small training samples are used (Tu 1996, Candade and Dixon 2004). Consequently, recent research has been focusing more on other non-parametric methods which are simple to implement and require less training data.

SVM is a machine learning algorithm which was introduced in the 1970s (Vapnik 1979) and has become popular in remote sensing in recent years (Mountrakis *et al.* 2011). The algorithm uses training samples to construct an optimal separating hyperplane (or decision boundary) with which a

dataset (image) can be separated into a discrete predefined number of classes (Tso and Mather 2009, Mountrakis *et al.* 2011). A condition for the determination of the optimal hyperplane is that the margin of separation between the different class samples be maximized (Vapnik 1979). Due to the "support vector" concept, only a subset of the training samples are selected as support vectors to define the classifier's hyperplane, without necessarily using all. This is a unique attribute of SVMs, which mostly results in their insensitivity to training sample size (Camps-Valls *et al.* 2004). Candade and Dixon (2004) observed that even with a small number of training samples, SVMs can achieve comparable accuracies with ANNs. Numerous studies have reported the superior performance of SVMs to traditional classifiers (e.g. MLC) (Huang *et al.* 2002, Pal and Mather 2005), while they have performed comparably or better than other state-of-the-art non-parametric classifiers. Common limitations of the method noted by numerous studies is the selection of key parameters such as kernel functions and the parameter value (denoted by C) which controls the trade-off between maximizing the margin and minimizing the error due to training samples located on the wrong side of the decision boundary (Tso and Mather 2009, Mountrakis *et al.* 2011).

DT algorithms use a hierarchical splitting (top-down) mechanism to label unknown patterns based on a sequence of decisions (Tso and Mather 2009). Basically, DTs are composed of a root node, a set of interior nodes and terminal nodes (also called leaf nodes). Based on the relationship between training samples and the classes under consideration, a decision is made at each non-terminal node to determine the path to the next node. The terminal nodes represent the final classification. This structure makes the handling of DTs very simple, while their training time is low compared to ANNs (Friedl and Brodley 1997, Pal and Mather 2003). Two broad approaches to the construction of DTs have been noted in literature - manual and automatic (Tso and Mather 2009). In manual DTs, an analyst studies extracted class statistics from spectral bands (training data) and identifies appropriate thresholds that are used to manually construct a decision tree to separate the classes of interest. This approach has been found to be time consuming, especially when the classes to be separated are many and there are spectral overlaps between the classes (Tso and Mather 2009).

DTs that are automatically designed (e.g. C4.5/SEE5, Classification and Regression Trees (CART)) overcome the challenges of manual approaches, and have become popular in recent years due to their superior performance compared to traditional classifiers such as the MLC (Pal 2005, Waske and Braun 2009). With these classifiers, selection of an appropriate threshold and the best predictor (spectral band) to split a non-terminal node is automatically determined from the training data. Thus, these methods are suitable for handling large data that are required for large area mapping (Wardlow and Egbert 2008). Additionally, they can integrate a wide variety of datasets (e.g. from different sensors) to achieve high classification accuracies (Breiman *et al.* 1984). The Random Forest (RF) Classifier (Breiman 2001), which has received widespread usage in recent years (Gislason *et al.* 2006, Rodriguez-Galiano *et al.* 2012), falls under this category of classifiers. RF has a special advantage in that large sets of independent classification trees are generated, with each tree trained on a bootstrapped sample (randomly selected) of the original training samples. Each tree cast a vote for the most popular class, and the final classification output is determined by a majority vote of the

trees. This approach has been found to increase classification accuracies (Briem *et al.* 2002, Pal 2005, Gislason *et al.* 2006). Studies that compared the performance of DTs to other non-parametric classifiers (e.g. ANN, SVM) reported mixed results. Whereas some studies noted a comparable performance (Adam *et al.* 2014), others reported a lower performance for DTs (Watanachaturaporn *et al.* 2008) while Otukei and Blaschke (2010) reported a higher performance for DTs.

### 2.5. Classification approaches

The overall objective of classifying a remotely sensed image is to reveal thematic classes such as forested areas, agricultural plots or urban structures. Apart from selecting the appropriate data (section 2.3) and classification algorithm (section 2.4), the selection of a suitable classification approach is essential depending on the intended thematic classes to be mapped vis-a-vis the data. Various approaches have been developed to classify satellite images. Four of such approaches are discussed in this section: (1) per-pixel, (2) sub-pixel, (3) object-based and (4) per-field approaches.

#### 2.5.1. Pixel-based classification

The per-pixel classification approach, which is adopted by many traditional classifiers (e.g. MLC), identify thematic classes by analyzing the spectral information contained in each individual pixel (Mather 1987, Gong and Howarth 1990, Richards 1993). Thus, this approach ignores the spatial context of the pixel under consideration (Myint *et al.* 2011). In other words, the spatial (and textural) information surrounding a pixel is not considered in the classification process. Since remotely sensed data discretize space into pixels, this approach is easily implementable, and has been used for many years in the RS community. But, several studies have shown that this approach to classification can lead to inaccurate results depending on the spatial resolution of the imagery being used, characteristics of the landscape being mapped and the thematic classes of interest (Pedley and Curran 1991, Lobo *et al.* 1996, Smith and Fuller 2001, Myint 2006, Myint *et al.* 2011, Tran *et al.* 2014).

In crop mapping for instance, two frequently occurring problems associated with per-pixel classifications that leads to poor results have been discussed (Smith and Fuller 2001, De Wit and Clevers 2004). The first problem occurs when agricultural plots exhibit high within-field spectral variability owing to variations in soil fertility, soil moisture conditions or pest and diseases (De Wit and Clevers 2004, Peña-Barragán *et al.* 2011, Forkuor *et al.* 2014). This situation leads to misclassifications, where part of a field belonging to say class “A” is wrongly classified as class “B” due to spectral similarities between different parts of the two fields. The second problem arises when a pixel at the boarder of two fields/classes (mixed pixel) is assigned to a class other than the two classes of which it originally forms part, due to similarities between the spectral signatures of the mixed pixel and pixels of the class to which it has been assigned. Studies have shown that errors due to these two problems become even pronounced when per-pixel approaches are applied to heterogeneous landscapes characterized by small agricultural plots (Xiao *et al.* 2002, Tran *et al.* 2014). At the same time, the use of high spatial resolution imagery, which is required to adequately capture small agricultural fields in heterogeneous landscapes, leads to increased errors when per-

pixel approaches are adopted (Myint 2006, Myint *et al.* 2011). Consequently, other classification approaches have been developed to overcome these limitations. These include sub-pixel based (Lobell and Asner 2004, Gessner *et al.* 2013), object-based (Blaschke 2010, Peña-Barragán *et al.* 2011) and field-based (Turker and Arıkan 2005, Forkuor *et al.* 2014) classification approaches.

### **2.5.2. Sub-pixel based classification**

This classification approach is normally chosen to overcome the mixed pixel problem in heterogeneous landscapes. The fractional proportion of the different land cover types in a pixel is determined based on an appropriate training data. Two popular approaches that are often used are (1) spectral mixture analysis (SMA) and (2) regression based analysis

#### **Spectral mixture analysis**

In SMA, the mixed spectral signatures in a pixel (i.e. belonging to different land cover/surface types) are compared to a set of “pure” reference spectra to enable the detection of multiple land cover types within the pixel (Lillesand *et al.* 2004). The pure reference spectral is also known as endmembers, and their selection has been noted to be critical to the success or otherwise of any SMA (Elmore *et al.* 2000, Lobell and Asner 2004). A popular SMA approach is the linear mixture model (Lillesand *et al.* 2004), in which the spectral properties of a pixel are modelled as a linear combination of endmember spectra weighted by the percent ground coverage of each endmember (Elmore *et al.* 2000). This has found widespread application in vegetation studies (Smith *et al.* 1990a, 1990b, Adams *et al.* 1993, Roberts *et al.* 1997). However, owing to the high temporal changes in cropland, Lobell and Asner (2004) introduced a slight modification to linear mixture models in which endmembers are defined in terms of temporal signatures (i.e. from different images acquired at different times of the cropping season) of reflectance instead of, or in addition to, spectral signatures. A condition to this approach is that the endmember fractions must not vary between image dates (Quarmby *et al.* 1992, DeFries *et al.* 1999). Using this approach (which they called probabilistic temporal unmixing), they successfully estimated fractional cropland cover at MODIS scale in two agricultural regions in Mexico and the United States.

Recently, Ozdogan (2010) tested an alternative approach to the temporal unmixing introduced by Lobell and Asner (2004). The Independent Component Analysis (ICA) (Comon 1994), which is a special case of the Blind Source Separation (BSS) technique, does not require endmembers prior to the unmixing. In this sense, the method can be considered as an unsupervised approach where a clustering algorithm is used to extract temporal classes defined by characteristic time curves from each mixed pixel. These extracted time curves (or crop profiles) are then matched to crop distributions by an experienced interpreter. The non-reliance of this method on a priori temporal endmembers makes it suitable for data poor regions where training samples may be difficult to obtain.

### Regression based models

This approach estimates fractional land cover based on multi-resolution data and regression trees (RTs) (DeFries *et al.* 1997, Hansen and DeFries 2004, Tottrup *et al.* 2007). Like classification trees (see Section 2.4.2), RTs are composed of a root node, interior nodes and terminal nodes, and depend on training samples and a set of predictors to label unknown patterns based on a sequence of decisions rules. Training samples may be extracted from the classification of a high spatial resolution image (e.g. Quickbird, Aster, etc.) while coarser spatial, but temporally high resolution images (e.g. MODIS) may be used as predictors (independent or explanatory variables) in estimating the fractional proportions (dependent variable) of land cover classes in the training samples (Hansen and DeFries 2004, Tottrup *et al.* 2007).

RTs are constructed by recursively partitioning the training samples (from the root node) into disjointed regions (nodes) and providing a fitted value (fractional cover) within each region based on a set of predictors (independent variables). The recursive partitioning of the training samples allow an assessment of the predictor variables and can provide important information about the most important predictor variables in estimating the surface property of interest (Borak 1999). An important difference between DTs and RTs is that whereas DTs assign a categorical class/value at each terminal node, RTs assign real values, which in this case represents the fractional proportion of a land cover class.

A common problem of RTs is overfitting (Breiman *et al.* 1984), which occur as a result of the generated trees fitting too perfectly to the training data. This could lead to incorrect predictions for other real world data that were not included in the model generation process. To avoid this problem, several pruning methods have been proposed (Breiman *et al.* 1984).

Several studies have demonstrated the use of RTs to estimate sub-pixel proportions of land cover on varying satellite images and have pointed out its advantages over other sub-pixel proportion estimation methods such as linear mixture modelling (DeFries *et al.* 1997, Smith *et al.* 2003). Hansen and DeFries (2004), for instance, used regression tree modeling to predict percent tree cover at global scales using 8 km AVHRR data and Landsat images. An aggregation of the Landsat classification results to the spatial resolution of AVHRR served as the response vector, while the spectral channels of the AVHRR data served as predictor variables. Tottrup *et al.* (2007) also used regression based modeling to estimate the fractional cover of mature forest, secondary forest and non-forest in Southeast Asia. They estimated the fractional cover at MODIS resolution based on initial classification of high resolution Aster images. Recently, Gessner *et al.* (2013) incorporated three imagery with varying spatial and temporal resolution (IKONOS, QuickBird, Landsat and MODIS) to estimate fractional cover (at MODIS scale) of major land cover types (woody growth forms, herbaceous growth forms, bare surfaces) in two heterogeneous landscapes in Namibia using non-parametric ensemble regression trees from the Random Forest family. Sub-pixel land cover proportions at Landsat resolution was estimated by using the classification results of the IKONOS

and Quickbird images as training samples, while proportions at MODIS scale was calculated using the estimated proportions at Landsat resolution as training samples. Their results showed that the regression based approach adopted was suitable for characterizing heterogeneous landscapes in Africa and other regions.

### **2.5.3. Object-based classification**

This approach incorporates spectral, textural and contextual information in identifying thematic classes in an image. Here, an image is first segmented into homogeneous objects (cluster of pixels) based on some pre-defined parameters (e.g. compactness, shape, scale) which is derived from our real world knowledge of the features intended to be mapped (Mason *et al.* 1988). Thus in crop mapping, for instance, an idea of the average size and shape of agricultural plots is required to achieve optimal segmentation. In a second step, each object (segment) is classified based on one or more statistical properties of the pixels contained in it. This means all pixels in an object are assigned to one class, eliminating the within-field spectral variability and mixed pixels problems associated with per-pixel approaches. Several studies have confirmed the superiority of object-based over pixel-based classifications, especially in heterogeneous agricultural landscapes and urban areas (Myint 2006, Blaschke 2010, Myint *et al.* 2011, Peña-Barragán *et al.* 2011).

However, a common problem that is associated with this approach is over- and under segmentation which results from generating too many or too few segments respectively (Delves *et al.* 1992). This occurs due to the inability of many segmentation algorithms to adapt to variations in an object such as color and texture or variations caused by different environmental factors (Rao *et al.* 2012). This situation frequently leads to erroneous agricultural field boundaries, which could eventually affect classification accuracy. Consequently, recent studies have developed tools and methods to assess the accuracy of image segmentation prior to classification (Möller *et al.* 2007, Liu and Xia 2010).

### **2.5.4. Per-field classification**

This classification approach integrates a per-pixel classification result with vector field boundaries and assigns a class to each field based on the majority (modal) class within it (Brisco *et al.* 1989, Aplin and Atkinson 2001). This approach has gained widespread use in crop mapping in recent years due to the increasing availability of digital topographic vector databases in many countries (De Wit and Clevers 2004, Turker and Arikan 2005). Considering the limitations of image segmentation algorithms (see Section 2.5.3), availability of accurate field boundaries can greatly improve classification accuracies. Studies that adopted this classification approach has noted its superior performance compared to traditional per-pixel approaches, especially in heterogeneous landscapes (Pedley and Curran 1991, Lobo *et al.* 1996, Conrad *et al.* 2010, 2014, Forkuor *et al.* 2014).

However, two factors are critical to the successful implementation of this method. First is the accuracy of the per-pixel classification (Turker and Arikan 2005). For example, in instances where the number of classes being considered are high/many, interclass confusion in the per-pixel result could lead to a particular field having a majority class with a small proportion (e.g. 25%), which does not provide enough confidence in the class assignment. The second factor has to do with the reliability

## State of the Art

---

of the field boundaries used. This is especially important when an official topographic vector database does not exist. In such instances, most studies have derived same from high resolution images using standard segmentation algorithms (Conrad *et al.* 2010, Forkuor *et al.* 2014). It is necessary that the appropriate accuracy assessment is performed for the the segmentation prior to the integration with the per-pixel results (Möller *et al.* 2007, Liu and Xia 2010).

### 3. Study Area

#### 3.1. Geographical location

The study was conducted at two spatial scales in the Sudannian Savanna (SS) of West Africa (Figure 3.1). The first spatial scale is the watershed, where detailed analysis was conducted in three focal watersheds along an East-West gradient. The focal watersheds are located in three West African countries namely Burkina Faso, Ghana and Benin. Hydrologically, they fall within the Volta River Basin (VB), which drains 42 and 43% of the total land area of Ghana and Burkina Faso respectively. The second spatial scale comprises a broader region in the SS, in which detailed results obtained at the watershed level was upscaled.

In Burkina Faso, the watershed falls in the Dano Department which administratively belongs to the Ioba province (South-West Region). It has an area of about 580 km<sup>2</sup> and lies between latitudes 11° 21' 50" and 11° 04' 27"N and longitudes 003° 08' 37" and 002° 50' 15"W. The watershed also falls in the Black Volta (Mahoun), which is one of the four sub-basins of the VB. Neighboring towns/departments include Dissin, Baforo, Lebiele and Bilanbar.

The watershed in Ghana falls in the Upper East Region (UER) and cuts across two administrative boundaries – Bolgatanga municipal and Bongo district. It is close to the city of Bolgatanga, which is the regional capital of the UER. The watershed has an area of 300 km<sup>2</sup> and lies between latitudes 11° 00' 55" and 10° 34' 36"N and longitudes 000° 59' 57" and 000° 45' 20"W. Within the VB, it falls in the White Volta sub-basin system. Major towns close to the watershed include Pwalugu, Zuarungu and Navrongo.

In Benin, the watershed is located in the north western part of the country. It has an area of about 192 km<sup>2</sup> and lies between latitudes 10° 56' 06" and 10° 44' 15"N and longitudes 001° 01' 37" and 001° 11' 33"E. It falls in the Materi commune, which administratively belongs to the Atacora department. It is a rural watershed with scattered villages in and around it. Dassari, the biggest village in the watershed, is the capital of the Materi commune. The north eastern part of the watershed forms part of the Pendjari National Park in West Africa. Within the VB, it falls in the Oti-Pendjari sub-basin system.



## Study Area

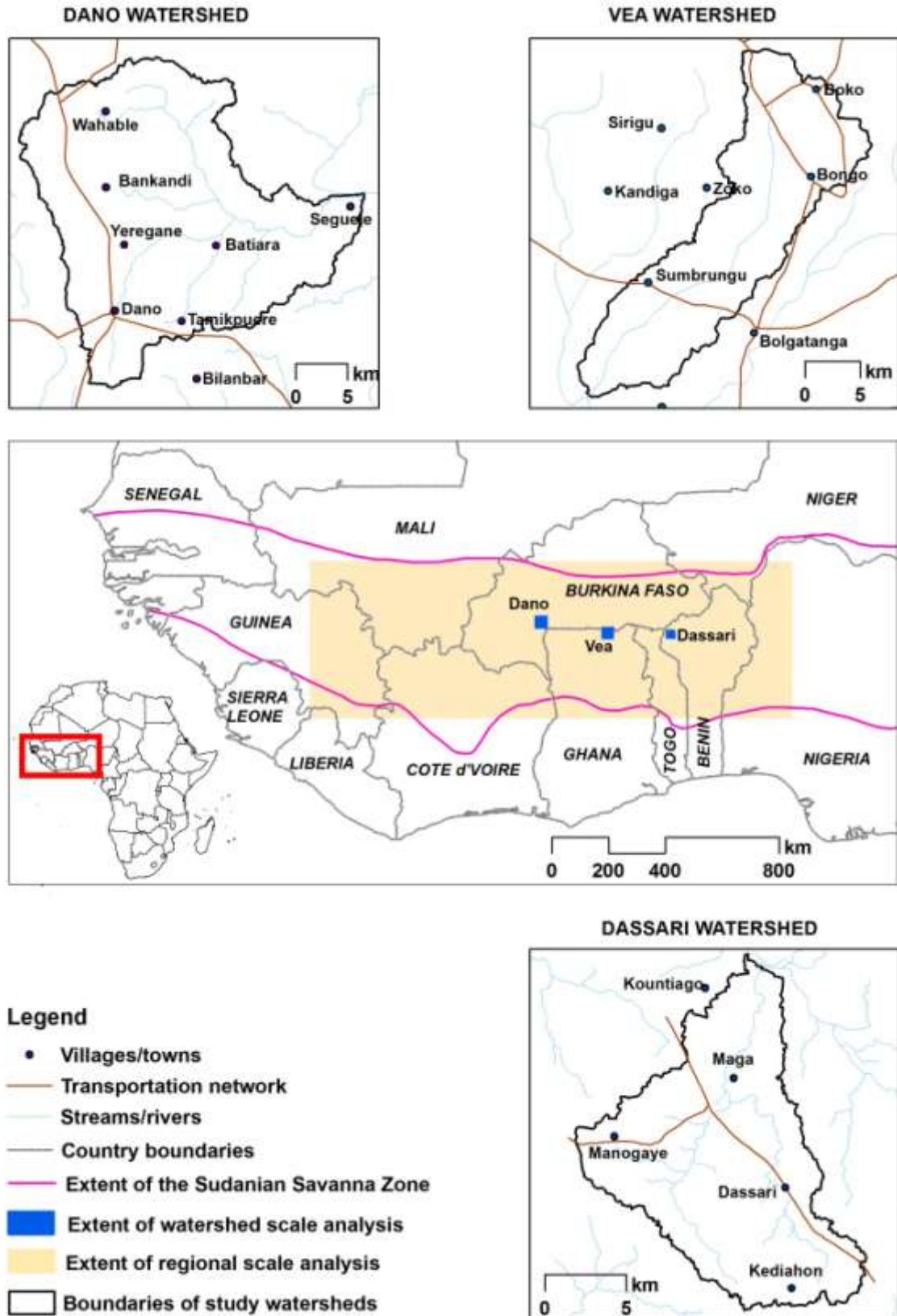


Figure 3. 1 Map showing the geographical locations of the watersheds as well as the extent of the regional scale analysis

### 3.2. Biophysical characteristics

#### 3.2.1. Climate

West Africa's climate is mainly controlled by the interaction of two air masses - the humid south-west monsoon winds and the dry north-eastern trade winds (Hayward and Oguntoyinbo, 1987). The inter-phase between these two air masses is known as the Inter Tropical Convergence Zone (ITCZ), whose annual position and latitudinal (north-south) movement results in distinct climatic zones in West Africa (Hayward and Oguntoyinbo 1987). The African Easterly Jet (AEJ), which overlay the south-west monsoon and north-east trade winds, is another system that influence climate in the sub-region, especially in the northern parts. Interaction between the south-west monsoon winds and the AEJ results in squall lines (Leroux 2001) which have been noted to produce most of the annual rainfall in some parts of WA. For example, Friesen (2002) found that in northern Ghana, rainfall at the end of the wet season almost exclusively originate from squall lines.

The climatic zone of the SS is characterized by high temperatures and a mono-modal (single peak) rainfall distribution. Typically, rainfall last from May till October during which major agricultural activities are undertaken. Rainfall reaches its peak in July or August, depending on the onset of the rains. The rainy season is followed by a long dry season between November and April, during which agricultural activities cease, except isolated cases of irrigated agriculture along major rivers and around irrigation dams.

**Rainfall:** Total annual rainfall in the SS ranges between 800 and 1200 mm, although this is highly variable in space and time (inter and intra-annual) (Nicholson and Palao 1993, Ingram *et al.* 2002, Yilma 2006). Studies conducted in the VB reported that between 1901 and 2002, average rainfall in the basin varied from 540 to 1370 mm/year with a coefficient of variation of 19 % (Oguntunde *et al.* 2006), suggesting a high inter-annual variation. Within the same period, spatial variation was twice as much as temporal variation (Oguntunde *et al.* 2006). These trends are evident in the study watersheds. Figure 3.2 shows the deviation of annual rainfall in Dano from a forty year mean (1970-2010). The figure depicts high inter-annual variation in rainfall totals, with deviations ranging between -314 mm to +280 mm. Sharp changes in annual rainfall totals from year to year occasionally occur. For instance, the difference in rainfall totals between 1980 and 1981 was 345 mm while that between 2003 and 2004 was 200 mm. These high inter-annual variations have dire consequences on agriculture, which is the main source of livelihood in the study areas. There's also considerable spatial variation in rainfall totals between the watersheds. A comparison of annual rainfall in Dano and Vea for a twenty-six year period (1980-2005) is presented in Figure 3.3. It shows significant differences of between 200 and 400 mm in corresponding rainfall totals between the two catchments. This high spatial variation does not exist only between countries, but also within countries. A studies conducted in Niger noted that in 1985, there was nearly a two-fold difference in total annual rainfall between stations 14 km apart (Flitcroft *et al.* 1989).

## Study Area

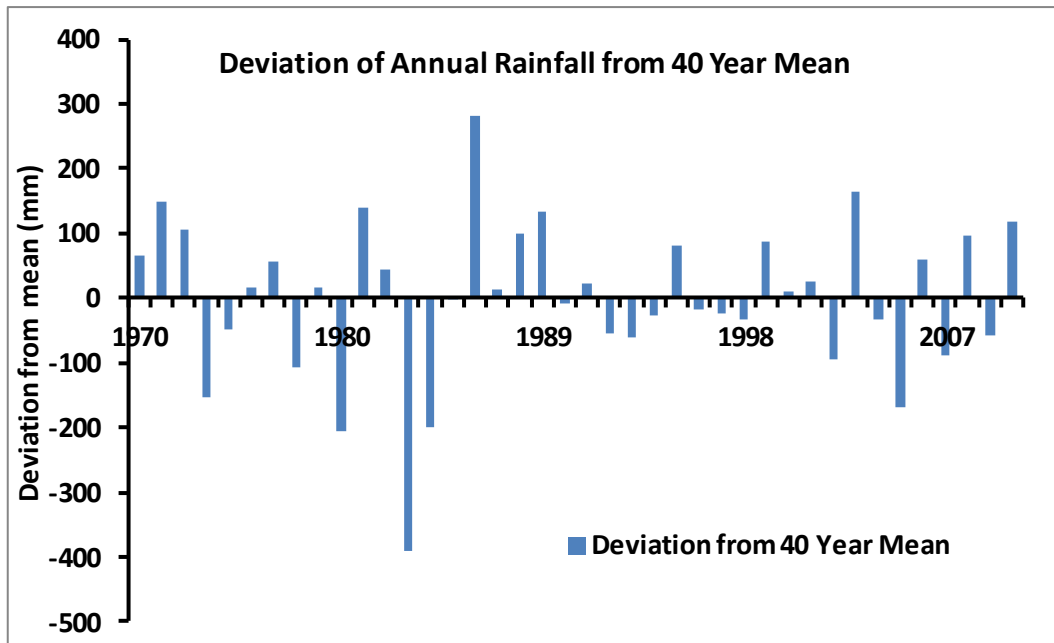


Figure 3. 2 Deviation of annual rainfall at Dano meteorological station from a 40-year mean

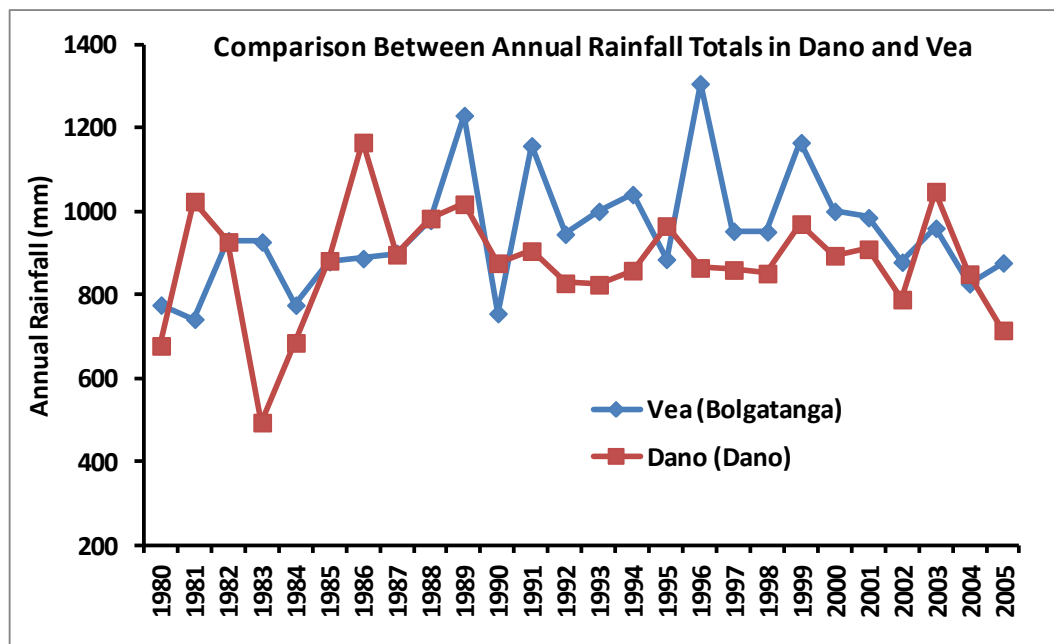


Figure 3. 3 Comparison between annual rainfall totals in Dano and Bolgatanga met stations in Burkina Faso and Ghana respectively.

Evidence of declining rainfall totals in WA in the past five decades has been presented by recent studies (Nicholson *et al.* 2000, L'HÔTE *et al.* 2002, Weldeab *et al.* 2007). This decline has been partly blamed on a general southward shift in the seasonal migration of the ITCZ (Owusu 2009). Oguntunde *et al.* (2006) noted that the VB experienced the driest period in its hydrological history between 1970 and 2002. They found that whereas rainfall in the basin increased at a rate of  $0.7 \text{ mm/yr}^2$  ( $49 \text{ mm/yr}$ ) between 1901 and 1969, a decreased of  $0.2 \text{ mm/yr}^2$  ( $6 \text{ mm/yr}$ ) was observed between 1970

## Study Area

and 2002. Kranjac Brisavljevic and Blench (1999) also noticed a decline in rainfall trend in northern Ghana when data between 1962-1991 were compared to that of 1932-1961.

**Temperature:** Temperature in WA increases from south to north. The Sahel region (northern Burkina Faso upwards) experiences higher temperatures compared to the Sudanian Savanna region (Figure 3.1), although this variation is not as high as that of rainfall (Walker 1962). Highest day-time temperatures occur during the dry season (March and April), while lowest day-time temperatures coincide with the months of highest rainfall (July-September). The Harmattan wind causes the lowest night-time temperatures to be recorded between December and February. Mean monthly temperatures in the study watersheds vary between 24<sup>o</sup>C in the wet season and 30<sup>o</sup>C in the dry season (Oguntunde 2004, Avohou and Sinsin 2009).

Studies have showed that temperature has been rising steadily in West Africa. For example, analysis of observations between 1960 and 1990 have revealed a rise in average temperature of 1<sup>o</sup>C (Ouedraogo 2004, Sandwidi 2007). Boko *et al.* (2007) also noted a general temperature rise of 0.74<sup>o</sup>C based on observations between 1906 and 2005, although the intensity of warming in the past 50 years was noted to be higher than previously. Numerous climate models agree that temperature in the sub-region will increase by 3-4<sup>o</sup>C by the end of the century (Boko *et al.* 2007). This development is expected to have consequences on the regions agricultural production.

Potential evapotranspiration in the study watersheds exceed monthly rainfall for most part of the year, except the three wettest months of July, August September. In a study of the Volta Basin, Oguntunde *et al.* (2006) noted that evapotranspiration is highest in March, while August experiences the lowest value.

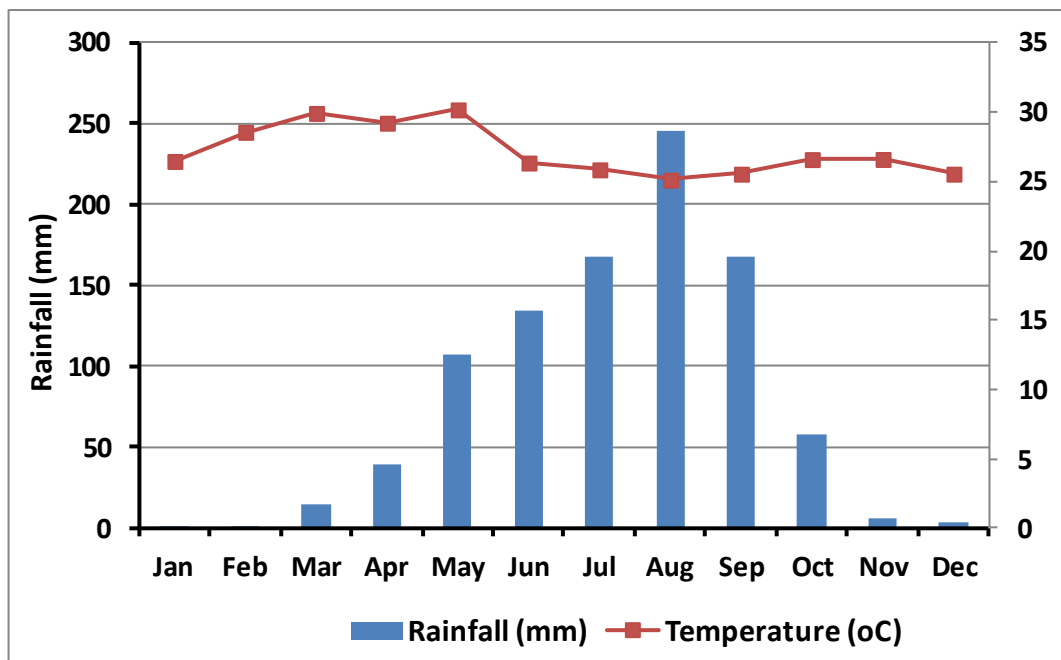


Figure 3. 4 Average monthly rainfall and temperature in Bolgatanga, Ghana from 1977 to 2004

### 3.2.2. Topography, Geology and Soils

The Sudannian Savanna is mainly flat, with elevation between 200 and 400 m. Average elevation in the study watersheds is less than 300 m (Farr and Kobrick 2000) while slopes rarely exceed five degrees. In Vea and Dano, rock outcrops occur in the eastern (i.e. Bongo granites) and western parts of the respective watersheds, where elevation exceeds 300 m. Slight depressions, also known as inland valleys, occur along rivers/streams and are mostly used for irrigated agriculture during the dry season due to proximity to water and high groundwater level. During the rainy season, these areas are used mainly for rice cultivation.

Geology of the study watersheds is dominated by Birimian rocks of Paleoproterozoic age which is associated with the West African craton (Wright *et al.* 1985). These rocks cover greater portions of Ghana, Burkina Faso and Cote d'Ivoire (Martin 2006). The Birimian rocks consist of granites, gneiss, phyllite, schist, migmatite and quartzite (Gyau-Boakye and Tumbulto 2006). Granites and gneiss are the major rocks in the watersheds under study.

The dominant soil type in the watersheds is lixisols, while acrisols, leptosols, fluvisols, cambisols and luvisols occur in relatively smaller proportions.

Lixisols are strongly weathered tropical soils with low organic matter content and a sandy loam to sandy clay loam composition. Lixisols have a topsoil with a lower, and subsoil with a higher, clay content (WRB 2006). Generally, lixisols have low levels of available nutrient, which is aggravated by a low cation retention. Consequently, recurrent fertilizer inputs are required to ensure continuous cultivation (WRB 2006). But the use of organic fertilizers in WA is low, leading to soils with low fertility in the sub-region. This situation is further exacerbated by management practices such as annual burning of vegetation and the transportation of crop residue (e.g. groundnut, sorghum/millet stalks) to homesteads, which leads to a continuous decline in soil organic matter (SOM) content and subsequently low soil fertility (Bationo *et al.* 2011). Loss in soil fertility also occurs as a result of upland/hill slope cultivation. Due to an unstable surface structure, lixisols are susceptible to slaking and soil erosion on hill slopes (WRB, 2006). In Dano, Schmengler (2011) modelled soil loss rates at hill slope and catchment level. She found that although average soil loss rates on hill slopes were moderate (less than  $5 \text{ t ha}^{-1} \text{ yr}^{-1}$ ), it could reach as high as  $50 \text{ t ha}^{-1} \text{ yr}^{-1}$  at particular hill slope positions (erosion hotspots).

In Vea, Fluvisols occur in the low lying areas along streams and rivers (inland valleys). Fluvisols have high clay content and its compact nature results in water logging during the rainy season. Cultivation of paddy rice on fluvisols is common. Leptosols occur in the elevated areas of Vea. These soils are shallow and gravelly, having a texture of loamy sand to sandy loam (Martin 2006). Late millet and other crops that have relatively low soil fertility requirements are cultivated on this soil.

Cambisols occur mainly on hill slopes in the western part of Dano. They have clay to silty-clay texture and are more fertile than lixisols, which occur in most parts of the Dano watershed. A variety of crops are cultivated on cambisols.

### 3.3. Socio-economic characteristics

#### 3.3.1. Demography

West Africa has experienced high population growth rate in recent years as a result of high fertility rates (Callo-Concha *et al.* 2012). The SS, and for that matter the study watersheds, is no exception. Data from the L'Institut national de la statistique et de la démographie in Burkina Faso indicate that population increase in the Ioba province (administrative region for the Dano watershed) more than doubled from 9% between 1985 and 1996 to 19% between 1996 and 2006 (INSD 2007). In Ghana, the Bolgatanga municipal and Bongo district both experienced a population increase of about 9% between 2000 and 2010 (GSS 2012).

Despite these increases, population density in the watersheds remain low ( $\leq 100$  persons / km<sup>2</sup>), with a high rural population. The percentage of rural population in the Ioba province in Burkina Faso, Bongo district in Ghana and Materi commune in Benin all exceed 90 % (INSAE 2004, GSS 2012)(INSD 2007). Bolgatanga municipal in Ghana has a relatively lower percentage of rural inhabitants (50%) due to the location of a regional capital in this municipal. Female population in the watersheds is higher than male, a situation that is consistent with that of West Africa. The percentage of young people has also been found to be high in the study watersheds. INSAE (2004) indicate that as of 2002, 60% of the populace in Dassari were less than 18 years, while the corresponding figure for Bongo and Bolgatanga was 50 and 44% respectively as of 2010(GSS 2012). This situation often leads to high migration rates (Sow *et al.* 2014).

#### 3.3.2. Livelihoods and income

Agriculture (crop farming and livestock rearing) is the main source of livelihood for the rural population living in the study watersheds (Ghana Statistical Service 2007, Sanfo 2010, Sissoko *et al.* 2011). According to Ghana Statistical Service (2005), agriculture employed 58 and 51% of the population in Bongo and Bolgatanga municipality respectively in 2000. Sanfo (2010) indicated that 86% of the work force in Burkina Faso is primarily employed in agriculture. Crop cultivation takes place during the rainy season which spans from May to October, while irrigated agriculture is done on a very limited scale during the dry season. Subsistence farmers generally use all their produce (especially the staples) for household consumption. Farmers who have access to credit and are able to cultivate cash crops sell them to generate income for the household. This income is used for household expenses, invested in farm inputs for the next farming season or invested in non-farm ventures (diversification).

Erratic rainfall patterns, frequent droughts/floods and poor access to markets occasionally lead to crop failure and income losses (Sissoko *et al.* 2011, Antwi-Agyei *et al.* 2012). In order to safeguard themselves against these shocks, rural farmers in the study watersheds frequently engage in other non-farm activities that can provide the necessary support in case of crop failure (Barrett *et al.* 2001). Livestock rearing is one such livelihood strategy (Barrett *et al.* 2001). Poultry, pig, goat, sheep and cattle are the main livestock reared. Farmers occasionally sell these livestock (especially goats and sheep) to provide income for the household. Additionally, they provide food for the household

(e.g. poultry) and are sometimes used ritually to make small payments (Callo-Concha *et al.* 2012). Apart from providing income and food supplement, livestock provides dung and manure for compound farms (Deng 2007).

Another livelihood strategy adopted by inhabitants of the study watersheds is outmigration (Wouterse and Taylor 2008, Sow *et al.* 2014). Most people (especially the youth) migrate to the southern parts of the respective countries during the dry season in search of employment opportunities (Kanchebe 2010, Schraven 2010). For example, farmers in Dano and Veia migrate to southern Ghana and provide labor on cocoa farms or engage in manual activities in the major cities such as Accra and Kumasi (Adepoju 1977, Cordell *et al.* 1996). In the UER, the rate of outmigration (to southern Ghana) in 2000 was estimated to be 22.2% (Ghana Statistical Service 2005). Farmers in Dassari migrate to southern Benin or Nigeria in the dry season, but also in the main cropping season in search of fertile lands for agriculture (Henson and Tomkins 2011, Sow *et al.* 2014). Incomes generated during the seasonal migration are often used as initial capital for the next cropping season as well as to purchase other items needed by the household. Inhabitants who migrate permanently occasionally send remittances to their families back home to be used for household expenses (Wouterse and Taylor 2008).

### **3.3.3. Land tenure and security**

Inhabitants in the study watersheds practice customary/traditional land tenure system. In this system, land is held or vested in traditional authorities (stools or skins) who hold it in trust for their subjects. The first settlers on a land are considered allodial owners who do not have any restrictions on their user rights and can, therefore, occupy/cultivate the land in perpetuity. Traditional authorities allocate lands to their subjects (substools, families, clans, etc.) under a customary freehold arrangement. The subjects also exercise perpetual rights over the lands so far as they acknowledge the superior title/authority of the stool/skin (Sarpong 2006). Family heads would normally divide their land among their children, and the interest in the land is inheritable upon the death of the family head. Inheritance is mostly patrilineal. Allodial owners and customary freeholders have the right to grant leasehold to a tenant for a specified period of time in return for money (rent). The rights in the land revert to the owner upon the expiration of the lease.

Apart from allodial owners and customary freeholders exercising perpetual rights in their land, migrants/strangers in the study watersheds (and other parts of WA) can derive secondary rights to land (mostly for agricultural purposes). In a West African study, Lavigne-Delville *et al.* (2001) identified between three and fifteen different arrangements for strangers/migrants to gain access to land, although similarities between some arrangements allowed for a categorization into five broad groups. These are: (1) open-ended long term loans, (2) short-term loans, (3) tenancies, (4) share-cropping contracts and (5) land pledge.

"Short-term loans", in which a land owner transfers his rights to a second party for a short period, have become popular in recent years as a result of increasing pressure on land, while "open-ended long term loans" are practiced only in areas where there's little pressure on land. "Tenancies" are

fixed-term contracts in which a tenant pays rent either at the beginning of the cropping season (in cash) or at the end (in kind, e.g. foodstuffs). "Share-cropping contract" is the practice where a landowner enters into an agreement with a tenant to either provide labor on, or cultivate a plot of land. The two parties share the produce after harvest. The harvest is either divided into two (abunu) or three (abusa) and the tenant gives half or a third respectively to the land owner (Sarpong 2006). "Land pledge" is an arrangement in which a land owner delegates his/her rights of access to land to a second party in return for a loan, with the lender using the land till the loan is repaid.

Security of tenure is an important factor that promotes or inhibits agricultural growth and investment in Africa (Commission for Africa 2005). Many countries have established formal legal systems that enable land owners to legally register their rights in a piece of land. However, most rural farmers (e.g. those in the study watersheds) do not have legal rights (title) to their land due to lack of knowledge of the process, exorbitant fees, cumbersome procedures and sometimes the seeming contradiction between the formal legal systems and local/traditional tenure arrangements (Sarpong 2006). Research has, however, shown that customary tenure systems provide enough tenure security that encourages investment and growth (Bruce 1993, Platteau 1996).

### **3.4. Cropping system**

Agriculture in the study area is mainly rainfed and dominated by smallholder farmers. Cultivation is mostly done around hamlets and in nearby bushes (Laube 2007). It is normal for most households to have more than a farm; one in close proximity to their house/hamlet and dedicated to specific crops, while the others are a few kilometers away from the house. Farm sizes are generally small due to low level of mechanization and the use of rudimentary tools for farming (Nin-Pratt *et al.* 2011). For instance, it has been estimated that about 50% of farms in northwestern Benin are less than 1.25 ha in size (Igue *et al.* 2000). Eguavoen (2008) also reported that about 70% of farms in northern Ghana have sizes between 0.5 and 2 ha. Low level of external inputs such as fertilizers and pesticides has also been observed, leading to low yields and declining productivity (Ouedraogo *et al.* 2001).

Shifting cultivation (fallow-based), a system in which a relatively long period of fallow follows a relatively short period of continuous cultivation (FAO and University of Ibadan 1982), was the main cropping system in West Africa (Callo-Concha *et al.* 2012) until recently, when rapid population growth and increasing land pressure has forced a change in this system to intercropping, where farmers cultivate multiple crops on the same piece of land on a yearly basis (Ouedraogo *et al.* 2010, Bado *et al.* 2012). Even in areas where some form of shifting cultivation is still practiced, a drastic shortening in the fallow periods has been reported (Igue *et al.* 2000, Kanchebe 2010). Intercropping has, thus, become the main cropping system in WA, since it enables farmers to derive the maximum benefit from their limited land resources. Recent uncertainties in rainfall patterns in the sub-region (Owusu *et al.* 2008, Ibrahim *et al.* 2014) have further encouraged the practice of this system in that cultivation of multiple crops on the same land serve as an insurance against crop failure, since different crops have different water requirements and can withstand varying degrees of heat.



## Study Area

---

Intercropping is predominant in the focal watersheds. The main types of intercropping are cereal-cereal (e.g. millet and sorghum), cereal-legume (e.g. millet, beans) and legume-legume (e.g. groundnuts and bambara beans). This is in line with the classification of the SS as a cereal-root-crop mixed system by Dixon *et al.* (2001). The growing period for most crops cultivated in this region range between 120 and 180 days in accordance with the mono-modal rainfall distribution (Dixon *et al.* 2001). Millet, maize, sorghum and rice are the main staple food crops cultivated in all the watersheds. Millet and sorghum are mostly cultivated for household consumption, while maize and rice may be sold in part to generate revenue for the household. In Vea, early maturing (2 months) millet is often intercropped with sorghum (and sometimes late maturing millet) to ensure an early availability of food for the household. Rice is often cultivated in inland valleys, although cultivation on uplands is also popular. Rice is also cultivated in the command area of irrigation dams in the respective watersheds. Cotton is the major cash crop in Dano and Dassari and is cultivated alone (mono-cropping). Cotton farmers receive governmental support in Burkina Faso and Benin in the form of seeds, fertilizer and pesticides. Their harvest is subsequently readily purchased by the government for export. Consequently, cotton fields tend to dominate and are normally bigger than other crop fields in the two watersheds. For example Igue *et al.* (2000) estimated that 50% of farm lands in northwestern Benin are under cotton cultivation. Due to the application of fertilizer on cotton fields, farmers usually implement a cotton-cereal (maize/sorghum)-cotton rotation based system in which cereals benefit from residual effects of cotton fertilizer (Ouattara *et al.* 2011).

In Vea, groundnut is the main cash crop. It is often intercropped with Bambara beans and may border cereal fields close to hamlets or located a few kilometers away. Like cereals, no fertilizer is applied on groundnuts fields. Yam is cultivated in Dassari either for subsistence or for generating household income. It is cultivated in mounds and is often intercropped mainly with rice (i.e. in gullies between mounds) and sometimes with maize, cassava and agushie.

The start of cultivation in the study watersheds is tied to the onset of the rainy season, which recent studies have identified uncertainties in its pattern (Laux *et al.* 2008, Lacombe *et al.* 2012). As a result of this linkage (i.e. start of the season with onset of rains), the cropping calendar could vary in, or between, countries (Vrieling *et al.* 2011). This results in variable planting dates as farmers subjectively decide when to plough or plant their fields, i.e. as to whether they are convinced that the pattern of rains will continue or not. Consequently, it is possible to have a variation of between two weeks to a month in the cropping calendar of the same crop. Differences in crop varieties could also lead to differences in cropping calendar for a crop. For example, 3- and 4-month maize varieties cultivated at the same time will have different peak periods as well as harvest times.

### 4. Data and Pre-processing

This chapter gives an overview of the data used in this study and the pre-processing steps that were carried out prior to analysis (chapter 5). The chapter is divided into three sections (4.1-4.3). The first section (4.1) gives details of the different optical image datasets employed in the study and the main pre-processing steps performed on each. The optical data used in this study are RapidEye (5m), Landsat (30m) and Moderate Resolution Image Spectrometer (MODIS; 232m) data. RapidEye and Landsat were used for watershed level analysis, while Landsat and MODIS were used for analysis performed at the regional scale (Sudanian Savanna). Section 4.2 presents the SAR data used in this study and the pre-processing steps carried out on the data. This data, which comes from the TerraSAR-X sensor were used only for the watershed level analysis. The final section details ancillary data used in this study. These include reference data collected through field campaigns and agricultural statistics and climate data obtained from secondary sources.

#### 4.1 Optical satellite images

##### 4.1.1. RapidEye

High resolution optical images from RapidEye's (RE) Multi-Spectral Imager (MSI) were used for the watershed level analysis. The RE MSI consist of five identical earth observation satellites that orbit the earth at an altitude of 630 km and produces imagery at a ground sampling distance of 6.5 m (Sandau 2010). It has a swath width of 77 km and a revisit time of 5.5 days at nadir (BlackBridge 2013). Data is provided in five optical bands in the 400-850 nm range of the electromagnetic spectrum. In addition to the traditional multi-spectral bands of Blue, Green, Red and Near-Infrared (NIR), RE MSI provides data in the so called rededge channel (Sandau 2010). The images used in this study were ordered as Level 3A, which are orthorectified and the original 6.5 m pixel resolution resampled to 5 m resolution (BlackBridge 2013). Table 4.1 presents the available time-series per watershed for the year 2013.

Table 4. 1 Available RapidEye data for the three watersheds and their acquisition dates

Year	Watershed/Available Time-series/Date of Acquisition		
	Dano	Vea	Dassari
2013	1 <sup>st</sup> April 3 <sup>rd</sup> May  29 <sup>th</sup> September 13 <sup>th</sup> October	1 <sup>st</sup> April 4 <sup>th</sup> May 3 <sup>rd</sup> June 19 <sup>th</sup> September 2 <sup>nd</sup> October 3 <sup>rd</sup> November	4 <sup>th</sup> April 2 <sup>nd</sup> May 13 <sup>th</sup> June 19 <sup>th</sup> September 12 <sup>th</sup> October 15 <sup>th</sup> November

##### RapidEye pre-processing

Atmospheric correction was performed for all RapidEye images using the ENVI ATCOR software (Richter and Schläpfer 2012). This application provides sensor specific (e.g. RapidEye, Landsat, SPOT) atmospheric database of look-up-tables (LUT) which contains results of pre-calculated radiative transfer calculations based on MODTRAN 5 (Berk *et al.* 2008). The application requires parameters

## Data and Pre-processing

such as date of image acquisition, satellite azimuth, illumination elevation and incidence angle. These parameters were obtained from the associated metadata files of the respective images. For images acquired in the dry season (see Chapter 3), a "dry tropical" atmosphere was selected while a "tropical" atmosphere was used for rainy season images.

For each time-step (monthly acquisition), image tiles covering the respective watersheds were mosaicked after atmospheric correction. Although the images were orthorectified (i.e. level 3A), initial analysis revealed that they were geometrically not aligned to other datasets such as transportation layers from topographical maps produced by the national mapping agencies of the respective countries. Therefore, the respective May images were georeferenced (with the image to map module in ENVI) using available topographical maps in the study watersheds. Subsequently, an image to image co-registration was performed for all other available images using the May image as the base. A root mean square error of less than one pixel was obtained for the initial georeferencing all subsequent co-registrations exercises. Clouds and their shadows were manually digitized and masked out from the multi-temporal images.

Spectral analysis was conducted for each image to extract difference, ratio and normalized vegetation indices (Table 4.2). Twenty-four spectral indices were initially extracted (after Schuster *et al.* 2012). However, only the indices in Table 4.2 were found to be useful based on initial analysis using the random forest variable importance measure (Genuer *et al.* 2010). These indices were used together with the original (five) bands of RE in subsequent analysis.

Table 4. 2 RapidEye spectral indices extracted for each available time-step

Difference Indices	Ratio Indices	Normalized Vegetation Indices
NIR-Red edge	NIR/Green	NDVI = (NIR-Red)/(NIR+Red)
NIR-Red	NIR/Red edge	NDVIrededge = (NIR-Rededge)/(NIR+Rededge)
NIR-Green		

### 4.1.2. Landsat

Landsat data were used in both the watershed and regional scale analysis. Historical Landsat data for the watersheds were classified to reveal changes in land use (especially cropland) between 2002 and 2013. The detected cropland areas at Landsat resolution were then upscaled unto MODIS resolution in the regional scale analysis so as to derive similar information for a broader region in the Sudanian Savanna of West Africa.

Data from the Landsat Thematic Mapper (TM), Enhanced TM (ETM) and Operational Land Imager (OLI) were downloaded free-of-charge from the United States Geological Survey's (USGS) GLOVIS website (<http://glovis.usgs.gov/>) for the years 2002 to 2013. Only images that had a cloud cover of less than twenty percent were considered for download. Due to poor Landsat data availability in the Dassari watershed, data were downloaded for only the Vea and Dano watersheds. The Vea watershed falls in the Landsat tile with path 194 and row 052, while Dano falls in the tile with path

## Data and Pre-processing

196 and row 052. Tables 4.3 - 4.4 details the multi-temporal images that were available for each year in the two watersheds. The months of acquisition suggest that most of the images were acquired during late/harvest season (October/November) or immediately after harvest (December). This is mainly due to persistent cloud cover during the main cropping season.

Table 4. 3 Landsat time-series available for the **Dano watershed**. Only images with a cloud cover of less than twenty percent were considered for download (Path 196, row 052)

Year	May	June	July	Aug	Sep	Oct	Nov	Dec
2002								
2005								
2006								
2007								
2008								
2010								
2011								
2013								
Legend		ETM+/OLI			ETM+ SLC-off			TM5

Table 4. 4 Landsat time-series available for Vea. Only images with a cloud cover of less than twenty percent were considered for download (path 194, row 052)

Year	May	June	July	Aug	Sep	Oct	Nov	Dec
2002								
2005								
2006								
2007								
2008								
2010								
2011								
2013								
Legend		ETM+/OLI			ETM+ SLC-off			TM5

In May 2003, the scan line corrector (SLC) of the Landsat ETM+ sensor, which compensates for the forward motion of the satellite and ensures a continuous coverage of the full Landsat swath (Chander *et al.* 2009), failed permanently. This resulted in data gaps which constitutes approximately 22% of each Landsat ETM+ acquired after May 2003 (Storey *et al.* 2005, Ju and Roy 2008, Wulder *et al.* 2011). Such images are referred to as SLC-off images. Thus, in downloading the Landsat data for this study, available Landsat TM data (which have no SLC errors) acquired between 2003 and 2012 were, as much as possible, downloaded instead of SLC-off Landsat ETM+. However, cloud-free images that were available for 2005 and 2008 in the study watersheds were SLC-off images. Therefore, the data gaps were filled prior to analysis. Although some previous studies that analyzed SCL-off images used them in their original form (i.e. with the data gaps) (e.g. Gessner *et al.* 2013), the gaps in the SLC-off images used in this study were filled due to two main reasons. First, the gap-filling was done to ensure that results obtained from analyzing the SLC-off images is comparable with that obtained from the analysis of the Landsat TM images (which have no gaps). Secondly, the regional scale analysis required that cropland areas detected at Landsat resolution be aggregated to

MODIS resolution (i.e. to calculate the percentage of cropland in each MODIS pixel). Because the locations of the scan gaps are different for each SLC-off image, classifying multiple SLC-off images (without filling the gaps) could lead to substantial gaps in the final results. Thus, aggregating Landsat results that have such gaps to MODIS resolution could lead to an erroneous aggregated layer.

Since the malfunctioning of the SLC in 2003, several approaches have been developed to fill the data gaps in the SLC-off images (Storey *et al.* 2005, Maxwell *et al.* 2007, Chen *et al.* 2011, Zeng *et al.* 2013). These approaches mostly use auxiliary data in the form of previously acquired SLC-on or SCL-off images to fill-in the missing gaps. In this study, a gap-filling approach proposed by Storey *et al.* (2005) and implemented in a freeware tool ("frame and fill") by (Irish and Scaramuzza 2005) was used to fill the SCL-off images of 2005 and 2008. This approach uses an adaptive local linear histogram matching technique to fill the gaps in a SLC-off image (primary image) using previously acquired SLC-on or SLC-off images (fill scenes). In its operation, a common window around each gap pixel (in the primary image) is defined from which a pre-defined number of corresponding pixel (non-zero) values are extracted from the primary and fill scenes. Based on these values (extracted from the defined window), a linear least-squares regression analysis is conducted to derive predictive equations that are used to fill the gaps in the primary image. Storey *et al.* (2005) noted that this gap-filling approach can yield poor results if the scenes being combined exhibit drastic differences in target radiance due to, for instance, the presence of clouds, snow or sun glint. Thus, a major constraint of this approach is obtaining cloud free fill scenes for the gap filling. However, this was not a major problem in this study since most of the TM images used as fill scenes were acquired during months (October-December) of minimal cloud cover in the study areas. Previous studies have utilized this approach for various mapping purposes (Brinkmann *et al.* 2011, Sanga-Ngoie *et al.* 2012).

Figure 4.1 depicts the processes undertaken in filling the gaps in the SLC-off images analyzed in this study. First, the "Frame and Fill" application (<http://l7gapfill.sourceforge.net/>) was used to fill the gaps in the SLC-off image using the approach described above. Previously acquired Landsat TM or SLC-on ETM+ data were used as "fill scenes". The output of the "Frame and Fill" processing was overlaid with the respective gap mask bands (which are supplied together with SLC-off images) in order to derive only the image data for the gaps (per band). The resulting gaps data, therefore, contains spectral information for the gaps originally present in the SLC-off ETM+ data. Subsequently, the gaps data were combined with the original SLC-off data (using band maths) to derive the final filled images. This means that, the original SLC-off data (i.e. portions that had data) was preserved, while the 22% no data areas (gaps) were filled with the output of the "frame and fill" procedure. The performance of the gap-filling exercise was assessed visually by comparing the gap-filled images with the original SLC-off image as depicted in Figures 4.2 and 4.3.

## Data and Pre-processing

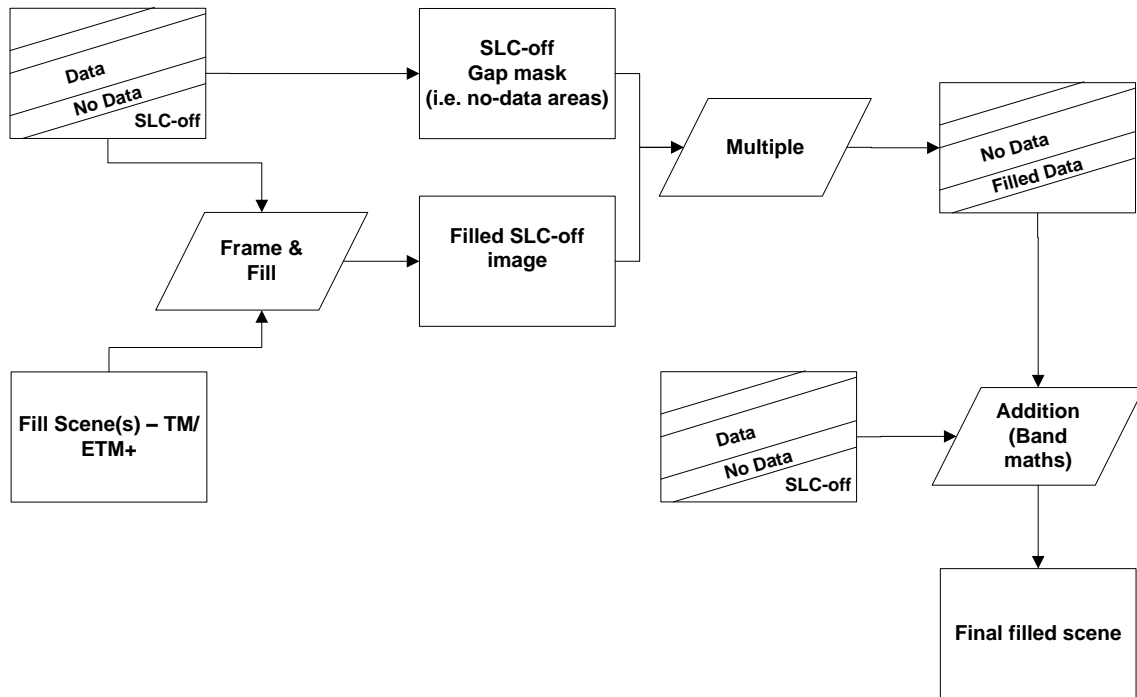


Figure 4. 1 Processing steps undertaken to correct SLC-off Landsat ETM+ data using previously acquired Landsat TM or SLC-on ETM+ images

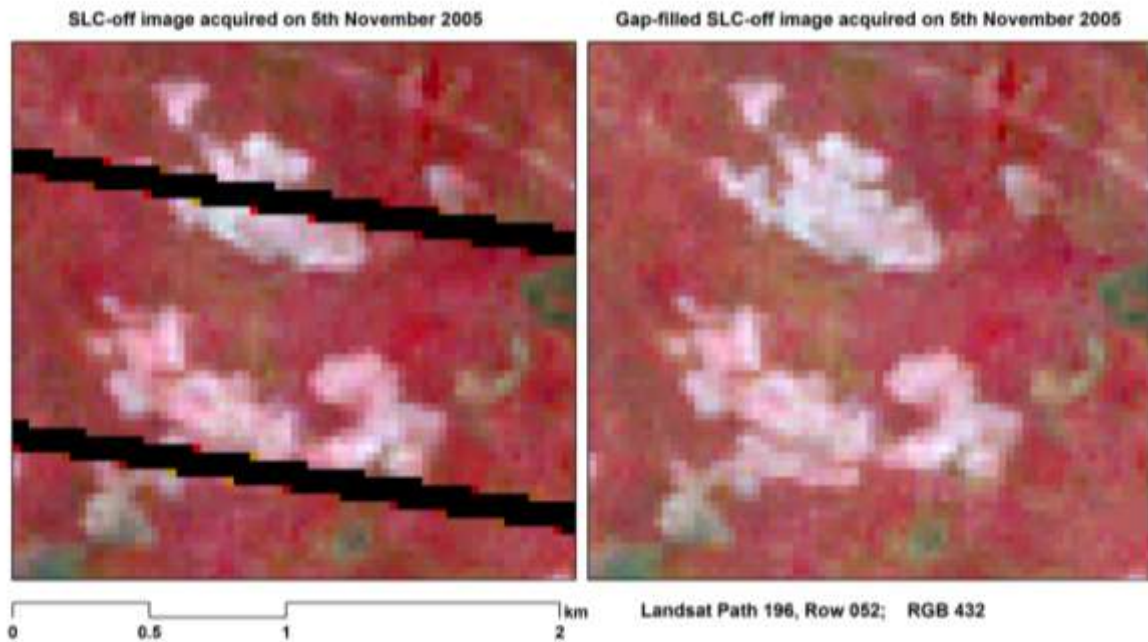


Figure 4. 2 Comparison of a SLC-off Landsat image with a corresponding gap-filled image for the Landsat tile: path 196 and row 052 (Dano watershed). The reddish features represent natural/semi-natural vegetation while the whitish features represent agricultural fie

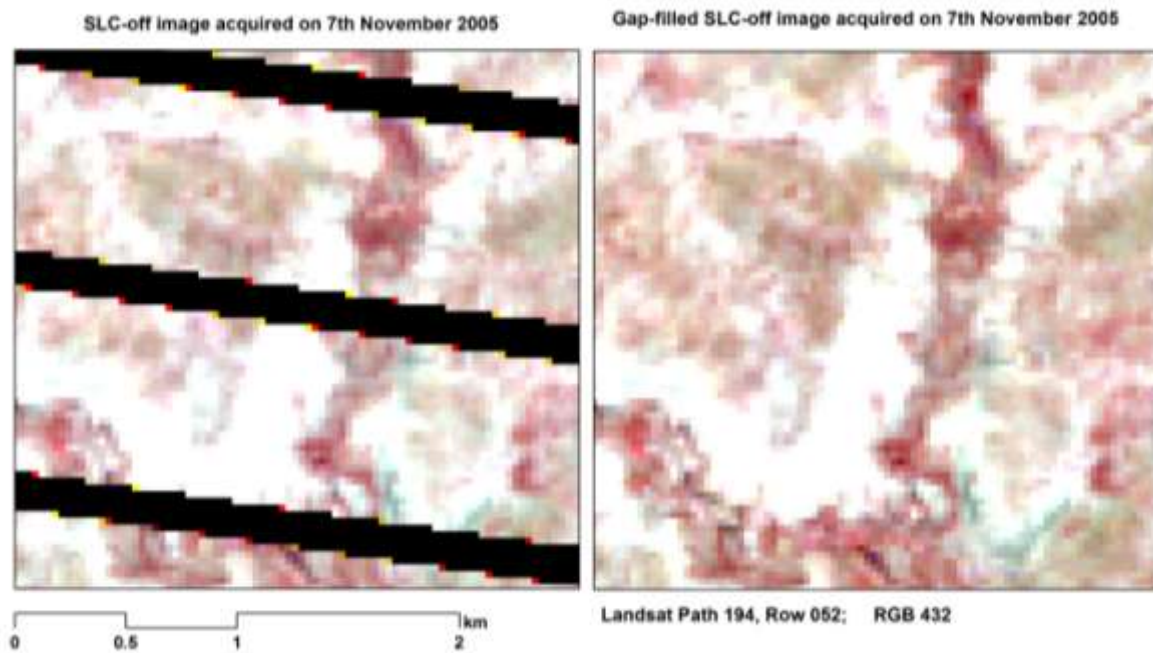


Figure 4. 3 Comparison of a SLC-off Landsat image with a corresponding gap-filled image for the Landsat tile: path 194 and row 052 (Veja watershed). The reddish features represent natural/semi-natural vegetation while the whitish features represent agricultural fields

### Landsat pre-processing

Atmospheric correction was performed for all Landsat images using ENVI ATCOR 2 (see Section 4.1.1). Parameters such as image acquisition dates, satellite azimuth, illumination elevation and incidence angle required for the correction were obtained from the associated metadata files. Georeferencing and co-registration was not performed due to a perfect alignment of the multi-temporal data with existing topographic maps and the geometrically corrected RapidEye data. In addition to the original spectral bands, nine spectral indices (difference, ratio and vegetation indices) were calculated for each image (Table 4.5). Due to some differences in the spectral channels of RapidEye and Landsat (e.g. rededge channel available only in RapidEye and mid-infrared (MIR) channels available only in Landsat), the spectral indices derived here are not exactly the same as those of the RapidEye (Table 4.2). Notable omissions here (Table 4.5) are the rededge related indices, while additions include MIR related indices, the simple ratio (SR; NIR/Red) and the soil adjusted vegetation index (SAVI; Huete 1988). Landsat derived SAVI and SR were included due to their widespread use in the remote sensing literature (Turner *et al.* 1999, Wu and Li 2012, Gessner *et al.* 2013) while the MIR related indices were included due to the usefulness of the MIR channels of Landsat in crop mapping (Panigrahy and Parihar 1992, Patnaik and Dadhwal 1995, Thenkabail 2003).

## Data and Pre-processing

Table 4. 5 Spectral Indices extracted for each available Landsat time-step in Tables 4.3-4.4

Difference Indices	Ratio Indices	Vegetation Indices
NIR-Red	NIR/Green; Red/NIR	NDVI = (NIR-Red)/(NIR+Red)
NIR-Green	Green/Red; MIR1/MIR2 MIR2/Green	SAVI = $\frac{(NIR - Red)}{(NIR + Red + 0.5)} * (1 + 0.5)$

MIR1=Landsat band 5; MIR2 = Landsat band 7

### 4.1.3. Moderate Resolution Image Spectrometer (MODIS)

MODIS data was used for the regional scale analysis primarily due to the large geographical coverage of MODIS tiles (10<sup>0</sup> X 10<sup>0</sup>) and its suitability for regional/global scale analysis (Friedl *et al.* 2002, Wardlow *et al.* 2007). Cropland areas detected at Landsat resolution (30m) were upscaled unto MODIS resolution (232m) by estimating the fractional cover of cropland in each MODIS pixel using regression based modeling.

Data from the standard MODIS product MOD13Q1 were used in this study. MOD13Q1 provides data as sixteen days composites. This means that daily acquisitions made within a sixteen day period are combined to produce the best layer for the period. There are twenty-three composites for each year. Table 4.6 shows the first date (and Julian day) of each 16-day compositing period for leap and non-leap years. The MOD13Q1 product has twelve layers which is made up of four reflectance channels (blue, red, NIR, MIR), two vegetation indices (Enhanced Vegetation Index (EVI), NDVI), two quality layers, three angle layers (zenith and azimuth angles) and a layer that gives information about the Julian day, during the sixteen day composite period, that the data for each pixel was recorded. In this study, the layers of interest were three reflectance bands (red, NIR, MIR), two vegetation indices (EVI, NDVI) and the reliability layer which provides a reliability rating for each pixel throughout the 16 day compositing period. These data were downloaded free-of-charge from the USGS' Land Processes Distributed Active Archive Center (LP DAAC) using their developed MRTWeb interface (<https://mrtweb.cr.usgs.gov/>).

Due to the intention to upscale Landsat level results unto MODIS resolution, the MODIS data were downloaded for the same years (2002 to 2013) as that of Landsat. Twenty-three images (i.e. 16-day composites) were downloaded for each year. The spatial extent of the regional scale analysis (Figure 3.1) falls within four MODIS tiles (h17v07; h17v08; h18v07; h18v08). Therefore, these tiles were mosaicked and subsetted with the MRTWeb tool prior to downloading. The native resolution of 232 m was preserved, while the projection of the data was set to the Universal Transverse Mercator Zone 30N.



## Data and Pre-processing

Table 4. 6 Numbers and corresponding first date of the composite periods of the MODIS product MOD13Q1

Composite Number	Composite first day of year (Julian day)	Date of first day (Non-leap years)	Date of first day (Leap years)
1	1	01-January	01-January
2	17	17-January	17-January
3	33	02-February	02-February
4	49	18-February	18-February
5	65	06-March	05-March
6	81	22-March	21-March
7	97	07-April	06-April
8	113	23-April	22-April
9	129	09-May	08-May
10	145	25-May	24-May
11	161	10-June	09-June
12	177	26-June	25-June
13	193	12-July	11-July
14	209	28-July	27-July
15	225	13-August	12-August
16	241	29-August	28-August
17	257	14-September	13-September
18	273	30-September	29-September
19	289	16-October	15-October
20	305	01-November	31-October
21	321	17-November	16-November
22	337	03-December	02-December
23	353	19-December	18-December

### MODIS pre-processing

Persistent cloud cover during the cropping season in West Africa inhibits optical sensors from acquiring quality data. Despite compositing daily acquisitions spanning sixteen days, the MOD13Q1 product (and other MODIS products) is regularly affected by low quality pixels mainly due to cloud cover or other atmospheric particles. This leads to noise in the time-series (i.e. the twenty-three images per year), with abnormally high or low pixel values during the cropping season months. Thus, the correction of such anomalies in each MODIS annual time-series data (i.e.) is necessary to ensure that reliable results are obtained in subsequent analysis. The provision of quality or reliability information for each pixel in the MOD13Q1 product data presents an opportunity to improve the overall quality of the time-series. In this regards, several approaches have been developed that analyzes the associated pixel quality or reliability layers and produces a temporally consistent or smooth time-series by replacing invalid pixels (i.e. low quality pixels) through temporal interpolation (Colditz *et al.* 2008) or curve fitting (Eklundh and Jönsson 2010).

In this study, the MODIS time-series were pre-processed using the TIMESAT software (Eklundh and Jönsson 2010). TIMESAT analyzes time-series satellite sensor data (e.g. AVHRR, MODIS) and generates a smooth time-series by fitting an appropriate smooth function (Savitzky-Golay filter,

least-squares fitted asymmetric Gaussian or double logistic) to the data (Eklundh and Jönsson 2010). It also permits the extraction of seasonality parameters such as start and end of vegetation greening (Eklundh and Jönsson 2010). Although numerous studies that used this software focused on the extraction of seasonality parameters (e.g. Jönsson *et al.* 2010, Davison *et al.* 2011), the use of TIMESAT in this study was only to generate a smoothed MODIS time-series for subsequent analysis. The pre-processing of the MODIS data to generate a smoothed time-series entailed three steps.

In the first step, a suitable function was identified for each of the time-series (i.e. red, NIR, MIR, NDVI, EVI) using the "TSM\_GUI" module of the TIMESAT software. Information contained in the pixel reliability layer was used as a quality indicator at this stage. The reliability layer has unique values that range from 0-3, where "0" signify good data, "1" is marginal data, "2" indicates pixels covered with snow or ice and "3" signify cloudy pixels. In processing the data, therefore, a subjective weight of "1" was given to all pixels with reliability of "0", "0.5" for pixels with reliability of "1 or 2" and "0" for pixels with reliability of "3". The analysis revealed that an adaptive Savitzky-Golay filter with a window size of two (Press *et al.* 2007) provided the best fit for all the time-series analyzed. The Savitzky-Golay filter operates with the moving window concept and replaces data values by a linear combination of nearby values in the window. In its operation, a quadratic polynomial is fitted to all points within a defined window by the method of linear least squares (Press *et al.* 2007).

In the second step, the "TSF\_Process" module of the software was used to fit the Savitzky-Golay function to the various time-series. Finally, the fitted/smoothed data (i.e. output of step two) were used to create a new set of images using the "TSF\_fit2img" module of TIMESAT. These new set of images, which represent a smoothed time-series devoid of invalid or cloudy pixels, were used in subsequent analysis. Figure 4.4 compares an original NDVI-time-series of 2012 to a corresponding fitted/smoothed time-series for a pixel. Notice the anomalous NDVI recordings for time-steps 13 and 14 in the raw data, and the smoothed version in the fitted data.

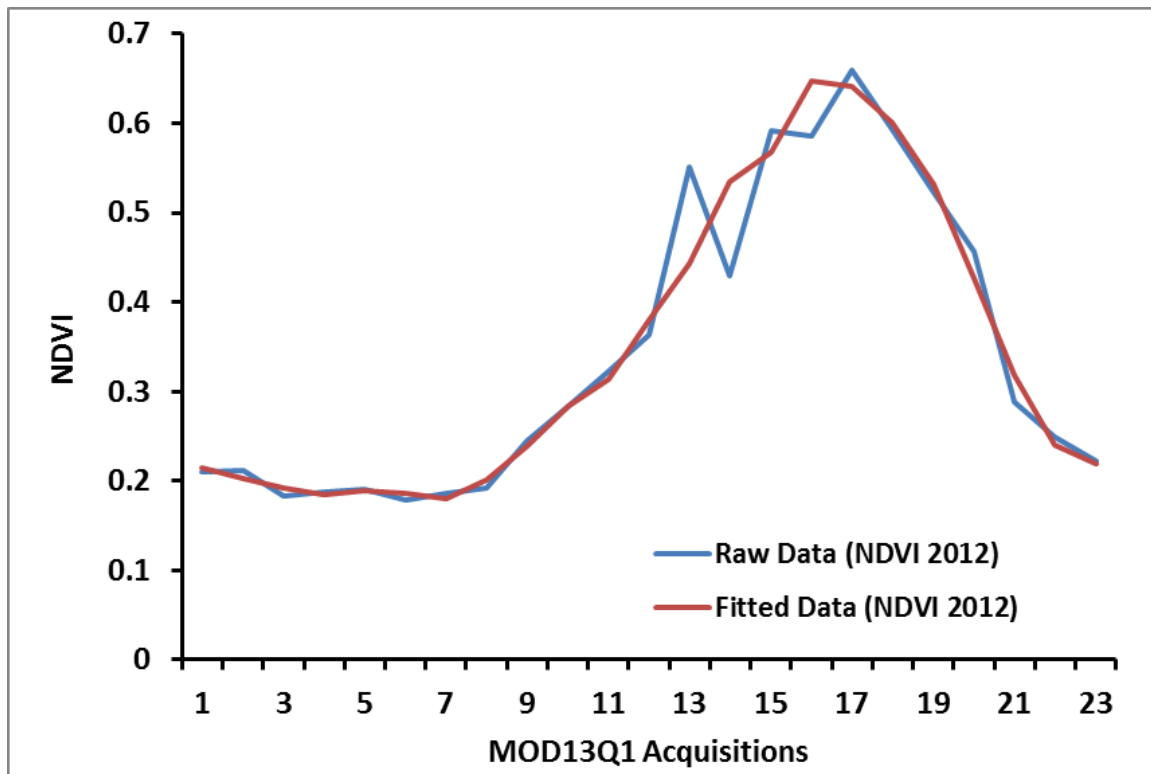


Figure 4. 4 Comparison of raw and fitted NDVI data (using the Savitzky-Golay adaptive filter) for the year 2012

#### 4.2. Synthetic Aperture Radar(SAR) data

SAR data from the TerraSAR-X (TSX) sensor was acquired for the three study watersheds and used, together with the RapidEye data, for the watershed scale crop classification analysis.

##### 4.2.1. TerraSAR-X

Multi-temporal TSX images were obtained for the year 2013 from the German Aerospace Center (DLR). TSX acquires high spatial resolution SAR images of the earth owing to its operation in the X-band segment (frequency 9.6 GHz, wavelength 31 mm) of the microwave region of the electromagnetic spectrum. The TSX instrument has a revisit time of 11 days and acquires data in four imaging modes (StripMap, high resolution spotlight, spotlight and ScanSAR). Images are acquired in either single or dual polarizations. StripMap (SM) is the basic acquisition mode, in which the ground swath is illuminated with a continuous sequence of pulses while pointing the antenna beam to a fixed angle in elevation and azimuth (DLR 2009). Single and dual polarization SM products have a swath width of 30 and 15 km, and spatial resolution of 3 m and 6-7 m respectively.

In this study, dual polarization SM data were requested in the VV and VH polarizations. Images acquired during the cropping season (May to October) were obtained for the three watersheds. Table 4.7 provides a summary of the acquisition dates for the three watersheds. Due to the limited width of the dual polarization SM data (i.e. 15km), multiple acquisitions, taken in an interval of 11 days, were made monthly in order to fully cover the respective watersheds. Incidence angle ranged between 43 and 45°, while ground range and azimuth resolutions ranged between 1.29-1.31 m and

## Data and Pre-processing

2.59-3.15 m respectively. Data were requested in two formats - Single Look Slant Range Complex (SSC) and Multi Look Ground Range Detected (MGD) formats.

The complex SSC product is the basic single look product of the focused radar signal (DLR 2009). The data are represented as complex numbers and pixels are spaced equidistant in azimuth and in slant range (DLR 2009). Owing to the availability of the full bandwidth and phase information in this product, it is suitable for scientific applications such as SAR interferometry and interferometric polarimetry. The MGD product, on the other hand, is a detected multi-look product with reduced speckle (DLR 2009). This product has approximately square resolution pixels on ground, with pixels spaced equidistant in azimuth and in ground range. This is achieved through a simple polynomial slant-to-ground projection in range using the WGS84 ellipsoid and an average constant terrain height (DLR 2009, Marzano *et al.* 2011). The advantage of this product is that image rotation to map coordinate system is not performed, hence interpolation artifacts are avoided (DLR 2009).

Both the SSC and MGD formats were analyzed in this study. A polarimetric analysis was conducted with the SSC data acquired for the Dassari watershed, while the MGD formats were used in the analysis of Vea and Dano watersheds.

Table 4. 7 Acquisition dates of the TerraSAR-X imagery analyzed in the study. Multiple acquisitions were made per month in 11 days interval (indicated by curly brackets) to cover the spatial extent of the respective watersheds

Watershed/Available Time-series/Date of Acquisition			
Dano		Vea	Dassari
			04/05/2013
			15/05/2013
			06/06/2013
			17/06/2013
08/07/2013	}		09/07/2013
19/07/2013			20/07/2013
30/07/2013			
10/08/2013	}		11/08/2013
21/08/2013			22/08/2013
01/09/2013	}		
12/09/2013		07/09/2013	
23/09/2013		18/09/2013	
04/10/2013	}	29/09/2013	
15/10/2013		10/10/2013	
26/10/2013	}	21/10/2013	
06/11/2013		01/11/2013	

### Polarimetric analysis for the Dassari watershed: SSC data

Analysis of the polarimetric information from the two channels (VV and VH) is necessary for discriminating different targets based on the type of backscattering they produce. In polarimetry, scattering matrices (e.g. Sinclair-matrix, Covariance Matrix, Müller M-matrix, Kennaugh K-matrix, etc.) are used to describe the polarization state of electromagnetic waves under different scattering

conditions (Boerner 2004). The fundamental quantities measured by a polarimetric SAR are the scattering matrix elements, i.e. the transmitted and received polarizations respectively (Boularbah *et al.* 2012). These matrices contain relevant information about the scattering processes (Boerner 2004). Thus, the use of these matrices can assist in the development of unique scattering signatures for different features, and improve their discrimination.

The dual polarimetric information contained in the SSC data acquired for the Dassari watershed was analyzed using the Kennaugh scattering matrix (Guissard 1994). Kennaugh Matrix (K) is a symmetric matrix, where the single elements of the matrix are real and linear combinations of the Sinclair matrix elements (Cloude 2009, Schmitt *et al.* 2012). It is also referred to as Stokes Matrix and can be converted to Covariance or Coherency Matrix (Cloude 2009). The Kennaugh matrix elements for the VV/VH cross-polarization (equations 1-5) were implemented in the "NEST ESA SAR toolbox" application (Engdahl *et al.* 2012). Equations (2) and (3) represent the total backscatter intensities from both polarizations and their difference respectively. (4) and (5) represents the information from the real and imaginary parts of the SSC data respectively. Terrain correction was performed for the four Kennaugh intensity bands with the Range Doppler Terrain Correction (RDTC) routine implemented in NEST (Infoterra 2008, DLR 2009). Elevation data required for the terrain correction was obtained from the Shuttle Radar Topographic Mission (SRTM) Digital Elevation Model (DEM). The raw Digital Numbers (DNs) of the Kennaugh intensity bands were converted to the backscatter coefficient sigma nought by applying radiometric normalization. To enable integration with the RE data, the data was resampled to 5 m resolution using bilinear interpolation and georeferenced to the Universal Transverse Mercator (UTM) projection (Zone 31 North). The multiple images acquired per month were then mosaicked and subsetting to match the dimensions of the RE data. Visual inspection of the Kennaugh intensity bands revealed a high level of noise in the elements "K5" and "K6" compared to the other two elements. For this reason, elements "K5" and "K6" were not considered in subsequent analysis.

$$K = \begin{bmatrix} K0 & 0 & K5 & K6 \\ 0 & K1 & 0 & 0 \\ K5 & 0 & 0 & 0 \\ K6 & 0 & 0 & 0 \end{bmatrix}, \text{ with} \quad (1)$$

$$K0 = 0.5(|S_{XX}|^2 + 2|S_{XY}|^2) \quad (2)$$

$$K1 = 0.5(|S_{XX}|^2 - 2|S_{XY}|^2) \quad (3)$$

$$K5 = \Re(S_{XX}S_{XY}^*) \quad (4)$$

$$K6 = \Im(S_{XX}S_{XY}^*) \quad (5)$$

Where K0, K1, K5, K6 are the Kennaugh matrix elements, Sxx and Sxy represent the VV and VH polarizations respectively, and  $\Re$  and  $\Im$  are the real and imaginary parts of the complex data respectively

In addition to the Kennaugh intensity bands, backscatter intensities from the individual polarizations (VV/VH) were processed by performing terrain and radiometric correction. Again the RDTC routine in NEST was used to convert the raw DNs to sigma nought and georeferenced to UTM Zone 31N. For each monthly time-step, the two Kennaugh intensity bands (K0 and K1) and the backscatter intensities of the two polarizations (VV/VH) were stacked together (i.e. four bands per time step) for subsequent analysis.

### **Pre-processing of MGD Data: Dano and Veja Watersheds**

Processing of the MGD data was carried out in the “NEST ESA SAR toolbox” application (Engdahl *et al.* 2012). Here, only the VV and VH polarization intensity bands were processed for subsequent analysis. Terrain and radiometric correction was applied to each intensity band using the RDTC routine in the NEST application. The raw DNs in the intensity bands were converted to sigma nought by applying radiometric normalization. Next, the data were resampled to 5 m resolution using bilinear interpolation and then georeferenced to UTM Zone 30N. The multiple acquisitions made per month for each watershed were mosaicked and subsetting to match the dimensions of the respective RE images.

#### **4.2.2. Filtering of the SAR data**

SAR data filtering is an important pre-step to analyzing SAR images. Traditionally, local mean filters (e.g. Lee, Frost, etc.) have been used. However, non-local mean (NLM) filters have an advantage over mean filters in that it improves the preservation of structure and texture (Buades *et al.* 2005). The use of NLM filters for SAR images have been demonstrated in recent years (Deledalle *et al.* 2010). NLM filters work with the assumption that, for every small window (patch) in an image, there are similar windows (i.e. in terms of grey level intensity) (patches) in the whole image or a defined search window. Thus, the estimated value of a pixel under consideration is based on a weighted average of all pixels in the image or a defined search window (Buades *et al.* 2005).

A NLM filter implemented with ENVI’s Interactive Data Language (IDL) was used for post filtering of the processed TSX data (SSC and MGD). The algorithm estimates the similarity (weight) between two pixels using the squared Hellinger Distance (Ullmann *et al.* 2013). A similarity window of 9 X 9 pixels was used while the search window used was set at 21 X 21 pixels. The algorithm was run twice on the data (i.e. the first result as input for the second run) to achieve enough averaging. Figure 4.5 demonstrates the advantages of using NLM filters on SAR data by comparing a portion of the July TSX image of the Dassari watershed in its unfiltered state, a corresponding filtered image using the Lee adaptive filter (with window size 7 x 7 – Wang *et al.* 2012) and a NL means filtered image. Like in the case of the NLM filter, the adaptive Lee filter was applied twice on the raw SAR. The red ellipses show that the NLM filter better preserves the structure of agricultural fields than the other two methods.

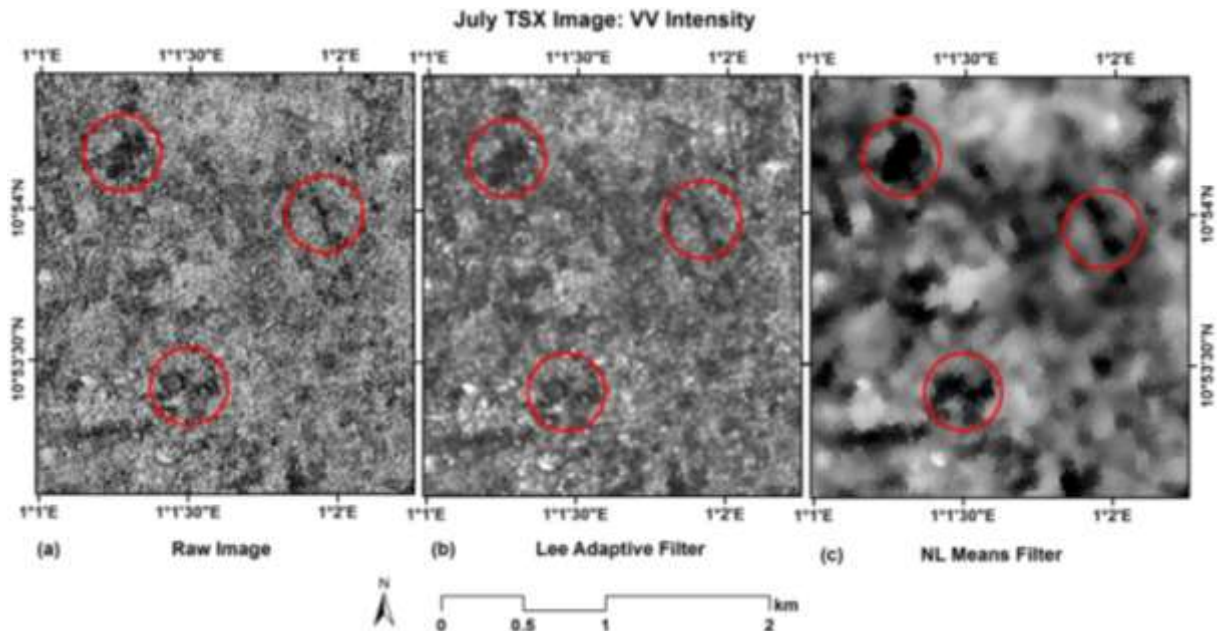


Figure 4. 5 Comparison between (a) a raw TSX image (b) a corresponding image filtered with the Lee adaptive filter (window size of 7x7) and (c) a non-local means filtered image (similarity window of 9x9 and search window of 21x21).

### 4.3. Ancillary data

#### 4.3.1. Field and reference data

Field campaigns to generate reference data (for training the classifier and validating results) were organized in 2013 in the three watersheds. Table 4.8 indicates the acquisition months of images analyzed and the periods of fieldwork. In each campaign, focal areas, each about 1 km<sup>2</sup>, were identified for mapping. Within each focal area, representative fields for all crop types and other land cover types (e.g. grassland, forest, etc.) were mapped using a handheld Global Positioning System (GPS) device. Occasionally, fields outside these focal areas were mapped due to the absence of certain crop or land cover types in the area. For example, rice fields were not always available in the focal areas due to their predominance in inland valleys. In order to derive adequate pixels for training or validation, the minimum field size mapped was 900 m<sup>2</sup> (i.e. 30 X 30 m). Fields were surveyed by walking around it with a handheld GPS in track mode, which were later downloaded and processed in a Geographic Information System (GIS). Historical LULC interviews were conducted to derive knowledge of the LULC changes that have occurred on the surveyed sites between 2002 and 2013.

The Land Cover Classification System (LCCS) (di Gregorio and Jansen 2005) protocol developed by the Food and Agricultural Organization (FAO) was modified and used in the survey/interview (see Appendix A). The form has three main sections (A, B and C). Section (A) deals with the general information of the field being surveyed. These include: area name, name of surveyor, date and time of survey, central coordinates of the field, general landform (slope) and a measure of the accessibility of the field. Additionally, five photographs were taken per field (i.e. one each to north, south, East, West and one from north position to the middle of the field). Section (B) deals with the

## Data and Pre-processing

land cover type of the field being surveyed, i.e. whether it is vegetated or non-vegetated, terrestrial or aquatic and the single major land cover aspect. In instances where the field being surveyed is predominantly natural/semi-natural vegetation, the composition (in terms of trees, shrubs, grass, etc.) were visually assessed. Section (C) is about cultivated terrestrial area and managed land. This section witnessed the main modification to the protocol as originally developed by the FAO. For each cultivated field surveyed, information such as: (1) the number and type of crops cultivated, (2) the date of ploughing, planting and the anticipated harvest date of each crop, the main cropping system being practiced and (4) historical information on crops cultivated in the past ten years (i.e. from 2002 to 2013) were recorded. Additionally, the type and quantity of fertilizer applied and information on pest and diseases were sought through the interviews. Data in this section provided information on the cropping system and calendar as well as historical land use on each of the surveyed farm plots. Table 4.9 provides information on the number of fields surveyed in each of the watersheds for the respective crops or crop groups, while Figure 4.6 shows the spatial distribution of the fields.

Table 4. 8 Periods of field campaigns in the three watersheds in 2013. Arrows indicate the start and end of each campaign.

Watershed	Jan	Feb	Mar	Apr	May	June	July	Aug	Sep	Oct	Nov	Dec
Dassari							↔			↔		
Vea							↔					
Dano							↔					

Green = RapidEye only; Blue = TSX only; Orange = RapidEye+TSX

Table 4. 9 Number of fields (crops only) surveyed in each of the watersheds during the field campaigns

Crops	Number of Fields Surveyed		
	Dassari	Vea	Dano
Cereals (millet, sorghum)	42	32	42
Maize	34	15	31
Cotton	38	-	32
Rice	25	29	29
Legumes (Groundnuts, beans)	-	33	-
Yam	21	-	-



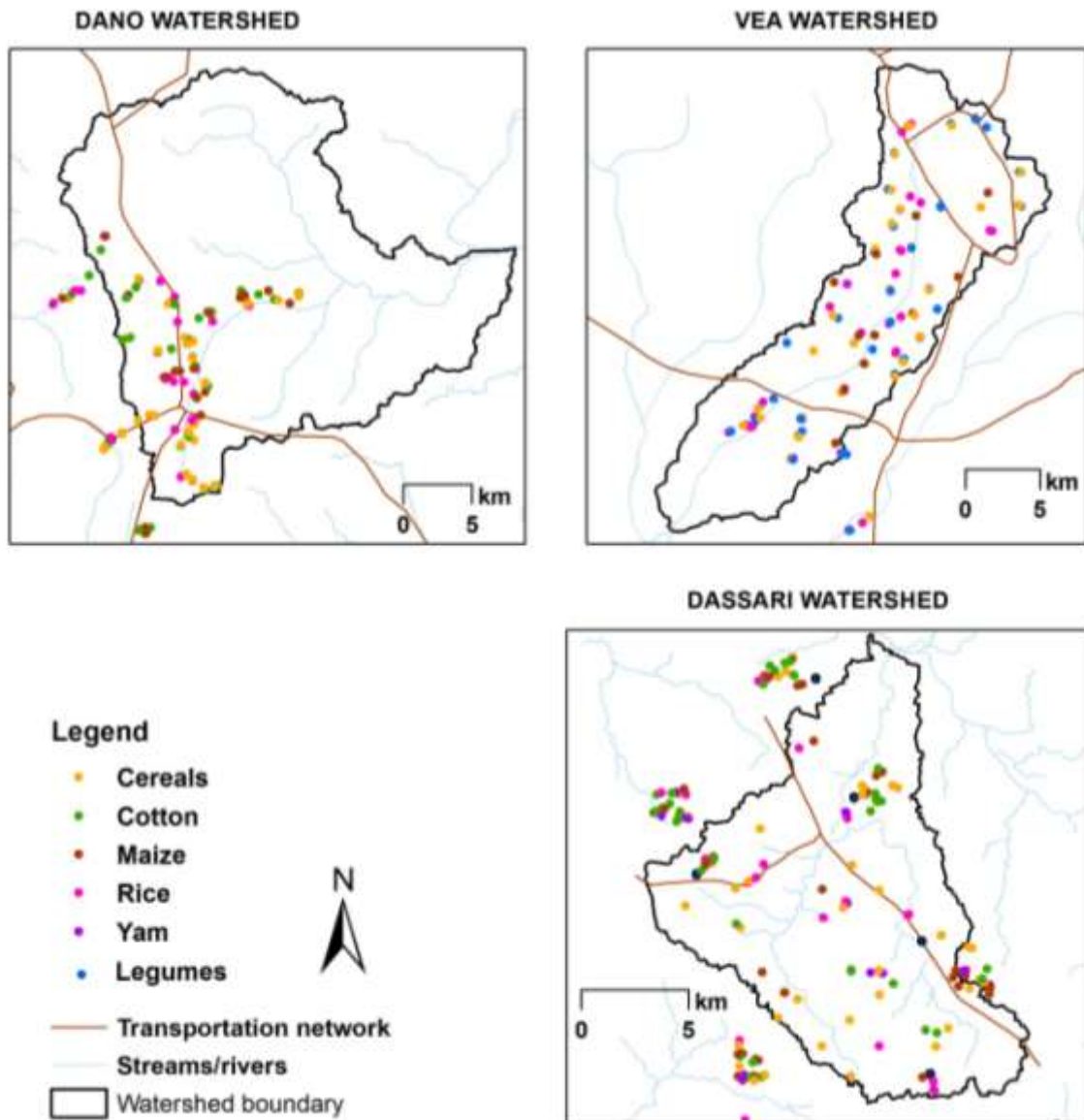


Figure 4. 6 Spatial distribution of crop fields surveyed during the 2013 field campaign

#### 4.3.2. Agricultural census data

District level (2nd administrative level) agricultural statistics for Ghana were obtained from the Statistics, Research and Information Directorate (SRID) of Ghana's Ministry of Food and Agriculture (MoFA). The data spans from 2002 to 2011 (except 2006) and consist of cropped area (ha), production (Mt) and yield (Mt/ha) of the major crops cultivated in each district of Ghana. The statistics are derived from surveys that are conducted by agricultural extension officers employed in each district. In order to determine the cultivated area for the major crops in a district, each district is divided into enumeration areas (EAs), from which a sample is randomly selected to be surveyed. Within each selected EA, a sample of farms are further selected, which are then surveyed with either prismatic compass and a tape (i.e. polygon method - De Groote and Traoré 2005) or a handheld GPS. Most districts in the country still use the compass and prismatic compass for area measurement, although some few districts (especially those in urban areas) now uses the handheld GPS. MoFA has

plans of gradually phasing out prismatic compasses and adopting handheld GPSs. Based on the survey results of these selected farms, MoFA uses statistical methods to estimate the total cropped area of the respective crops for the whole district.

### **4.3.3. Climate data**

Rainfall data for two climate stations in the Vea and Dano watersheds were obtained from the respective meteorological agencies of Ghana and Burkina Faso. The station in Ghana is situated in Bolgatanga (Latitude 10.8 N and Longitude 0.8667 W) while that in Burkina Faso is situated in Dano (Latitude 11.15N and Longitude 3.0667 W). The data comprised of monthly rainfall totals from 1970 to 2013 for Bolgatanga and 1970 to 2011 for Dano. The observed dynamics of cropland area derived from Landsat data at the watershed scale were discussed in the light of this rainfall data.

### 5. Methodology

This chapter describes the methodology used in this study. The chapter is divided into five sections. The first section describes the Random Forests algorithm (Breiman 2001, Liaw and Wiener 2002), which was used for all the analysis (classification and regression) in the chapter. The second section details the accuracy assessments carried out on all results obtained in the chapter.

The third to fifth sections (5.3-5.5) presents a two-scale analysis conducted at watershed and regional scales in West Africa. The watershed scale analysis was performed in three watersheds described in Section 3.1 while the regional scale analysis was conducted within a portion of the Sudanian Savanna agro-ecological zone in West Africa. In section 5.3, a methodology developed for classifying crop types/groups at watershed scale using high spatial resolution multi-sensor (optical and radar) satellite imagery is presented. Different image combinations and classification approaches were evaluated and their advantages/disadvantages in crop mapping are reported. Section 5.4 details the analysis of historical Landsat images (2002 - 2013) to reveal changes in cropland area in the watersheds under investigation. The final section (5.5) presents a methodology used to upscale the watershed scale cropland information (based on Landsat resolution) to the regional scale (Sudanian Savanna) using coarse resolution satellite imagery (MODIS). The possibility of improving national/sub-national agricultural statistics with the derived regional scale cropland information is further presented.

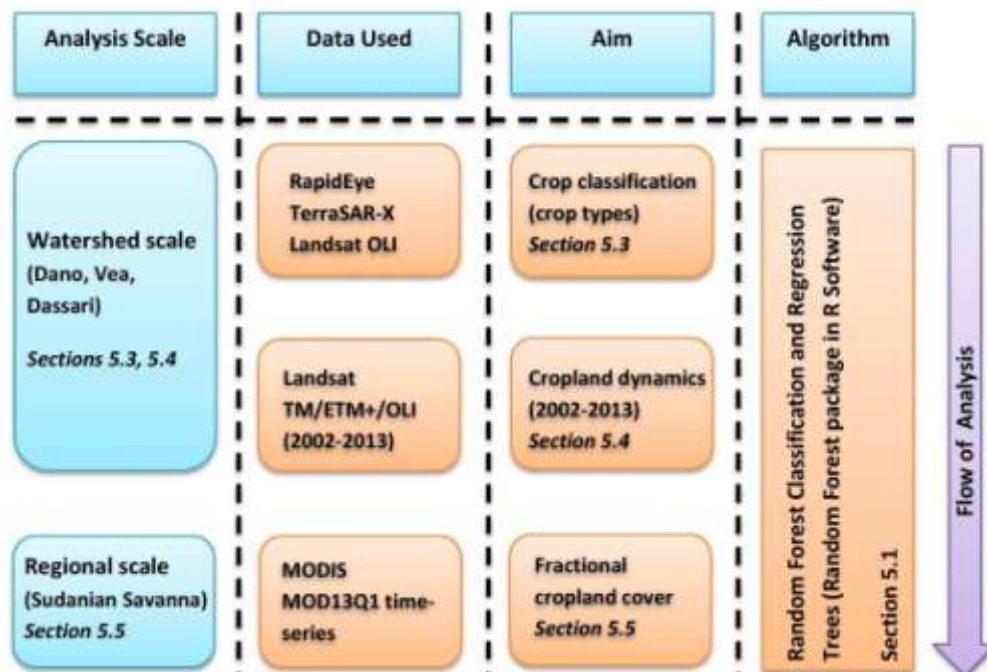


Figure 5. 1 Overview of the different scales of analysis conducted in the study

### 5.1. Random Forests (RF)

RF belongs to the family of ensemble learning algorithms that predicts a response or class from a set of inputs (training data) by creating multiple Decision Trees (DTs) and aggregating their results. Each tree is composed of a root node, a set of interior nodes and terminal nodes (also called leaf nodes). The terminal nodes represent the final decision in a tree. The training data is typically a table of values obtained by overlaying field reference data (e.g. polygons) on a stack of variables/predictors (e.g. spectral bands and indices) and extracting the corresponding values. Columns in the training data represent variables/predictors while rows represent training samples for the various classes/responses variables.

RF is used for both classification and regression problems. In classification, the response vector is categorical values (e.g. crop classes) while they are real values (e.g. fractional crop cover) in regression problems. The definition of the response variables in classification problems is straightforward (e.g. number of classes), while that of regression problems (e.g. continuous proportion of a certain land cover class between 0 and 100) is mostly determined based on the classification results of a high resolution image (Tottrup *et al.* 2007, Gessner *et al.* 2013). Such classifications are normally aggregated to the pixel size of a coarser resolution image, from which a random selection is made to serve as a response vector. In both classification and regression problems, each tree in the forest is independently constructed using a different bootstrap sample of the training data.

In the tree construction process, a decision is made at each non-terminal node (i.e. node splitting) to determine the path to the next node based on the relationship between a set of explanatory variables (predictors) and the response vector. Compared to other ensemble learning algorithms, e.g. boosting (Schapire *et al.* 1998) and bagging (Breiman 1996), RF introduces a new approach in the tree construction process that leads to computational efficiency and a better overall result. This is with regard to the selection of the best variable to split a node. Whereas other algorithms use the best split among all available variables for node splitting, RF chooses the best split from a randomly selected subset of variables (Mtry). The introduction of this additional randomness decreases the correlation between trees in the forest, and consequently increases accuracy (Gislason *et al.* 2006). In classification problems, the criterion for selecting the best variable (out of the Mtry) for splitting a non-terminal node is based on the so-called decrease in gini impurity (Breiman 2001). In other words, the variable that achieves the highest decrease in Gini impurity is chosen, out of the random selected (Mtry) to split a non-terminal node. On the other hand, the variable (out of Mtry) that maximizes the reduction in the deviance (i.e. residual sum of square) is used for node splitting in regression problems (Breiman 2001, Tottrup *et al.* 2007). The reduction in deviance,  $D_{red}$ , at each split is given by:

$$D_{red} = D_x - D_y - D_z \quad (5.1)$$

where  $y$  and  $z$  are the two descendant nodes from node  $x$ , and where the deviance,  $D$ , for each node,  $i$ , is calculated as:

$$Di = \sum_{j=1}^n (y_j - \bar{y}_i)^2 \quad (5.2)$$

where  $n$  is the number of cases,  $y_j$  is the response value for case  $j$ , and  $\bar{y}_i$  is the mean of the response in node  $i$ .

The implementation of RF (classification and regression) requires two parameters to be defined. These are (1) total number of trees to be constructed ( $N_{tree}$ ) and (2) the number of variables to be randomly selected as candidates at each node split ( $M_{try}$ ). " $N_{tree}$ " must be set to ensure that every training sample gets predicted at least a few times (Liaw 2012). " $M_{try}$ " is by default set to the square root and one-third of the total number of variables for classification and regression problems respectively. The best parameter values can be obtained through a try and error approach by studying accuracy estimates (Breiman 2002). It has, however, been found that RF is not very sensitive to these parameters (Breiman 2002, Liaw and Wiener 2002, Gislason *et al.* 2006).

RF uses the training samples that are omitted from the bootstrapped samples used in the tree construction (i.e. out-of-bag, OOB) to provide accuracy estimates. To do this, the trees grown with the bootstrap samples are used to predict the OOB data which is aggregated and compared to the actual labels. For classification problems, this error estimate is known as the "OOB estimate of error rate", while the equivalent in regression problems is the "mean of squared residuals" (equation 5.3). The OOB estimate of error rate is an accurate measure of classification error, provided enough trees are grown (Liaw and Wiener 2002).

$$MSE_{OOB} = n^{-1} \sum_1^n \{y_k - \bar{y}_k^{OOB}\}^2 \quad (5.3)$$

Where " $n$ " is the number of observations,  $y_k$  is the average prediction of the  $k^{th}$  observation and  $\bar{y}_k^{OOB}$  is the average prediction for the  $k^{th}$  observation from all trees for which the observation was OOB.

RF optionally provides additional information on the relative importance of the variables used in the construction of the forest (Liaw and Wiener 2002). In classification problems, four such importance measures are possible while only one is possible with regression (Breiman 2002, Liaw and Wiener 2002). Two widely used variable importance measures, which are also implemented in the RF package in the R computing software are (1) mean decrease accuracy (MDA) and (2) mean decrease gini (MDG) (Calle and Urrea 2011). In the first measure (also known as permutation importance), the importance of a variable is determined by noting the difference in prediction error, when values of the variable is randomly permuted in the OOB samples compared to the original observations (Breiman 2002). The second measure estimates a variable's importance by considering the total decrease in node impurity due to the variable (i.e. at all nodes in the forest where the variable was

used to make a split), normalized by the number of trees (Breiman 2002). This measure is used in both classification and regression problems. In classification, the Gini index provides a measure of the node impurity while the residual sum of squares provides the equivalent in regression. Previous studies have shown that compared to the MDA, the MDG importance measure is more stable and provides more robust results (Calle and Urrea 2011). For this reason, the MDG was used in all analysis in this study. This measure was useful in selecting the most important variables (bands/indices) for each classification based on preliminary runs (Genuer *et al.* 2010).

### 5.2. Classification accuracy

Classification accuracies were determined for all classifications using an independent set of field data. Confusion matrices were produced for all assessments. Overall accuracy, producer's accuracy and user's accuracy (Congalton and Green 2009) were also determined. A confusion matrix provides information on the correct and incorrect prediction made by a classification algorithm by comparing a classified map with ground information. The overall accuracy is the ratio of correctly classified pixels to all pixels considered in the evaluation. The producer's accuracy refers to the errors of omission and indicates the probability that a certain land cover/use on the ground is classified as such on the map. User's accuracy, on the other hand, is the errors of commission and indicates the probability that a pixel/feature labeled as a certain class in the map is really the same class on the ground. Additionally, the F1 score (equation 5.4) (Van Rijsbergen 1979, Schuster *et al.* 2012), which combines producer's and user's accuracy into a composite measure was computed for each class. This measure enables a better assessment of classwise accuracies. The score has a theoretical range between "0" and "1", where "0" represents the worst results while "1" is the best.

$$F_1 score = 2 * \frac{precision * recall}{precision + recall} = 2 * \frac{user's\ accuracy * producer's\ accuracy}{user's\ accuracy + producer's\ accuracy} \quad (5.4)$$

The McNemar's statistical test (Foody 2004a, de Leeuw *et al.* 2006a) was used to evaluate the statistical significance of the differences between confusion matrices derived from different classification approaches in the watershed scale analysis. McNemar's test is a non-parametric test which determines whether column and row frequencies of two confusion matrices are equal (null hypothesis) or not (de Leeuw *et al.* 2006b, Yan *et al.* 2006, Dingle Robertson and King 2011). Unlike other test (e.g. Cohen's Z-test (Cohen 1960)) that assumes independence of validation samples (i.e. samples used to derive the two confusion matrices), McNemar's test allows for the comparison of confusion matrices derived from related validation samples (Foody 2004b). This test was, therefore, appropriate for this study since the same validation samples were used to evaluate the classification accuracies of the different classification approaches. The test is based on the standardized normal test chi-square (equation 5.5) and requires the two confusion matrices to be summarized into a 2 x 2 contingency matrix which indicates the correctly and incorrectly classified pixels in both classifications. The test statistic is given by:

$$\chi^2 = \frac{(f_{12} - f_{21})^2}{f_{12} + f_{21}} \quad (5.5)$$

where  $f_{12}$  represents the number of cases that are correctly classified by classifier one but incorrectly classified by classifier two, and  $f_{21}$  denotes the number of cases that are correctly classified by classifier two but wrongly classified by classifier one (Petropoulos *et al.* 2012). The derived value of  $\chi^2$  is compared against tabulated chi-squared values (with one degree of freedom) to determine its statistical significance (Foody 2004).

### 5.3. Crop mapping at watershed scale

Multi-temporal RE, TSX and Landsat images acquired between April and November, 2013 (see Chapter 4) were used to map crops and crop groups in the study watersheds. Timing of the acquisitions were planned to coincide with the main cropping season (May-October) and enable accurate crop discrimination. The methodology proposed for improved crop mapping in West Africa entails two steps. In the first step, a separation between cropped and non-cropped areas was carried out. In step two, crop classification to discriminate crop types/groups was performed only on the derived crop mask in step one. Details of the two steps are provided in the next two sub-sections.

#### 5.3.1. Derivation of a crop mask

Derivation of a crop mask prior to crop classification is important for three main reasons:

1. Similarities between the spectral signatures of crops and natural/semi-natural vegetation often cause confusion between the two classes and lead to poor classification results (Braimoh 2004, Cord *et al.* 2010, Pringle *et al.* 2012). This situation is aggravated in the study watersheds due to cultivation in bushes (Callo-Concha *et al.* 2012) and the existence of an integrated crop-livestock system which results in high proximity of agricultural fields to pasture lands (Bationo *et al.* 2011). Consequently, separation of cropland from non-cropland prior to crop mapping is essential to reduce confusion between crops and surrounding natural/semi-natural vegetation. Arvor *et al.* (2011) argued that different image time-series and ancillary data are required to separate vegetation types and crop classes. Thus, whereas layers of vegetation indices may be appropriate to separate different vegetation types, crop classes may be better discriminated using spectral information plus data on cropping calendar. Crop classification on a crop mask can, therefore, lead to better results than when crops are classified together with vegetative classes. Previous studies that implemented this approach noted improvements in classification accuracy (Wardlow and Egbert 2008, Arvor *et al.* 2011, Forkuor *et al.* 2014).
2. The derivation of an accurate crop mask can be beneficial to crop mapping in subsequent years (at least till substantial changes in cropped area is witnessed), and eliminate the need for the derivation of a crop mask annually. This is essentially useful for regions with moderate inter-annual changes in cropped areas. In the Vea watershed, for instance, where compound farms are popular (cultivation around hamlets), few changes in cropped area

## Methodology

occur from year to year due to unavailability of “new” lands for cultivation. Thus, derivation of a crop mask for a particular year can be used in subsequent crop mapping exercises, which could save financial and human resources.

3. An accurate crop mask can improve crop area statistics at local and regional levels. This is particularly true for areas where official crop area statistics are irregular or unreliable due to methodological and logistical constraints.

In deriving a crop mask for the respective watersheds, a general LULC classification was performed to identify four broad classes. Table 5.1 details the classes and their description.

Table 5. 1 Land use and land cover classes considered in the derivation of a crop mask for the focal watersheds.

Class	Description
Cropland	Area under cultivation
Natural/semi-natural vegetation	Grassland, forest, mixed grass, shrub and trees
Artificial Surfaces	Buildings, roads (asphalt, laterite), bare areas, etc.
Water	Reservoirs, streams, rivers

Early season images that cover the ploughing and planting stages are important for separating cropland from other land covers (Turner and Congalton 1998). This is primarily due to the unique spectral characteristics of ploughed fields and fields in early vegetative stages, which is caused by high reflectance from the background soil. Since most farmers in the study watersheds plough their fields between late April and July (depending on the onset of the rains and the crop type), images acquired between this period can be essential for the derivation of a crop mask. Figure 5.2 presents NDVI profiles for some LULC classes in the Veia watershed. The figure indicates, for example, a decrease in NDVI from May to June for a cereal (intercropping of millet and sorghum) field which was ploughed in mid-May (Field Survey Results, 2013). This decrease, which was as a result of the ploughing, provides an opportunity to separate all such fields from, for example, grasslands, which registered an increase in NDVI from May to June.



## Methodology

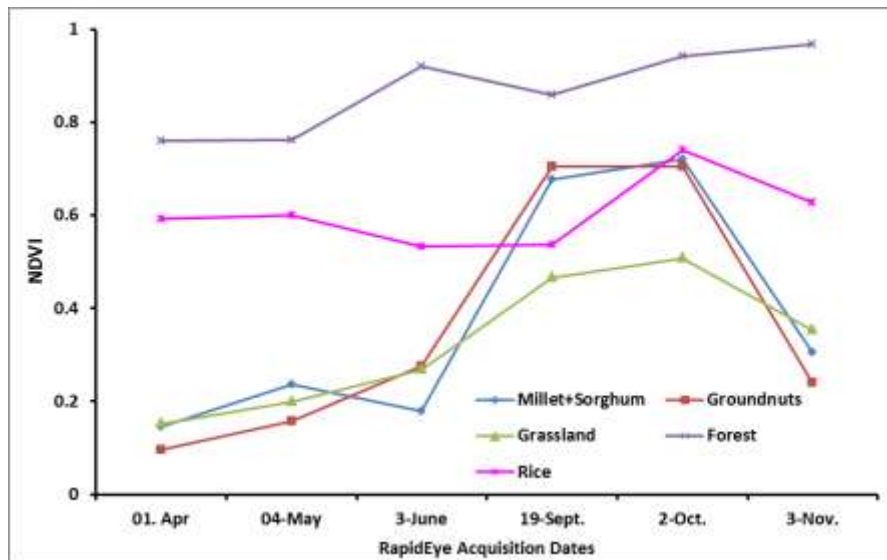


Figure 5. 2 Phenological profiles of some LULC classes in the Veia watershed. Each profile represents the mean signature of a field.

But not all fields in the study watersheds are ploughed in the early stages of the season. A number of reasons cause some farmers to plough their fields later in the season. Field interviews conducted revealed some of the reasons for late ploughing as:

1. Farmers who own many plots are unable to plough all of them at the same time when the rains start. Due to low levels of mechanization (Nin-Pratt *et al.* 2011), ploughing and preparing a plot progresses slowly. Consequently, some fields belonging to multiple plot owners could be ploughed after two weeks or a month from the onset of the rainy season.
2. Dual season (wet and dry) cultivation, especially in irrigation schemes, also result in late cultivation. For example, some farmers in the Veia irrigation scheme cultivate dry season rice in late February /early March and harvest them in May/June. Late harvesting of these crops often results in late ploughing and planting of the same field for the next rainy season. For example, the NDVI profile for rice presented in Figure 5.2 represents a rice field in the Veia irrigation scheme that was ploughed and planted in late August 2013.
3. Some crops, such as groundnuts, require ample soil moisture prior to planting (Collinson *et al.* 1996). Thus, such fields are normally planted later (e.g. a month or more after the onset of the rainy season), when there is enough soil moisture. In the Veia catchment, for example, most groundnut fields (for the 2013 cropping season) were ploughed in mid-July/early August, a clear month or more after early millet and sorghum was planted. Figure 5.2 shows an increase in NDVI from May to June for a groundnut field ploughed in mid-July. In Dassari, some maize fields were also ploughed and planted in August, after millet, sorghum, rice and cotton had been planted between late May and early July.
4. Due to the erratic nature of rainfall in the region, some farmers would wait a bit to be convinced that the pattern of the rains will continue before they start ploughing.

## Methodology

---

Consequently, late cultivated fields behaved spectrally similar to natural/semi-natural vegetation with respect to the June image.

As a result of the late ploughing of some fields, the use of early season images alone will fail to produce an accurate crop mask. Late season images (e.g. October/November) can provide additional information on late cultivated fields. A late season image is, thus, required in addition to an early season one to improve the detection of cropland in the cropping season.

Therefore, in deriving a crop mask for each watershed, multiple RF classifications were performed with all possible combinations of the available optical image time-series (i.e. RE and Landsat). Since all the three watersheds had sufficient optical image time-series (i.e. three early – April, May, June and three late season – September, October, November), the SAR data were not included in the classifications at this stage. The aim for classifying all possible combinations of available optical image time-series was to determine (1) the combination(s) that produces the best accuracies for deriving a cropmask and (2) the optimal number of images required to produce a cropmask with an acceptable accuracy. Determining the optimal number of acquisitions that deliver acceptable accuracies can help achieve a good balance between cost and accuracy in future mapping exercises (Murakami *et al.* 2001, Conrad *et al.* 2014).

In the Vea and Dassari watersheds, six available RE time steps (April, May, June, September, October, November) produced a total of sixty-three possible image combinations which were all classified using the RF classification algorithm. In Dano, Landsat images acquired in June and November were used to augment the RE images (April, May, September, October) in order to obtain a comparable time-series as in Vea and Dassari.

A RF classification script was automated to classify all possible image combinations for the respective watersheds. Single date images, as well as all possible permutations of two, three, four and five images, were classified. All six images were also classified. Training and validation data for the respective runs were fixed throughout all classifications for a watershed. Table 5.2 provides information on the number of training and validation samples used for each of the classifications. For every image combination classified, the OOB error rate, test set error rate as well as the producer's and user's accuracy for all classes were recorded in a database. A total of 500 trees were constructed for each RF, while the number of predictors to be tested at each node was set to the default value (square root of total number of predictors). The MDG variable importance measure (Breiman 2002) was recorded for all runs.

## Methodology

Table 5. 2 Training and validation samples used in the general land use/land cover mapping in the respective watersheds. Water samples for Dassari are relatively few due to fewer water bodies in this watershed.

Class	Dassari		Veja		Dano	
	Training	Validation	Training	Validation	Training	Validation
Cropland	1500	2000	1500	2000	1500	2000
Natural/semi-natural Vegetation	1500	2000	1500	2000	1500	2000
Artificial Surfaces	1500	2000	1500	2000	1500	2000
Water	350	370	1500	2000	1500	2000

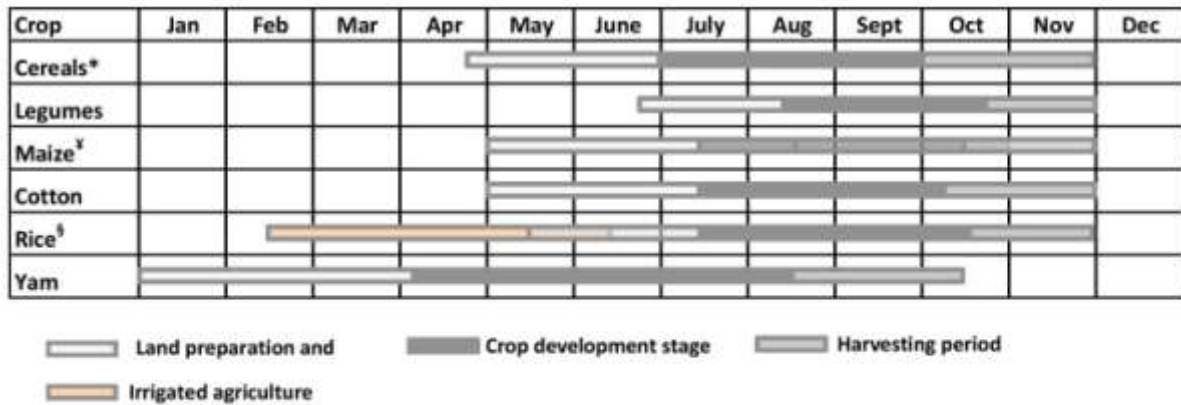
### 5.3.2 Crop classification at watershed scale

A per-pixel crop classification was conducted on the respective crop masks using the RF algorithm. Table 5.3 contains information on the crop types that were mapped in each watershed and the number of training and validation samples used in the classification. Due to frequent inter-cropping of certain crop types and similarities in their structure and cropping calendar, they were grouped into a single class (crop group) in the classification scheme. The two main crop groups considered are (1) “cereals”, which represents millet or sorghum or their intercropping and (2) “legumes”, which is made up of groundnuts and bambara beans (*vigna subterranea*). Although maize is considered a cereal, it was separated because it is normally cultivated alone. Figure 5.3 shows the cropping calendar for the various crops based on the 2013 field survey.

Table 5. 3 Training and validation samples used in crop classification in the focal watershed

Crop class/group	Veja		Dano		Dassari	
	Training	Validation	Training	Validation	Training	Validation
Cereals (Millet and Sorghum)	800	1000	800	1000	800	1000
Legumes (Groundnuts+Beans)	800	1000	-	-	-	-
Maize	800	500	800	1000	800	1000
Cotton	-	-	800	1000	800	1000
Rice	800	1000	800	1000	800	1000
Yam	-	-	-	-	800	1000

## Methodology



\* Early millet (an early maturing millet variety) in Vea is harvested between July and August

<sup>2</sup> Maize is cultivated earlier in Dano and Vea than Dassari. This is indicated by the overlap between land preparation and planting and the crop development stage

<sup>3</sup> Dry season rice cultivation is undertaken mainly in the irrigation command area of the Vea dam in the Vea watershed. These fields are harvested late and prepared again on the dry season.

Figure 5. 3 Cropping calendar for major crops in the focal watersheds based on the 2013 field survey results.

Varying agronomic practices and environmental conditions often lead to differences in the phenology of same crops or similarities in the phenologies of different crops (Wardlow *et al.* 2007, Peña-Barragán *et al.* 2011). Varying planting and harvesting dates of same or different crops is a major agronomic aspect that leads to difficulties in mapping crops from RS data. Figure 5.4 show example NDVI temporal profiles for some crops in the Vea and Dassari watersheds that depict the effects of agronomic practices.

In Figure 5.4 (a), two cereal fields depict different NDVI temporal profiles due to a lag of about a month in their ploughing and planting dates. This could be due to farmer decision, weather conditions or ownership of multiple farms (see Section 5.3.1). Consequently, whereas one field reaches a peak in September, the other reaches a peak in October. This situation affects the harvesting dates, which means one field could be harvested a month after the other. A similar pattern is depicted for three rice fields in Figure 5.4 (b), which shows different spectral profiles for the three fields. Likewise, Figure 5.4 (c) show different phenological patterns for two cotton fields cultivated in June and July respectively (i.e. different ploughing and peak dates). Pictures of these fields are shown in Figure 5.5 (a,b).

In addition to same crops having different phenological patterns, varying agronomic practices also cause different crop types to have similar phenological profiles. This is depicted in Figure 5.4 (c), where a maize and a cotton field ploughed and planted in early July in the Dassari watershed exhibit similar phenological behavior (ploughing, peak and harvesting dates) expressed by the NDVI. Figure 5.4 (d) also shows a rice and a yam field that, although planted months apart, display similar NDVI patterns. The similarity between profiles of rice and yam is attributable to the intercropping of yam with rice as depicted in Figures 5.5 (c, d).

## Methodology

This temporal inter- and intra-class variability/similarity poses a major challenge in crop classification, since some crops could easily be classified as belonging to different crops and vice versa. A previous study by Conrad *et al.* (2011) that noted similar challenges in the Khorezm region of Uzbekistan found that temporal segmentation of image time-series (MODIS NDVI) reduces the errors due to inter- and intra-class temporal variability in crop classification. They divided MODIS time-series into several temporal segments and used each segment (or a combination) as input to classification. They found that a combination of temporal segments improved classification accuracy by 6-7% over the use of the original MODIS time-series. However, comparative low temporal resolution of the input data at the high geometric resolution used in this study hampered the adaption of such an approach.

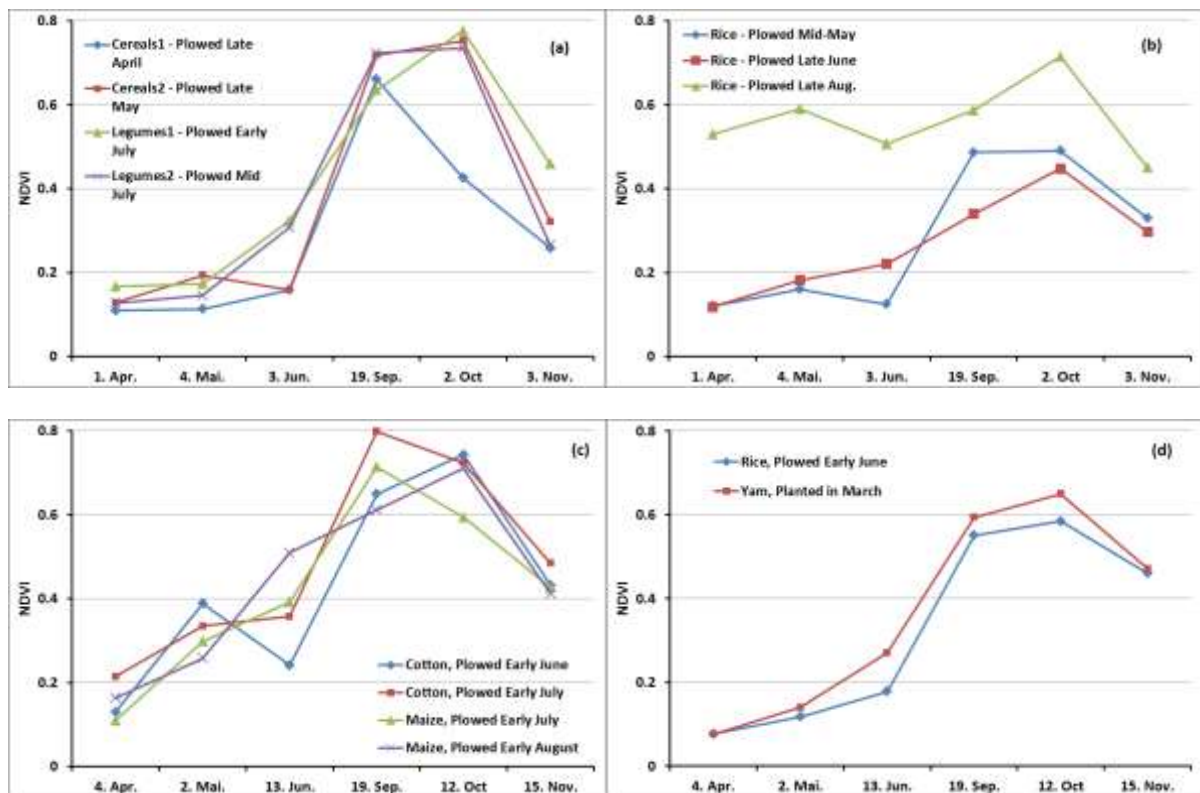


Figure 5. 4 Phenological profiles of same crops ploughed at different periods of the cropping season and different crops ploughed at similar periods in the cropping season. Each profile represents the mean signature of a field.



Figure 5.5 Example of (1) same crops ploughed and planted at different periods of the cropping season and (2) effect of intercropping. Top left: a cotton field ploughed and planted in June and at early vegetative stage as of early July; top right: a cotton field ploughed as of early July. Bottom left: a rice only field; bottom right: a yam field intercropped with yam in the “gullies”.

In order to overcome the challenges outlined above, a sequential masking classification approach (Van Niel and McVicar, 2004; Turker and Arıkan 2005) was implemented to classify crops in the three watersheds. This classification approach is premised on the notion that, some image combinations classify certain crop classes better than when all images are included in the classification (Murakami *et al.* 2001). In implementing this process, a set of available images is first used to accurately classify a single crop class, the pixels belonging to the mapped class are masked out from the images, and a subsequent classification is conducted to classify a second class using a different image combination, and so on.

Figure 5.6 demonstrates this idea using some crop classes in the Veia watershed. Figure 5.6(a) shows that the cereal class can be separated from the other classes using the September TSX image (VV polarization) and the June RE image. Inclusion of the June RE improves the separation primarily due to the early cultivation of cereals in the watershed (see Figure 5.3). Although it is possible to have cereal fields cultivated later in the season, most of them are cultivated between April and June. On the other hand, Figure 5.6(c) indicates that a late season image (October RE) improves the separation of legumes from the other classes. Similarly, this can be explained by the general late cultivation of legumes in Veia, compared to cereals. Further, a combination of the TSX and RE images

## Methodology

acquired in September achieves a good separation between rice and the other crop classes in the Veia watershed (Figure 5.6b).

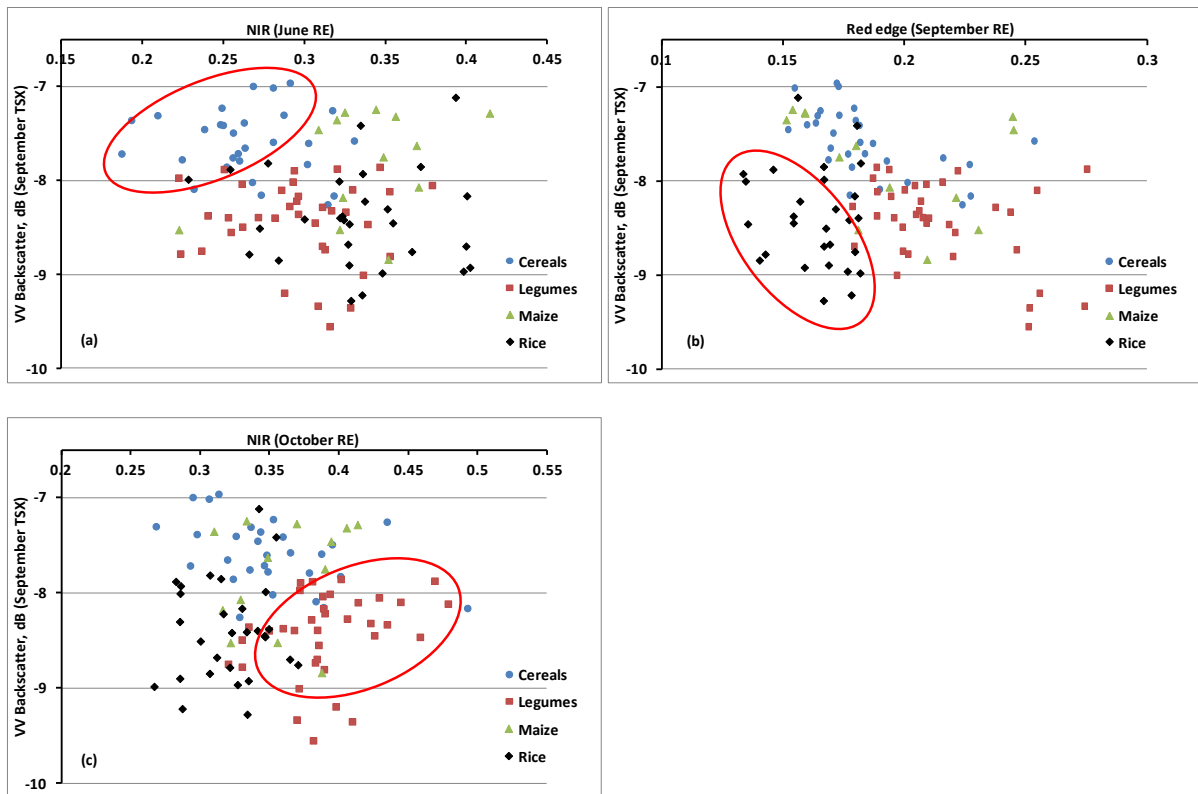


Figure 5. 6 Feature space plots of the main crop classes in Veia. The images used in each plot demonstrate their ability to better discriminate a certain crop type.

Figure 5.7 shows the main processing steps in the implementation of the sequential masking classification. The first step in the approach was to determine the best image combinations for discriminating the various crop classes. This was achieved by performing initial RF classifications using all possible permutations of the available imagery (RE, Landsat and TSX) for each watershed. In Veia for instance, the eight available time-steps (i.e. six RE and two TSX) produced a total of two hundred and fifty-five (255) classifications, while the ten time-steps available for Dassari (six RE and four TSX) and Dano (four RE, four TSX and two Landsat) each produced a total of one thousand and twenty-three (1023) classifications.

Out of these permutation runs, two sets of information were extracted. First, the classification (or image combination) that produced the best overall results was noted (hereinafter referred to as one-time classification). Second, image combinations that produced the best results for the individual crop classes under investigation were noted and extracted for the subsequent sequential masking classification. To do this, the user's and producer's accuracies were combined into a composite measure - the F1 score (see Section 5.2). Image combinations that produced the highest F1 score for a particular class was selected to classify that class in the sequential masking classification scheme. For example in the Veia watershed, four time-steps (May RE, September TSX,

## Methodology

---

October TSX and October RE) produced an F1 score of 0.89 (producer's and user's accuracy of 96% and 83% respectively) for the legumes class. On the other hand, four other image time-steps (April RE, May RE, June RE, September TSX) produced an F1 score of 0.86 (producer's and user's accuracy of 88% and 84% respectively) for the cereals class.

In the sequential masking classification scheme, therefore, the class with the highest F1-score (among all other classes, e.g. Legumes in the case of Veja) was classified first using its corresponding image combination. Pixels belonging to that class were masked out and the class with the second highest F1-score (cereals) was classified using its corresponding image combination. Results of the various classes were eventually combined into a single classification output using a simple decision rule. In order to assess the contribution of radar in crop mapping in the watersheds, the classification process described above was repeated without the SAR images. All image combinations in the initial RF runs involving SAR data were discarded. Thus, new image sets (other than the ones used previously) including only RE and Landsat data were used to classify the crop types.

Finally, the efficiency of the sequential masking approach was assessed by comparing the final results obtained for each watershed with results of the classification that produced the overall best accuracy in the initial permutation runs (i.e. one-time classification). Accuracy assessment was performed for results of both approaches (i.e. sequential masking and one-time classification) using the same set of validation data. The McNemar's test was then used to evaluate the statistical significance of the differences between confusion matrices derived from the two classification approaches.



## Methodology

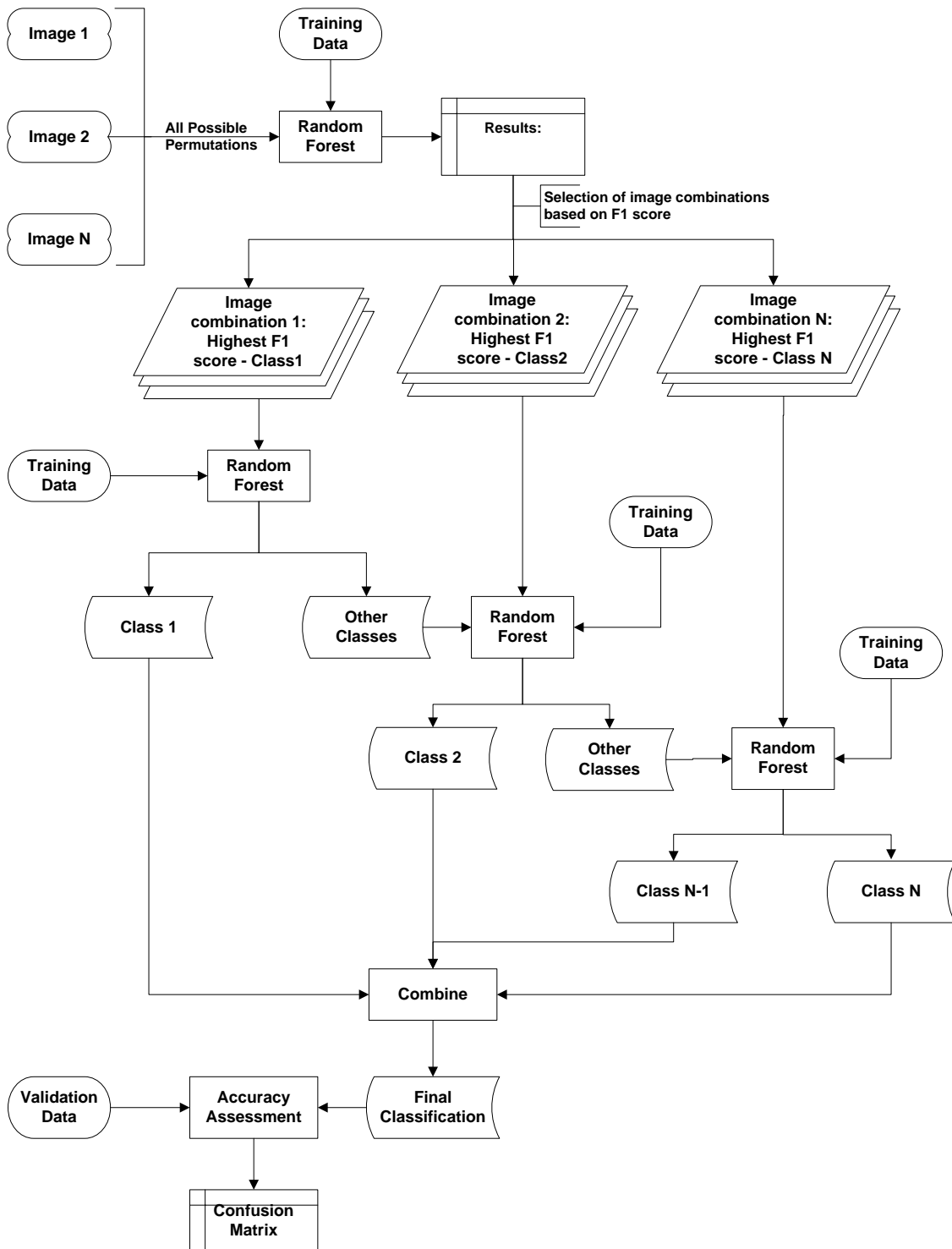


Figure 5. 7 Schematic of the main processing steps in the sequential masking approach adopted to classify crops and crop groups in the focal watersheds.

### 5.4 Mapping cropland area at watershed scale

This section presents analysis of historical Landsat images of the watersheds acquired between 2002 and 2013 (see time-series in Tables 4.3-4.4). The objective of performing the historical analysis was twofold. The first was to obtain an annual crop mask for the watersheds between 2002 and 2013 and study the inter-annual changes in cropland (extensification or reduction) vis-à-vis other land

## Methodology

cover types such as forest and mixed vegetation. The second objective was to enable an upscaling of the results obtained (at Landsat resolution) unto a coarser resolution, but spatially large satellite imagery (MODIS), in order to obtain similar information (cropland areas) for a wider region in the Sudanian Savanna of West Africa. Details for the second objective are provided in the regional scale analysis present in section 5.5

The cropland change analysis was conducted for the Vea and Dano watersheds only. The Dassari watershed was excluded due to poor availability of historical Landsat images. The Dano watershed falls in the Landsat tile “Path 196, Row 52” while Vea falls in the tile “Path 194, Row 52”. Although the scale of analysis at this stage was the Dano and Vea watersheds, classification of the Landsat images was conducted for a geographical region bigger than the respective watersheds due to the relatively larger footprint of Landsat images compared to RapidEye and TerraSAR-X (Figure 5.8). Classification of the bigger geographical extent was also necessary for the subsequent regional scale analysis reported in Section 5.5.

A general LULC classification was performed for the respective annual Landsat time-steps available for the watersheds (Tables 4.3-4.4). Table 5.4 provides details of the classes considered in the general LULC classifications. Due to poor annual temporal sequence, all crop classes were lumped into one class – cropland.

Table 5. 4 Name and description of classes considered in the Landsat historical analysis

Class	Description
Cropland	Area under cultivation
Natural/semi-natural vegetation	Grassland, Forest, mixed grass, shrub and trees
Mixed Vegetation	Buildings, roads (asphalt, laterite), bare areas, etc.
Artificial Surfaces	Buildings, roads (asphalt, laterite), bare areas, etc.
Water	Reservoirs, streams, rivers

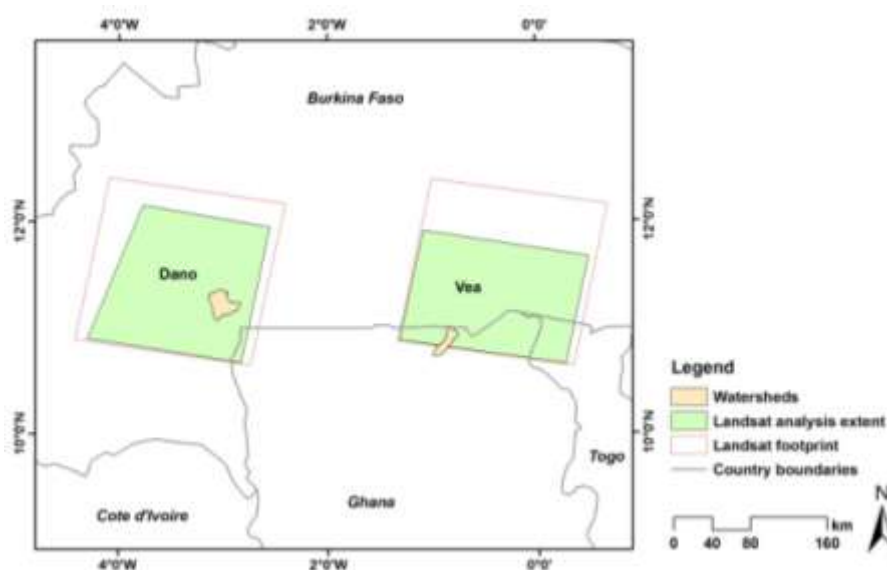


Figure 5. 8 Geographical extents of Landsat images analyzed for the Dano and Vea watersheds

## Methodology

---

Data from the field campaigns carried out in 2013 served as the basis for deriving training and validation data for classifying the Landsat images. As alluded to in section 4.3.1, a historical land use survey was conducted using the adapted LCCS protocol (Appendix A). For each field surveyed, information on the historical land use/cover from the year 2002 to 2013 was obtained from the respondents (e.g. farm owners) or residents close to the surveyed site (i.e. in cases where the site being surveyed was natural/semi-natural vegetation). Based on this information, it was possible to determine the historical LULC of each of the fields surveyed during the fieldwork in 2012 and 2013.

Since the analysis window for the Landsat classifications was bigger than the respective watersheds, it was necessary to identify additional training and validation data outside the watershed boundaries prior to classification. To do this, the spectral properties of the already existing training and validation data within the watersheds were analyzed. Figure 5.9 shows a feature space plot of the NIR and MIR2 bands of a Landsat image acquired in October 2007 for the Dano watershed. The plot shows a high reflectance in the MIR2 channel for most cropland and artificial surfaces while water and the vegetative classes have a relatively lower reflectance. Croplands and artificial surfaces have similar spectral reflectance in this channel due to the fact that the image was acquired during the harvest season. During harvesting, farmers normally transport crop residues to their houses for various purposes (e.g. as animal feed). Thus harvested fields could spectrally behave as bare areas.

Using information in such plots (similar plots were created for the other years), training and validation data for areas beyond the watershed extent (where field data were not collected) were collected through visual analysis. First, MIR2 reflectance thresholds (e.g. as indicated by vertical bars in Figure 5.9) were used to separate the image into (1) cropland and artificial surfaces, (2) vegetative classes and (3) water bodies. Then with the aid of other spectral channels and indices (e.g. NDVI), visual analysis was conducted to identify additional training and validation data beyond the extent of the watersheds.

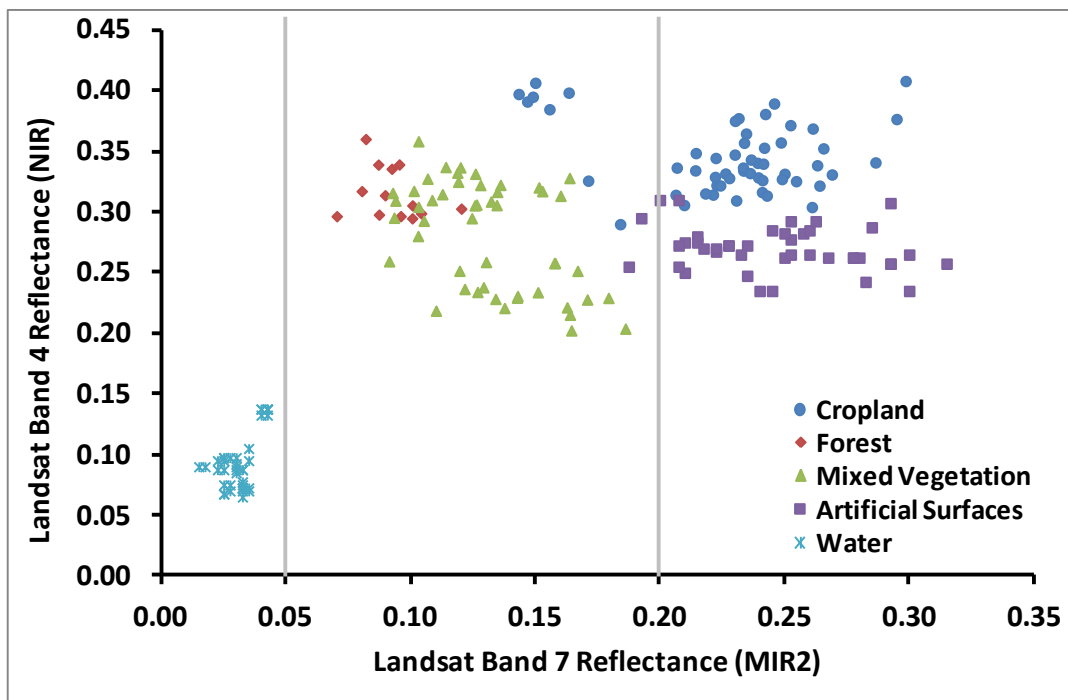


Figure 5.9 Feature space plots of the five LULC classes considered in the Landsat scale classification.

A per-pixel classification was then conducted for each annual image time-series using the RF algorithm. As indicated in Section 4.1.2 classifications were conducted with the original Landsat spectral bands together with derived spectral indices. For each of the classifications, one thousand pixels each were used for training the classifier and validating the results. A maximum of 500 trees were constructed, while the number of variables to be tried for splitting at each node (Mtry) was set to the default (square root of the total number of variables) . The option to calculate variable importance was activated.

LULC change analysis was conducted between the different years based on the classification results. Special attention was given to expansion or reduction in cropland in relation to other LULC types.

### 5.5 Mapping cropland area at regional scale (Sudanian Savanna)

The detected cropland areas based on the Landsat classifications of Section 5.4 were upscaled to a broader region in the Sudanian Savanna (SS) agro-ecological of West Africa (Figure 3.1). The aim of the upscaling was to improve information on the spatial distribution and extent of cropland in the SS of West Africa, and to investigate possibilities of using such information to improve national/sub-national agricultural statistics.

Spatial distribution and extent of cropland in West Africa has remained poor for decades (Ramankutty 2004). Agricultural surveys conducted by national agricultural institutions fail to provide information on the spatial distribution of cropland in the coarse administrative units on which the surveys are based. Global LULC products (e.g. GLC2000, GLOBCOVER, etc.) which provide some spatial information on cropland extent in the region have been found to be inconsistent (Hannerz and Lotsch 2008, Fritz *et al.* 2010, Vintrou *et al.* 2012). Moreover, the coarse spatial

## Methodology

resolution of images used in these products (e.g. 1 km AVHRR) are unable to adequately represent the heterogeneous landscape of the region which is characterized by small agricultural plots mixed with natural/semi-natural vegetation (Cord *et al.* 2010, Forkuor *et al.* 2014). Although mixed cover classes have been introduced in some of the products to overcome the heterogeneity challenge, estimation of cropland extent from these classes has been found to be problematic (Hannerz and Lottsch 2008). For example, it is challenging to determine the exact proportion of cropland in a class defined as having less or equal to 60% cropland (Friedl *et al.* 2010, Vintrou *et al.* 2012). A better approach to represent heterogeneous landscapes using coarse spatial resolution datasets is to estimate the fractional cover of different LULC classes within each pixel (DeFries *et al.* 1995, Tottrup *et al.* 2007, Herold *et al.* 2008, Gessner *et al.* 2013).

In this study, therefore, fractional cropland cover at MODIS resolution was estimated with non-parametric RF regression tree ensembles based on the Landsat classification results obtained in Section 5.4. The benefits of using tree ensembles over single trees have been outlined in sections 2.5.2 and 5.1. In this approach, the proportion of cropland within a MODIS pixel was predicted based on a regression model developed from the Landsat classifications and MODIS time-series. Figure 5.10 details the main processing steps used to derive the fractional cover maps.

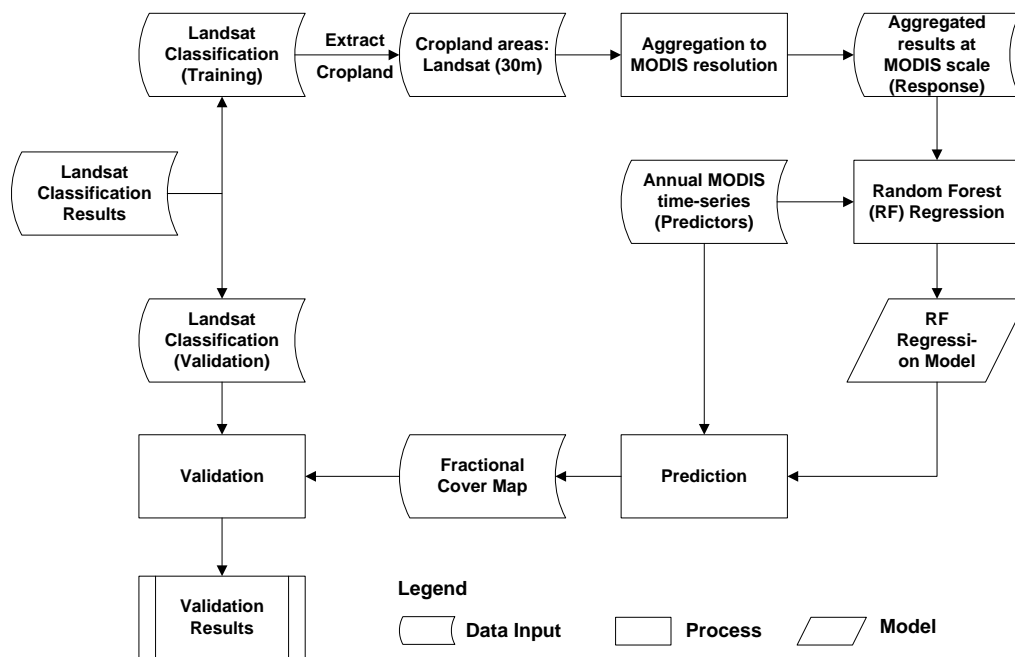


Figure 5. 10 Schematic representation of the main processes involved in upscaling Landsat level results onto MODIS resolution

First, the Landsat classification results for the Vea and Dano watersheds were each divided into two. One-half of each site was used as training and the other used for an independent validation of the fractional cover maps (see Figure 5.11). Next, cropland areas in the training dataset were extracted and aggregated to MODIS resolution. The aggregation was achieved by determining the proportion

## Methodology

of Landsat cropland pixels within a MODIS pixel. Based on a sample of this aggregated layer (as response) and MODIS time series made up of the MIR, NIR, NDVI, and Red channels of the MOD13Q1 product (as predictors), a RF regression model was developed using the RF function in the R software.

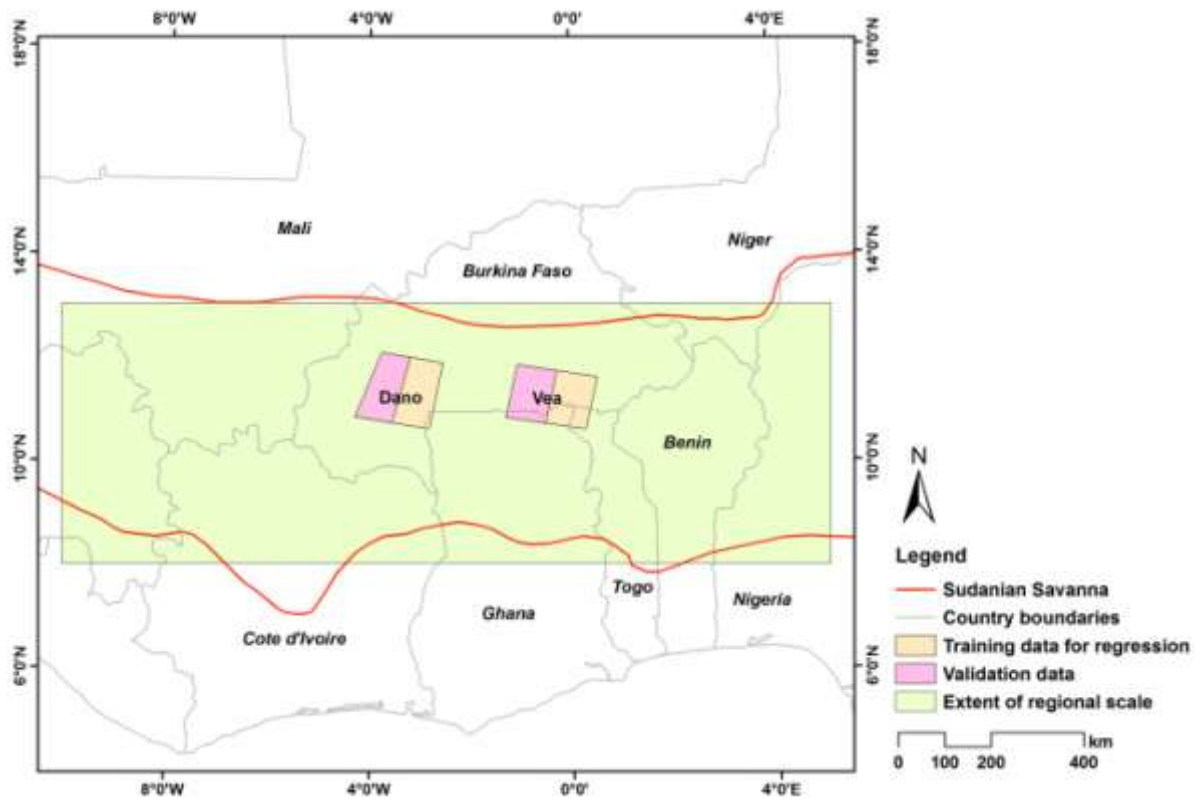


Figure 5. 11 Extent of Landsat and MODIS data in the upscaling analysis

In order to derive optimal parameters for the generation of the RF regression model, a number of initial experiments were conducted. This was achieved by testing different parameter sets while noting their effects on accuracy estimates (i.e. OOB and Test set Mean Squared Error (MSE)). The parameters considered in the experiments included:

1. Training samples: a regular sampling approach was used to select training and validation data from the aggregated Landsat results (response) and the MODIS data (predictors) to build the regression model. Regular sampling ensures that the selected samples are equally distributed over the range of response values (i.e. 0-100). Experiments were conducted with five, ten and fifteen thousand samples each for training and validation.
2. Number of trees: experiments were conducted with two, three and five hundred regression trees during the generation of the model.
3. Node size: Node size was varied between five, ten and fifteen during the experiments

Table 5.5 presents results of the initial experiments conducted. The first three runs revealed that construction of more than two hundred trees did not lead to any change in accuracy; therefore two

## Methodology

hundred trees were built in the subsequent experiments. With regards to training samples, error estimates reduced appreciably when samples were increased from 5,000 to 10,000, while maintaining a node size of five (experiment 1 and 5). However, an increase from 10,000 to 15,000 resulted in a relatively insignificant reduction in error estimates (experiments 5 and 8). The table also indicates that an increase in the node size from five to ten resulted in insignificant change in the error estimates (experiments 5 and 6) while an increase from five to fifteen resulted in an increase in the error estimates (experiments 5 and 7). Therefore, all regression models (from 2002 to 2013) were developed with ten thousand training samples, a node size of five and two hundred trees built. The number of variables/predictors to be tried at each node split was set to the default (i.e. number of variables/3). The resultant regression models were used to predict the respective MODIS scenes to derive fractional cropland maps for the area of interest.

Table 5. 5 Experiments to determine optimal parameters for the development of random forest regression tree models

Experiment	No. of Training Samples			Node Size			No. of Trees			Error Estimate	
	5000	10000	15000	5	10	15	200	300	500	OOB MSE	Test Error
1	X			X			X			347.3	355.3
2	X			X				X		347.0	355.4
3	X			X					X	347.6	355.9
4	X				X		X			348.1	359.2
5		X		X			X			334.4	335.3
6		X			X		X			335.3	335.9
7		X				X	X			334.8	337.6
8			X	X			X			335.9	329.8
9			X		X		X			333.7	330.2
10			X			X	X			337.9	331.0

### 5.4.2.1 Validation of cropland fractional cover maps

An independent validation was performed for each modeled fractional cropland cover map (i.e. from 2002 to 2013) with its corresponding half of the Landsat classification (see Figure 5.14) that was excluded from the development of the map. Cropland areas were extracted from the Landsat classifications and aggregated to MODIS resolution by determining the percentage of cropland pixels in each MODIS pixels (hereinafter referred to as reference data). In performing the validation, ten different samples, each containing seven thousand five hundred samples randomly selected from the reference data, were used to validate the fractional cropland cover map. In other words, validation of each fractional cropland cover map was performed ten times, each time with seven thousand five hundred reference samples. This was done to determine the consistency of errors inherent in the modeled fractional cover maps. At each round of validation, three error statistics were extracted: (1) Mean Absolute Error (MAE), (2) Mean Error (ME) and (3) Root Mean Square Error (RMSE). The average and standard deviation of the above-mentioned statistics over the ten validation rounds was noted for each fractional cover map.

$$ME = n^{-1} \sum_{i=1}^n P_i - O_i \quad (5.6)$$

$$MAE = n^{-1} \sum_{i=1}^n |P_i - O_i| \quad (5.7)$$

$$RMSE = \left[ n^{-1} \sum_{i=1}^n (P_i - O_i)^2 \right]^{1/2} \quad (5.8)$$

where “ $P$ ” is the predicted or modeled fractional cover, “ $O$ ” is the reference, and “ $n$ ” is the number of samples included in the evaluation.

### **5.4.2.2 Plausibility analysis**

Plausibility analysis was conducted by comparing extracted cropped area from the fractional cropland cover maps with official agricultural statistics obtained from Ghana's Ministry of Food and Agriculture (MoFA) (see Section 4.3.2). The comparison was performed for sixteen districts in the north of the country.



## 6. Results

This chapter presents results of the multi-scale analysis conducted in this study. It is divided into three main sections (6.1-6.3). Section 6.1 deals with the crop mapping results obtained at the watershed scale. First, findings of the general LULC mapping conducted to derive a crop mask are presented. Second, results of the crop classification conducted on the crop mask are presented. In section 6.2, results of the Landsat (historical) classifications conducted at watershed scale are shown. Changes in cropland area between 2002 and 2013 are presented and as well as statistics on the changes in different LULC types. The last section (6.3) of the chapter presents findings of the upscaling of watershed scale cropland information unto regional scale to derive cropland fractional cover maps. Comparison between cropped area statistics derived from these fractional cover maps and official cropped area statistics for seventeen districts (second administrative units) in Ghana are shown.

### 6.1 Crop mapping at watershed scale

#### 6.1.1 Derivation of a crop mask

Tables 6.1-6.3 present a subset of the results obtained for the derivation of a crop mask in the study watersheds. The crop mask was derived by classifying all possible permutations (sixty-three) of available optical imagery in each watershed. The tables indicate the image or image combination that produced the highest overall accuracy at each round of permutations. For example, "Perm No. 1" indicates the single date image that produced the best overall accuracy out of all single date classifications while "Perm No. 2" indicates the pair of images that produced the highest accuracy out of all possible combinations of two images. This means in Table 6.1, for example, the RapidEye image acquired in November in the Vea watershed (Nov RE) achieved the highest overall accuracy out of all single date classifications. F1 scores for the four main LULC classes considered in the derivation of the crop mask (see Table 5.1) are reported in the tables.

Table 6. 1 Results of the permutation of all possible combinations of available optical images in the **Vea watershed** for the derivation of a crop mask. The image combination that produced the best overall accuracy in each of the six permutation rounds is present (marked by "X")

Perm. No.	Available image time-steps						Overall Accuracy	F1 score - LULC Classes			
	April RE	May RE	June RE	Sep. RE	Oct. RE	Nov RE		Cropland	Vegetation	Artificial Surfaces	Water
1						X	84.5	0.809	0.855	0.827	0.943
2	X					X	89.9	0.901	0.904	0.834	0.943
3	X			X		X	93.2	0.943	0.941	0.868	0.943
4	X			X	X	X	94.4	0.953	0.942	0.901	0.972
5	X		X	X	X	X	94.2	0.951	0.942	0.891	0.972
6	X	X	X	X	X	X	94.0	0.949	0.942	0.886	0.964

## Results

Table 6. 2 Results of the permutation of all possible combinations of available optical images in the **Dano watershed** for the derivation of a crop mask. The image combination that produced the best overall accuracy in each of the six permutation rounds is present (marked by "X")

Perm. No.	Available image time-steps						Overall Accuracy	F1 score - LULC Classes			
	April RE	May RE	June LS	Sep. RE	Oct. RE	Nov LS		Cropland	Vegetation	Artificial Surfaces	Water
1						X	81.6	0.785	0.712	0.820	0.985
2					X	X	89.5	0.826	0.798	0.958	0.985
3				X	X	X	89.6	0.836	0.811	0.961	0.986
4	X			X	X	X	89.6	0.823	0.794	0.963	0.985
5	X	X		X	X	X	87.7	0.809	0.767	0.963	0.985
6	X	X	X	X	X	X	86.2	0.793	0.707	0.968	0.987

LS = Landsat; RE = RapidEye

Table 6. 3 Results of the permutation of all possible combinations of available optical images in the **Dassari watershed** for the derivation of a crop mask. The image combination that produced the best overall accuracy in each of the six permutation rounds is present (marked by "X")

Perm. No.	Available image time-steps						Overall Accuracy	F1 score - LULC Classes			
	April RE	May RE	June RE	Sep. RE	Oct. RE	Nov RE		Cropland	Vegetation	Artificial Surfaces	Water
1						X	84.7	0.818	0.828	0.894	0.832
2					X	X	91.1	0.871	0.898	0.946	1.000
3			X		X	X	92.0	0.880	0.909	0.956	1.000
4		X		X	X	X	92.4	0.884	0.915	0.959	0.997
5		X	X	X	X	X	92.3	0.883	0.917	0.956	0.993
6	X	X	X	X	X	X	91.6	0.873	0.901	0.960	0.992

The results indicate that images acquired in November consistently produced the highest accuracy in single date classifications in all the three watersheds. In addition, the November acquisitions were included in all other image combinations that produced the highest accuracies in each round of permutations. This suggest that images acquired during or immediately after harvest are important for deriving an accurate crop mask since the cropping season in all watersheds ends in November (see Figure 5.3). This is corroborated by the fact that the combination of October and November acquisitions produced the best results out of all pairwise combinations in Dassari and Dano. In Vea, the April and November acquisitions produced the best accuracy (89.9%) for all pairwise combinations, while October and November achieved a slightly lower accuracy of 87.8%. In Vea, the inclusion of the April acquisition in image combinations that produced the highest accuracies for five permutation rounds (i.e. Perm No. 2 to 6) indicate the contribution of early season images to the derivation of an accurate crop mask. The relative importance of the April acquisition in Vea can be explained by early ploughing in this watershed compared to the other two.

It is clear from the results that two, or at most three, monthly acquisitions is sufficient for deriving a crop mask in the three watersheds. It is interesting to note that the use of all available optical image time-series did not produce the highest overall accuracy in any of the watersheds. In Dano, for instance, classification of two late season images (October and November) produced an overall

## Results

accuracy of 89.5% compared to 86.2% when all six available time-steps were classified (Table 6.2). In Dassari, one early and two late season images (June, October, November) produced an overall accuracy of 92%, only 0.4% lower than the highest accuracy (92.4%) produced by two early and two late season images. Again, the three images produced a slightly better result than when all six time-steps were classified (91.6%). The situation is similar in the Vea watershed, where the use of one early and two late season images (April, September, November) produced comparable overall accuracy (93.2%) to that achieved when all six time-steps were used in the classification (94%).

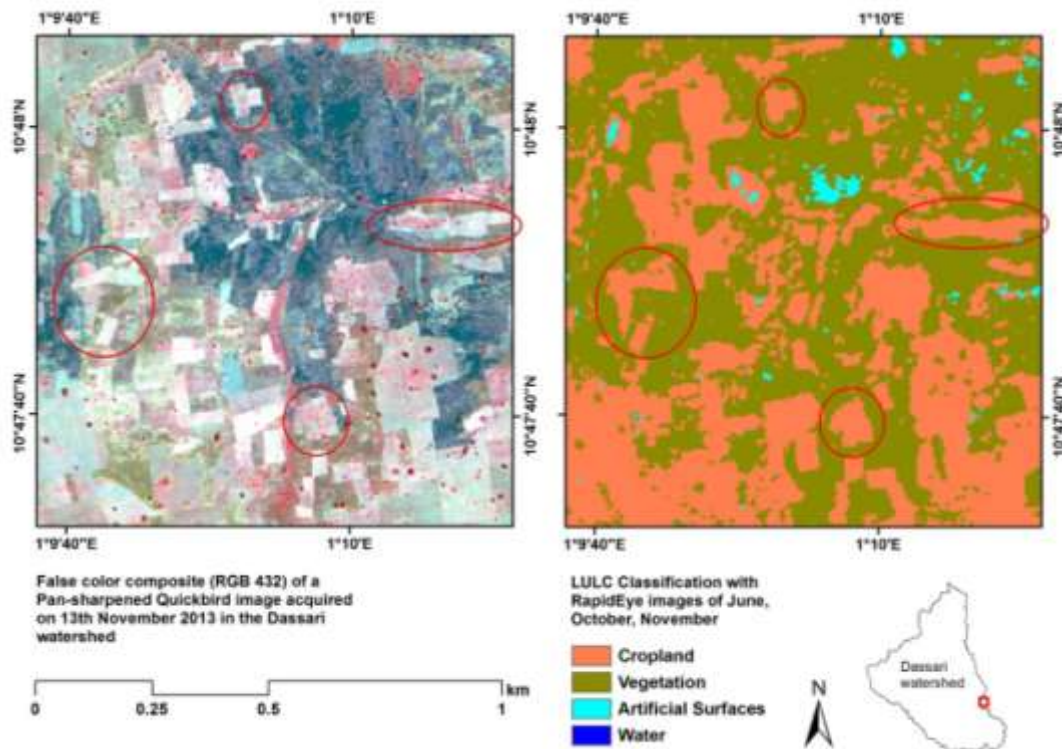


Figure 6. 1 Comparison of a pan-sharpened Quickbird image (0.6 m resolution) acquired on 13th November 2013 with the RapidEye cropland mask derived by classifying the June, October and November RE images of Dassari

Figure 6.1 compares the Dassari crop mask derived from the classification of three image time-steps (June, October, November) with a false color (RGB 432) pan-sharpened Quickbird image acquired in November 2013. The figure (red ellipses) shows that the high spatial resolution of RE adequately captures the typical small fields in the heterogeneous landscapes of West Africa and achieves a good recognition of cropland structure. Fields having a surface area of as low as 0.2 hectares were accurately delineated.

### Spatial distribution and statistics of general LULC classes

Table 6.4 presents the area coverage of the general LULC classes considered in the derivation of a crop mask for the respective watersheds. Figures 6.2-6.4 show the spatial distribution of the classes. In all the study watersheds, cropland and natural/semi-natural vegetation are the dominant LULC types. The Vea watershed has the highest percentage of cropland of about 52%, followed by Dano

## Results

(45%) and Dassari (40%). Conversely, the percentage of natural/semi-natural vegetation in Dassari is highest (59%), with Vea having the lowest (42%). Artificial surfaces constitute 4% of the Vea watershed, compared to 1.9% and 1% for Dano and Dassari respectively. The high percentage in Vea is indicative of its relative "urban" nature (compared to the other two), which is due to its proximity to the regional capital (Bolgatanga) of the Upper East region of Ghana. The low percentage in Dassari also confirms its rural nature compared to Vea and Dano. The Vea watershed has, by far, the highest percentage of water bodies, which forms 1.6% of the watershed compared to 0.17% and 0.01% for Dano and Dassari. The presence of a large reservoir in Vea, which serves as irrigation water as well as the main source of water supply (after treatment) for the city of Bolgatanga and its environs, is the main reason for the high percentage of water in Vea. The very low percentage of water bodies in Dassari is as a result of the existence of only one small reservoir in the whole watershed.

Table 6. 4 Area statistics of the four main LULC classes in the study watershed

LULC Type	Dassari		Vea		Dano	
	<i>Area (ha)</i>	<i>% watershed</i>	<i>Area (ha)</i>	<i>% watershed</i>	<i>Area (ha)</i>	<i>% watershed</i>
Cropland	7609.4	39.60	15671.1	51.93	26327.1	45.20
Nat./semi vegetation	11406.6	59.36	12813.6	42.46	30724.9	52.45
Artificial Surfaces	197.5	1.03	1200.0	3.98	1096.7	1.88
Water bodies	1.6	0.01	493.0	1.63	96.2	0.17
Total	19215.1	100	30177.7	100	58244.9	100

Croplands are dominant in the northern part of the Vea watershed, while the southernmost part consists of mainly natural/semi-natural vegetation (Figure 6.2). Hamlets are scattered all over the watershed, with the exception of the southernmost part which is uninhabited. Due to the practice of an integrated crop-livestock system, grasslands, meant for animal grazing, are normally in close proximity to the hamlets.

In the Dano watershed, croplands and natural/semi-natural vegetation are mixed in equal measure, although the northern part seems to have a slightly higher percentage of croplands than the south (Figure 6.3). Large expanses of natural/semi-natural vegetation frequently occur (southern, western and eastern) in the watershed. The Dano township is located in the southern part of the watershed, while agglomerations of hamlets occur in a few more places.

Croplands are dominant in the western and south-western part of the Dassari watershed (Figure 6.4). Croplands and natural/semi-natural vegetation are mixed in equal measure in the southern, south-eastern and eastern part of the watershed. Natural vegetation is dominant in the north-eastern section because it forms part of the Pendjari national park. The Dassari village is located in the eastern part of the watershed.

## Results

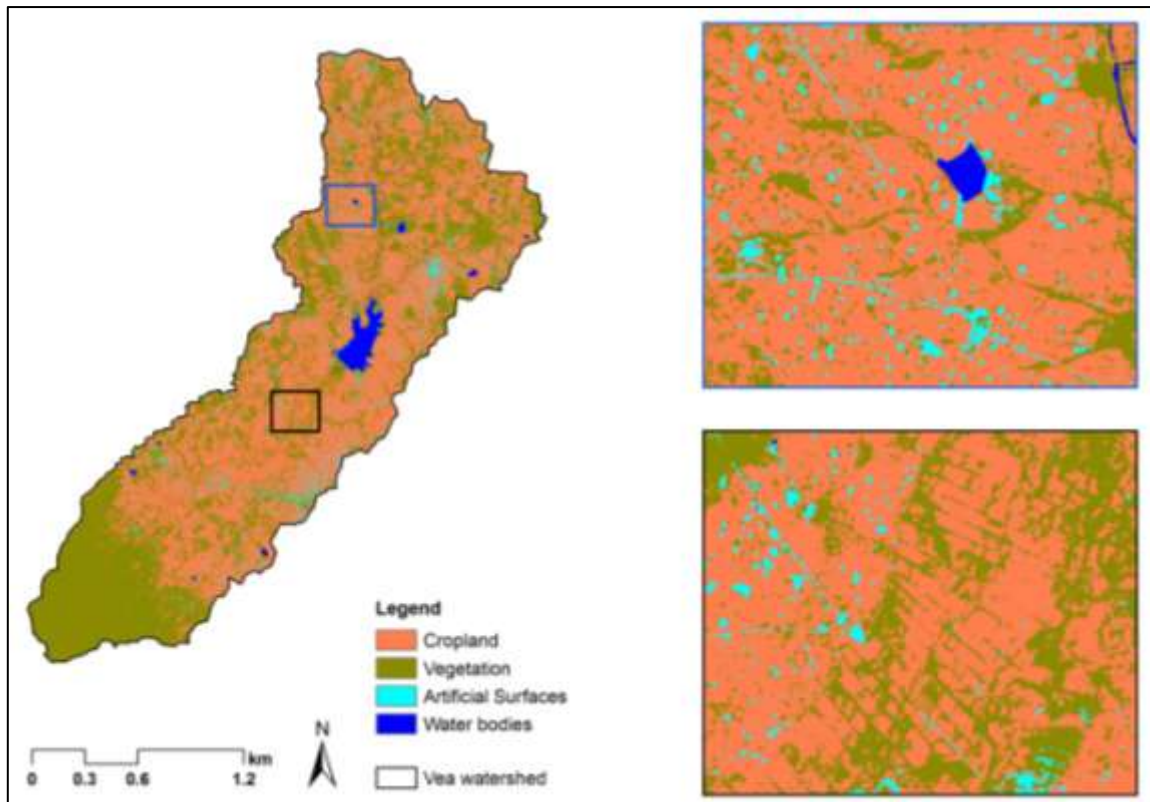


Figure 6. 2 Spatial distribution of the four main LULC classes in the **Vea watershed**. Crop classification was subsequently conducted on only the cropland areas.

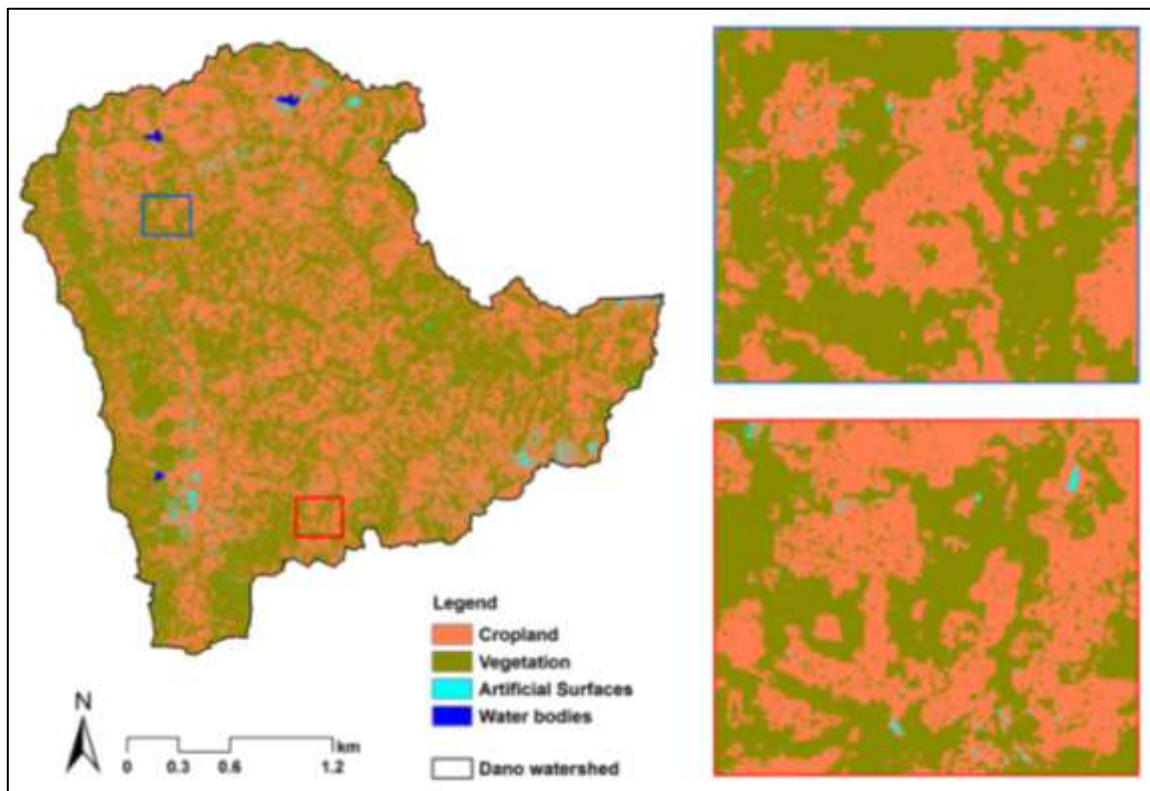


Figure 6. 3 Spatial distribution of the four main LULC classes in the **Dano watershed**. Crop classification was subsequently conducted on only the cropland areas

## Results

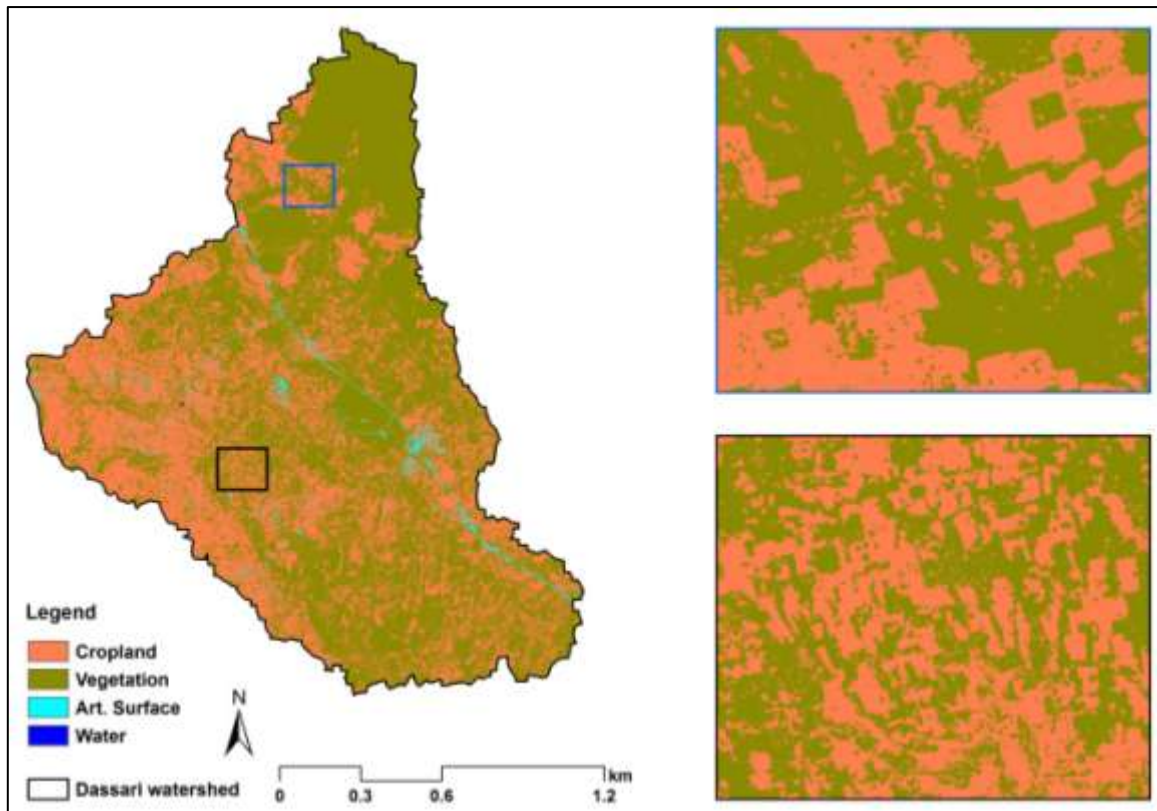


Figure 6. 4 Spatial distribution of the four main LULC classes in the **Dassari watershed**. Crop classification was subsequently conducted on only the cropland areas.

### 6.1.2 Crop mapping

This sub-section presents results of the crop classification conducted in the three study watersheds. A sequential masking classification approach was implemented in which different crops were classified sequentially using different image combinations. These image combinations were determined from initial classifications of all possible permutations (255 for Vea, 1023 each for Dano and Dassari) of all images (optical and SAR) available for the respective watersheds. Thus, the section begins with a presentation of the image combinations that were found to be most suitable for discriminating the different crop types. Next, a comparison between results (overall and classwise accuracies) obtained from the sequential masking approach and results obtained by classifying all crops with all images at the same time ("one-time classification") are presented. The one-time classification was the results of the image combination that achieved the highest overall accuracy out of all permutation runs in a watershed. Further, results of classification with, and without, SAR are presented and compared. The sub-section ends with a presentation of the statistics and spatial distribution of the different crop classes in the respective watersheds.

#### 6.1.2.1 Image combinations for discriminating crop types

Figures 6.5 – 6.7 presents a summary of the results obtained from the classification of all possible permutations of available images in each watershed. There were eight available images in Vea (255 permutations), while Dano and Dassari each had ten images (1023 permutations). The x-axis represents the permutation number and the number of classifications conducted in the round of

## Results

permutations is given in parenthesis. The y-axis represents the minimum, maximum and mean of the overall accuracies achieved in a particular round of permutations. For example, permutation number 1 indicates all single date classifications while number 2 indicate all pairwise (two images) classifications.

Figure 6.5 shows that in *Vea*, classification accuracy increased steadily from the classification of single images (permutation number 1) to classification of four images (permutation number 4). For the single date classifications, the June RE achieved the highest accuracy of 54% while the October, November, May, September and April RE followed with 52%, 49%, 48%, 46% and 43% respectively. The SAR images of September and October achieved the lowest accuracies of 39% and 34% respectively. The good performance of the June image can be attributed to differences in the ploughing period of cereals on one hand and legumes/maize on the other. Early ploughing of cereals (April to June) is believed to have improved separation between the classes. The figure shows that maximum classification accuracy of 80% was achieved when only four images were classified (April RE, June RE, September TSX, October RE), while inclusion of additional images did not appreciably increase the accuracy. It is interesting to note that the maximum accuracy actually decreases to 76% and 71% when seven or eight images respectively are involved in the classification. This result suggests that, when only four images can be purchased for crop mapping in *Vea*, acquisition in the above-mentioned months may be beneficial, provided environmental conditions (e.g. rainfall pattern) and farmer management practices (e.g. ploughing) remain largely constant.

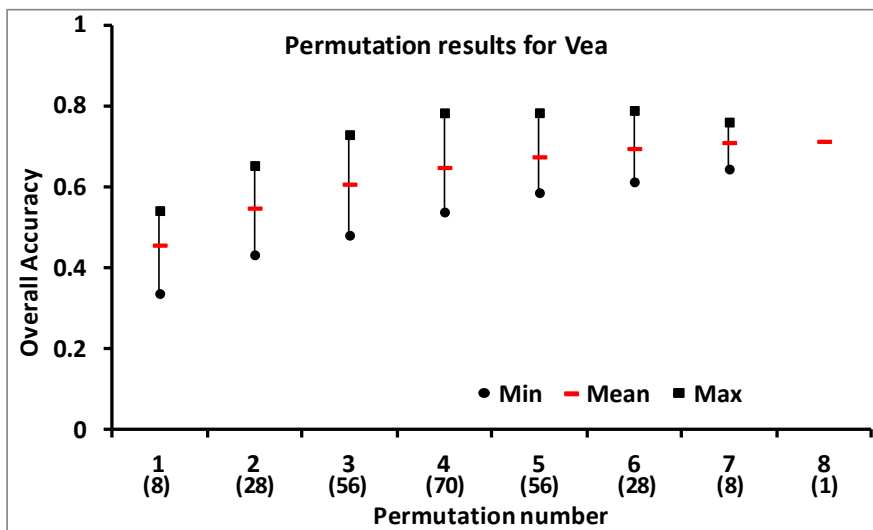


Figure 6. 5 Classification of all possible permutations of available imagery in the **Vea watershed**. The number of classifications performed at each round of permutations is provided in parenthesis on the x-axis

Figure 6.6 presents a similar trend as in Figure 6.5 (*Vea*) for the *Dano watershed*, although classification accuracies are relatively lower. The figure also shows a steady increase in classification accuracy from permutation number 1 till 4, after which there is no appreciable increase in classification accuracy. For the single date classifications, the September RE achieved the highest accuracy of 56%, while 54%, 48% and 45% were obtained for the SAR images of August, September

## Results

and October. The early season images – April RE, May RE, June LS and July TSX – achieved the lowest accuracies of 39%, 33%, 33% and 29% respectively. Compared to Vea, the increase in maximum classification accuracy from permutation number 2 (two-image combinations) to number 4 (four-image combinations) was much smaller (i.e. 4% as against 13% in Vea). However, the increase in maximum accuracy from single date to two-image combinations was substantial (10%) and comparable to that of Vea (11%). Similar to Vea, the highest accuracies were obtained when four or five images were combined in classification, while the accuracies decrease as more images are included. In fact, a difference of only 0.4% was observed between the maximum accuracy of image combination in permutation number 5 (April RE, August TSX, September RE and TSX, October RE) and that of the permutation number 4 (April RE, August TSX, September RE and TSX). The inclusion of the October RE in the former was found to have slightly increased the classwise accuracy of rice.

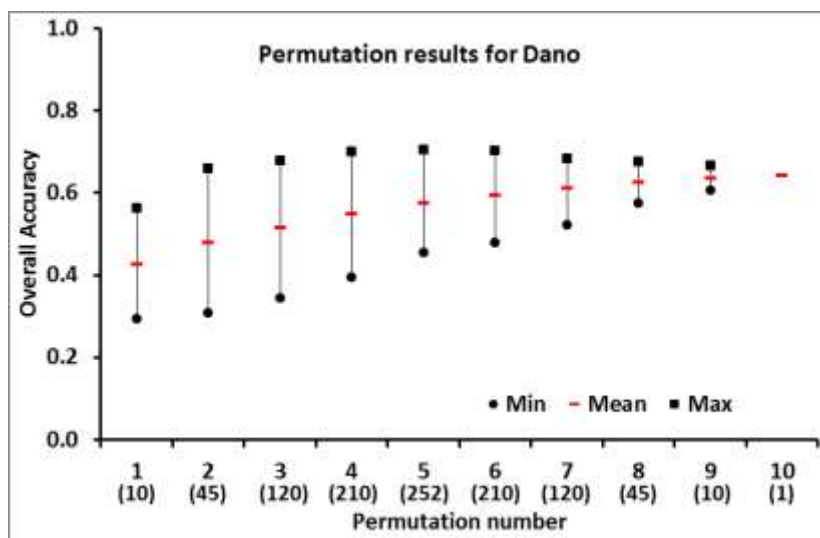


Figure 6.6 Classification of all possible permutation of available imagery in the **Dano watershed**. The number of classifications performed at each round of permutations is provided in parenthesis on the x-axis

Figure 6.7 shows the results for Dassari. Similar to the other watersheds, maximum classification accuracy steadily increases from single date classifications till four-band combinations (permutation number 4), after which no appreciable increase in accuracy was observed. Considering the single date classifications, the September RE produced the highest accuracy of 48% while the June RE and August TSX achieved an accuracy of 43% and 40% respectively. All other time-steps produced an accuracy of less than 35%. The image combination that achieved the highest classification accuracy (55%) was found to be the June RE, June TSX, July TSX and September RE.

The results obtained in the permutation runs suggest that increasing the number of images in crop mapping may not necessarily increase classification accuracy. However, a careful selection of image dates in accordance with the cropping calendar of the crops under investigation may produce similar or even better results than when a lot of images are included. It can be observed in all the results (Figures 6.5-6.7) that, four, or at most five, images produce better classification accuracy than when all images are included in the classification. Particularly, classification accuracy declined in all



## Results

watersheds when six or more images were involved in the classification. A possible explanation for the lower accuracy when six or more images are involved is that, some dominant layers may cause accurate discrimination of certain classes while other classes may be poorly discriminated, leading to an overall poor result.

The range of classification accuracy (i.e. minimum and maximum) for the respective permutation runs suggest how different combinations of the same number of images (acquired at different stages in the cropping calendar) can result in varying overall accuracies classification. For example, when one considers permutation number 4, the range in accuracy for Vea, Dano and Dassari were found to be 25%, 30% and 28% respectively. This further suggests that satellite images acquired during the cropping season have to be carefully selected in order to achieve the best results in crop discrimination. The results obtained in this section confirms results of other studies that stressed the need to determine the best temporal window(s) for crop mapping (Murakami et al., 2011; Conrad et al., 2014).

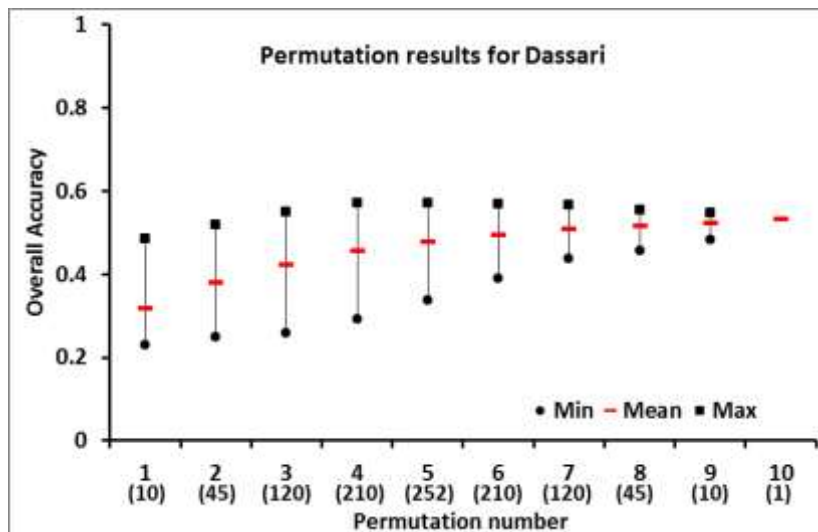


Figure 6. 7 Classification of all possible permutations of available imagery in the Dassari watershed. The number of classifications performed at each round of permutations is provided in parenthesis on the x-axis

Another important aspect of the results obtained from the permutation runs was a determination of image combinations that best discriminate the individual crop classes. This determination is based on the classwise accuracies of the crops (i.e. F1 score) instead of the overall accuracy. Thus, the optimal image combinations for discriminating the individual classes can be different from the image combination that produces the overall best classification. As previously explained in Chapter 5, a sequential masking of the individual crop types, based on different image combinations can improve the detection of crops.

Tables 6.5-6.7 provide information on the optimal image combinations that achieved the best discrimination (based on F1 score) of the individual crop classes in each watershed. In addition, the

## Results

---

image combination that achieved the highest overall accuracy out of all permutation runs (“one-time classification”) is presented.

Tables 6.5-6.7 indicate that good classwise accuracies were achieved for different crop types when different image combinations were classified in the permutation runs. For instance, in Veia (Table 6.5), the use of three early season images (April RE, May RE and June RE) and one late-season image (Sep TSX) achieved the highest F1 score of 0.86 for the cereals class while all other classes had a lower F1 score. On the other hand, one early season image (May RE) and three late season images (Sep TSX, Oct RE and Oct TSX) produced the highest F1 score of 0.89 for the legumes class while all other classes had a lower F1 score. This suggests that early season images best discriminate the cereal class while late season images are better for discriminating the legumes class. This difference can be attributed to differences in the cropping calendar of the two crops (Figure 5.3), especially with regards to their planting dates. Land preparation and planting is done much earlier in the Veia watershed for cereals than legumes. Thus, whereas early season images may identify cereal fields as ploughed, legume fields may be seen as grasslands/unploughed. Table 6.7 presents a similar situation for maize in the Dassari watershed, which is better discriminated with two early season images (June RE, July TSX) and one late-season image (November RE). Ploughing of most maize fields in the watershed for the 2013 cropping season started later in July, while other crops were mostly ploughed earlier. Thus, the spectral differences between ploughed and unploughed fields on early season images contributed to the detection of maize fields using the above stated image combination.

## Results

Table 6. 5 The best image combination used to separate different crop classes in the **Vea watershed**

Discriminating Crop		Image Combination								Classwise Accuracy (F1 Score)			
		April RE	May RE	June RE	Sep. RE	Sep. TSX	Oct. RE	Oct. TSX	Nov	Legumes	Cereals	Rice	Maize
Sequential	Legumes		X			X	X	X		0.89	0.67	0.79	0.07
	Cereals	X	X	X		X				0.76	0.86	0.70	0.45
	Rice	X			X	X	X	X	X	0.76	0.73	0.86	0.02
	Maize			X		X		X		0.62	0.75	0.54	0.52
One-time classification		X		X		X	X			0.87	0.83	0.81	0.50

Table 6. 6 The best image combination used to separate different crop classes in the **Dano watershed**

Discriminating Crop		Image Combination										Classwise Accuracy (F1 Score)			
		April RE	May RE	June LS	July TSX	Aug. TSX	Sep. RE	Sep. TSX	Oct. RE	Oct. TSX	Nov. LS	Rice	Cotton	Cereals	Maize
Sequential	Rice			X	X			X	X		X	0.84	0.48	0.67	0.36
	Cotton	X	X			X	X	X				0.61	0.81	0.71	0.49
	Cereals	X			X	X	X			X		0.71	0.54	0.79	0.33
	Maize		X			X	X	X	X			0.64	0.79	0.71	0.60
One-time classification		X				X	X	X	X			0.73	0.79	0.71	0.57

Table 6. 7 The best image combination used to separate different crop classes in the **Dassari watershed**

Discriminating Crop		Image Combination										Classwise Accuracy (F1 Score)				
		April RE	May RE	May TSX	June RE	June TSX	July TSX	Aug. TSX	Sep. RE	Oct. RE	Nov. RE	Cotton	Maize	Cereals	Rice	Yam
Cotton			X		X		X		X		X	0.71	0.54	0.44	0.64	0.51
Maize					X		X				X	0.33	0.59	0.27	0.34	0.47
Cereals				X		X		X	X		X	0.64	0.27	0.55	0.68	0.27
Rice		X		X				X	X	X		0.50	0.30	0.43	0.75	0.48
Yam		X			X	X	X				X	0.40	0.44	0.36	0.50	0.60
One-time classification					X	X	X		X			0.69	0.55	0.46	0.65	0.51

## Results

In general, tables 6.5-6.7 show that mid to late season images (August-October) are essential for crop discrimination, although early season images occasionally proved beneficial for discriminating certain crop types (e.g. cereals in Veá). Images acquired in this temporal window (August-October) had a higher frequency of occurrence considering all the time-steps used in discriminating the different crops in the respective watersheds. In Veá, for example, RE and TSX images acquired in September and October constituted ten, out of the seventeen, time-steps used to classify the four crop types in the watershed. In Dano, twelve, out of the twenty, time-steps used to discriminate the different crop types were acquired between August and October, while the remainder were acquired in April, May, June, July and November. In Dassari, a relatively fewer number (seven out of twenty-three) was used, primarily due to the high number of early season images (six), compared to three and four in Veá and Dano respectively. Apart from Dassari, the November acquisitions were rarely useful in the discrimination of crop classes. In Veá and Dano, the November acquisitions were only involved in the discrimination of rice, which can be attributed to the characteristic high reflectance of rice fields during or even after harvesting (Figures 5.4*b, d*). In Dassari, however, the November RE acquisition was useful in discriminating four, out of the five, crop classes. This could be due to late harvesting of certain crops in this watershed.

### 6.1.2.2 Sequential masking vs one-time classification

Table 6.8 compares the overall accuracy of the final sequential masking classification results with the highest overall accuracy obtained from the classification of all possible permutations (one-time classification). The accuracy assessments are based on the same set of validation data. This comparison was performed to ascertain the advantages or disadvantages of the sequential masking approach adopted. Additionally, results obtained from classifying with, and without, SAR data are presented to determine the contribution of SAR data to improving crop classification in the study watersheds.

Table 6. 8 Summary results of the sequential masking and one-time classification performed with and without SAR data. Detailed confusion matrices for the various classifications can be found in Appendix B

	Dano		Veá		Dassari	
	One-time classification	Sequential masking	One-time classification	Sequential masking	One-time classification	Sequential masking
Optical + SAR	69.5%	78.8%	80.0%	86.0%	55.2%	64.6%
Optical only	55.4%	64.0%	69.8%	71.1%	50.8	56.5

Table 6.8 shows that the sequential masking approach consistently produced better overall accuracies than the one-time classification in all cases. Compared to the one-time classification, overall accuracies obtained in the sequential masking improved by 6%, 9.3% and 9.4% for Veá, Dano and Dassari respectively when optical and SAR data were combined in the classification. When only optical data were used for classification, the corresponding increases were 1.3%, 8.6% and 5.7% for Veá, Dano and Dassari respectively.

## Results

The McNemar's test was used to test the statistical significance of these differences. Table 6.9 summarizes the results obtained. The test proved that the observed differences in accuracy between the sequential and one-time classifications for all the watersheds were significant at the 1% significance level, except the Veia classification involving only optical data that was found to be significant at the 5% level of significance.

Table 6. 9 McNemar's test results based on a comparison of the sequential masking and one-time classifications for the study watersheds

Watershed		$f_{11}$	$f_{12}$	$f_{21}$	$f_{22}$	Total	Chi-square ( $\chi^2$ )	p-Value
Optical and SAR	Dano	2580	572	200	648	4000	179.3	< 0.001
	Veia	2536	418	211	269	3434	68.1	< 0.001
	Dassari	2160	1071	598	1171	5000	134.0	< 0.001
Optical only	Dano	1767	793	450	990	4000	94.6	< 0.001
	Veia	2233	209	165	827	3434	5.2	< 0.05
	Dassari	1226	649	446	2679	5000	37.6	< 0.001

Tables 6.10-6.12 shows the confusion matrices derived for the sequential masking classification involving the optical and SAR datasets for the three watersheds. Only these are shown here due to the superiority of the sequential masking approach over their one-time counterparts. All other confusion matrices have been provided in Appendix B. Tables 6.10-6.12 are discussed in detail in the next chapter (Discussion of results).

Table 6. 10 Confusion matrix for the sequential masking classification in **Veia** with optical+SAR

Class		Cereals	Maize	Legumes	Rice	Total	Prod. Acc	User. Acc	F1 score
Reference	Cereals	869	36	94	1	1000	86.9	86.7	0.86
	Maize	51	300	60	23	434	69.1	69.4	0.69
	Legumes	3	85	886	26	1000	88.6	84.3	0.86
	Rice	79	11	11	899	1000	89.9	94.7	0.92

Table 6. 11 Confusion matrix for the sequential masking classification in **Dano** with optical+SAR

Class		Cotton	Maize	Cereals	Rice	Total	Prod. Acc	User. Acc	F1 score
Reference	Cotton	755	122	121	2	1000	75.5	90.9	0.83
	Maize	59	586	232	123	1000	58.6	71.9	0.65
	Cereals	9	69	921	1	1000	92.1	68.8	0.79
	Rice	7	38	65	890	1000	89.0	87.6	0.88

## Results

Table 6. 12 Confusion matrix for the sequential masking classification in **Dassari** with optical+SAR

	Class	Cotton	Maize	Cereals	Rice	Yam	Total	Prod. Acc	User. Acc	F1 score
<b>Reference</b>	<b>Cotton</b>	753	137	109	1	0	1000	75.3	73.2	74.2
	<b>Maize</b>	167	539	245	36	13	1000	53.9	53.2	53.5
	<b>Cereals</b>	95	243	526	70	66	1000	52.6	49.2	50.8
	<b>Rice</b>	1	24	20	842	113	1000	84.2	74.8	79.2
	<b>Yam</b>	13	71	169	176	571	1000	57.1	74.8	64.8

### 6.1.2.3 Classwise accuracies

Tables 6.13-6.15 compares the classwise accuracies (F1 score) of the two approaches (sequential masking and one-time classification) for the respective watersheds. The tables reveal that, compared to the one-time classification, the sequential masking approach produced better classwise accuracies for most classes when optical and SAR data were combined in the classification. Exceptions are legumes in the Vea watershed (Table 6.13) and maize in the Dassari watershed (Table 6.15), where the one-time classification produced slightly higher accuracies than the sequential masking method. The tables depict a similar trend for classifications involving only optical data, with maize (Vea watershed) and cotton and maize (Dano watershed) being the only exceptions where the one-time classification produced a better classwise accuracy than the sequential masking approach.

Table 6. 13 Comparison of classwise accuracies derived for the **Vea watershed** using based on the one-time classification and sequential masking classification

Crop type/group	One-time classification		Sequential masking classification	
	Optical only	Optical + SAR	Optical only	Optical + SAR
Cereals	0.77	0.83	0.77	0.87
Maize	0.18	0.50	0.14	0.69
Legumes	0.71	0.87	0.76	0.86
Rice	0.79	0.81	0.81	0.92

Table 6. 14 Comparison of classwise accuracies derived for the Dano watershed using based on the one-time classification and sequential masking classification.

Crop type/group	One-time classification		Sequential masking classification	
	Optical only	Optical + SAR	Optical only	Optical + SAR
Cereals	0.46	0.74	0.66	0.78
Cotton	0.58	0.76	0.54	0.83
Maize	0.56	0.51	0.54	0.65
Rice	0.63	0.73	0.83	0.88

## Results

Table 6. 15 Comparison of classwise accuracies derived for the **Dassari watershed** using based on the one-time classification and sequential masking classification

Crop type/group	One-time classification		Sequential masking classification	
	Optical only	Optical + SAR	Optical only	Optical + SAR
Cereals	0.45	0.47	0.46	0.51
Cotton	0.68	0.69	0.68	0.74
Maize	0.45	0.55	0.47	0.54
Rice	0.52	0.57	0.69	0.79
Yam	0.44	0.51	0.49	0.69

In Dano and Dassari, both sequential masking and one-time classifications produced better classwise accuracies for cotton and rice than maize, cereals and yam when optical and SAR data were combined in the classification (Tables 6.14-6.15). This suggests the relative ease with which these crop types can be discriminated when images acquired during the cropping season are available. An F1 score of 0.7 or greater was consistently achieved for cotton in all classifications, while the same was achieved for rice with the exception of the one-time classification in Dassari where an F1 score of 0.57 was achieved. This is attributable to a higher confusion between rice and yam when the two classes were classified together, instead of being sequentially classified.

In Veia, F1 scores of 0.8 were consistently achieved for rice, legumes and cereals in both classification approaches when optical and SAR data were included in the classification (Table 6.13). Relatively lower accuracies were, however, achieved for maize (F1 score of 0.69 and 0.50 for sequential and one-time respectively) due to confusion with the legumes and cereals classes. In Dano, an F1 score of 0.7 or greater was consistently achieved for the cereal class, while lower accuracies were recorded for maize (F1 score of 0.65 and 0.51 for sequential and one-time respectively). Lowest accuracies for the cereals and maize classes were obtained for the Dassari watershed, where F1 scores of less than 0.6 was consistently obtained for both classes irrespective of the approach or data used in the classification. Results of all classifications suggest a general difficulty in discriminating maize from cereals, although their cropping calendar may differ in some of the watersheds (e.g. Dassari). Structural similarities between the two crops could be one of the reasons for this confusion. Further discussion is provided in the next chapter.

### **6.1.2.4 Optical+SAR versus Optical only**

Table 6.8 shows how the inclusion of SAR data improved classification accuracies compared to the use of only optical data. This is evident irrespective of the classification approach adopted. In the sequential masking approach, the integration of optical and SAR data increased overall accuracy by 8% for Dassari and 15% for Veia and Dano over the use of only optical data. The corresponding figures for the one-time classification were 4%, 10% and 14% for Dassari, Veia and Dano respectively. The relatively low improvements (4%, 8%) in the Dassari classifications can be attributed to the unavailability of SAR images acquired in September and October, which according to Tables 6.5 and 6.6 contributed to achieving the accuracy improvements in Dano and Veia. For example, in Veia, TSX images acquired in September and October constituted seven, out of the seventeen, time-steps used

in the sequential masking classification (Table 6.5). Additionally, image combinations used for the one-time classifications in Dano and Veja both included the respective TSX images acquired in September.

Tables 6.13-6.15 further shows that classifications involving optical and SAR produced better classwise accuracies over the optical only classifications. In Veja, the maize class witnessed the most significant increment in the F1 score when it increased from 0.14 (optical only) to 0.69 (optical and SAR) in the sequential masking approach (Table 6.13). This is not surprising, as Table 6.5 shows that, two, out of the three, time-steps that were suitable for discriminating the maize class were SAR data (September and October TSX). Other classes in Veja (cereals, legumes, rice) also witnessed minimal increments (0.1) in F1 score when optical only and optical plus SAR results were compared. In Dano, the F1 score of the cotton class increased from 0.54 (optical only) to 0.83 (optical and SAR) in the sequential masking classification (Table 6.14). The maize and cereals classes each witnessed increments in F1 score of about 0.11, while rice had the least increment of about 0.05. In Dassari, highest F1 score increments were achieved for the yam and rice classes when comparing the optical only and optical plus SAR sequential masking classification results. The F1 score of yam increased from 0.49 to 0.65 while that of rice increased by 0.1. According to Table 6.6, three, out of the four, SAR images available (i.e. June, July, August TSX) were useful in discriminating the yam class. In addition, the Table reveals that the June and July TSX images were two, out of the four, time-steps that achieved the highest overall accuracy (one-time classification) when all possible permutations of available images were considered.

### **6.1.2.5 Crop statistics**

Area statistics for the different crop types/groups classified in the study watersheds are presented in Table 6.16. The area statistics was extracted from the classification results of the sequential masking approach involving both optical and SAR data due to the superior results obtained for these classifications.

Cereals, which comprise of the staples millet, sorghum and their intercropping, were found to be the dominant crop group in Veja and Dano. It constituted about 20% and 16% of Veja and Dano watersheds respectively. The dominance of this group (in comparison with other crops) is not surprising, since they are the main staples that are cultivated by almost every household for household consumption. In Dassari, cereals and maize were found to be the dominant crops and recorded similar percentages of about 11% each. However, the general difficulty in separating these two classes, and the resultant low F1 scores compared to that achieved in other watersheds (0.53 and 0.51 for maize and cereals respectively) could have positively or negatively affected their area estimates.



## Results

Table 6. 16 Crop area statistics derived from the crop classification results at watershed scale

Crop type/group	Dassari*		Vea*		Dano*	
	Area (ha)	% watershed	Area (ha)	% watershed	Area (ha)	% watershed
Cereals	2049.7	10.8	6116.5	20.3	9324.5	16.0
Maize	2070.0	10.7	1383.2	4.6	7054.0	12.1
Cotton	1410.4	7.3	-	-	7303.3	12.5
Rice	1449.4	7.5	2821.4	9.3	2645.4	4.5
Yam	630.1	3.3	-	-	-	-
Legumes	-	-	5350.0	17.7	-	-

\* Watershed area of Dassari, Vea and Dano are 19,215 ha, 30,178 ha and 58,245 ha respectively

Maize constitutes 4.6% and 12.1% in the Vea and Dano watersheds respectively. The low percentage cover of maize in Vea is expected, since very few farmers cultivate maize in the watershed. Field interviews conducted in 2013 revealed that the inability of most farmers to purchase fertilizers was the main reason for the non-cultivation of maize in Vea. Although some private agricultural agencies have started supporting farmers by providing them with fertilizers at the start of the season (which they pay back after harvest), most farmers are yet to subscribe to the program. In Dano, however, cultivation of maize is popular due to the cultivation of cotton. Cotton farmers in this watershed are supported by the Government of Burkina Faso by providing fertilizers. Most cotton farmers, therefore, alternate cotton and maize on an annual or bi-annual basis, in which maize benefits from the residual effects of the previous year(s) cotton fertilizer (Ouattara *et al.* 2011).

Cotton constitutes 7.3% and 12.5% of the area of the Dassari and Dano watersheds respectively. Considering that previous literature had indicated the general dominance of cotton in northwestern Benin (Igue *et al.*, 2000), a much higher percentage area for cotton in Dassari was expected. A possible explanation for this low figure is the cotton-maize/sorghum-cotton rotation based system that is practiced in the watershed (and in many other cotton cultivation areas) (Ouattara *et al.* 2011, Saidou *et al.* 2012). This system could affect the total area under cotton cultivation during years that most cotton farmers decide to cultivate maize or sorghum instead of cotton.

The percentage coverage of rice was 9.3%, 7.5% and 4.5% in the Vea, Dassari and Dano watersheds respectively. Yam in Dassari covers only 3.3% of the area of the watershed. Confusion between rice and yam in the Dassari classification could affect the estimated areas of rice and yam. Legumes were found to be the second dominant crop group in Vea, and constituted about 18% of the watershed area. This is in line with local knowledge (of author) and agricultural statistics from MoFA for the district in which the watershed falls (Bongo).

### 6.1.2.6 Spatial distribution of crops

Figures 6.8-6.10 show the spatial distribution of crops/crop groups in the study watersheds. Detailed looks of approximately 2 km x 2 km have been provided for a closer assessment of the distribution of crops/crop groups.

Rice occurs mainly in inland valleys in all the watersheds due to the relatively high and secure water availability of inland valleys compared to the uplands. Several studies have noted the potential of inland valleys for rice cultivation in West Africa (Hideto *et al.* 2011, Rodenburg 2013, Rodenburg *et*

## Results

---

*al.* 2014). Therefore, the predominance of rice in the valley bottoms of the watersheds is expected. However, rice fields are also located on uplands (Becker and Johnson 2001), where farmers make bunds on relatively flat terrain to hold water and provide the rice plants with sufficient water during development stages. In Dassari, most yam fields occur next to rice fields, whether in valley bottoms or uplands. In Vea and Dano where an irrigation scheme exist, rice occurs in the irrigation command area (i.e. downstream of the reservoir) (in Dano), while rice, cereals, maize and legumes were found in the irrigation command area in Vea.

Cereals are mostly located close to hamlets in Vea, while in Dano and Dassari, they are located in bushes although a few can be found around hamlets. The predominance of cereals around hamlets in Vea can be explained by the relatively "urban" nature of this watershed compared to Dano and Dassari. Legumes fields in Vea are also close to hamlets, but they are a bit farther than cereals. Due to the predominance of the two crop groups (cereals and legumes) in Vea, their boundaries normally adjoin each other.

In Dassari and Dano, cotton, maize and cereals occur together and are mostly located in bushes (i.e. away from households), with their boundaries adjoining each other. Farmers may own multiple farms at a location, with each being one of the three crops mentioned above. Maize is occasionally cultivated in inland valleys, where soil fertility is believed to be high.

As previously alluded to, compared to Vea and Dano, a better cropland structure is recognizable in Dassari, where fields have regular shapes with clear boundaries. In Vea, fields are mostly irregular in shape, except those in the irrigation command area, which were properly demarcated by the management of the irrigation company.

## Results

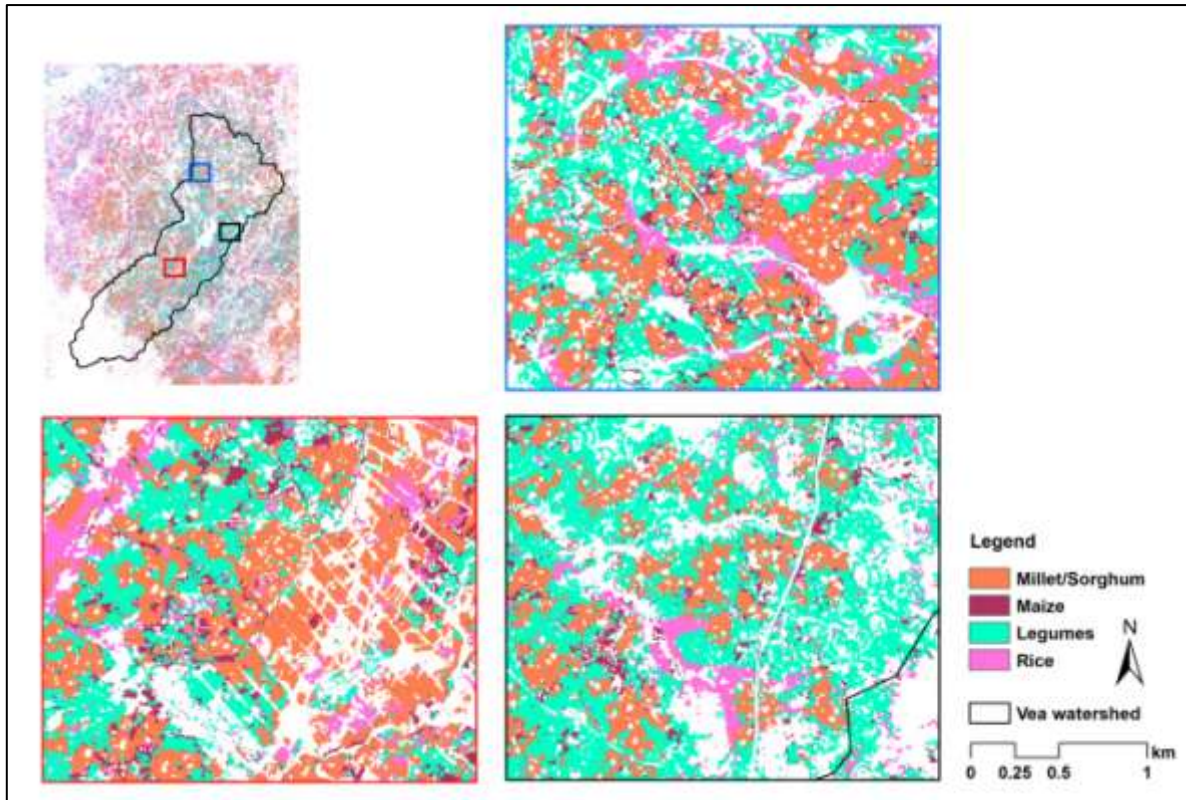


Figure 6. 8 Spatial distribution of crop types in the **Vea watershed**. Each detailed look is approximately 2km by 2km

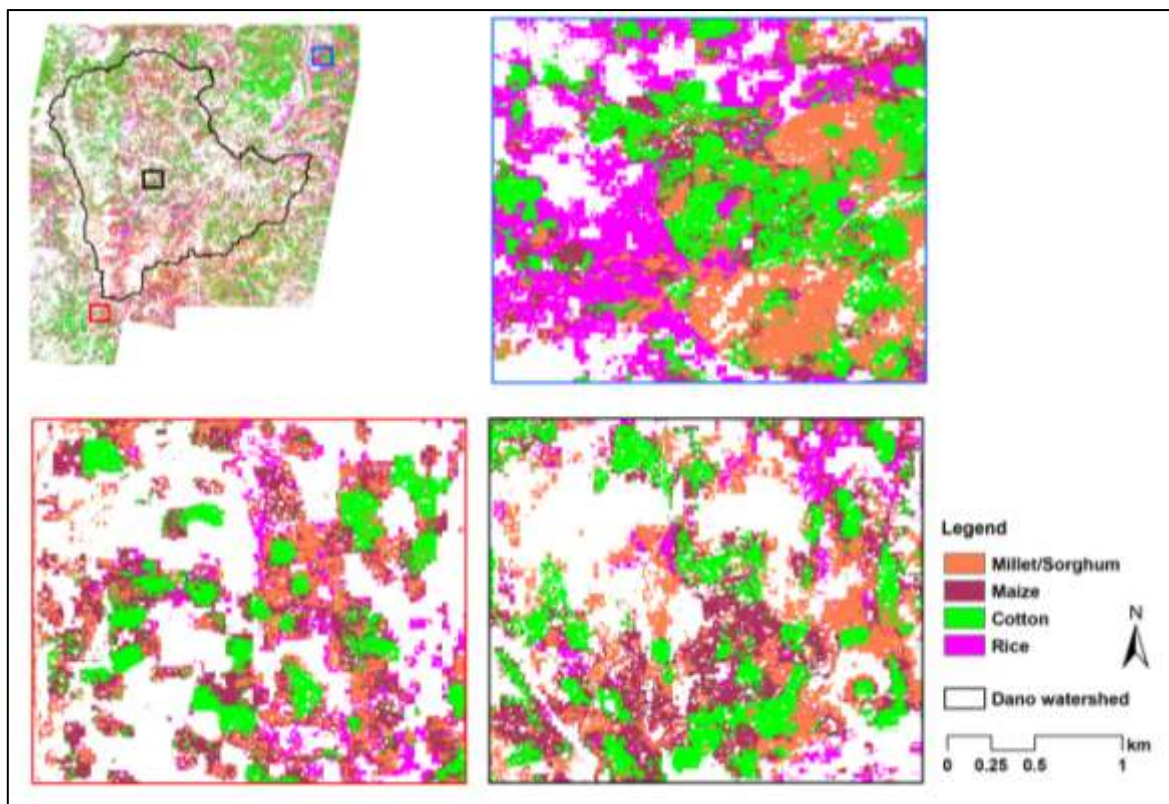


Figure 6. 9 Spatial distribution of crop types in the **Dano watershed**. Each detailed look is approximately 2km by 2km

## Results

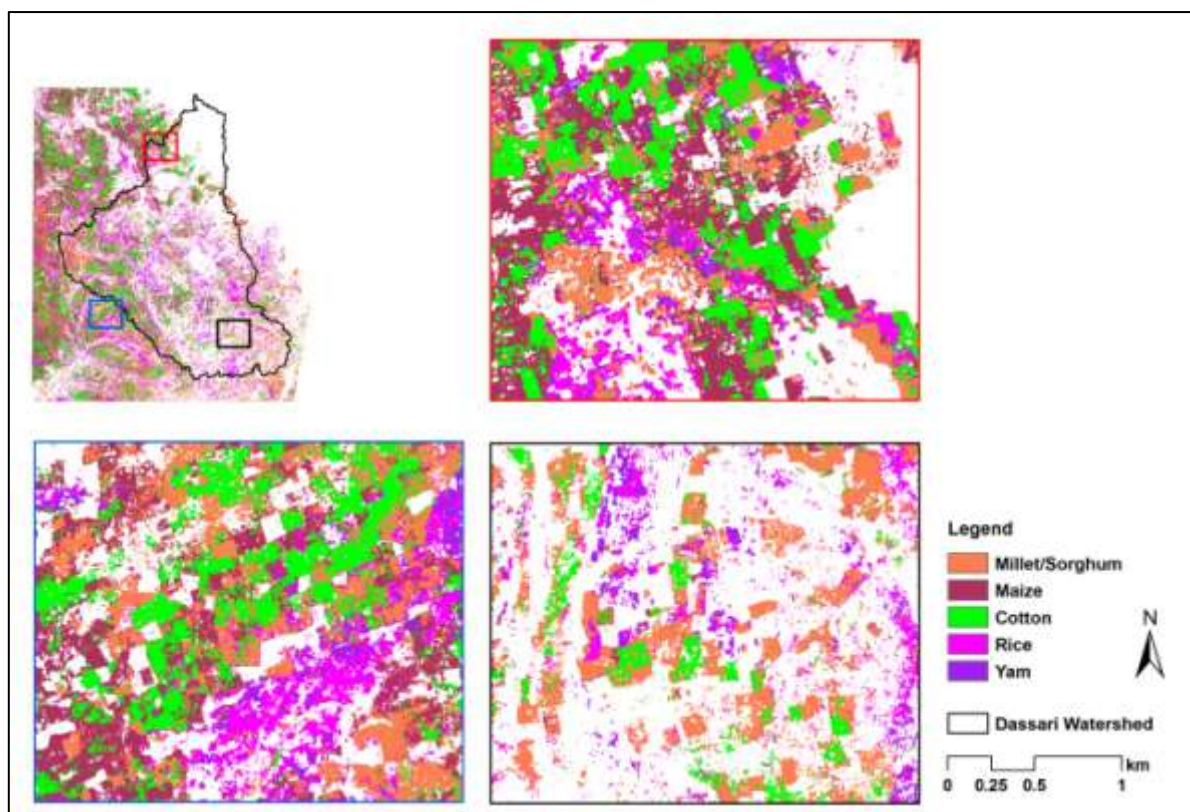


Figure 6. 10 Spatial distribution of crop types in the **Dassari watershed**. Each detailed look is approximately 2km by 2km

### 6.2 Cropland mapping at watershed scale

This sub-section presents results of the classification of historical Landsat images between 2002 and 2013. Due to data constraints, the analysis was conducted for only the Vea and Dano watersheds. The first part (6.2.1) of this sub-section deal with the classification accuracies (overall and classwise) obtained in each of the classifications. The second part - 6.2.2 - presents inter-annual or short term changes in cropland area in the last ten years. The last part of the sub-section presents statistics and changes in the other LULC classes considered in the classification.

#### 6.2.1 Classification accuracies

Tables 6.17 and 6.18 summarize accuracy estimates obtained for the time-series Landsat classifications performed for the Dano and Vea watersheds respectively. Five broad LULC classes (cropland, forest, mixed vegetation, artificial surfaces, water) were mapped in each classification (see Table 5.4 for definitions). The tables present the overall accuracy achieved for each classification as well as the classwise accuracies (producer's, user's accuracy and F1 score) obtained for the cropland class. Detailed confusion matrices for each classification have been provided in Appendix C.

The results show that, despite differences in the number of images used per year for the classification, an overall accuracy of 85% or more was achieved for all classifications conducted in both watersheds. In Dano, the lowest overall accuracy of 85.2% was obtained for the year 2010 while the highest of 97.7% was obtained for the 2008 classification. The 2011 classification in the

## Results

Vea watershed produced the lowest overall accuracy of 84.8%, while that of 2008 produced the highest of 92.4%. Spectral confusion between the forest and mixed vegetation classes were mostly the cause of the low overall accuracies obtained for some classifications. For example, in the 2010 classification of Dano, 20% of forest pixels were wrongly classified as mixed vegetation while 13% of mixed vegetation pixels were wrongly classified as forest. This confusion can partly be attributed to the acquisition period of the images used vis-a-vis the spectral response of vegetation. Most natural vegetation will have similar spectral response at the end of the rainy season (October, early November), which is the period most of the analyzed images were taken. Additionally, the use of mono-temporal data occasionally resulted in lower overall accuracies. For example, the Vea classification of 2011 (which had the lowest overall accuracy of 84.8%) was based on a mono-temporal acquisition, while all other classifications (in Vea) were based on multi-temporal datasets. This is in line with previous studies that have noted better performance of multi-temporal data as against mono-temporal (McNairn *et al.* 2009).

Table 6. 17 Overall and classwise accuracies achieved for the historical Landsat classifications conducted in the **Dano watershed**

Year	Overall accuracy (%)	Cropland		F1 score
		Producer's accuracy (%)	User's accuracy (%)	
2002	85.7	89.4	89.8	0.90
2005	89.6	90.6	94.1	0.92
2006	89.4	96.9	93.3	0.95
2007	85.6	91.9	92.3	0.92
2008	97.7	99.4	97.5	0.98
2010	85.2	93.5	92.5	0.93
2011	87.9	96.4	89.3	0.93
2013	87.5	92.5	87.4	0.90

Table 6. 18 Overall and classwise accuracies achieved for the historical Landsat classifications conducted in the **Vea watershed**

Year	Overall accuracy (%)	Cropland		F1 score
		Producer's accuracy (%)	User's accuracy (%)	
2002	87.1	87.3	96.3	0.87
2005	87.5	96.1	97.0	0.92
2006	87.7	91.7	93.5	0.90
2007	86.3	95.4	87.8	0.91
2008	92.4	96.3	97.4	0.94
2010	89.3	93.8	96.4	0.92
2011	84.8	83.4	88.5	0.84
2013	90.1	95.8	97.8	0.93

The results further reveal that an F1 score of at least 0.9 was achieved for the cropland class in all classifications except the Vea classifications of 2002 and 2011. The classifications of 2008 produced the highest F1 scores of 0.98 and 0.94 for the cropland class in the Dano and Vea watersheds respectively. In both watersheds, the classifications of 2005, 2006, 2008 and 2010 consistently

## Results

---

produced a producer's and user's accuracy of more than 90% for the cropland class, suggesting a very good detection of croplands.

The high level of accuracy achieved for the cropland class can be attributed to the use of harvest season images in the classifications. Tables 4.3 and 4.4 reveal that most of the images classified were acquired either during late crop developmental stages/harvesting (October and November) or immediately after harvest (December). This period affords the best separation between agricultural fields and surrounding natural vegetation due to a reduction in, for example, vegetation indices on the former. Harvesting of fields normally leads to a sharp decline in NDVI, which can assist in discriminating croplands from other surrounding LULC classes.

However, the use of harvest season images has its own limitations mainly due to the harvesting mechanism in the watersheds. Farmers in most of West Africa transport crop residues after harvest to their homes to be used as animal feed, preparation of manure or as building materials (Bationo and Mokwunye 1991, Ouédraogo *et al.* 2001). For instance, farmers who cultivate sorghum normally cut down the stalks after harvest and transport them to their houses to be used as materials for roofing, fencing or cooking fuel (Bationo and Mokwunye 1991). Legume (especially groundnuts) farmers also uproot the whole plant, plug the nuts, and transport the residue home to be used as animal feed (Karbo and Agyare 2002, Bado *et al.* 2012). These harvesting techniques, thus, result in harvested fields having bare patches and grasses/herbs which are mostly not weeded once the crops reach maturity stage. Figure 6.11 (left) shows a harvested sorghum field in Dano with the stalks ready to be transported while 6.6 (right) shows a harvested groundnut field in the Veia watershed with bare patches and grasses/herbs. The figures suggest that harvested fields could behave spectrally similar to bare areas (and other artificial surfaces) and/or mixed vegetation/grasses.



Figure 6. 11 Left: Harvested sorghum field in the **Dano** watershed with the sorghum stalks cut down and ready to be transported; right: A harvested groundnut field in the **Veia** watershed. The plants have been uprooted and transported home, leaving on a mixture of bare patches and grasses

Consequently, the artificial surfaces and mixed vegetation classes were the two main sources of spectral confusion with the cropland class in the classifications conducted. Compared to other classes (forest and water), these two classes had the highest confusion with the cropland class in all

## Results

classifications where the classwise accuracies of cropland were relatively poor. For example in the 2002 Dano classification, about 10% of cropland pixels were wrongly classified as artificial surfaces while 4% each of artificial surfaces and mixed vegetation pixels were wrongly classified as cropland. Similarly, 6% of cropland pixels were wrongly classified as artificial surfaces in the 2013 classification, while 10% and 8% of artificial surfaces and mixed vegetation pixels respectively were wrongly classified as cropland. In the Vea classification of 2011, 15% of cropland pixels were wrongly classified as mixed vegetation, while 4% and 7% of artificial surfaces and mixed vegetation pixels respectively were wrongly classified as cropland. These confusions, together with the use of mono-temporal data in some cases, contributed to the relatively low classwise accuracies achieved for the cropland class in some classifications.

### 6.2.2. Watershed-scale cropland dynamics between 2002 and 2013

Annual cropland area in the Vea and Dano watersheds between 2002 and 2013 are presented in Figure 6.12. Due to spatial limitations of the Landsat scene (path 194, row 52) that covers the Vea watershed (see Figure 5.11), the area statistics presented in the figure represents about half of the Vea watershed. The figure also shows annual rainfall totals for the analyzed years. It can be seen from the figure that generally, the Vea watershed has a higher cropland percentage than Dano, which is a confirmation of the results obtained from the watershed scale analysis using RapidEye data (see Section 6.1.1). Cropland area in Vea consistently constituted more than 50% of the watershed area, while it was consistently below 50% in Dano. In both watersheds, annual cropland area fluctuated between 2002 and 2013, although the patterns are different for each. In Vea, the major changes occurred in 2006/2007 and 2011 when cropland area declined, while high cropland areas were recorded in 2005, 2008, 2010 and 2013. In Dano, there was a decline in cropland area in 2005, 2007 and 2013, while increases were recorded in 2006 and between 2008 and 2011. These changes can be explained by a number of reasons including: (1) climatic factors (floods or dry spells during the cropping season), (2) declining soil fertility, (3) demographic changes and (4) changes in agricultural policies. Further discussions of these points are provided in the next chapter (Discussion of results).

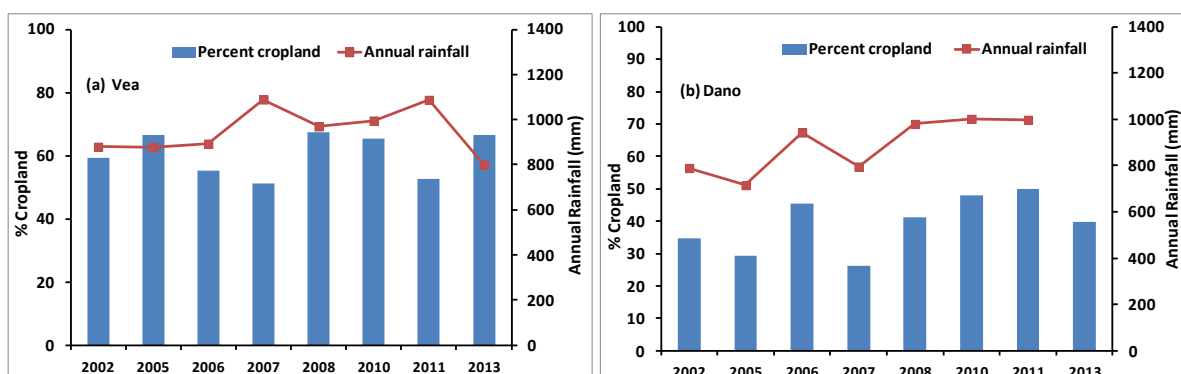


Figure 6. 12 Annual cropland area in the **Vea** (a) and **Dano** (b) watersheds between 2002 and 2013 and relationship with total annual rainfall. Blue bars represent annual cropland area while red line represents total annual rainfall

## Results

### 6.2.3. Spatial distribution of land use and land cover classes

Tables 6.19 and 6.20 present area statistics for all LULC types mapped in the Vea and Dano watersheds respectively. Similar to croplands, percentage coverage of the mixed vegetation class exhibited high fluctuations between the years analyzed. This can be attributed to the variety of vegetation types (grasslands/fallows, shrubland, and their mixtures) included in this class. Changes in cropland extent mostly occurred with a corresponding, but opposite, change in the extent of mixed vegetation. For example, in Dano, a reduction of 19% in cropland coverage between 2006 and 2007 resulted in an increase of 20% in mixed vegetation coverage between the same years. A similar pattern can be observed in Vea, where between 2007 and 2008, an increase of 16% in cropland coverage resulted in a corresponding decrease of 15% in mixed vegetation coverage.

Apart from cropland and mixed vegetation, all other LULC types had a fairly stable percentage coverage throughout the period of analysis. Forest land in Dano decreased from 20% of the catchment area in 2002 to about 15% in 2013, with the most significant decrease occurring between 2002 and 2005. Forest in the Dano watershed is mainly riverine and occurs along the main river channels (see Figure 6.13). The relatively high percentage of artificial surfaces in 2002 (in Dano) can be attributed to a higher confusion between cropland and artificial surfaces in the classification. Although high population increases have been reported in West Africa, it is not reflective in the study watersheds (by way of percentage increases in artificial surfaces). This is mainly due to the rural nature of the watersheds, and the fact that the high population increases have been happening mostly in big urban cities. Other studies also found that bare soils and steppes witnessed very little change over a 40 year period in Mali (Ruelland *et al.* 2010). The relatively high percentage cover of water in Dano in 2007 was due to flooding of the Black Volta River, which runs along the eastern part of the Dano watershed. Figure 6.13 shows changes in LULC in the Dano watershed between 2007 and 2008. The low coverage of cropland in 2007 is possibly due to flooding that occurred during the cropping season of 2007.

Table 6. 19 Changes in general LULC classes in the **Vea watershed** between 2002 and 2013

LULC	2002	2005	2006	2007	2008	2010	2011	2013
Cropland	59.4	66.6	55.3	51.1	67.4	65.4	52.5	66.7
Forest	3.9	4.3	4.8	5.4	4.3	4.5	4.7	5.0
Mixed vegetation	31.9	25.1	35.6	38.6	23.4	25.7	38.1	24.3
Artificial surfaces	2.1	1.8	1.4	2.2	2.0	1.5	1.5	1.8
Water	2.7	2.2	2.8	2.8	3.0	3.0	3.2	2.3

Table 6. 20 Changes in general LULC classes in the **Dano watershed** between 2002 and 2013

LULC	2002	2005	2006	2007	2008	2010	2011	2013
Cropland	34.8	29.2	45.3	26.2	41.1	47.8	49.9	39.7
Forest	20.0	17.4	17.8	17.0	17.0	15.1	14.9	14.7
Mixed vegetation	44.1	52.6	36.1	56.0	41.2	36.1	34.5	44.6
Artificial surfaces	1.1	0.8	0.8	0.8	0.6	0.9	0.7	0.9
Water	0.1	0.2	0.1	0.3	0.2	0.2	0.1	0.2



## Results

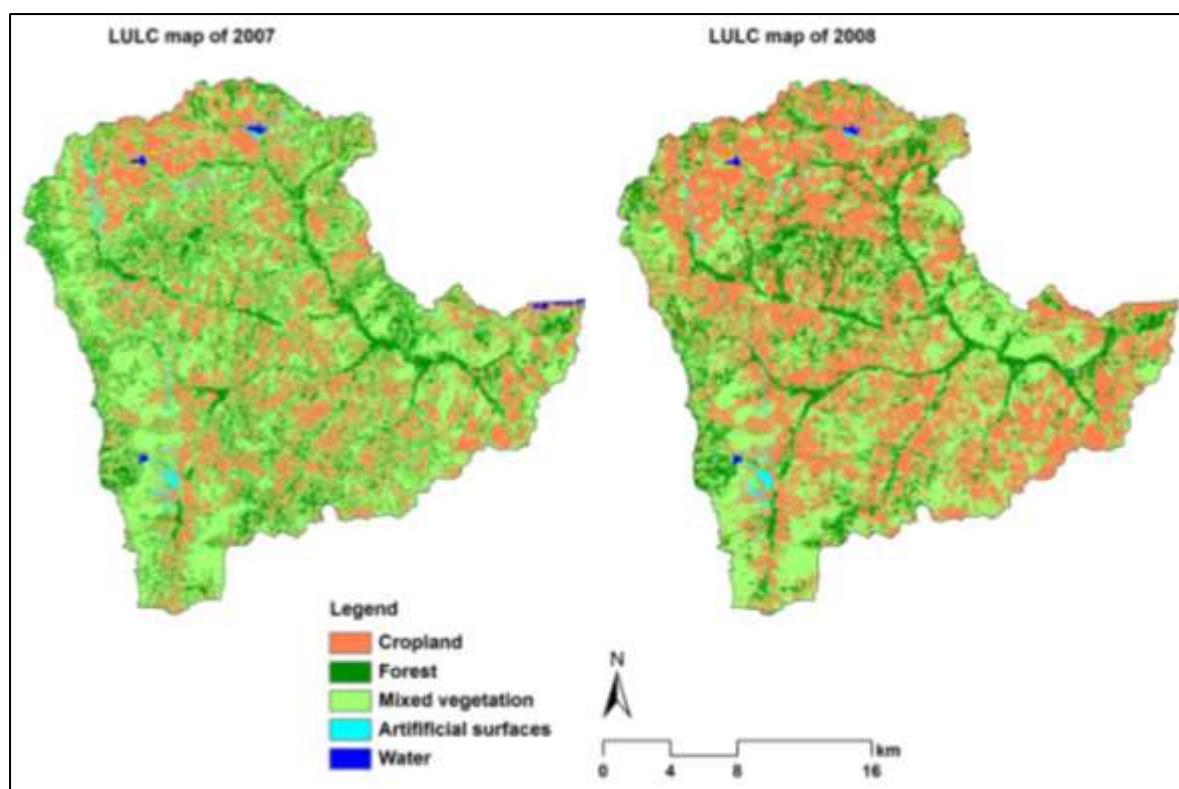


Figure 6. 13 Changes in the major LULC classes in the Dano watershed between 2007 and 2008. Low cropland coverage in 2007 is believed to be as a result of floods that year.

### 6.3 Upscaling of watershed cropland information unto regional scale

Cropland areas detected at Landsat resolution (section 6.2) were upscaled to MODIS resolution by calculating the proportion of cropland per each MODIS pixel using an ensemble of Random Forest regression trees. The resultant cropland fractional cover was independently validated with a portion of the Landsat classification (reference data) that was not used in the regression analysis (Figure 5.14). For each fractional cover map, ten different samples, each containing seven thousand five hundred samples randomly selected from the reference data, were used for validation. Table 6.21 presents the mean and standard deviation of the accuracy estimates obtained for the ten samples for each of the analyzed years. Mean error (ME), mean absolute error (MAE), root mean square error (rmse) and the coefficient of determination ( $R^2$ ) are presented for each fractional cover map.

Table 6. 21 Accuracy estimates derived from the validation of the modeled fractional cover maps.

Year	ME		MAE		RMSE		$R^2$	
	Average*	Std Dev <sup>§</sup>	Average*	Std Dev <sup>§</sup>	Average*	Std Dev <sup>§</sup>	Average*	Std Dev <sup>§</sup>
2002	-0.241	0.207	17.168	0.184	23.197	0.189	0.543	0.008
2005	0.247	0.307	15.416	0.089	19.807	0.154	0.703	0.005
2006	1.255	0.207	14.204	0.096	19.590	0.178	0.601	0.009
2007	-1.228	0.288	17.250	0.112	22.244	0.170	0.622	0.004
2008	-0.858	0.309	19.050	0.170	23.923	0.203	0.561	0.006
2010	0.434	0.192	16.781	0.184	21.717	0.203	0.666	0.007
2011	-0.970	0.198	17.194	0.198	22.085	0.200	0.629	0.008
2013	-0.268	0.274	16.974	0.134	21.557	0.180	0.617	0.007

\* Average of results of ten different validation samples each consisting of 7500 samples

<sup>§</sup> Standard deviation of results of ten different validation samples each consisting of 7500 samples

## Results

---

In general, the low standard deviations observed for the four computed statistics indicate a high level of consistency of the errors inherent in each modeled results. The average ME values indicate that the model results of the 2002, 2007, 2008, 2011 and 2013 cropland fractional cover were, on average, negatively biased. This means that cropland area estimations derived from these products will likely to be an underestimation of the actual area. On the other hand, model results obtained for 2005, 2006 and 2010 were, on average, positively biased, suggesting a possible overestimation in terms of cropland area calculation.

The MAE and RMSE give an indication of the average error of the respective model results. Although the RMSE is an often used statistic in the literature to describe average model error, Willmott and Matsuura (2005) noted that the MAE was a better statistic to describe the average error of a model's results. They argued that the RMSE is a function of three characteristics of a set of errors, which include MAE (the others being variability of the distribution of error magnitudes and square root of the number of errors), and therefore tends to make RMSE values generally larger than MAE for the same set of validation data. RMSE has a lower limit fixed at MAE, while its upper limit is the product of the square root of the number of samples and MAE ( $n^{1/2}MAE$ ) (Willmott and Matsuura 2005). This fact explains the generally higher RMSE values obtained in this study compared to the MAE. However, both statistics depicts a similar pattern of model performance for the years analyzed.

Based on the average MAE, the 2005 and 2006 model results (i.e. fractional cropland cover) achieved the lowest mean error while that of 2008 was the worst. Generally, the positively biased results (2005, 2006, 2010) achieved a lower mean error ( $MAE < 17$ ) than the negatively biased results ( $MAE \geq 17$ ). This can be attributed to the better detection of cropland in the Landsat classifications of 2005, 2006 and 2010, where a producer's and user's accuracy of 90% were consistently achieved for cropland (see Tables 6.17 and 6.18). The slightly higher mean error ( $MAE > 17$ ) of the 2002, 2007 and 2011 model results can similarly be attributed to the relatively lower accuracies achieved in the Landsat classifications. However, the poor performance of the 2008 results ( $MAE = 19.1$ ) was not expected, considering the high overall and classwise (cropland) accuracies obtained in the Landsat classifications.

### 6.3.1 Spatial distribution of croplands at regional scale

Figure 6.14 compare the Landsat classifications of the Veia and Dano watersheds for the year 2010 with the corresponding modelled fractional cover at MODIS resolution. A visual assessment of the figure reveals that the fractional cover maps reasonably replicated the pattern of croplands as depicted in the Landsat classifications. Fractional cropland cover in, and around, the Veia watershed (upper left of figure 6.14) is sixty percent or more, which is comparable to earlier findings in the watershed scale analysis using RapidEye (Table 6.4) and Landsat (Table 6.19). The northern part of the Dano watershed is also depicted as having a slightly higher cropland cover than other parts, which is also in line with earlier findings made at the watershed level analysis.

Most of the vegetated areas detected at Landsat scale were modeled as having a fractional cropland cover of less than 10% (white areas in Figure 6.14). However, other vegetated areas were modeled

## Results

as having a cropland cover of between 10 and 20%. Although there may not be croplands at all in these vegetated areas, the assignment of a fractional cropland cover to these vegetated areas can be explained by misclassifications between cropland and natural vegetation at the Landsat scale. In other words, a wrongful assignment of a vegetated pixel as cropland or vice versa at the Landsat scale could result in such errors. The wrongful assignment of vegetated areas as having crop cover of between 0 and 20% is in with the MAE of the fractional cover maps, which ranged between 14 and 19% (16% for 2010). Consequently, areas with fractional cropland cover of between 0 and 20% are classified as one class in subsequent maps (see Figure 6.15).

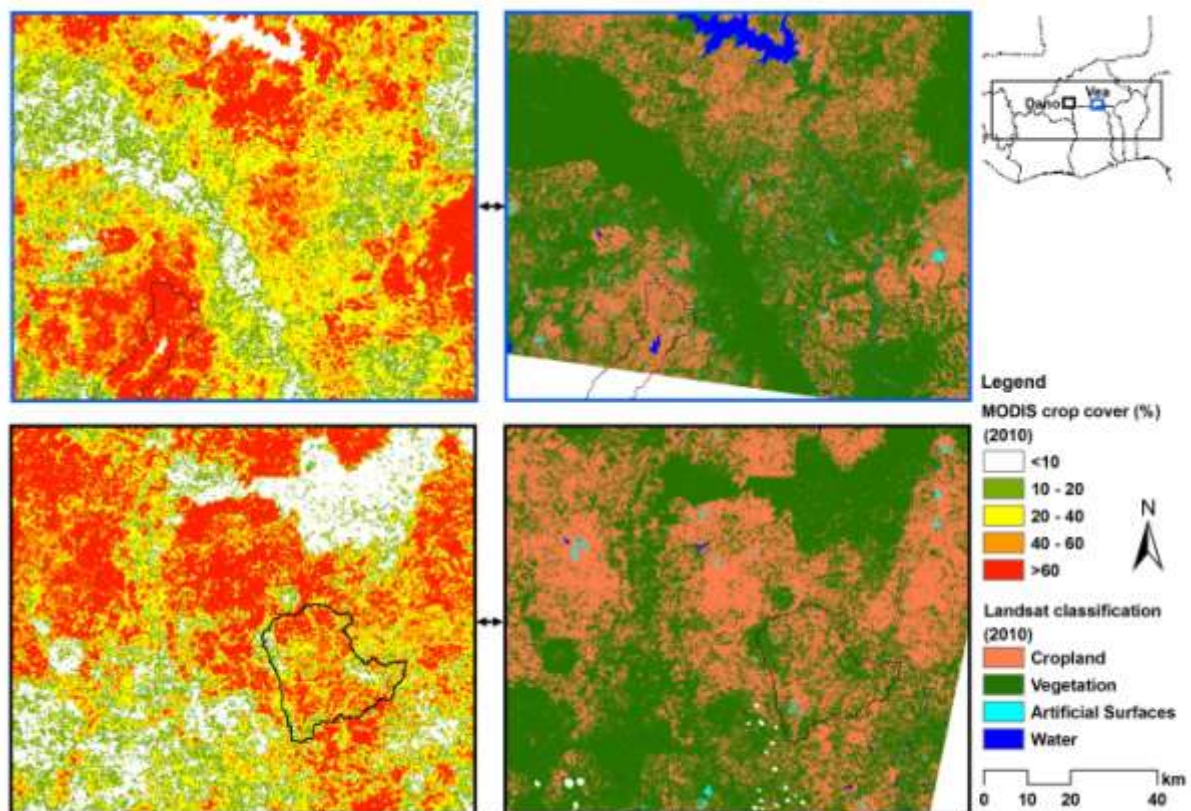
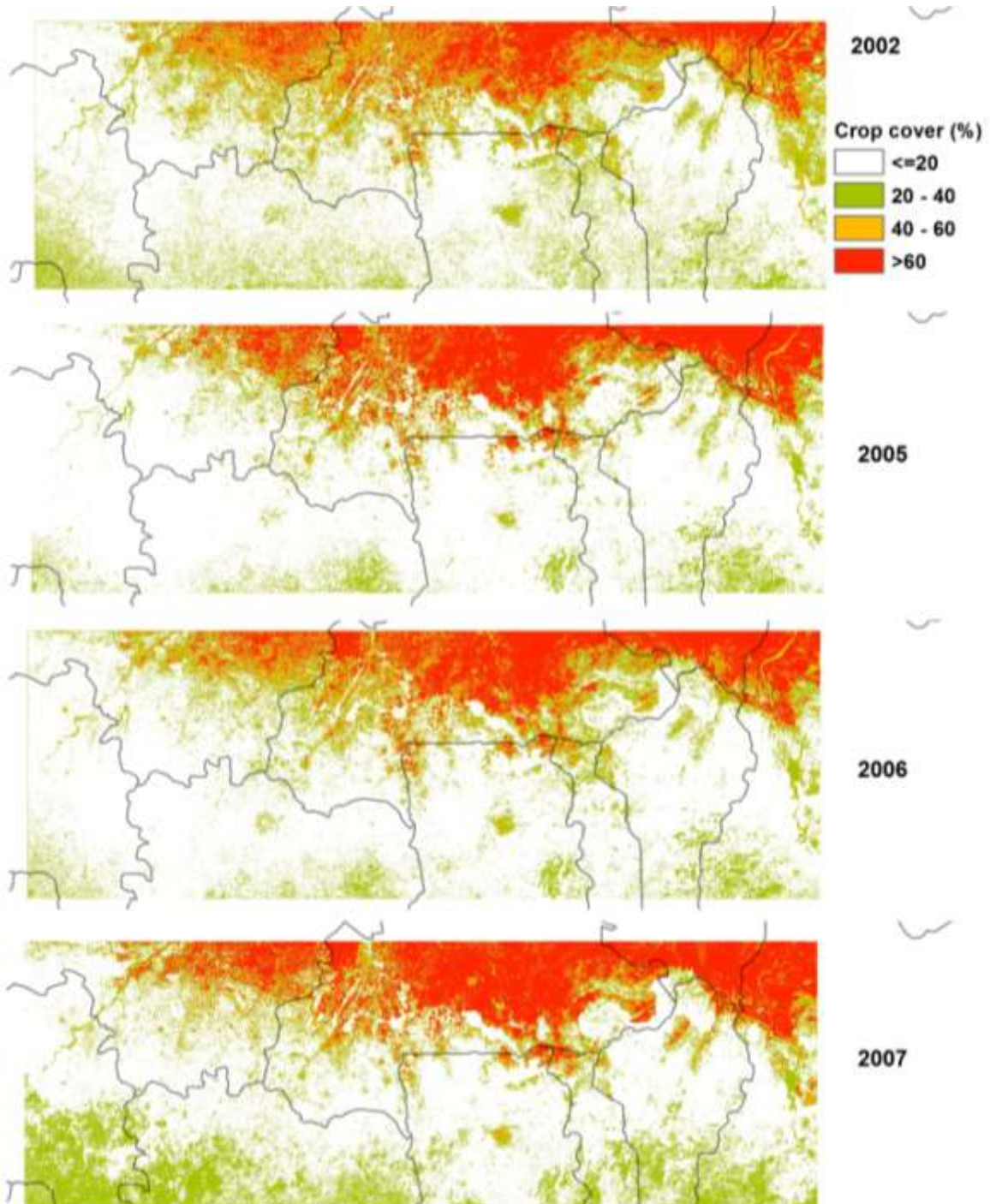


Figure 6. 14 Comparison of modeled cropland cover maps at MODIS scale with corresponding Landsat classification

The spatial distribution of croplands at the regional scale for the years analyzed (2002 to 2013) is shown in Figure 6.15. It can be seen from the maps that the northern part of the Sudanian Savanna region generally has a higher percentage of croplands than the south part. Areas from latitude  $11^{\circ} 30'$  to  $13^{\circ}$  consistently had a fractional crop cover of sixty percent (per MODIS pixel) or more from 2002 to 2013. The 2008 map, however, shows relatively fewer areas in the northern part as having cropland cover of sixty percent or more. This can be attributed to errors in the model (as revealed by the accuracy estimates) and not necessarily a reduction in cropland. On the other hand, the lower portions of the Sudanian Savanna have a lower percentage of croplands compared to the north. Most of the areas south of latitude  $11^{\circ} 30'$  have a cropland percentage (per MODIS pixel) of either below 20% or between 20 and 40%. A visual inspection of Google Earth images confirmed the observed north-south gradient in cropland areas in the Sudanian Savanna. Additionally, comparison

## Results

of the modeled results with other regional LULC maps in Figure 6.16 (i.e. the MODIS V051 - [https://lpdaac.usgs.gov/products/modis\\_products\\_table/mcd12q1](https://lpdaac.usgs.gov/products/modis_products_table/mcd12q1)), largely shows the existence of the north-south gradient in cropland areas, with the northern parts having a larger percentage of croplands than the southern part. Although the legends of the two parts maps are not exactly comparable, the emphasis over here was to highlight the similarities in the cropland distribution.



## Results

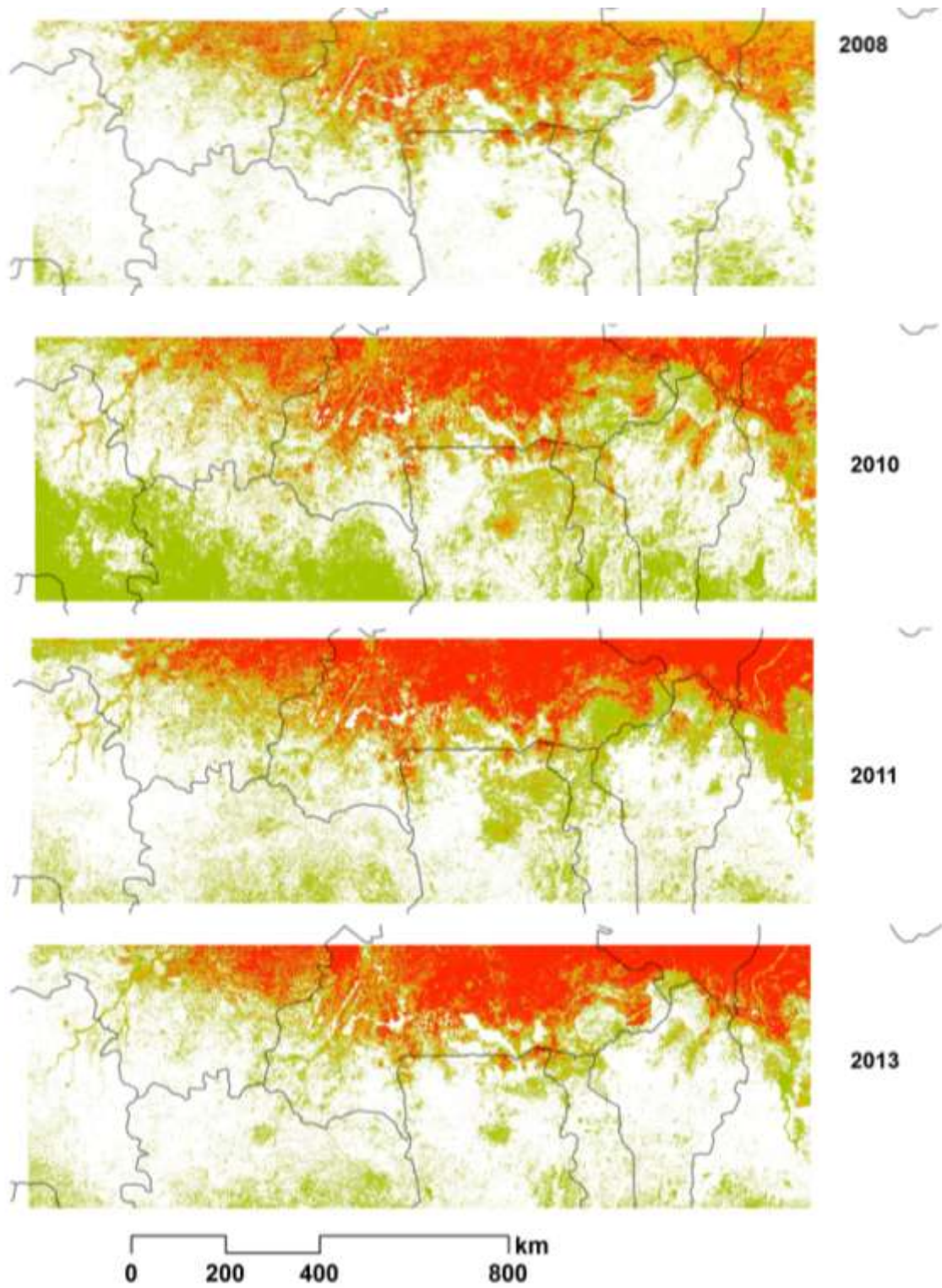
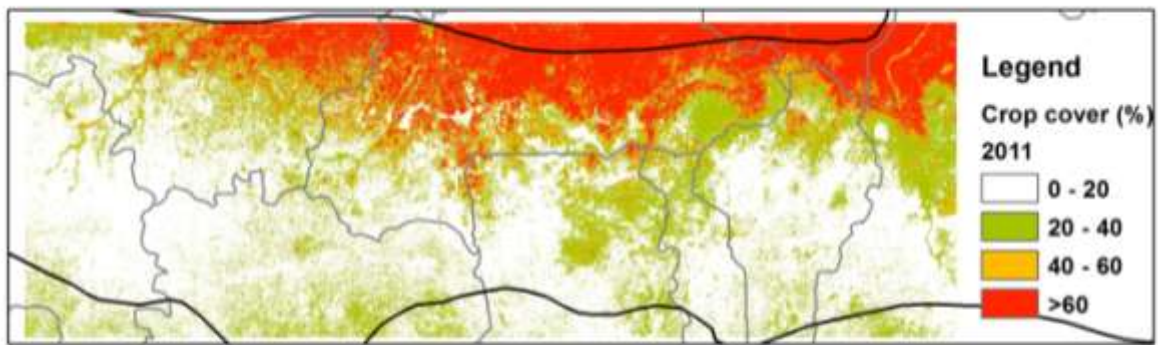


Figure 6. 15 Regional scale cropland distribution maps between 2002 and 2013

## Results

Fractional cropland cover map (2011)



MODIS V051 2011 (MOD12Q1): IGBP classification

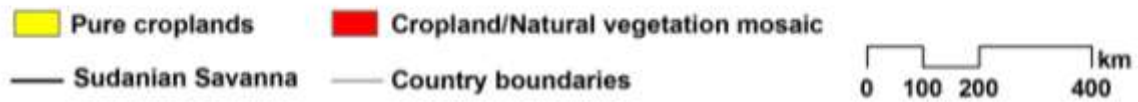
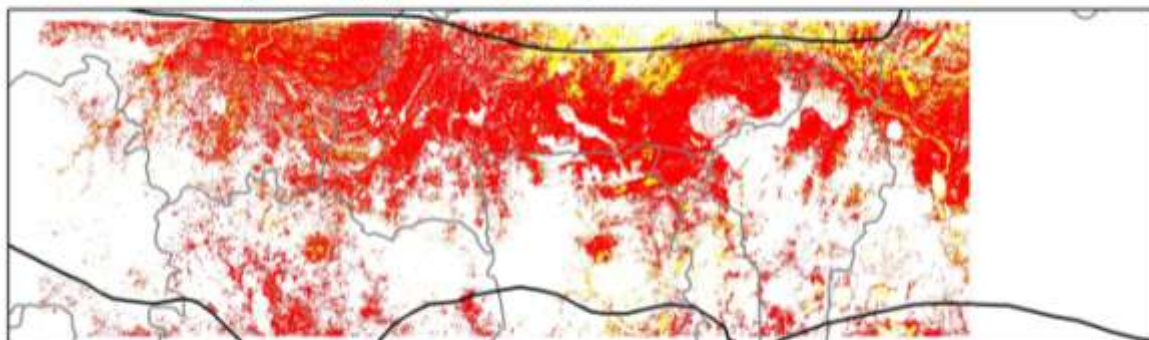


Figure 6. 16 Comparison of fractional cropland cover for the 2011 with the MODIS V051 LULC product of 2011 developed by the MODIS land team.

Figure 6.17 shows regional scale changes in cropland area over the period of analysis (2002-2013). Changes in three different fractional cover categories are presented: (1) cropland cover of between 20 and 40%, (2) between 40 and 60% and (3) greater than sixty percent. Areas having cropland cover of less than 20% was left out due to the confusion with vegetation as explained above. The figure shows a fluctuating pattern for all the categories as witnessed in the watershed scale analysis.

When one considers areas with a cropland cover of greater than 60% (blue line), for example, there was an increase in this category from 2002 to 2005 while a decrease was witnessed in 2006 relative to 2005. This pattern is similar to what was observed in the Veia watershed, and the reverse of the pattern noted in Dano (Figure 6.12). However, the graph shows an increase in the >60% areas from 2006 to 2007, which is the reverse of what was found in the watershed scale analysis using the Landsat classifications (Figure 6.12). This difference (between Landsat and MODIS results) can be attributed to the use of the full annual MODIS time-series in the regression analysis as against the use of only harvest season images in the Landsat classifications. In other words, availability of additional time-steps in the MODIS imagery could have revealed additional information that was not identifiable in the Landsat images. As already alluded to, the low percentage of cropland areas >60% in 2008 can be attributed to the poor modeling results. The graph further shows that areas with cropland cover >60% increased from 2010 to 2011 and decreased between 2011 and 2013. Again,

## Results

this pattern is similar to that observed on Dano in the watershed analysis, while the pattern in Vea is the reverse. Further discussions of the possible causes of these fluctuations are provided in the next chapter.

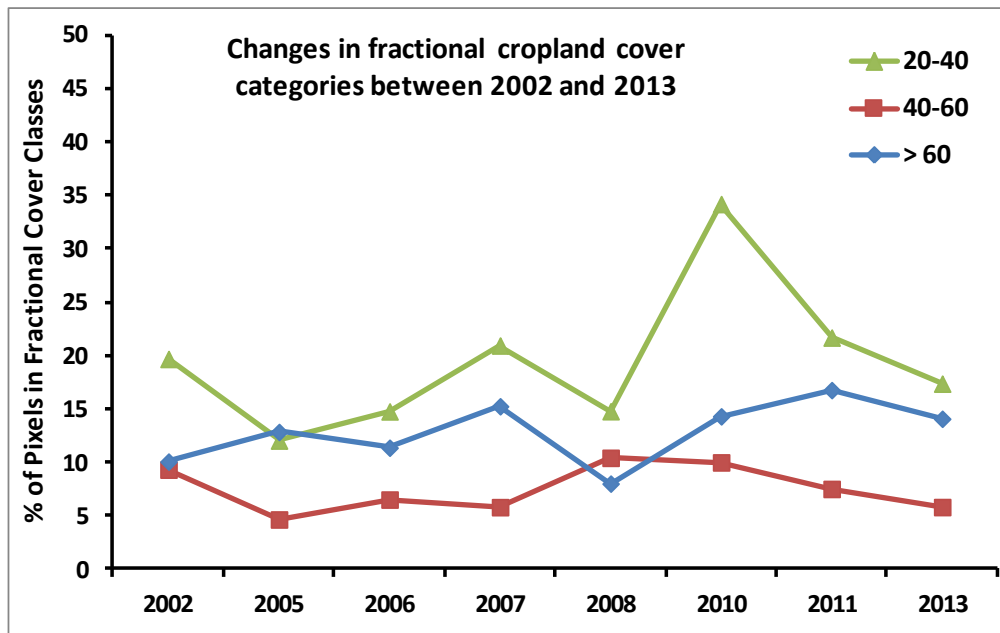


Figure 6. 17 Changes in cropland area in the Sudanian Savanna agro-ecological zone in West Africa between 2002 and 2013

### 6.3.2 Plausibility analysis

Plausibility analysis was conducted by comparing official cropped area statistics obtained from Ghana's Ministry of Food and Agriculture (MoFA) with cropland area estimates derived from the MODIS fractional cover maps. MoFA's statistics (per year) include: (1) crop production (in metric tonnes), (2) cropped/harvested area (in hectares) and (3) yield (in metric tonnes per hectare) for all crops cultivated in each district. For purposes of this comparison, the total cropped area for each district was determined by summing the cropped/harvested area for all crops in the district.

The comparison was done for seventeen districts (second administrative boundary) in the northern part of Ghana (Figure 6.18). Between 2006 and 2012, the number of Ghana's districts has changed from one hundred and ten (110) to two hundred and sixteen (216). Since the agricultural statistics for 2002 and 2005 were reported at the previously 110 level, the comparison in this study was done at that level. Due to unavailability of official statistics for 2006 and 2013, the comparison was done for 2002, 2005, 2007, 2008, 2010 and 2011. Figure 6.19 shows the comparisons between the MoFA and MODIS cropland estimates expressed as a percentage of the district area. The x-axis of the graphs represents the districts under consideration, which have been expressed with abbreviations for clarity (see Figure 6.18 for definitions).

# Results

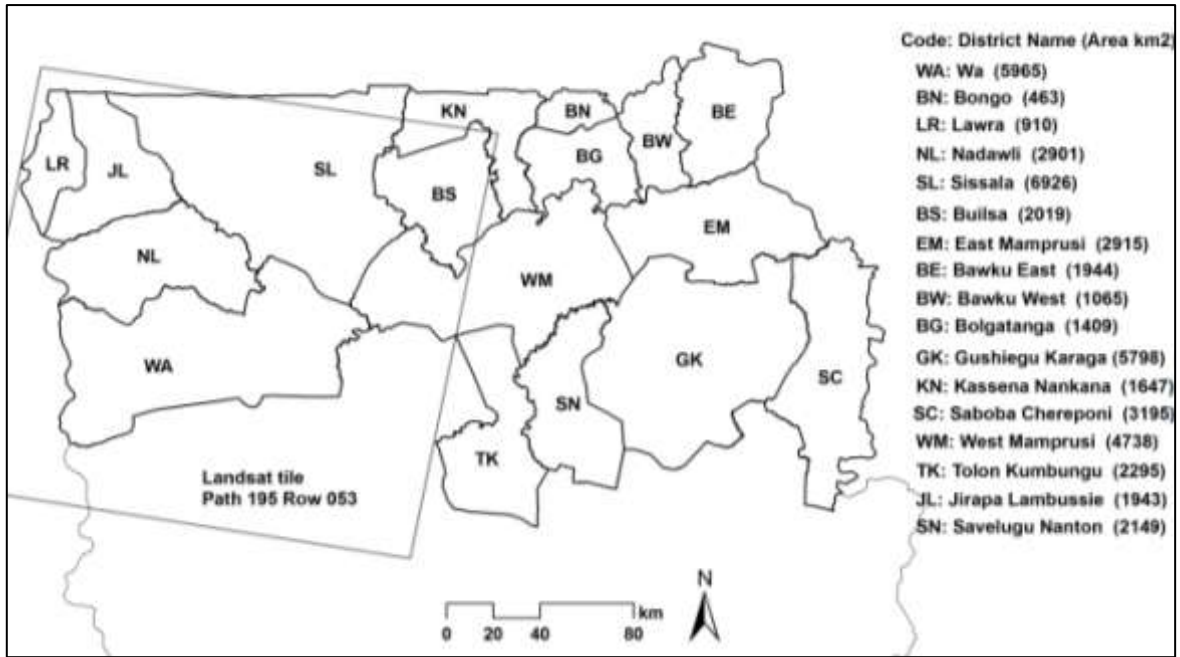
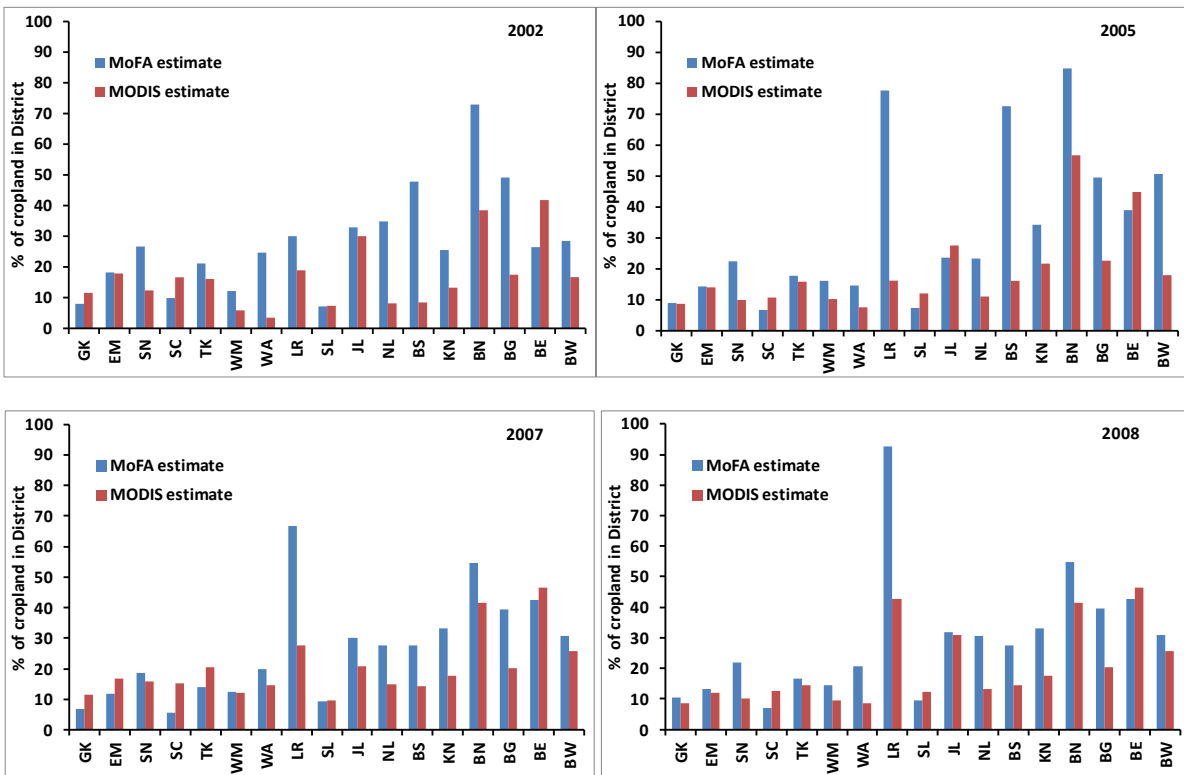


Figure 6. 18 Districts (2nd administrative unit) of Ghana used in the plausibility analysis.





## Results

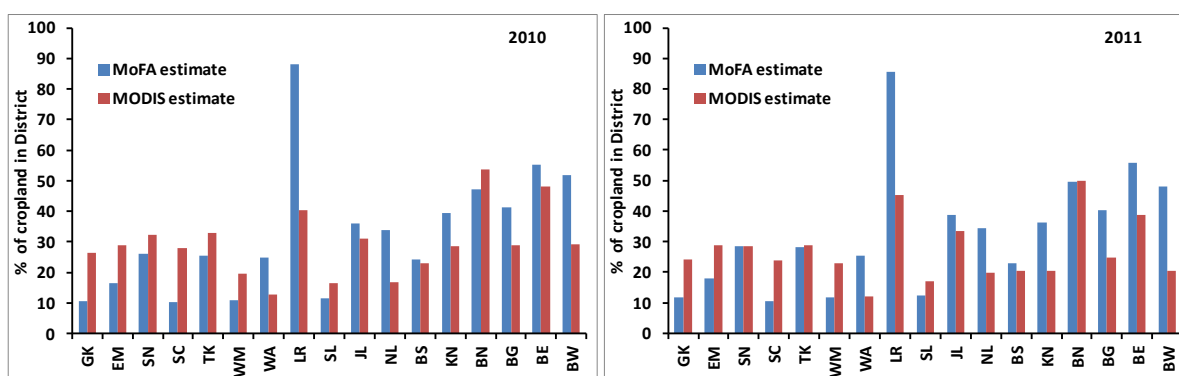


Figure 6.19 Comparison between cropland area derived from the MODIS fractional cover and official cropped area statistics from Ghana's agricultural ministry for seventeen districts in northern Ghana. Cropland area is expressed as the percentage of the district area

The plots show a general disparity between the two estimates, with the MoFA estimates being higher than that of the MODIS in most cases. In seven, out of the seventeen districts (Wa, Lawra, Nadawli, Builsa, Kassena/Nankana, Bolgatanga and Bawku West), the MoFA estimate was consistently higher than the MODIS estimate for all the years analyzed. The difference between the two estimates (i.e. MoFA-MODIS) ranged from 1.1% to 61%. The MoFA estimate for Lawra was consistently very high from 2005 to 2011, constituting about 92%, 88% and 85% of the total district area in 2008, 2010 and 2011 respectively. The difference between some of the districts was relatively high in 2002 and 2005, but reduced significantly from 2007 to 2011. An example is the Builsa district, where the difference between MoFA and MODIS estimates was 39% and 56% respectively for 2002 and 2005, but reduced to 1.1% and 2.6% respectively for 2010 and 2011. The differences in estimates of other districts, e.g. Bawku West, fluctuated between the years, with a value of 33% in 2005, 5% in 2008 and 28% in 2011.

In two of the districts (Saboba/Chereponi and Sissala), the MODIS estimate was consistently higher than that of MoFA for all the years analyzed. However, the differences in this situation were relatively lower. In Sissala for instance, the difference between the two estimates (i.e. MODIS-MoFA) ranged from 0.2% in 2002 to about 5% in 2010.

In the other eight districts (Gushiegu/Karaga, East Mamprusi, Savelugu/Nanton, Tolon/Kumbungu, West Mamprusi, Jirapa/Lambussie, Bongo, and Bawku East), the differences between the two estimates were not consistent. The MoFA estimate was higher than the MODIS estimate in some years while the reverse happened in other years. Generally, the differences for these districts (either way) ranged between 0.1% and 16%, with the exception of Bongo where the MoFA estimate was higher than that of MODIS by about 35% and 28% for 2002 and 2005 respectively. Interestingly, the difference between the two estimates reduced to 6.4% and 0.2% for 2010 and 2011.

The poor agreement between the two estimates, and the inconsistent nature of their differences in most of the districts, suggest that comparison with a third estimate deemed to be accurate than the two is necessary to ascertain the "correctness" or otherwise of the MODIS/MoFA estimates.

## Results

---

Datasets that are available for such purposes are global LULC datasets (GLC2000, MODIS V05, GLOBECOVER, etc.) that cover the whole of West Africa. However, these datasets have already been noted to have errors (Vintrou *et al.* 2012). Therefore, an additional classification of Landsat data was carried out for this purpose. The Landsat tile classified (Path 195, Row 53) covers almost five, out of the seventeen, districts considered in the comparison (see Figure 6.18). A small portion of the Sissala district is not covered by the tile. The aim of this extra classification was to derive a crop mask and subsequently use the extracted cropland area for the five districts as reference with which the corresponding MoFA and MODIS estimates were compared. A Landsat ETM+ image acquired in 2002 was classified. Unavailability of good images (i.e. SLC-on or TM) between 2003 and 2012 was the main reason for considering only the image of 2002.

Figure 6.20 compares the Landsat derived statistics against the MoFA and MODIS estimates for the five districts within the Landsat tile (path 195, row 53). The Landsat estimate for the Sissala district is expected to be slightly lower than the actual because the Landsat scene did not fully cover the district (Figure 6.18). The figure shows that, compared to the Landsat estimates, the MODIS fractional cover (for 2002) consistently underestimated the total cropland area for the five districts. This is not surprising, because the validation results for this product showed that it was negatively biased (ME = -0.241). However, the underestimation varied from 29% in Wa to 43% in Sissala, with an average underestimation (for all five districts) of 38%. This indicates a major challenge of the fractional cover map in correctly estimating district level cropland area.

Comparison of the Landsat estimates with the MoFA estimates did not reveal a consistent pattern. In two of the districts (Wa and Nadowli), the MoFA estimates were higher than that of the Landsat (overestimation), while the reverse (underestimation) occurred in three districts (Lawra, Sissala, Jirapa). The overestimation of MoFA estimates relative to the Landsat were 55% and 45% respectively for Wa and Nadowli, while the underestimation were 12%, 39% and 62% for Lawra, Jirapa and Sissala respectively. This apparent inconsistency in the MoFA estimates can be attributed to the independence of the MoFA staff in each district to estimate the cropped area with little coordination from the national office. Differences in the methods and gadgets used (e.g. GPS or compass/tape) as well as varied financial and logistical constraints across the different districts could lead to the inconsistencies in the estimation of cropland area in the districts. Further discussion of these constraints, and the possibilities of improving the statistics using satellite derived estimates, are provided in the next chapter.

## Results

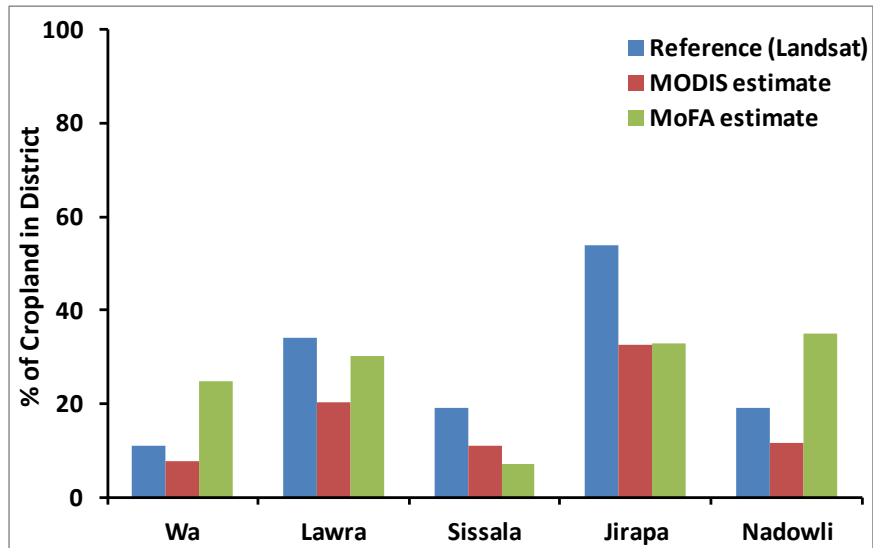


Figure 6. 20 Comparison of Landsat, MODIS and MoFA cropland area estimates for five districts in northern Ghana

### 7. Discussion of Results

This section discusses the results presented in Chapter 6. It is divided into three main sub-sections. The first (7.1) deals with the watershed level results obtained for mapping crops and crop groups. It discusses challenges in crop mapping in West Africa and points out the advantages of the implemented classification approach. The ease or difficulty in mapping the different crop types is further discussed. The second sub-section (7.2) discusses results obtained for mapping croplands at watershed scale. Possible reasons for the fluctuation in cropland area between 2002 and 2013 are discussed. The last sub-section discusses the spatial distribution and pattern of croplands within the Sudanian Savanna region. It also discusses the comparison between district level crop area estimations derived from the regional scale fractional cover maps and official statistics from the government of Ghana. Limitations of the fractional cover maps are discussed, and possible solutions proffered.

#### 7.1 Crop mapping at watershed scale

##### 7.1.1 Challenges in crop mapping

###### 7.1.1.1 Crop calendar overlaps and variable planting dates

An underlying challenge to crop separability that was identified in all classifications is the overlap of the cropping calendars of most crops considered in the respective watersheds. The reliance of agriculture in the sub-region on rainfall means that all crops are cultivated in a single cropping period which coincides with the rainy season. In addition, variable planting dates often lead to similarities in the spectral profiles of different crops and differences in the spectral profiles of same crops (Forkuor *et al.* 2014). But the identification of unique crop spectral profiles is essential for the success of crop mapping (Odenweller and Johnson 1984). Reasons for the prevalence of variable planting dates in most places in Africa have been discussed by a number of studies (Cooper *et al.* 1987, Kamara *et al.* 2009). Hassan (1996), for example, identified three reasons that could lead to variable planting dates for the same crop: (1) farmers who own tractors or oxen are able to prepare their lands faster and can therefore plant earlier than those who have to do it manually or rent a tractor or oxen; (2) farmers who have large families, and therefore, ready availability of labor, may be able to plant earlier than a farmer with a relatively small family; (3) farmers who have plans of planting multiple crops on the same land may start cultivation earlier than those who practice mono-cropping. These factors are applicable in the study watersheds, and led to confusion between most of the crop classes investigated.

Previous crop mapping studies conducted in other parts of the world also noted challenges owing to overlaps in the cropping calendars of certain crop types (Quarmby *et al.* 1993). In a study in south-eastern Australia, Van Niel and McVicar (2004), noted that an overlap in the planting dates of maize on the one hand and rice and sorghum on the other was a limiting factor in accurately mapping these crop classes. This overlap, they found, was as a result of the cultivation of early and late maize by farmers, resulting in a long planting date window for maize (90 days). In another study in Canada,

McNairn *et al.* (2009) found that variances in the planting dates of cereals (wheat, barley, oats) led to significant confusion between the individual cereals classes due to differences in the phenological stages of fields belonging to each of the cereals classes. Peña-Barragán *et al.* (2011) also attributed the major confusion between some summer crops (safflower, sunflower and tomatoes) to similarities in their development stages and cropping calendar.

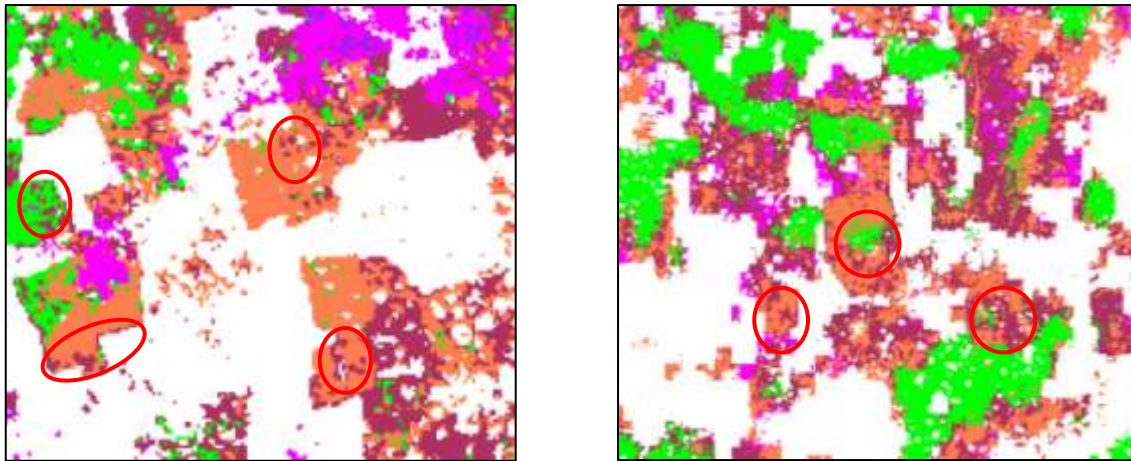
Despite the challenge of cropping calendar overlaps, the implemented approach, and availability of satellite imagery (optical and radar) for the whole cropping season, achieved good separability for most of the crop classes considered in the respective watersheds.

### **7.1.1.2 Landscape heterogeneity and per-pixel classification**

All classifications conducted in this study were based on an evaluation of the spectral information contained in each individual pixel (per-pixel classification). This means that the spatial context of a pixel under consideration is ignored (Myint *et al.* 2011). The use of this approach in classifying images often result in a "speckled" output, with pixels of other classes found within fields of a different class. This situation is even pronounced when SAR data are involved. Figure 7.1 (red ellipses) demonstrates the effects of the per-pixel approach on the classification results. In Dano and Dassari, maize and cereals pixels were frequently mixed as wells as rice and yam pixels. The figure reveals that the use of per-pixel classification in the study contributed to the lower classwise accuracies achieved for some crop classes (e.g. maize, cereals, yam, etc.).

High spectral within-field heterogeneity, which could be caused by variations in soil fertility, soil moisture conditions and pest or diseases, often results in a classifier assigning different classes to pixels in the same field (Smith and Fuller 2001, De Wit and Clevers 2004). In West Africa, the heterogeneity of the landscape (Cord *et al.* 2010) and frequent intercropping aggravates this situation. Several studies have overcome this challenge by adopting a per-field classification in which results of a per-pixel classification was overlaid with field/parcel boundaries and assigning the modal class within each field as its class (Berberoglu *et al.* 2000, Turker and Arikan 2005, Conrad *et al.* 2010). This ensures that each field is assigned only one crop class, thereby removing the "speckled" effect. Several studies that adopted this approach noted an increase in classification accuracies (Lobo *et al.* 1996, Tso and Mather 1999, Ban 2003, Blaschke *et al.* 2008). Thus, the accuracy of the classifications in this study could be improved by adopting a per-field classification approach.

## Discussion of Results



Legend: Green = Cotton; Coral = Cereals; Magenta = Rice; Maroon = Maize

Figure 7. 1 Demonstration of the effects of per-pixel classification in Dassari (left) and Dano (right).  
Emphasis on red circles

But, per-field approaches require the availability of a topographic vector database of field boundaries. This is a major limitation for the implementation of such approaches in most parts of West Africa, since vector databases of field boundaries do not exist. In such instances, similar information has been obtained through segmentation of high resolution images (Conrad *et al.* 2013). However, the heterogeneity of the landscape in most of West Africa makes it largely unsuitable for image segmentation, especially for crop mapping (Lobo *et al.* 1996, Zhou *et al.* 2014). In Veve, for example, the irregular shape of most fields as a result of cultivation around hamlets poses a challenge. Additionally, there is poor spectral contrast between the boundaries of adjoining fields due to the high spatial contiguity of the fields, with no clear boundaries. This situation could lead to poor segmentation results. In Dano, the presence of trees on fields is the main limitation to image segmentation (Figures 7.2). Excessive tree coverage results in different coloration within fields, which can lead to high incidence of over-segmentation.

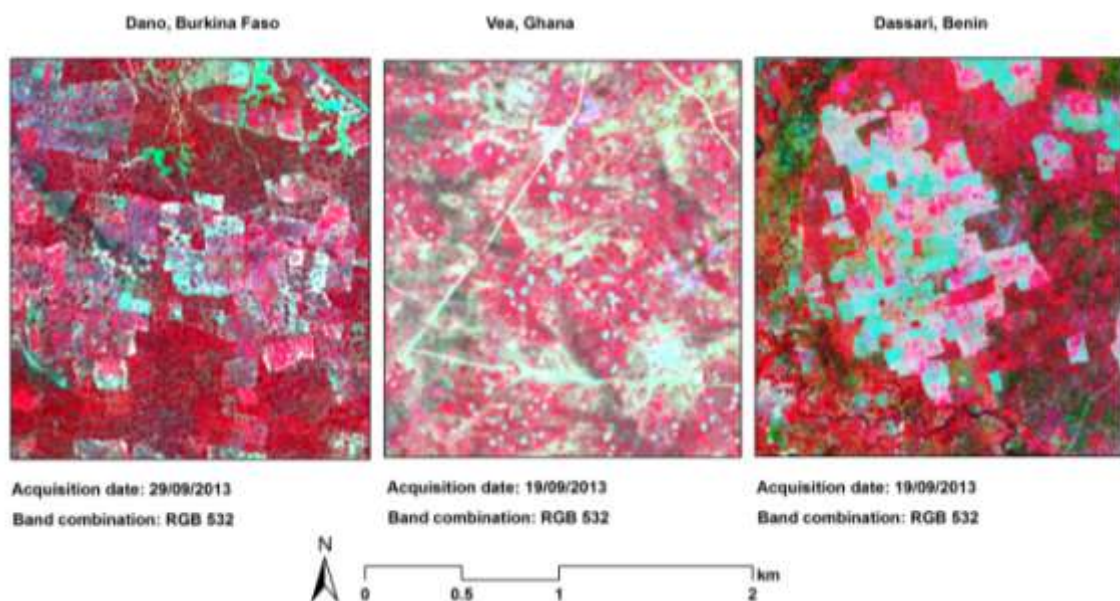


Figure 7. 2 Suitability of the watershed's landscape for segmentation

In Dassari, however, the presence of regularly shaped fields with fewer trees on them makes it relatively suitable for image segmentation (Figure 7.2). Forkuor *et al.* (2014), for example, successfully implemented a per-field classification in this watershed by overlaying a per-pixel classification results on field vector boundaries generated through segmentation of a high resolution RapidEye image. They achieved a better overall accuracy (75%) than has been obtained with the per-pixel classification in this study (65%), which is a confirmation of findings of previous studies (Lobo *et al.* 1996, Tso and Mather 1999, Ban 2003, Blaschke *et al.* 2008). This suggest that, West African landscapes that have regularly shaped fields with fewer trees can benefit from the use of per-field approaches since image segmentation can be performed using high spatial resolution images. However, unsuccessful attempts to apply field based approaches to the highly heterogeneous landscapes of Dano and Vea suggest that most of the heterogeneous landscape in West Africa may be better mapped using per-pixel approaches.

### 7.1.2 Advantages of sequential masking classification

The implementation of a sequential masking classification approach largely overcame the problem of cropping calendar overlaps and improved the identification of crops and crop groups in the study watersheds. Compared to the one-time classifications (where all crop classes were classified at the same time), the sequential masking classifications improved overall classification by between 6 and 9%. The improvement in the overall classification accuracy can be attributed to two main aspects of the sequential masking approach. (1) the initial determination of optimal temporal window(s) for discriminating individual crop classes prior to classification and (2) sequentially classifying the different crop classes based on the optimal temporal windows in (1) above.

Preliminary classification of all possible permutations of available images provided information on the best image combination/temporal window(s) for discriminating the individual crop classes. This ensured the attainment of the best classwise accuracy obtainable for each crop class. The need to determine the optimal temporal window(s) for discriminating individual crop classes was already noted by previous studies to be essential for improving overall crop classification accuracy (Dawbin and Evans 1988, Murakami *et al.* 2001, Niel and McVicar 2003). For example, based on separability analysis involving nine multi-temporal SPOT images, Murakami *et al.* (2001) found that individual crop classes were better discriminated using different images acquired at varying stages of the cropping season. They found that the segmentation of available imagery is necessary to ensure accurate discrimination of different crop types and subsequently improve overall classification accuracy. Consequently, they found that only four, out of the nine images, could achieve results comparable to that achieved when all nine images were used in the classification. Conrad *et al.* (2014), based on the cropping calendar of crops in the Khorezm region, also conducted a careful segmentation of nine RapidEye images and found that five, out of nine RapidEye scenes, were sufficient to achieve optimal crop discrimination. They noted that individual crop classes were better discriminated with different images/image combinations acquired at various stages of the cropping season. However, the above mentioned studies conducted a one-time classification of all the crops under investigation using the best image combinations earlier determined.

## Discussion of Results

---

In this study, the coupling of a sequential masking approach with information on the optimal images for discriminating individual crop classes was found to have further improved the overall classification as well as the classwise accuracy of all crops. This improvement in accuracy owing to the sequential masking approach confirms the findings of earlier studies that used similar approaches in crop mapping in other parts of the world. For example, based on initial single date classification of seventeen Landsat images acquired throughout the cropping season, Van Niel and McVicar (2004) were able to determine the best temporal window (or image combination) for discriminating four different crops in Australia. They showed that an iterative (or sequential) classification of the crops based on the respective image combinations previously identified increased classification accuracy by between 6 and 12% compared to a standard (or one-time) classification of all the crops. They found that the sequential masking approach improved the classwise accuracy of certain crop classes that exhibited confusion when a one-time classification of all crops was conducted. This fact was also evident in this study when the classwise accuracy of rice and yam (in Dassari watershed) increased in F1 score by 0.22 and 0.18 respectively (Table 6.15) when the sequential masking results were compared to that of the one-classification. Turker and Arikan (2005) also emphasized the advantages of performing sequential masking on different image dates acquired in line with the phenological evolution of different crops. They observed an improvement of 10% in overall classification accuracy compared to one-time classification of the respective image dates.

Despite their advantages, the sequential masking approach can lead to poor results due to the propagation of errors from one classification level to the other (Van Niel and McVicar, 2004; Turker and Arikan, 2005; Forkuor et al., 2014). Since each classified crop is masked out from the images, it is important to ensure that classes that are masked in the initial steps of the classification scheme are classified with a high accuracy. High classification errors in the initial classes that are masked may propagate to other classes that will be classified later and thereby lead to poor overall results. Consequently, Van Niel and McVicar (2004) suggested that the sequential masking approach may work best when the crop classes to be discriminated are few. This was mainly the case in this study, where the first two classes in Vea (rice, legumes) and Dano (rice, cotton) were accurately classified with an F1-score of more than 0.85. This means that little errors were propagated to the other classes. In Dassari, however, the first two crops (rice, cotton) masked out achieved a relatively low accuracy (F1 score = 0.75; 0.71). This could have contributed to the relatively poor overall results obtained for the Dassari watershed compared to Vea and Dano.

### 7.1.3 Crop separability

This sub-section discusses the ease or difficulty of mapping the different crop classes in the respective watersheds and West Africa in general. In particular, the contribution of the SAR data (TSX) in improving the accuracy with which the classes were mapped is highlighted. Due to persistent cloud cover in the tropics, and the inability of optical systems to acquire useful images, the contribution of SAR data in crop mapping is of paramount interest. All discussions are based on



Tables 6.10 and 6.12 in the results chapter, which reports accuracy estimates for the sequential masking classification involving optical and radar data.

### Rice and Yam

Rice achieved the highest classwise accuracy in all watersheds. F1 scores of 0.79, 0.88 and 0.92 were achieved in the Vea, Dano and Dassari watersheds respectively. Producer's and user's accuracy of 84% and 75% respectively were achieved for Dassari, 89% and 88% respectively for Dano and 90% and 95% respectively for Vea. In Dassari, yam was the class most confused with the rice class, with about 11% of rice pixels wrongly labelled as yam. This confusion can be attributed to the intercropping of rice on some yam fields as explained in section 5.3.2. The highest confusion with rice in Vea came from the cereals class, with 8% of rice pixels wrongly classified as cereals. This confusion occurred mostly in the Vea irrigation command area, where the predominant crop cultivated is rice. In Dano, 12% of maize pixels were wrongly classified as rice. This was mainly due to occasional cultivation of maize in inland valleys, where soil fertility is normally high. Minimal confusion occurred between rice and cereals in Dano, where about 6% of rice pixels were wrongly classified as cereals. This minimal confusion was found to have occurred due to the misclassification of an upland rice field as cereals.

The relatively high classwise accuracy obtained for rice (compared to other classes) in all the watersheds can be attributed to the cultivation of rice in flooded fields which make it easily distinguishable from other land cover or crop classes due to the effect of water in the NIR channel (McCloy *et al.* 1987, Casanova *et al.* 1998, Van Niel and McVicar 2001). Additionally, the relatively high reflectance of rice fields during or immediately after harvest (Figures 5.2 and 5.4) enabled a better discrimination of the crop. The inclusion of SAR data in the classification further improved the accuracies achieved for rice. Several studies that used SAR data (RadaSat, ENVISAT, TerraSAR-X) to map rice fields identified the distinctive backscatter response of inundated vegetation that enables an easy discrimination of rice fields from other crops and land uses (Kurosu *et al.* 1997, Shang *et al.* 2009, Zhang *et al.* 2009, Bouvet and Le Toan 2011, Koppe *et al.* 2013).

In this study, for example, the inclusion of SAR data improved the discrimination between the rice and yam classes in the Dassari watershed compared to when only optical data were used. F1 scores of rice and yam increased from 0.69 and 0.49 respectively when only optical data were included in the classification (sequential) to 0.79 and 0.65 respectively when SAR data were included in the classification. Table 6.7 indicates that, three, out of the four, available SAR time-steps (in Dassari) were included in the image combination that produced the best F1 score for the yam class. The sensitivity of radar systems to land surface characteristics, such as soil moisture and roughness (Aubert *et al.* 2011) is a possible reason for the improved separation between the two classes when SAR data were included. Due to the cultivation of yam in mounds (soil heaps, see Figure 5.5), these fields have a rougher surface characteristic compared to rice-only fields. Thus, backscatter intensities are expected to be higher for yam fields than rice. Moreover, a distinction between "broad leafed" and "fine/narrow leaf" have been made by some studies that used SAR data for crop mapping and noted to be useful in separating certain crop types (Soria-Ruiz *et al.* 2009, Bargiel and Herrmann

## Discussion of Results

2011). Broad-leaved crops have higher backscatter intensity than fine-leaved crops, due to a high absorption of the radar signal in the latter (Macelloni *et al.* 2001). In this regard, yam, which can be categorized as broad leaf, will have higher backscatter intensities than rice, which can be considered as fine leaf. Figure 7.3 shows a feature space plot of the July TSX VV and VH intensities for rice and yam in the Dassari watershed. The figure shows higher intensity values for most yam fields compared to rice, which is believed to have contributed to a better separation between the two classes.

Previous crop mapping studies also reported relatively high accuracies for rice and noted the relative ease with which rice was discriminated based on the factors highlighted above. Barbosa *et al.* (1996) used Landsat 5 data to map nine crops (including maize, wheat, rice, winter cereal, etc.) and found that, rice achieved the highest classification accuracy among all the other crops based on producer's and user's accuracy. Rice achieved a high producer's and user's accuracy of 80% and 100% respectively in another study conducted by Turker and Arikan (2005). In a recent study in the Khorezm region of Uzbekistan, Conrad *et al.* (2014) noted that rice was one of the crops that achieved the highest classification accuracy (the others being cotton and wheat).

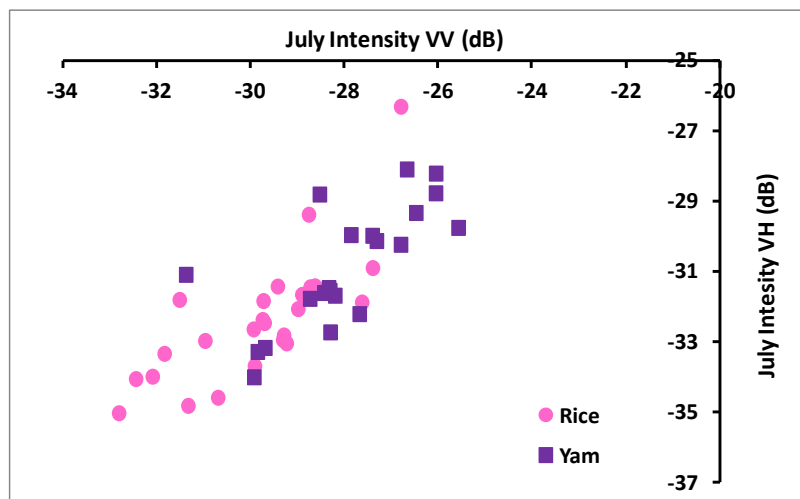


Figure 7. 3 Feature space plot of yam and rice fields in the Dassari watershed using the July VV and VH TSX intensities. Each point represents the average values in a field

### Cotton

In Dano and Dassari, cotton achieved the second highest classwise accuracy (after rice). F1 scores of 0.83 and 0.74 were obtained for Dano and Dassari respectively. Producer's (user's) accuracy of 76% (91%) were achieved for Dano while 75% (73%) were achieved for Dassari. Classes that had the highest confusion with cotton in both watersheds were cereals and maize. This confusion was reported by other crop mapping studies (Conrad *et al.*, 2014). On the other hand, very minimal confusion was found between cotton and rice (or yam). In Dassari, 25% of cotton pixels were wrongly classified as maize (14%) or cereals (11%) while 17% and 10% of maize and cereals pixels respectively were wrongly classified as cotton. Similarly, 24% of cotton pixels in Dano were wrongly

## Discussion of Results

---

classified as maize (12%) or cereals (12%) while 6% and 1% of maize and cereals pixels respectively were wrongly classified as cotton. There are two possible reasons for this confusion: (1) overlaps between the cropping calendars of the three crops as discussed above could easily cause one crop type to be mislabeled as the other, and (2) the three crops are mostly cultivated on uplands (although occasionally in valley buttons, especially maize) with their boundaries normally adjoining each other.

Despite these challenges, differences in the bio-physical characteristics (e.g. canopy moisture, leaf area and level of greenness) of cotton and maize/cereals in the optical feature space and differences in the canopy architecture (e.g. leaf shape and size) of the crops in the SAR feature space allowed for a reasonably good discrimination of cotton from maize/cereals in the two watersheds (Dano and Dassari). When only optical data were included in the classification (sequential), an F1 score of 0.54 and 0.68 respectively were achieved for cotton in Dano and Dassari. The better accuracy in Dassari can partly be explained by the late cultivation of most maize fields in this watershed, compared to Dano where cultivation of all crops started around the same time. Thus, maize and cotton (in Dassari) were likely at different developmental stages by the middle of the season (September). This enabled a better discrimination between cotton and maize in Dassari using optical images acquired in mid to late season, compared to Dano, where the cultivation of most cotton and maize fields around the same time lead to similar developmental stages and hence difficulty in separating the two classes using optical imagery.

In this regard, the sensitivity of radar systems to different canopy structures (leaf shape and size) greatly improved the separation of the cotton and maize/cereals classes, since these two crops essentially have different canopy architectures. In particular, the X-band TSX (which was used in this study) has been noted to be highly sensitive to vegetation canopy due to its relatively shorter wavelength and low penetration depth (compared to, e.g., C-band Radarsat and L-band ENVISAT). Studies that used TSX for the classification of agricultural areas highlighted its capability to observe small-scale vegetation changes due to its lower penetration depth (Baghdadi *et al.* 2010, Bargiel and Herrmann 2011, Lopez-Sanchez *et al.* 2011), and subsequently achieve better results than other radar sensors such as the C-band Radarsat-2 (Shang *et al.* 2009). Thus, the integration of the TSX data (with the optical), especially those acquired at crop maturity stages (August, September), provided additional information that resulted in improved classwise accuracies for cotton in the two watersheds. In Dano, for instance, the F1 score of cotton increased from 0.54 when only optical images were used to 0.83 when optical and SAR data were used. A corresponding increase 0.68 to 0.74 was observed for Dassari. In order to demonstrate the contribution of the TSX to the discrimination of the cotton class from the maize/cereal classes, a feature space plot of the August and September VV and VH intensities for all the crop classes (cotton, maize, cereals, rice) in the Dano watershed has been presented in Figure 7.4. The figure shows the potential of TSX images acquired during mid to late season (August, September) to discriminate crops with different canopy structures. The plots show that generally, cotton and rice can be reasonably well discriminated whereas maize and cereals are comparatively inseparable due to similarities in their structure.

## Discussion of Results

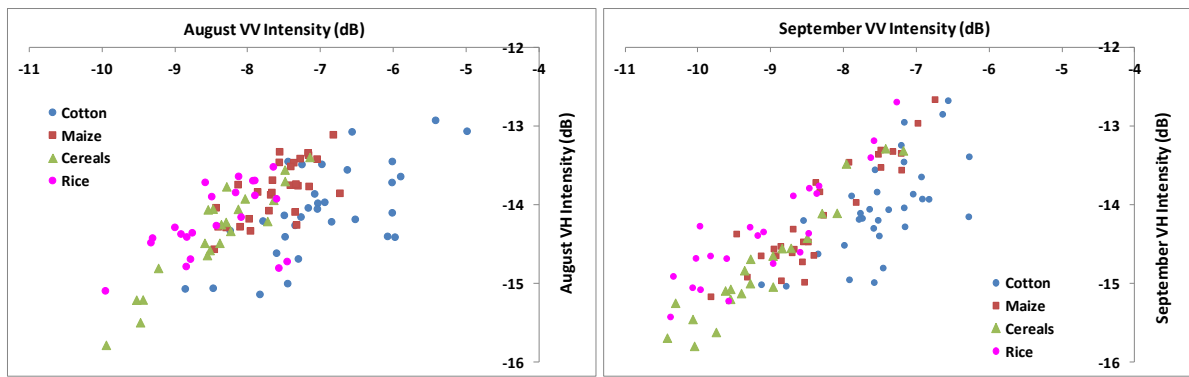


Figure 7. 4 Potential of the TSX image acquired in August (left) and September (right) to separate cotton from other crop classes in the Dano watershed. Each point represents the mean values in each field.

### Cereals and Maize

The accuracy with which maize and cereals were mapped varied for Veia (on the one hand) and Dano and Dassari (on the other).

In Veia, cereals were discriminated with a good accuracy, achieving the second highest F1 score of 0.87 (after rice). Producer's and user's accuracy were both 87%. Even when only optical images were used in the classification, a good F1 score of 0.77 was achieved. The inclusion of the SAR data, therefore, moderately improved the classwise accuracy (F1 score) of cereals in Veia by 0.1. Structural differences between cereals and certain crops (e.g. rice), especially at maturity stage, was the main reason for the improvement in the classwise accuracy when SAR data was included. There was minimal confusion between cereals and other crops in the Veia watershed. Nine percent and 4% of cereals pixels were wrongly classified as legumes and maize respectively. The confusion with legumes was found to have occurred along the edges of some cereal fields that border legume fields. Additionally, one cereal field within a legume dominated area was misclassified as legumes. A possible explanation for the good detection of cereals in Veia is the early ploughing of cereal fields compared to other crops. Most cereal crops are ploughed early (late April to June) due to the cultivation of an early maturing millet, which is often intercropped with late maturing sorghum. Farmers harvest this millet in the middle of the season (August), which serves as an early source of food for the household. Thus, the general late cultivation of legumes and maize in this watershed resulted in a slight shift in the cropping calendar of these crops. However, some farmers also cultivate late maturing millet, for which land preparation can be done latter in the season.

Unlike cereals, maize achieved the lowest F1 score of 0.69 in the Veia watershed. Producer's and user's accuracies were each 69%. This relatively low classwise accuracy of maize can be attributed to two factors. First is an overlap in the cropping calendars of maize and legumes, which resulted in a higher confusion between the two classes than between cereals and rice. Maize and legume fields in the watershed were generally ploughed at the same time (late July to early August), which resulted in similarities in their development stages and a possible confusion between them. The use of only

## Discussion of Results

the RE time-series for classification resulted in even high confusion between the two classes, with about 40% of maize pixels being wrongly classified as legumes. This means that the RE images acquired during crop maturity stages (September, October) was unable to adequately separate the two classes due to similarities in their phenological profiles. Integration of the TSX data acquired in September and October improved the separation between the classes. F1 score improved from 0.14 when classification was performed with only optical to 0.69 when SAR and optical data were integrated. As previously alluded to, the sensitivity of SAR data to differences in canopy structure (Baghdadi *et al.* 2010, Bargiel and Herrmann 2011, Lopez-Sanchez *et al.* 2011) was the main reason for this improvement. Figure 7.5 shows a feature space plot of the VV and VH polarizations of the September TSX image for the maize and legume fields. It can be seen that the TSX data achieves a moderate separation between the two classes.

Another possible reason for the relatively low accuracy of the maize class is its low area coverage in the watershed. Table 6.16 shows that maize is clearly a minority crop in the Veia watershed, with a percentage cover of just 4.6%. Due to the general lack of use of fertilizers in this watershed, farmers have always avoided the cultivation of maize, which according to them require fertilizer. Consequently, the number of maize fields surveyed was about half of the number surveyed for the other crops (see Table 4.8), which led to fewer reference pixels for maize (Van Niel and McVicar, 2004).

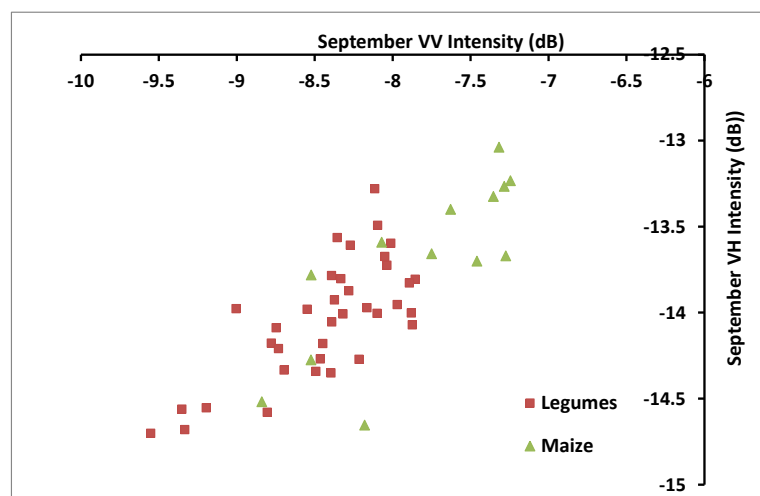


Figure 7. 5 Potential of the TSX image acquired in September to separate maize from legume fields in the Veia watershed. Each point represents field means.

In Dano and Dassari, the highest interclass confusion was found to be between maize and cereals, which culminated in the two classes having the lowest F1 scores in the respective watersheds. Although the integration of the SAR data improved the accuracies of these classes, relatively high interclass confusion remained. The integration of the SAR data increased the F1 scores of maize and cereals in Dano from 0.54 to 0.65 and 0.66 to 0.78 respectively compared to when only optical data were considered. In Dassari, corresponding increases of 0.47 to 0.54 and 0.46 to 0.51 were recorded for maize and cereals respectively when the SAR data were included in the classification. In both

## Discussion of Results

---

watersheds, the confused pixels between maize and cereals were higher than that of all other classes put together (Tables 6.11 and 6.12). In Dassari, 25% of maize pixels were wrongly labelled as cereals while 24% of cereals pixels were wrongly labelled as maize. Similarly in Dano, 23% of maize pixels were wrongly classified as cereals whereas 7% of cereals pixels were wrongly classified as maize. This relatively high confusion between the two classes can be attributed to a number of reasons.

In Dano, overlap between the cropping calendars as discussed above was a contributory factor. The lumping of millet, sorghum and their intercropping into one class (cereals) further aggravated the errors due to cropping calendar overlaps, since individual crops within the cereal class, which were cultivated at the same time as some maize fields, could have developmental stages similar to that of maize. Another factor is the cultivation of different varieties of same crops. For example, three- and four months maturing maize may exhibit different phenological behavior although they were planted at the same time. Similarity of the phenological behavior of either of them with any of the individual crops in the cereal class could result in confusion between the two classes.

In Dassari, however, the level of confusion between maize and cereals was not expected, considering that most maize fields were ploughed and planted a month or two (late July to August) after most cereal fields were planted (May to early July). Therefore, the phenological characteristics of the two crops were expected to be different, and hence the possibility to separate them with minimal confusion. Analysis of NDVI profiles revealed that the best time-step/period for separating cereals and maize was the June 13<sup>th</sup> RE image (Table 4.1). The spectral characteristics of ploughed fields as of June 13<sup>th</sup> (mostly cereals, cotton and rice) were markedly different from unploughed fields (mostly maize) which were essentially grassy. But, this image could not provide a complete separation between the classes because cereal fields which were ploughed after the June 13<sup>th</sup> acquisition behaved spectrally similar to maize fields. Unfortunately, the July and August TSX acquisitions provided only limited separability between the two classes as depicted in Figure 7.6, because all fields ploughed within this period would have been in early developmental stages, hence similarities in their backscatter response. Structural similarities between maize and cereals (i.e. leaf shape, size, etc.), especially at maturity stage, made it difficult for the RE acquisitions acquired during this stage (September, October) to significantly improve on the separability of the two classes. Table 6.7 reveals that apart from the June RE and July TSX acquisitions, the November RE acquisition was the only image that provided additional information concerning the discrimination of the maize class. This is most likely due to the early harvest of some cereal fields.

## Discussion of Results

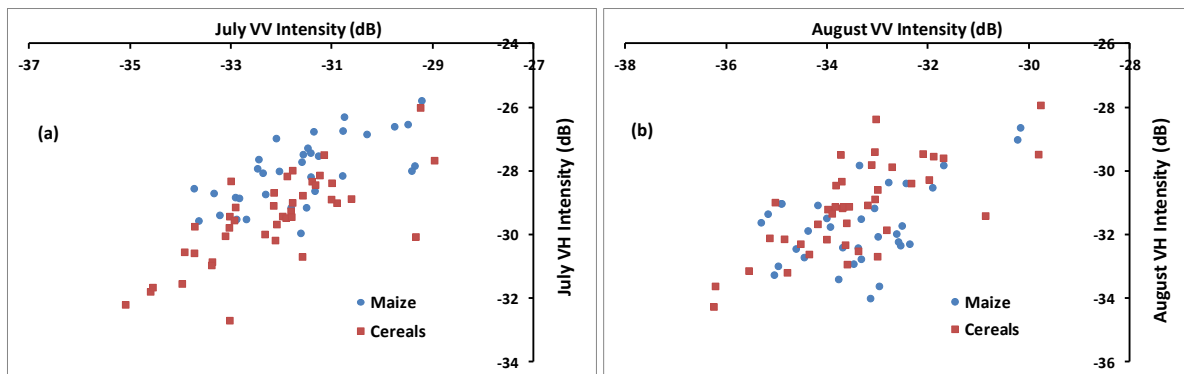


Figure 7. 6 (a) Feature space plot of the maize and cereals classes in the Dassari watershed using the VV and VH intensities of the July TSX image; (b) same plot as (a) for the August TSX image. Each point represents class means.

### Legumes

Legumes in the Vea watershed were discriminated with a good accuracy, having an F1 score of 0.86. Producer's and user's accuracies of 89% and 84% respectively were achieved. Like the cereal class, a good classwise accuracy (F1 score = 0.76) was obtained for the legume class when only optical data was used in the classification. The inclusion of the SAR data moderately improved the F1 score from 0.76 to 0.86. The planting of maize and legumes around the same time caused a similarity in their phenological behavior, resulting in minimal confusion between the two classes. About 9 percent of legume pixels were wrongly classified as maize, while less than 3% and of legume pixels were wrongly classified as rice and cereals. As earlier discussed, slight shift in the planting dates of the legumes and cereals classes led to minimal confusion between them.

### 7.2 Cropland dynamics at watershed scale between 2002 and 2013

Previous studies that investigated changes in LULC in various parts of West Africa and between different dates reported increases in cropland area in the periods investigated (Tappan *et al.* 2004, Wood *et al.* 2004, Forkuor and Cofie 2011, Brinkmann *et al.* 2012). Most of these studies calculated changes in cropland area based on analysis of satellite images that spanned between ten or more years. For example, Ruelland *et al.* (2010) reported increases of between 7% and 24% in cropland area when they analyzed time-series of satellite images (Corona, Aster, Landsat) acquired between 1967, 1986/1990 and 2003/2004 in three different areas of Mali. Paré *et al.* (2008) reported an increase of 60% in cropland area when they classified satellite images acquired between 1986 and 2002 (16 years) in southern Burkina Faso, and subsequently estimated an annual rate of increase of +3.8% in cropland areas. By analyzing images that span a decade or more, most of these studies, based on their results, assumed an inter-annual increase in cropland area. In other words, they assume a continuous increase in cropland area from year-to-year. However, few studies that analyzed image time-series with finer temporal scales revealed that year-to-year or short term (e.g. 2-3 years) fluctuations in cropland area do occur in West Africa due to a number of reasons (e.g. Amissah-Arthur *et al.* 2000). Results obtained from the historical Landsat classifications in this study (see Section 6.2) confirm the results obtained by these studies, and revealed that the study

## Discussion of Results

---

watersheds (and possibly other parts of West Africa) experienced inter-annual or short-term (2-3 years) fluctuations in cropland area between 2002 and 2013.

Numerous factors could account for the observed fluctuations in cropland area. One obvious factor is the rainfall pattern (quantity and distribution) during the period of investigation. Reliance of agriculture in West Africa on rainfall means that abnormal rainfall patterns, especially during the cropping season, can cause crop failure and lead to a reduction in the total harvested area for a year (Leisinger *et al.* 1995). Farmers are, therefore, very particular about rainfall patterns within the cropping season, and may hinge most of their decisions on this. Ingram *et al.* (2002) noted that the most important rainfall parameters that many farmers in Burkina Faso wanted in a climate forecast (in declining order of priority) were: (1) the onset and end of the rainy season, (2) likelihood of water deficits in the rainfall distribution, and (3) total rainfall amounts. This suggests the major role that rainfall quantity and distribution within the cropping season play in the agricultural sector (e.g. farmers' decision whether to cultivate or not, what crop to cultivate, etc.), and how delays in the onset of rains and dry spells during the cropping season could affect the total cultivated area.

In Dano, for instance, poor rainfall distribution in 2005 is a possible cause of the reduction in cropland area from 35% in 2002 to 29% in 2005. Based on a 40-year mean of annual rainfall from a meteorological station in Dano (Figure 3.2), annual rainfall in 2005 was found to be below average. Additionally, analysis of the monthly rainfall totals for the year (2005) revealed a very low rainfall amount for the month of August (118 mm), which was only 50% of a ten year (2001-2010) average for the month (235 mm). Considering that August is an important month in the developmental stages of most crops (based on the cropping calendar – see Figure 5.3), the low rains in this month (August) could have resulted in crop failure and subsequently a reduction in the total harvested area. On the other hand, high annual rainfall totals in 2006 (which was above the 40 year mean) could have contributed to the relatively higher total cropland area in 2006 relative to 2005.

In 2007, both Vea and Dano watersheds experienced a decline in total cropland area relative to previous years. The percentage of cropland in Dano declined from 45% in 2006 to 26% in 2007, while that of Vea changed from 55% in 2006 to 51% in 2007. The simultaneous reduction in cropland area in both watersheds (in 2007) can possibly be attributed to widespread flooding in West Africa and other parts of Sub Saharan Africa (SSA) in September 2007 which destroyed properties, farmlands and led to the loss of lives (BBC 2007, Levinson and Lawrimore 2008, Armah *et al.* 2010, Braman *et al.* 2013). Although annual precipitation in Dano was lower in 2007 compared to 2006, a study of the monthly rainfall totals revealed that the flooding (in both watersheds) was mainly caused by anomalous rainfall amounts in July and August 2007. These anomalous rainfall events have been reported by other studies (e.g. Paeth *et al.* 2011). Relative to 2007, 2008 witnessed an increase in total cropland area in both watersheds. In Dano, percentage of cropland area increased from 26% in 2007 to 41% in 2008, while the corresponding increase in Vea was from 51% to 67%. This could be farmers' response to a possible crop failure in the previous year (2007) due to the flooding.



## Discussion of Results

---

Other studies conducted in West Africa drew a linkage between rainfall and inter-annual or short term fluctuations in agricultural productivity. For example, Leisinger *et al.* (1995) observed that above-average rainfall in 1988 and 1989 in most Sahelian countries (including Burkina Faso) led to a high agricultural production while low rainfall totals in 1990 (below average) led to a 15% and 5% reduction in agricultural production relative to 1988 and 1989 respectively. Although agricultural production may not be the same as cultivated area, studies have shown that increases in agricultural production in West Africa (and SSA in general) are mainly driven by expansion in cropland area due to poor soils and low mineral inputs such as fertilizers (Enyong *et al.* 1999). Thus, an increase in cropland area can be assumed in case of an increase in agricultural production.

The results obtained in this study, however, show that a higher annual rainfall (e.g. above normal rainfall) does always translate into an increase in cultivated area. Rather, a regular distribution of rainfall within the cropping season is important. In Ve, for instance, a high annual rainfall of 1087 mm in 2011 resulted in a percentage cropland area of 52.5% while a relatively low annual rainfall of 800 mm in 2013 led to a cropland area of 66.7%. The difference in rainfall in the two years was found to have been caused mainly by anomalous rainfall in August 2011 (441.6 mm), as against a 10 year (2001-2010) average of 247 mm. Thus, monthly events such as this, although could increase the annual rainfall, may not translate into higher cropland area. Other studies conducted in West Africa also noted a decline in cropland area despite increasing pattern in annual rainfall. Based on classification of a time-series of SPOT images, Amissah-Arthur *et al.* (2000) observed a decreasing trend in cultivated area between 1990 and 1996 in the Hapex-Sahel area of Niger, although the area experienced normal or above average rainfall amounts (i.e. relative to the 1961-1990 base) between this period. According to FAO /GIEWS (1996), the normal or above normal rainfall experienced between 1990 and 1996 was happening for the first time since 1970. This, together with what was observed in this study suggest that annual rainfall alone may not always be correlated with cropland area, and that there are other important factors that may influence cropland dynamics in West Africa.

A review of some previous studies reveals that a sole linkage between cropland area and rainfall is ambiguous, and that other climate variables (e.g. relative humidity, temperature), biophysical (e.g. soil fertility) and socio-economic factors (e.g. population growth, agricultural policy) influence inter-annual changes in cropland area. For example, Tottrup and Rasmussen (2004) analyzed positive and negative trends in agricultural productivity (using NDVI as proxy) in Senegal between 1981 and 2000 in relation to rainfall patterns. Average NDVI values (NOAA AVHRR) were extracted from a 12.5 km buffer around four meteorological stations for which monthly rainfall data was available from 1981 to 2000. They found that, out of the four localities (each having a meteorological station), a significant relationship between agricultural productivity and annual rainfall was observed for only one station, while there was no relationship between the two factors in the other three localities. Population growth and declining soil fertility were found to be the other factors affecting agricultural productivity. Paeth *et al.* (2008) investigated the relationship between climatic variables (rainfall, relative humidity, temperature) derived from a regional climate model (Paeth *et al.* 2005) and the

## Discussion of Results

---

yield of eight major crops in Benin, West Africa between 1979-2003. They found a strong, and statistically significant, relationship between the inter-annual variations in crop yield and all the climatic variables, with relative humidity turning out to be a better indicator of crop yield changes than rainfall and temperature for most crops. Their study also revealed varying effects of the climatic variables on different crops. For example, inter-annual variations in the yield of cotton, maize and beans were found to be less affected by the climatic variables. Recently, Schmidt *et al.* (2014) analyzed the relationship between NDVI patterns (i.e. changes in vegetation cover) and climatic variables derived from a regional climate model (Paeth *et al.*, 2005) for different land use and land cover types in tropical and northern Africa. By using a regional climate model, climatic variables such as relative humidity, global radiation and temperature which have been absent in previous studies (e.g. Herrmann *et al.* 2005, Camberlin *et al.* 2007) were obtainable. They showed that the climatic variables that have the strongest links to cropland in most of West Africa were (in decreasing order): relative humidity, rainfall, minimum, maximum temperature and global radiation. The seeming importance of relative humidity to agricultural productivity in these studies is interesting, and suggests the need for more climatic variables, other than rainfall, to be considered in understanding cropland dynamics in West Africa.

Other studies have also identified non-climatic factors as a cause of inter-annual changes in cropland. Amissah-Arthur *et al.* (2000), for example, attributed the decline in cropland area in the Hapex-Sahel area of Niger despite increasing rainfall to declining soil fertility and productivity. They reported that poor soil fertility and productivity cause farmers to occasionally abandon their agricultural lands. Mutsaers *et al.* (1997) noted that intensive cultivation of land (i.e. continuous cultivation over a long period of time) often lead to more runoff, increased soil erosion and reduced water retention. Thus, an increase in rainfall amount may not necessarily improve soil moisture conditions to benefit crop growth, especially in the cropping season. This may frequently occur on uplands/hill slopes or marginal lands, and could lead to dry conditions and possible crop failure. The effects of long term continuous cultivation, coupled with poor nutrient inputs (e.g. fertilizer), on soil fertility in West Africa have been noted by a number of studies (Bationo *et al.* 1995a, 2007, Zougmore 2003, Ouedraogo 2004). For example, Soil Organic Carbon (SOC) levels have been found to rapidly decline with continuous cultivation in West Africa, with average annual losses of about 4.7% and 2% for sandy and sandy loam soils (Bationo *et al.* 1995b, 2007). Tottrup and Rasmussen (2004) attributed negative trends in crop productivity in two sites in Senegal to prolonged cultivation of lands that had led to soil deterioration. Continuous depletion of soil fertility causes the land to be unproductive, which may lead farmers to temporarily or permanently abandon it and migrate to previously uncultivated lands (Amissah-Arthur *et al.* 2000, Braimoh and Vlek 2004, Adjei-Nsiah *et al.* 2007). In this study, unavailability of soil fertility data for the years analyzed prevented an analyses to be conducted in relation to the observed changes in cropland.

Rapid population growth is another factor that could be responsible for the observed changes in cropland area in the watersheds. Several studies have noted that increasing population growth has often led to increases in cropland area in West Africa (Leisinger *et al.* 1995, Lambin *et al.* 2003,

## Discussion of Results

---

Tottrup and Rasmussen 2004, Braimoh 2009, Ouedraogo *et al.* 2010). However, the effect of population increases on cropland area will more likely affect the Dano watershed, which has experienced higher population increases in recent years than Vea, which has a relatively lower figure. Available statistics indicate that between 1996 and 2006, population in the Ioba province (in which Dano falls) increased by 19% (INSD 2007) while population in the Bongo and Bolgatanga districts (where Vea falls) in Ghana each increased by 9% between 2000 and 2010. The relatively higher decadal increase in Dano can be attributed to migration of farmers from drought-affected areas in northern Burkina Faso into the more humid southwestern parts where rainfall patterns are favorable for cultivation (Paré *et al.* 2008, Ouedraogo *et al.* 2010). This migration naturally results in the conversion of natural/semi-natural vegetation into croplands, thereby increasing cropland area. But, population increases may be more responsible for long term changes in cropland area rather than the abrupt inter-annual changes witnessed, for example, between 2006, 2007 and 2008, which are most likely due to climatic factors as explained above. For example, the increase in cropland area in the Dano watershed from 34.8% in 2002 to 45.3% in 2006 can be partly attributed to the population increases witnessed between 1996 and 2006. Ouedraogo *et al.* (2010) studied the relationship between LULC and population changes in southwestern Burkina Faso by analyzing satellite images acquired in 1986, 1992, 2002 and 2006. They found significant correlations between population increase and changes in cropland area throughout the four time series, with the highest correlations occurring in 2002 and 2006. This confirms a possible linkage between the observed cropland increase in Dano between 2002 and 2006 and population increases.

Other studies have noted that certain agricultural and political policies have led to increases in cultivated area in some West African countries. Braimoh (2009) found increases in cropland expansion rates in most of northern Ghana after the structural adjustment program in the early and mid 1980s. Policy shifts from agricultural sector protection to trade liberalization was found to be a major influencing factor in this regard. In addition, occasional fertilizer subsidy from the government of Ghana could also influence an increase in cultivation area. For example, the government of Ghana embarked on a fertilizer subsidy program in 2008 (Banful 2011). This could have contributed to the high cropland area reported in Vea in 2008 (67.4%), which was the highest among all the years analyzed. In Burkina Faso, Ouedraogo *et al.* (2010) stated that the government provided incentives such as ploughs and fertilizers to farmers in the 2000s as part of an agricultural policy to increase cotton production. These incentives normally encourage farmers to increase cultivated areas in anticipation of a higher yield and increased income.

### 7.3 Regional scale cropland dynamics

This sub-section discusses results of the regional scale analysis. It is divided into three sections. The first discusses the accuracy of the fractional cover maps in relation to other studies. In the second section, the spatial distribution and pattern of croplands in the Sudanian Savanna are discussed. The third section discusses the possibilities of using cropped area estimates from the fractional cover maps to improve government-derived agricultural statistics in West Africa.

### 7.3.1 Accuracy of fractional cover maps

In this study, the spatial distribution of cropland in the Sudanian Savanna region of West Africa between 2002 and 2013 was modeled by upscaling Landsat level (30 m resolution) cropland information unto MODIS scale (232 m resolution) and determining the proportion of cropland in each MODIS pixel (cropland fractional cover) using an ensemble of non-parametric regression tree models. A robust validation of each cropland fractional cover was conducted by comparing it with 75,000 samples extracted from an independent Landsat classification results (aggregated to 232 m) that was not used in the regression analysis. Four statistics - ME, MAE, RMSE, and  $R^2$  - were determined.

The  $R^2$  obtained from the validation exercise ranged from 0.54 for the 2002 fractional cover map to 0.70 for that of 2005 with an average of 0.62. This result compares favorably with previous studies that estimated fractional crop cover for a whole country, e.g. Verbeiren *et al.* (2008), who reported the highest  $R^2$  of 0.6 when they conducted pixel level validation of the fractional cover maps of two major crops (winter wheat and maize) in Belgium. With respect to MAE, the results achieved in this study (MAE of between 14.2% and 19.1%) are similar to accuracy estimates reported by Tottrup *et al.* (2007) who estimated the fractional cover of mature forest, secondary forest and non-forest using regression tree modeling and MODIS data. They obtained a MAE of 14.6%, 21.6% and 17.1% for mature forest, secondary forest and non-forest respectively.

In terms of RMSE, the range of accuracies obtained in this study (19.6 for 2006 and 23.9 for 2008 – Table 6.21) were found to be significantly lower than other studies e.g. Gessner *et al.* (2013), that reported RMSEs of between 3.1% and 9.9% for the estimation of fractional cover of natural vegetation and bare surfaces in Namibia. A possible explanation for the relatively better RMSEs obtained by Gessner *et al.* (2013) could be their use of very high resolution images (Quickbird and IKONOS) to map the growth forms before upscaling the results unto Landsat and MODIS resolutions. The use of very high resolution images can enable a better detection of land cover units and subsequently the derivation of a more realistic cover proportions to be used as training data (response) in the regression analysis.

In this regard, the spatial resolution limitations of Landsat vis-à-vis the heterogeneous landscape in the study watersheds is believed to be the primary source of error in the cropland fractional cover maps derived in this study. Due to the fact that a per-pixel classification approach was adopted at the Landsat scale, a pixel classified as cropland could have a portion of it as natural vegetation (Xiao *et al.* 2003). This is particularly the case in Dano, where the prevalence of sub-canopy cultivation results in many trees on agricultural plots (Figure 7.2). Thus, the aggregated proportions of the Landsat classification at MODIS resolution (which was used as the response in the regression analysis) could be under- or overestimated. Such errors will be inherent in both the training (response) and validation data.

### 7.3.2 Spatial distribution of croplands in the Sudanian Savanna zone

The fractional cropland cover maps (Figure 6.15) showed that the northern part of the Sudanian Savanna zone (north of latitude  $11^{\circ} 30'$ ) has a higher percentage of croplands than the south. Most of these areas consistently had a cropland cover (per MODIS pixel) of more than 60% between 2002 and 2013. A possible explanation for the high percentage of croplands in the northern part could be due to a higher reliance of the population in these areas on agriculture, compared to those in the south (i.e. areas south of latitude  $11^{\circ} 30'$ ). For example, Sanfo (2010) reported that more than 86% of the population in Burkina Faso is employed by the agricultural sector, while the figure is between 50 and 60% for Ghana (Ghana Statistical Service 2012, Kolavalli *et al.* 2012). This could lead to cultivation of extensive areas in Burkina Faso (which forms part of northern Sudanian Savanna) than Ghana which is in the south.

Another reason for the high percentage of croplands in the northern part of the Sudanian Savanna could be the occurrence of relatively poor soils and low rainfall distribution in the northern part compared to the south. Whereas some studies have reported that declining soil fertility can lead to farmers abandoning their lands (Brimoh and Vlek 2004, Adjei-Nsiah *et al.* 2007), others have also reported that declining soil fertility, which results in low yields, cause farmers to expand production into marginal land as a survival strategy and insurance against low yields (Enyong *et al.* 1999; Amissah-Arthur *et al.* 2000; Ruelland *et al.* 2010). This normally happens in areas of land scarcity, where the traditional fallowing system of abandoning land for a period can no longer be supported (Enyong *et al.*, 1999). Consequently, poor soil fertility areas such as the northern part of the Sudanian Savanna could have high cropland areas as observed in the regional scale maps. In addition, declining rainfall and a drier climate has been found to be an incentive for some farmers, especially those in the Sudano-Sahelian region, to expand cultivated area as an insurance against poor yields or crop failure (Tappan *et al.* 2000; Tottrop and Rasmussen, 2004; Ruelland *et al.* 2010).

The regional scale cropland maps (Figure 6.15) shows that generally, the southern part of the Sudanian Savanna has a lower crop cover compared to the north. Most areas have a cropland cover (per MODIS pixel) of between 20 and 40%. Visual inspection of Google Earth imagery and other global LULC maps revealed a similar pattern. A probable explanation for this is the high occurrence of vegetation (especially trees) and the predominance of agroforestry (cultivation under trees) in this part of the agro-ecological zone. In addition, tree plantations (e.g. mangoes in South-western Burkina Faso and northern Ghana) are common in the south part of the Sudanian Savanna compared to the north due to the relatively favorable climatic and environmental conditions there (Ruelland *et al.* 2010). Thus, spectral similarities between such plantations and ordinary trees can result in confusion between natural vegetation and cropland. The low percentage of croplands observed in the southern part of the Sudanian Savanna, therefore, could be: (1) a concealment of cropland due to sub-canopy cultivation and (2) inability of remotely sensed images to separate tree plantations from ordinary trees. Consequently, the percentage of croplands in the south of the Sudanian Savanna could be higher than what was detected using remotely sensed (Landsat/MODIS) data.

## Discussion of Results

---

Cropland areas at the regional scale were found to have experienced inter-annual or short term (2-3 years) fluctuations as witnessed in the watershed analysis. The reasons ascribed for the fluctuations observed at watershed scale in Section 7.2 are applicable here as well. However, a notable difference between the two patterns (watershed and regional) is the low cropland area detected at watershed scale in 2007 (Figure 6.12) using Landsat images against the high cropland area in the regional scale results for the same year using MODIS data (Figure 6.16). This can be attributed to differences in the temporal scales of the Landsat and MODIS data analyzed at the two spatial scales. As it was already explained in section 7.2, widespread flooding in September 2007 is believed to have caused the reduction in cropland area observed at the watershed scale. Since the Landsat images analyzed at the watershed scale were mostly acquired during the harvest season, possible crop failure or destruction of farmlands caused by the floods prior to harvest would have prevented all croplands to be identified on the harvest season images. In other words, croplands could have been poorly discernible on the 2007 harvest season Landsat images due to the floods. On the other hand, the MODIS data used for the regional scale analysis consisted of an annual time-series that spanned the entire cropping season. Thus, the availability of early season images (e.g. May - July) in the MODIS data could have provided additional information about croplands in 2007 than what could be observed at harvest period using the Landsat data. Based on the random forest variable importance measure (see Section 5.1), it was found that the first ten most important MODIS time-steps used in calculating the 2007 fractional crop cover included early season time-steps acquired in May and June, while late season time-steps acquired in November and December were also included. This means that information on croplands prior to the floods (in September) was considered in estimating the fractional cropland cover at the regional scale, a possible reason for the dissimilarity in the regional scale cropland area compared to that of the watershed scale. This finding suggest that, in the event of crop failure or farmland destruction due to floods or other natural disasters, the use of harvest season images alone to map croplands could be misleading.

### 7.3.3 Regional scale cropland maps and agricultural statistics

Comparison of area estimates derived from the fractional cover maps (MODIS) with official cropped area statistics from the Government of Ghana (MoFA) for seventeen districts revealed significant disparities between the two for some districts. MoFA's estimates were far higher than that of MODIS in most cases, with questionable estimates for some districts. For example according to MoFA, the total cropland area for the Lawra district increased from 30% of the district area in 2002 to 77% in 2005 and rose to 92% in 2008. These increases are questionable, considering that no district in the country witnessed such huge increases in cropland area between 2002 and 2005. In fact, other districts within the same geographical area as Lawra witnessed declines in cropped area between 2002 and 2005 (e.g. Wa, Jirapa-Lambussie and Nadawli). MoFA's reported estimates for Builsa also showed interesting patterns. Total cropland area increased from 48% of the district area in 2002 to 73% in 2005 and declined to 28%, 28%, 24% and 23% in 2007, 2008, 2010 and 2011 respectively. Although the floods of 2007 might have led to a reduction in cropland area, the magnitude of reduction between 2005 and 2007 (45%), and the consistency in the reported figures from 2008 to

## Discussion of Results

---

2011 (averaging 26%), suggest that the reported figures for 2002 and 2005 may be in error. Comparison of the 2002 MoFA estimates with Landsat derived estimates for five, out of the seventeen, districts (Figure 6.14) further revealed a level of inconsistency in the MoFA data, with high over estimations for some districts and underestimations for other districts. Studies in other parts of the world have reported discrepancies in crop area statistics from governmental sources. Xiao *et al.* (2003) and Seto and Kaufmann (2003) both noted that official crop area statistics from the Chinese government were underestimated. Ramankutty (2004) explained that such errors in official crop area statistics could be due to either: (1) a deliberate under- or overestimation due to certain incentives (e.g. reducing tax burdens and artificially inflating crop productivity figures – Yuyun and Zheng (2000)) or (2) the lack of resources or adequate infrastructure to conduct rigorous and reliable surveys. For example, Belshaw (1983) observed that cropped area in Uganda was underestimated in 1965 due to farmers' non-disclosure of the location of all their distant plots for fear of increased tax.

In the case of Ghana (and many other West African countries), lack of resources (human and financial) and inadequate infrastructure (e.g. road access) is the main cause of the discrepancies observed in the official crop area statistics. During agricultural census, MoFA divides a district into enumeration areas (EAs), from which a sample is selected to be surveyed. Within each selected EA, a sample of farms are further selected and surveyed by trained agricultural extension officers. From 2002 to about 2010, farm measurements (to estimate cultivated area) were done with a tape and prismatic compass for all districts (i.e. using the polygon method, De Groote and Traoré 2005), while some districts (e.g. Bolgatanga) introduced the use of handheld GPS in 2011. Since each district conducts its own survey with limited coordination, different estimation accuracies could be obtained for each district depending on: (1) size of the district vis-a-vis the number of EAs selected (i.e. statistical significance of the sample), (2) availability of adequate road access to enable enumerators reach all sampled EAs, (3) level of training and experience of enumerators, and (4) availability of adequate and accurately/regularly calibrated tools (e.g. compasses, measuring tapes, GPS handsets, etc.). Additionally, most enumerators, per FAO recommendation (Ramankutty 2004), subjectively estimate the area proportion of crops on an intercropped field, which could introduce further errors. Thus, differences in the financial, logistical, infrastructural and human resource base of the different districts could lead to a good estimation for one district and a poor estimation for the other. Inter-annual differences in accuracy estimations are also possible.

Although the area estimations derived from the 2002 MODIS fractional cover map mostly underestimated the actual cropped area by about 38% on average (based on comparison with Landsat estimates), the results show that the errors are systematic compared to that of the MoFA estimates (Figure 7.7). The validation results (e.g. ME) for other years (i.e. ME of 2005, 2006, 2010 - Table 6.21), however, indicated that the fractional cover maps of those years could overestimate cropland area in some instances, although such errors will be expected to be systematic as that of the 2002 output. As earlier stated, the over- and underestimation of cropland area by the fractional cover maps can be attributed primarily to inaccuracies in the underlying Landsat classifications. Other studies that estimated cropland area for the whole of Africa also observed systematic

## Discussion of Results

overestimation of their product, and attributed it to the underlying data and the effect of certain farming practices (e.g. shifting cultivation) in Africa (Vancutsem *et al.* 2012).

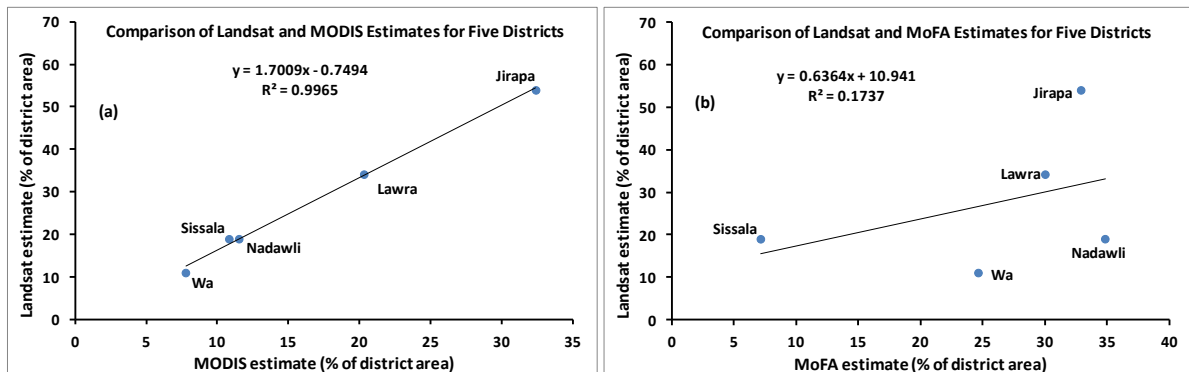


Figure 7. 7 Comparison of Landsat derived (reference) cropland estimate with estimates from the 2002 fractional cover map for five districts; (b) same graph as (a) between Landsat and MoFA estimates

Despite the apparent under- or overestimation of cropland by the generated fractional crop cover maps, the systematic nature of the errors can enable a "correction" of the MODIS results using regression estimation techniques (Alonso *et al.* 1991, Gallego *et al.* 1993, Haack and Rafter 2010). The regression estimate method allow for the results obtained with a coarse resolution image to be corrected based on an established statistical relation between samples of the coarse resolution results (auxiliary variable) and a corresponding fine spatial resolution results (primary variable). Thus, the established statistical relationship between the MODIS and Landsat estimates for the five districts (Figure 7.7a) can be used to correct the whole 2002 MODIS fractional crop cover map to derive near-actual area estimates. In this case, the Landsat classification is regarded as the primary variable (y) while the MODIS fractional cover map is regarded as the auxiliary variable. This approach has been successfully tested by other studies (Nelson 1989, Eva and Lambin 1998, Fraser *et al.* 2004). Successful application of the regression estimation method in this manner will make the MODIS fractional cover maps a viable alternative to the MoFA estimates in that: (1) the spatial distribution of cropland within a district can be known and allow for efficient implementation of agricultural programs and (2) consistent cropland area estimates can be obtained for all administrative units.

It is admitted, however, that the use of only five districts in a regression estimation analysis may not be statistically significant to determine a robust statistical relationship. But this was purely due to poor Landsat data availability for areas covering other districts due to the malfunction of the Landsat scan line corrector between 2003 and 2012. With the launch of Landsat 8, and the widespread availability of other optical and SAR sensors, remote sensing based crop area estimation can be significantly improved.



### 8. Conclusions and Outlook

Agricultural land use is the most pervasive of all land uses in the world today. In West Africa, rapid population growth has led to expansion in croplands due to the need to grow more food to meet the rising food demand of the burgeoning population. At the same time, these expansions negatively impact the sub-region's ecosystem, with implications for water and soil quality, biodiversity and climate. In order to appropriately monitor the changes in croplands and assess its impact on the ecosystem and other environmental processes, there is the need for regular agricultural land use mapping (i.e. mapping the spatial distribution of crops and croplands) in West Africa. Accurate and up-to-date information on agricultural land use can benefit a wide range of biophysical and economic models and improve decision making based on their results. For example, simulation models that integrate climate and crop data to assess climate change impacts on crop yields can improve their results when explicit information on the spatial distribution of the crops under investigation is available.

But agricultural land use mapping in West Africa has been challenging due to a number of reasons. First is the heterogeneity of the landscape, which is characterized by small agricultural plots, high incidence of inter-cropping, sub-canopy cultivation and cultivation around hamlets. Consequently, the use of medium spatial resolution satellite data such as Landsat leads to high spectral heterogeneity and poor results. Secondly, persistent cloud cover during the cropping season prevents optical sensors from acquiring useful images during critical crop development stages. In order to overcome these challenges (1) satellite data with high spatial and temporal resolution is required to map the typical small farm plots (spatial resolution) as well as improve chances of obtaining more useable images (temporal) during the cropping season and (2) images from sensors that are near-independent of weather conditions such as Synthetic Aperture Radar (SAR) systems must be integrated with optical images to improve the temporal coverage of available images within the cropping season.

In line with the above, this study investigated the use of high spatial and temporal resolution optical and radar imagery to improve agricultural land use mapping in three watersheds in the Sudannian Savanna (SS) of WA. Optical data from the RapidEye sensor (spatial resolution = 5 m and revisit period = 5.5 days) and dual polarimetric radar data from the TerraSAR-X sensor acquired in Strip Map mode (spatial resolution = 6 m and revisit period = 11 days), were used to map crops and crop groups. The classes considered are: cereals (millet and sorghum), maize, cotton, legumes (groundnuts and beans), rice and yam. In addition, inter-annual or short term changes in cropland area between 2002 and 2013 were investigated using historical Landsat data. Finally, the possibility of upscaling watershed level cropland information to regional level to improve sub-national/national agricultural statistics was investigated. Based on the above objectives, the following conclusions can be drawn.

### 8.1 Spatial resolution, field size and landscape heterogeneity

The high spatial resolution of the RapidEye imagery was found to adequately represent the heterogeneous landscape in the study watersheds. Farm plots that have sizes as low as 0.2 ha were correctly captured (Figure 6.1). The spatial resolution also permitted the identification of trees on farms. Small hamlets around which cultivation normally takes place (especially in Vea) were well identified by the RapidEye images. This permitted the derivation of an accurate crop mask prior to crop classification.

### 8.2 Crop classification

Dependence of agriculture on rainfall, coupled with variable planting dates, causes overlaps in the cropping calendar of most crops. This culminates in widespread confusion between crop classes when all crops are classified at the same time. This study has found that, sequentially classifying crops based on different image combinations reduces the confusion due to crop calendar overlaps. The implemented sequential masking approach improved classification accuracies by between 6% and 9% over the classification of all crops at the same time (one-time classification). Additionally, the accuracy with which the respective classes were mapped (classwise accuracies) improved by between 5% and 38%. The McNemar's test confirmed that differences in the accuracies obtained from the two approaches (sequential masking and one-time classification) were statistically significant.

In general, rice, cotton and legumes were found to be relatively easy to map in all watersheds provided images (optical and SAR) are available throughout the cropping season. Rice achieved the highest classwise accuracy in all watersheds, while cotton and legumes achieved the second best classwise accuracy. Cereals (millet and sorghum) and maize were generally difficult to separate due to similarities in their structure. However, early cultivation of cereals in Vea ensured a good separation of the class from other crop types using early season images, resulting in a good classwise accuracy. Minority crops (e.g. maize in Vea) achieved relatively low accuracies.

### 8.3 Crop classification using only optical imagery

Crop classification using only optical data achieved moderate classification accuracies for the three watersheds. Overall accuracies ranged from 57% to 71%. The available optical images failed to adequately separate crop classes that have similar cropping calendars. For example similarities between the cropping calendars of maize and legumes in Vea resulted in a very low classwise accuracy of the maize class (F1 score =0.14). In addition, certain inter-croppings (e.g. rice and yam in Dassari) cause difficulty for optical images to adequately discriminate between the respective classes. However, good classwise accuracies (F1 score > 0.8) can be achieved for crops that: (1) have a unique physical condition at certain periods of cultivation (e.g. rice, which is inundated at the peak of season) or (2) have a slightly different cropping calendar from that of other crops (e.g. early ploughing and cultivation of cereals in Vea). When only optical data are used for crop mapping, the absence of an acquisition made in September could lead to much poorer results than what has been achieved in this study.

### 8.4 Crop classification using optical and SAR data

Integration of the optical and SAR images in classifying crops improved overall and classwise accuracies compared to what was achieved with only the optical images. Overall accuracy increased by between 8% and 15%, depending on the available number of SAR images and their acquisition dates. Classwise accuracies (F1 score) of all crop classes increased by between 13% and over 100%. The sensitivity of radar systems to different crop canopy architectures improved the separation of crops with similar cropping calendars such as (1) maize and legumes in Vea and (2) cotton and maize/cereals in Dano and Dassari. The classwise accuracy (F1 score) of maize in Vea increased by about 390% (0.14 to 0.69) while cotton in Dano witnessed an increase of 54% (0.54 to 0.83) when SAR and optical data were integrated compared to only optical data. Furthermore, the sensitivity of radar systems to land surface characteristics such as soil moisture and roughness improved the separation between yam and rice, due to the cultivation of yam in mounds, which may have a rougher surface than rice only fields. Thus, the integration of the SAR and optical data increased the F1 score of yam in Dassari by 33% (0.49 to 0.65) compared to only optical data. In line with the findings of previous crop mapping studies, this study found that the VV polarization was more useful than the VH polarization.

### 8.5 Best temporal window(s) for cropland and crop mapping

**Cropland mapping:** Late/harvest season (October, November) images were found to be the best for mapping croplands. When available, combination of an early and a late season image may also achieve good results. The unique characteristics of ploughed or harvested fields ensure a good discrimination of croplands from surrounding land use and cover classes. Two, or at most three, image time-steps (e.g. one early and two late season images) are sufficient to achieve a good accuracy. In this study, overall accuracies of greater than 90% were consistently achieved for cropland mapping (or crop mask) using two or at most three time-steps. The MIR channels in Landsat were found to contain very useful information in mapping croplands.

**Crop classification:** This study has established that mid- to late season images (i.e. August to October) achieve the best separation between most of the crop types investigated. In instances where the cropping season starts a bit later (due to delays in the onset of the rainy season) (e.g. Dassari watershed), acquisitions in November can be useful for crop discrimination. Early season images (i.e. ploughing stage) were found to be useful for discriminating crops that are cultivated much earlier in the season (e.g. cereals in Vea). Acquisitions in September (optical or SAR) were found to be extremely useful in discriminating the different crop types. For example in Dassari, the use of the September RE image alone for classifying all crops (at the same time) achieved an overall classification of 48%, while the addition of three other time-steps (i.e. June RE, June TSX and July TSX) improved the accuracy by only 7%. In Vea, the TSX acquisition of September was the only image that was useful in discriminating all crop classes in the watershed. This is probably due to structural differences in crops as of September, since most crops would have reached maturity at this time of the season.

### 8.6 Spatial distribution of cropland and crops at watershed scale

**Cropland:** The three watersheds have different characteristics in terms of the spatial distribution of croplands and other land use/cover classes. In Vea, croplands are dominant in the northern part of while the southernmost part consists of mainly natural/semi-natural vegetation. Croplands and natural/semi-natural vegetation are mixed in equal measure in Dano, although the northern part seems to have a slightly higher percentage of croplands than the south. In Dassari, croplands are dominant in the western and south-western parts, while the north-eastern part is predominantly natural/semi-natural vegetation. In terms of area, the Vea watershed has the highest percentage of croplands (52%) followed by Dano and Dassari with 45% and 40% respectively. On the other hands, the percentage of natural/semi-natural vegetation is highest in Dassari (59%) while that of Dano and Vea were 52% and 42% respectively.

**Crops:** Rice and yams are found in low lying areas/inland valleys, although cultivation of rice on uplands is also popular. Cereals in Vea occur mainly around hamlets, while legumes and maize occur a little farther from the hamlets. Cotton, maize and cereals occur mainly in bushes in Dano and Dassari, although occasional cultivation around hamlets occurs. In terms of area coverage, cereals were found to be the dominant crop in all the watersheds, constituting 20.3%, 16% and 10.8% in Vea, Dano and Dassari respectively. This is mainly due to the fact that almost every family in the watersheds cultivates cereals for household consumption. Maize constituted a similar percentage (10.7%) as cereals in Dassari. In Vea, legumes are the second dominant crop with about 18% coverage while maize and cotton are the second dominant crops in Dano with a percentage cover of about 12% each. Cotton and rice each occupy about 7% of the Dassari watershed, while yam has the least coverage of 3%.

### 8.7 Cropland dynamics at watershed scale between 2002 and 2013

Cropland area in the Dano and Vea watersheds experienced fluctuations between 2002 and 2013. The observed fluctuation in cropland area suggest that croplands in West Africa do not continually increase on an annual basis as has been suggested by some previous studies. However, the predominant use of harvest season images in the classifications means that only the harvested areas were identified as croplands. Thus, in instances where extreme events such as floods and droughts cause crop failure or destructions prior to harvest, the identified cropland area could be below the actual. Factors that are believed to be responsible for the observed fluctuations in cropland area include: (1) inter-annual changes in climatic factors, e.g. rainfall (floods or droughts), relative humidity and temperature, (2) declining soil fertility, (3) population increases, which often leads to increases in cropland area and (4) agricultural policies such as fertilizer subsidies or provision which could motivate farmers to cultivate larger areas. Changes in cropland area in the watersheds was found to mostly occur with a corresponding, but opposite, change in the extent of mixed vegetation (grasslands/fallows, shrubland, trees or their mixtures). Compared to croplands and mixed vegetation, other LULC classes (i.e. forest, artificial surfaces and water) experienced minimal changes between 2002 and 2013.

### 8.8 Upscaling watershed cropland information to regional scale

Estimation of fractional crop cover on low spatial resolution images (MODIS) was found to be a suitable means of representing the heterogeneous agricultural landscape of West Africa at the regional or sub-regional scale. The large geographical extent of MODIS makes it suitable for regional scale analysis. Regression based modeling was successfully used to upscale watershed level Landsat classification results unto MODIS resolution by calculating the fraction of cropland in each MODIS pixel. Pixel level validation of the fractional cover maps revealed a mean absolute error (MAE) of between 14.2% and 19.1% which is similar to accuracy estimates obtained by other studies that used regression tree models to estimate fractional cover. The accuracy of the underlying Landsat classifications was found to influence the accuracy of the resulting fractional cover maps. Consequently, some of the fractional cover maps overestimated cropland cover while underestimations were witnessed in others. However, for each fractional cover map, these errors were found to be systematic in nature.

The regional scale maps showed that the northern part of the Sudanian Savanna (north of 11° 30' N) had a higher percentage of croplands than the southern part. The higher percentage in the north is believed to be due to a higher reliance of the population in these areas on agriculture than those in the south. Additionally, declining rainfall and soil fertility in these areas could be driving farmers to expand cultivated area to offset crop failure or low yields. The predominance of trees and agroforestry in the southern part of the Sudanian Savanna was found to be a contributory factor to the relatively low percentage of cropland in these areas.

### 8.9 Improving agricultural statistics with regional scale cropland maps

Comparison of extracted cropland area from the fractional cover maps with government's agricultural statistics (MoFA) for seventeen districts (second administrative units) in Ghana revealed high disparities between the two estimates. A further comparison of the two estimates with Landsat derived estimates (which was deemed to be more accurate than both) for five, out of the seventeen districts, revealed inconsistencies in the MoFA estimates, with some districts overestimating the actual cropped area while others underestimated it. On the other hand, errors in the MODIS fractional cover map (relative to the Landsat estimates) were found to be consistent, with a systematic underestimation of cropland area for all the five districts. A high correlation ( $R^2 = 0.9$ ) was observed when the Landsat and MODIS fractional cover estimates were compared, while a low correlation ( $R^2 = 0.2$ ) was obtained in the Landsat-MoFA comparison. The inconsistency in the government's statistics is attributable to differences in the financial, logistical, infrastructural and human resource base of the different districts, which results in good cropped area estimation for some districts and a poor estimation for others.

Thus, satellite derived cropped area estimations from regional scale maps such as generated in this study can be a viable alternative to current agricultural censuses in many developing countries that are fraught with financial, logistical and technical challenges. Based on the good correlation achieved between the Landsat and MODIS estimates, the systematic nature of errors in the MODIS fractional

cover maps can be “corrected” using regression estimation techniques to derive near-actual cropped areas. Successful implementation of such techniques in developing countries will be beneficial in that: (1) the spatial distribution of cropland within an administrative unit (which current censuses don't provide) can be known and allow for efficient targeting and implementation of agricultural development programs and (2) consistent cropland area estimates can be obtained for all administrative units in a country.

### **8.10 The way forward for crop mapping in West Africa**

#### **Satellite data availability**

One major constraint that has limited previous crop mapping efforts in West Africa has been availability of satellite images during the cropping season. Persistent cloud cover during the cropping season has always inhibited optical systems from acquiring useful images during critical crop growth periods (e.g. July to September). In this study, crop mapping was made possible due to the provision of high spatial resolution optical (RapidEye) and SAR (TSX) imagery throughout the cropping season. Although these data come from commercial sensors, they were obtained free of charge from the RapidEye and TSX science teams of the German Aerospace Center (DLR) for the WASCAL project. Thus, future mapping efforts may be required to purchase these datasets, which could be financially unsustainable, especially when large areas are intended to be mapped.

Freely available satellite images throughout the cropping season will greatly boost crop mapping efforts in West Africa and enable a possible operationalization in the future. Till date, data from the Landsat archive, which is publicly available, have been the most used satellite data for LULC mapping in Africa (Roy et al., 2010). The launch of Landsat 8 in February 2013 by the National Aeronautics Space Agency (NASA) will further provide high quality satellite data (devoid of the scan line corrector challenges of Landsat 7) for mapping purposes in the region. But, as an optical system, Landsat 8 will be limited in acquiring useful images during the peak of the cropping season (July to September) due to persistent cloud cover. For instance, analysis of historical Landsat acquisitions between 1984 to 2011 for two Landsat tiles - path 194, row 52 and path 196, row 52 – revealed that the percentage of acquisitions (cloud cover < 20%) that were made between May and September was only 16% and 24% respectively, while those made between October and April made up 84% and 76% respectively. Considering that Landsat has been the widely used satellite data in the sub-region, the statistics above suggest a general lack of data in the cropping season, except October and November. Consequently, future crop mapping efforts are likely to suffer the same fate as before, with limited availability of images during critical crop growing periods.

But this study has shown that SAR images greatly complement optical data, and contribute to improving separability of certain crop classes. In this regard, the European Space Agency's sentinel-1 satellite, which has become operational and will provide free and open access SAR data for global landmasses (Torres *et al.* 2012), will be an excellent addition to already available optical data such as Landsat 8 in improving crop mapping in West Africa. Sentinel-1 will provide day-and-night, all-weather acquisition of SAR imagery in the C-band portion of the microwave spectrum for various

## Conclusions and Outlook

---

applications. With a revisit time of less or equal to fourteen days (Torres et al., 2012), Sentinel-1 will ensure availability of monthly or sub-monthly time-steps to augment optical data. Most essentially, provision of data in the VV/VH polarization mode (Torres et al., 2012), which have been noted to be useful for crop mapping by this study and previous studies (McNairn et al., 2009) makes Sentinel-1 an important source of data for crop mapping efforts in the sub-region. Although the X-band (which was used in this study) has been found to be more useful for crop mapping than the C-band (Shang et al., 2009), the general sensitivity of SAR data to differences in crop canopy architecture as well as to land surface characteristics will greatly assist in improving the separability between certain crop classes. The free availability of Landsat 8 (optical) and Sentinel-1 (SAR) data will also improve chances of operationalizing crop mapping in West Africa.

A residual limitation of the combined use of Landsat 8 and Sentinel-1 data (in relation to the RapidEye and TSX data used in this study) is the spatial resolution of the two data sources. The panchromatic and multi-spectral bands of Landsat 8 have a spatial resolution of 15 m and 30 m respectively, while the Strip map mode of Sentinel-1 will offer a range of spatial resolutions between 5 and 100 m depending on the product (Torres et al., 2012). Thus, whereas both the RapidEye and TSX images used in this study were at 5 m resolution and achieved a good recognition of cropland structure, the relatively lower spatial resolution of Landsat may present challenges in this regard. Nonetheless, the spatial resolution of the Landsat multi-spectral bands can be improved to 15 m using the panchromatic band for improved recognition of cropland structure in the heterogeneous landscape of West Africa.

### Reference and ancillary data

This study found that different planting/harvesting dates of same crops is a major challenge to crop mapping in West Africa. The practice leads to different spectral responses for same crops, and causes confusion between classes. A possible solution to this problem is to continuously monitor as many fields as possible throughout the cropping season. Since ploughing in most parts of West Africa can be done anytime between April and August, ploughed fields of different crop types have to be identified every month and monitored throughout the cropping season. This will aid in understanding the different unique spectral responses of same/different crops cultivated at different stages of the cropping season. Continuous monitoring (year-to-year) of fields in this manner is necessary to understand the dynamics in cropping patterns and inure to the benefits of future attempts at operationalizing agricultural land use mapping in the region.

However, such an operation will be tedious and costly for a single organization or project to undertake, especially when required for larger areas. Therefore, a collaboration between scientist (remote sensing experts) and the national agricultural ministries of West African states is needed to improve the chances of obtaining sufficient and reliable reference data to aid in crop mapping exercises in West Africa. A sub-regional body, such as the West African Science Service Center on Climate Change and Adapted Land use (WASCAL) can spearhead such an initiative. Agricultural extension officers, who are employed by national agricultural ministries and visit farms regularly, can

## Conclusions and Outlook

---

be adequately trained and incentivized to map representative fields in their respective enumeration areas, which can be transferred to a central database and serve as reference data for crop mapping purposes. Such a collaboration can also aid in efforts to operationalize crop mapping in the sub-region, whereby annual satellite feeds from sensors such as Landsat 8 and Sentinel-1 can be processed with annual survey results from the national agricultural ministries.

Integration of other ancillary data in future crop mapping exercises can improve the discrimination of certain crop types and subsequently overall classification accuracy. Ancillary data such as soil type, elevation, distance to roads, distance to hamlets and distance to streams/water bodies can be beneficial to the classification process. For example, crop classification on different soil types can eliminate differences in phenological behavior of the same crop due to different soil fertility levels. It is recommended that future crop mapping exercises investigate the contribution of such ancillary data in improving the detection of crops and crop groups in West Africa.



### References

- Adam, E., Mutanga, O., Odindi, J., and Abdel-Rahman, E.M., 2014. Land-use/cover classification in a heterogeneous coastal landscape using RapidEye imagery: evaluating the performance of random forest and support vector machines classifiers. *International Journal of Remote Sensing*, 35 (10), 3440–3458.
- Adams, J.B., Smith, M.O., and Gillispie, A.R., 1993. Imaging spectroscopy: Interpretations based on spectral mixture Analysis. In: C.M. Pieters and P.A. Englert, eds. *Remote Geochemical Analysis: Elemental and Mineralogical Composition*. Cambridge: Cambridge University Press, 145–166.
- Adams, J.B., Smith, M.O., and Johnson, P.E., 1986. Spectral mixture modeling: A new analysis of rock and soil types at ley to Supply the Second Los Angeles Aqueduct; 1970 to 1990, and 1990 Onward, Pursuant to a Long Term Ground- the Viking Lander 1 site. *Journal of Geophysical Research: Atmospheres*, 91, 8098–8112.
- Adepoju, A., 1977. Migration and development in tropical Africa: Some research priorities. *African Affairs*, 76 (303), 210–225.
- Adjei-Nsiah, S., Kuyper, T.W., Leeuwis, C., Abekoe, M.K., and Giller, K.E., 2007. Evaluating sustainable and profitable cropping sequences with cassava and four legume crops: Effects on soil fertility and maize yields in the forest/savannah transitional agro-ecological zone of Ghana. *Field Crops Research*, 103 (2), 87–97.
- African Development Bank, 2011. *REGIONAL INTEGRATION STRATEGY PAPER FOR WEST AFRICA 2011 – 2015*.
- Alexandratos, N. and Bruinsma, J., 2012. *WORLD AGRICULTURE TOWARDS 2030/2050: The 2012 Revision*. Rome, No. 12-03.
- Alonso, F.G., Soria, S.L., and Cuevas Gozalo, J., 1991. Comparing two methodologies for crop area estimation in Spain using Landsat TM images and ground-gathered data. *Remote Sensing of Environment*, 35 (1), 29–35.
- Amissah-Arthur, A., Mougenot, B., and Loireau, M., 2000. Assessing farmland dynamics and land degradation on Sahelian landscapes using remotely sensed and socioeconomic data. *International Journal of Geographical Information Science*, 14 (6), 583–599.
- Andrew Wardell, D., Reenberg, A., and Tøttrup, C., 2003. Historical footprints in contemporary land use systems: forest cover changes in savannah woodlands in the Sudano-Sahelian zone. *Global Environmental Change*, 13 (4), 235–254.
- Antwi-Agyei, P., Fraser, E.D.G., Dougill, A.J., Stringer, L.C., and Simelton, E., 2012. Mapping the vulnerability of crop production in Ghana using rainfall, yield and socioeconomic data. *Applied Geography*, 32 (2), 324–334.
- Aplin, P. and Atkinson, P.M., 2001. Sub-pixel land cover mapping for per-field classification. *International Journal of Remote Sensing*, 22 (14), 2853–2858.

## Appendices

---

- Arino, O., Bicheron, P., Achard, F., Latham, J., Witt, R., and Weber, J., 2008. GLOBCOVER The most detailed portrait of Earth. *Esa Bulletin-European Space Agency*, 136, 24–31.
- Armah, F.A., Yawson, D.O., Yengoh, G.T., Odoi, J.O., and Afrifa, E.K.A., 2010. Impact of Floods on Livelihoods and Vulnerability of Natural Resource Dependent Communities in Northern Ghana. *Water*, 2 (2), 120–139.
- Arvor, D., Jonathan, M., Meirelles, M.S.P., Dubreuil, V., and Durieux, L., 2011. Classification of MODIS EVI time series for crop mapping in the state of Mato Grosso, Brazil. *International Journal of Remote Sensing*, 32 (22), 7847–7871.
- Atkinson, P.M. and Tatnall, A.R.L., 1997. Introduction Neural networks in remote sensing. *International Journal of Remote Sensing*, 18 (4), 699–709.
- Aubert, M., Baghdadi, N., Zribi, M., Douaoui, A., Loumagne, C., Baup, F., El Hajj, M., and Garrigues, S., 2011. Analysis of TerraSAR-X data sensitivity to bare soil moisture, roughness, composition and soil crust. *Remote Sensing of Environment*, 115 (8), 1801–1810.
- Avohou, H.T. and Sinsin, B., 2009. The Effects of Topographic Factors on Aboveground Biomass Production of Grasslands in the Atacora Mountains in Northwestern Benin. *Mountain Research and Development*, 29 (3), 250–254.
- Bado, B. V, Bationo, A., Lompo, F., Traore, K., Sedogo, M.P., and Cescas, M.P., 2012. Long Term Effects of Crop Rotations with Fallow or Groundnut on Soil Fertility and Succeeding Sorghum Yields in the Guinea Savannah of West Africa. In: A. Bationo, B. Waswa, J. Kihara, I. Adolwa, B. Vanlauwe, and K. Saidou, eds. *Lessons learned from Long-term Soil Fertility Management Experiments in Africa SE - 2*. Springer Netherlands, 27–40.
- Baghdadi, N., Cresson, R., Todoroff, P., and Moinet, S., 2010. Multitemporal observations of sugarcane by TerraSAR-X images. *Sensors (Basel, Switzerland)*, 10 (10), 8899–919.
- Ban, Y., 2003. Synergy of multitemporal ERS-1 SAR and Landsat TM data for classification of agricultural crops. *Canadian Journal of Remote Sensing*, 29 (4), 518–526.
- Banful, A.B., 2011. Old Problems in the New Solutions? Politically Motivated Allocation of Program Benefits and the “New” Fertilizer Subsidies. *World Development*, 39 (7), 1166–1176.
- BARBOSA, P.M., CASTERAD, M.A., and HERRERO, J., 1996. Performance of several Landsat 5 Thematic Mapper (TM) image classification methods for crop extent estimates in an irrigation district. *International Journal of Remote Sensing*, 17 (18), 3665–3674.
- Bargiel, D. and Herrmann, S., 2011. Multi-Temporal Land-Cover Classification of Agricultural Areas in Two European Regions with High Resolution Spotlight TerraSAR-X Data. *Remote Sensing*, 3 (12), 859–877.
- Barrett, C.B., Reardon, T., and Webb, P., 2001. Nonfarm income diversification and household livelihood strategies in rural Africa: concepts, dynamics, and policy implications. *Food Policy*, 26 (4), 315–331.
- Bationo, A., Buerkert, A., Sedogo, M.P., Christianson, B.C., and Mokwunye, A.U., 1995a. A critical review of crop residue use as soil amendment in the West African semi-arid tropics. In: J.M.

## Appendices

---

- Powell, S. Fernandez Rivera, T.O. Williams, and C. Renard, eds. *Livestock and Sustainable Nutrient Cycling in Mixed Farming Systems of SubSaharan Africa*. Addis Ababa: International Livestock Center for Africa, 305–322.
- Bationo, A., Buerkert, A., Sedogo, M.P., Christianson, B.C., and Mokwunye, A.U., 1995b. A critical review of crop residue use as soil amendment in the West African semi-arid tropics. *In: J.M. Powell, S. Fernandez Rivera, T.O. Williams, and C. Renard, eds. Livestock and Sustainable Nutrient Cycling in Mixed Farming Systems of SubSaharan Africa*. Addis Ababa: International Livestock Center for Africa, 305–322.
- Bationo, A., Kihara, J., Vanlauwe, B., Waswa, B., and Kimetu, J., 2007. Soil organic carbon dynamics, functions and management in West African agro-ecosystems. *Agricultural Systems*, 94 (0308), 13–25.
- Bationo, A. and Mokwunye, A.U., 1991. Role of manures and crop residue in alleviating soil fertility constraints to crop production: With special reference to the Sahelian and Sudanian zones of West Africa. *In: A.U. Mokwunye, ed. Alleviating Soil Fertility Constraints to Increased Crop Production in West Africa SE - 19*. Springer Netherlands, 217–225.
- Bationo, A., Waswa, B., Okeyo, J.M., Maina, F., Kihara, J., and Mokwunye, U., 2011. Comparative Analysis of the Current and Potential Role of Legumes in Integrated Soil Fertility Management in West and Central Africa. *In: A. Bationo, B. Waswa, J.M. Okeyo, F. Maina, J. Kihara, and U. Mokwunye, eds. Fighting Poverty in Sub-Saharan Africa: The Multiple Roles of Legumes in Integrated Soil Fertility Management*. Dordrecht: Springer Netherlands, 117–150.
- Bauer, E., Claussen, M., Brovkin, V., and Huenerbein, A., 2003. Assessing climate forcings of the Earth system for the past millennium. *Geophysical Research Letters*, 30 (6), n/a–n/a.
- Bayala, J., Sileshi, G.W., Coe, R., Kalinganire, a., Tchoundjeu, Z., Sinclair, F., and Garrity, D., 2012. Cereal yield response to conservation agriculture practices in drylands of West Africa: A quantitative synthesis. *Journal of Arid Environments*, 78, 13–25.
- BBC, 2007. Million hit by floods in Africa [online]. Available from: <http://news.bbc.co.uk/2/hi/africa/6998651.stm> [Accessed 27 Jul 2014].
- Becker, M. and Johnson, D.E., 2001. Cropping intensity effects on upland rice yield and sustainability in West Africa. *Nutrient Cycling in Agroecosystems*, 59 (2), 107–117.
- Belshaw, D.G.R., 1983. *Crop production data in Uganda: a statistical evaluation of international agricultural census methodology*. Norwich, UK, No. 7.
- Berberoglu, S., Lloyd, C.D., Atkinson, P.M., and Curran, P.J., 2000. The integration of spectral and textural information using neural networks for land cover mapping in the Mediterranean. *Computers & Geosciences*, 26 (4), 385–396.
- Berk, A., Anderson, G., Acharya, P., and Shettle, E., 2008. *MODTRAN 5.2.0.0 USER'S MANUAL*. Burlington, MA: SPECTRAL SCIENCES, INC.
- Biro, K., Pradhan, B., Buchroithner, M., and Makeshin, F., 2013. LAND USE / LAND COVER CHANGE ANALYSIS AND ITS IMPACT ON SOIL PROPERTIES IN THE NORTHERN PART OF GADARIF REGION, SUDAN. *Land Degradation & Development*, 24, 90–102.

## Appendices

---

- BlackBridge, 2013. Satellite Imagery Product Specifications [online]. Available from: [http://blackbridge.com/rapideye/upload/RE\\_Product\\_Specifications\\_ENG.pdf](http://blackbridge.com/rapideye/upload/RE_Product_Specifications_ENG.pdf) [Accessed 16 Jul 2014].
- Blaes, X., Vanhalle, L., and Defourny, P., 2005. Efficiency of crop identification based on optical and SAR image time series. *Remote Sensing of Environment*, 96 (3–4), 352–365.
- Blaschke, T., 2010. Object based image analysis for remote sensing. *ISPRS Journal of Photogrammetry and Remote Sensing*, 65 (1), 2–16.
- Blaschke, T., Lang, S., and Hay, G., 2008. *Object-Based Image Analysis: Spatial Concepts for Knowledge-Driven Remote Sensing Applications*. Springer Science & Business Media.
- Boerner, W.M., 2004. Basics of SAR polarimetry I. Radar polarimetry and interferometry. In: *RTO SET Lecture Series*. Brussels, Belgium, 14–15 October 2004/Washington, DC, USA, 18–19 October 2004/Ottawa, ON, Canada, 21–22 October 2004, 100.
- Boko, M., Niang, I., Nyong, A., Vogel, C., Githeko, A., Medany, M., Osman-Elasha, B., Tabo, R., and Yanda, P., 2007. Africa. In: M.L. Parry, O.F. Canziani, J.P. Palutikof, P.J. van der Linden, and C.E. Hanson, eds. *Climate Change 2007: Impacts, Adaptation and Vulnerability. Contribution of Working Group II to the Fourth Assessment Report of the Intergovernmental Panel on Climate Change*. Cambridge: Cambridge University Press, 433–467.
- Borak, J.S., 1999. Feature selection and land cover classification of a MODIS-like data set for a semiarid environment. *International Journal of Remote Sensing*, 20 (5), 919–938.
- Bossa, A.Y., Diekkrüger, B., Giertz, S., Steup, G., Sintondji, L.O., Agbossou, E.K., and Hiepe, C., 2012. Modeling the effects of crop patterns and management scenarios on N and P loads to surface water and groundwater in a semi-humid catchment (West Africa). *Agricultural Water Management*, 115 (0), 20–37.
- Boularbah, S., Ouarzeddine, M., and Belhadj-Aissa, A., 2012. Investigation of the capability of the Compact Polarimetry mode to Reconstruct Full Polarimetry mode using RADARSAT2 data. *Advanced Electromagnetics*, 1 (1), 19.
- Bouvet, A. and Le Toan, T., 2011. Use of ENVISAT/ASAR wide-swath data for timely rice fields mapping in the Mekong River Delta. *Remote Sensing of Environment*, 115 (4), 1090–1101.
- Braimoh, a. K. and Vlek, P.L.G., 2004. The impact of land-cover change on soil properties in northern Ghana. *Land Degradation & Development*, 15 (1), 65–74.
- Braimoh, A.K., 2004. Modeling land-use change in the Volta Basin of Ghana. Centre for Development Research, University of Bonn.
- Braimoh, A.K., 2009. Agricultural land-use change during economic reforms in Ghana. *Land Use Policy*, 26 (3), 763–771.
- Braman, L.M., van Aalst, M.K., Mason, S.J., Suarez, P., Ait-Chellouche, Y., and Tall, A., 2013. Climate forecasts in disaster management: Red Cross flood operations in West Africa, 2008. *Disasters*, 37 (1), 144–164.

## Appendices

---

- Breiman, L., 1996. Bagging predictors. *Machine Learning*, 24 (2), 123–140.
- Breiman, L., 2001. Random Forests. *Machine Learning*, 45 (1), 5–32.
- Breiman, L., 2002. Manual on setting up, using, and understanding random forests v3.1 [online]. Available from: <http://oz.berkeley.edu/users/breiman/> [Accessed 11 Jul 2014].
- Breiman, L., Friedman, J.H., Olshen, R.A., and Stone, C., 1984. *Classification and Regression Trees*. London: Chapman & Hall.
- Briem, G.J., Benediktsson, J.A., and Sveinsson, J.R., 2002. Multiple classifiers applied to multisource remote sensing data. *Geoscience and Remote Sensing, IEEE Transactions on*.
- Brink, A.B. and Eva, H.D., 2009. Monitoring 25 years of land cover change dynamics in Africa: A sample based remote sensing approach. *Applied Geography*, 29 (4), 501–512.
- Brinkmann, K., Dickhoefer, U., Schlecht, E., and Buerkert, A., 2011. Quantification of aboveground rangeland productivity and anthropogenic degradation on the Arabian Peninsula using Landsat imagery and field inventory data. *Remote Sensing of Environment*, 115 (2), 465–474.
- Brinkmann, K., Schumacher, J., Dittrich, A., Kadaore, I., and Buerkert, A., 2012. Analysis of landscape transformation processes in and around four West African cities over the last 50 years. *Landscape and Urban Planning*, 105 (1–2), 94–105.
- Brisco, B. and Brown, R.J., 1995. Multidate SAR/TM synergism for crop classification in western Canada. *Photogrammetric engineering and remote sensing*, 61 (8), 1009–1014.
- Brisco, B., BROWN, R.J., and Manore, M.J., 1989. Early season crop discrimination with combined SAR and TM data. *Canadian Journal of Remote Sensing*, 15 (1), 44–54.
- Bruce, J., 1993. Do indigenous tenure systems constrain agricultural development? In: T. Bassett and D. Crummey, eds. *Land in African agrarian systems*. Madison, Wisconsin: University of Wisconsin Press, 35–56.
- Buades, A., Coll, B., and Morel, J., 2005. A Review of Image Denoising Algorithms, with a New One. *Multiscale Modeling & Simulation*, 4 (2), 490–530.
- Budreski, K.A., Wynne, R.H., Browder, J.O., and Campbell, J.B., 2007. Comparison of Segment and Pixel-based Non-parametric Land Cover Classification in the Brazilian Amazon Using Multitemporal Landsat TM/ETM+ Imagery. *Photogrammetric engineering and remote sensing*, 73 (7), 813–827.
- Calle, M.L. and Urrea, V., 2011. Letter to the editor: Stability of Random Forest importance measures. *Briefings in bioinformatics*, 12 (1), 86–9.
- Callo-Concha, D., Gaiser, T., and Ewert, F., 2012. *Farming and cropping systems in the West African Sudanian Savanna*. Bonn, No. 100.
- Camberlin, P., Martiny, N., Philippon, N., and Richard, Y., 2007. Determinants of the interannual relationships between remote sensed photosynthetic activity and rainfall in tropical Africa. *Remote Sensing of Environment*, 106 (2), 199–216.

## Appendices

---

- Camps-Valls, G., Gomez-Chova, L., Calpe-Maravilla, J., Martin-Guerrero, J.D., Soria-Olivas, E., Alonso-Chorda, L., and Moreno, J., 2004. Robust support vector method for hyperspectral data classification and knowledge discovery. *Geoscience and Remote Sensing, IEEE Transactions on*.
- Candade, N. and Dixon, B., 2004. Multispectral classification of Landsat images: a comparison of support vector machine and neural network classifiers. *In: ASPRS Annual Conference Proceedings*. Denver, Colorado.
- Casanova, D., Epema, G.F., and Goudriaan, J., 1998. Monitoring rice reflectance at field level for estimating biomass and LAI. *Field Crops Research*, 55 (1-2), 83–92.
- Chander, G., Markham, B.L., and Helder, D.L., 2009. Summary of current radiometric calibration coefficients for Landsat MSS, TM, ETM+, and EO-1 ALI sensors. *Remote Sensing of Environment*, 113 (5), 893–903.
- Chen, J., Zhu, X., Vogelmann, J.E., Gao, F., and Jin, S., 2011. A simple and effective method for filling gaps in Landsat ETM+ SLC-off images. *Remote Sensing of Environment*, 115 (4), 1053–1064.
- Chen, K.S., Huang, W.P., Tsay, D.H., and Amar, F., 1996. Classification of multifrequency polarimetric SAR imagery using a dynamic learning neural network. *Geoscience and Remote Sensing, IEEE Transactions on*.
- Clinton, B., 1995. Release of Imagery Acquired by Space-Based National Intelligence Reconnaissance System.
- Cloude, S., 2009. *Polarisation—Applications in Remote Sensing*. Oxford, UK: Oxford University Press.
- Cohen, J., 1960. A coefficient of agreement for nominal scales. *Educational and Psychological Measurement*, 20, 37–46.
- Cohen, Y. and Shoshany, M., 2002. A national knowledge-based crop recognition in Mediterranean environment. *International Journal of Applied Earth Observation and Geoinformation*, 4 (1), 75–87.
- Cohen, Y. and Shoshany, M., 2005. Analysis of convergent evidence in an evidential reasoning knowledge-based classification. *Remote Sensing of Environment*, 96 (3–4), 518–528.
- Colditz, R.R., Conrad, C., Wehrmann, T., Schmidt, M., and Dech, S., 2008. TiSeG: A Flexible Software Tool for Time-Series Generation of MODIS Data Utilizing the Quality Assessment Science Data Set. *Geoscience and Remote Sensing, IEEE Transactions on*.
- Collinson, S.T., Azam-Ali, S.N., Chavula, K.M., and Hodson, D.A., 1996. Growth, development and yield of bambara groundnut (*Vigna subterranea*) in response to soil moisture. *The Journal of Agricultural Science*, 126 (03), 307–318.
- Commission for Africa, 2005. *Our common interest*.
- Comon, P., 1994. Independent component analysis, A new concept? *Signal Processing*, 36 (3), 287–314.

## Appendices

---

- Congalton, R.G. and Green, K., 2009. *Assessing the Accuracy of Remotely Sensed Data. Principles and Practices*. 2nd ed. London: CRC Press Inc.
- Conrad, C., Colditz, R.R., Dech, S., Klein, D., and Vlek, P.L.G., 2011. Temporal segmentation of MODIS time series for improving crop classification in Central Asian irrigation systems. *International Journal of Remote Sensing*, 32 (23), 8763–8778.
- Conrad, C., Dech, S., Dubovyk, O., Fritsch, S., Klein, D., Löw, F., Schorcht, G., and Zeidler, J., 2014. Derivation of temporal windows for accurate crop discrimination in heterogeneous croplands of Uzbekistan using multitemporal RapidEye images. *Computers and Electronics in Agriculture*, 103 (0), 63–74.
- Conrad, C., Fritsch, S., Zeidler, J., Rücker, G., and Dech, S., 2010. Per-Field Irrigated Crop Classification in Arid Central Asia Using SPOT and ASTER Data. *Remote Sensing*, 2 (4), 1035–1056.
- Conrad, C., Rahmann, M., Machwitz, M., Stulina, G., Paeth, H., and Dech, S., 2013. Satellite based calculation of spatially distributed crop water requirements for cotton and wheat cultivation in Fergana Valley, Uzbekistan. *Global and Planetary Change*, 110, 88–98.
- Cooper, P.J.M., Gregory, P.J., Tully, D., and Harris, H.C., 1987. Improving Water use Efficiency of Annual Crops in the Rainfed Farming Systems of West Asia and North Africa. *Experimental Agriculture*, 23 (02), 113–158.
- Cord, A., Conrad, C., Schmidt, M., and Dech, S., 2010. Standardized FAO-LCCS land cover mapping in heterogeneous tree savannas of West Africa. *Journal of Arid Environments*, 74 (9), 1083–1091.
- Cordell, D.D., Gregory, J.W., and Piche, V., 1996. *No TitleHoe and wage: A social history of a circular migration system in West Africa*. Boulder, Colorado: Westview Press.
- Davison, J.E., Breshears, D.D., van Leeuwen, W.J.D., and Casady, G.M., 2011. Remotely sensed vegetation phenology and productivity along a climatic gradient: on the value of incorporating the dimension of woody plant cover. *Global Ecology and Biogeography*, 20 (1), 101–113.
- Dawbin, K.W. and Evans, J.C., 1988. Large area crop classification in New South Wales, Australia, using Landsat data. *International Journal of Remote Sensing*, 9 (2), 295–301.
- DeFries, R., Hansen, M., Steininger, M., Dubayah, R., Sohlberg, R., and Townshend, J., 1997. Subpixel forest cover in central Africa from multisensor, multitemporal data. *Remote Sensing of Environment*, 60 (3), 228–246.
- DeFries, R.S., Field, C.B., Fung, I., Justice, C.O., Los, S., Matson, P.A., Matthews, E., Mooney, H.A., Potter, C.S., Prentice, K., Sellers, P.J., Townshend, J.R.G., Tucker, C.J., Ustin, S.L., and Vitousek, P.M., 1995. Mapping the land surface for global atmosphere-biosphere models: Toward continuous distributions of vegetation's functional properties. *Journal of Geophysical Research: Atmospheres*, 100 (D10), 20867–20882.
- DeFries, R.S., Townshend, J.R.G., and Hansen, M.C., 1999. Continuous fields of vegetation characteristics at the global scale at 1-km resolution. *Journal of Geophysical Research: Atmospheres*, 104 (D14), 16911–16923.

## Appendices

---

- Deledalle, C.-A., Tupin, F., and Denis, L., 2010. Polarimetric SAR estimation based on non-local means. *Geoscience and Remote Sensing Symposium (IGARSS), 2010 IEEE International*.
- DELVES, L.M., WILKINSON, R., OLIVER, C.J., and WHITE, R.G., 1992. Comparing the performance of SAR image segmentation algorithms. *International Journal of Remote Sensing*, 13 (11), 2121–2149.
- Deng, Z., 2007. *Vegetation Dynamics in Queme Basin, Benin, West Afrika*. Göttingen, Germany: Cuvillier Verlag Göttingen.
- Deutsches Zentrum für Luft- und Raumfahrt (DLR), 2009. TerraSAR-X Ground Segment Basic Product Specification Document, V. 1.6; TX-GS-DD-3302 [online]. Available from: file:///C:/Users/[Accessed 11 Jul 2014].
- Dingle Robertson, L. and King, D.J., 2011. Comparison of pixel- and object-based classification in land cover change mapping. *International Journal of Remote Sensing*, 32 (6), 1505–1529.
- Dixon, B. and Candade, N., 2007. Multispectral landuse classification using neural networks and support vector machines: one or the other, or both? *International Journal of Remote Sensing*, 29 (4), 1185–1206.
- Dixon, J., Gulliver, A., and Gibbon, D., 2001. *Farming systems and poverty: improving farmers' livelihoods in a changing world*. Rome: FAO.
- Dong, J., Zhuang, D., Huang, Y., and Fu, J., 2009. Advances in Multi-Sensor Data Fusion: Algorithms and Applications. *Sensors*, 9, 7771–7784.
- Donner, S.D. and Kucharik, C.J., 2003. Evaluating the impacts of land management and climate variability on crop production and nitrate export across the Upper Mississippi Basin. *Global Biogeochemical Cycles*, 17 (3), n/a–n/a.
- Duadze, S.E., 2004. *Land Use and Land Cover Study of the Savanna Ecosystem in the Upper West Region (Ghana) Using Remote Sensing*. Bonn: Cuvillier Verlag Göttingen.
- ECOWAP, 2008. *Regional Agricultural Policy for West Africa*. Abuja: ECOWAS.
- Eguavoen, I., 2008. *The political ecology of household water in Northern Ghana*. Social Anthropology. Munster, Germany: LIT Verlag.
- Eklundh, L. and Jönsson, P., 2010. TIMESAT 3.0 Software Manual [online]. Available from: [www.nateko.lu.se/timesat/docs/timesat30\\_software\\_manual.pdf](http://www.nateko.lu.se/timesat/docs/timesat30_software_manual.pdf) [Accessed 7 Aug 2013].
- Ellis, E.C., Klein Goldewijk, K., Siebert, S., Lightman, D., and Ramankutty, N., 2010. Anthropogenic transformation of the biomes, 1700 to 2000. *Global Ecology and Biogeography*, 19 (5), 589–606.
- Elmore, A.J., Mustard, J.F., Manning, S.J., and Lobell, D.B., 2000. Quantifying Vegetation Change in Semiarid Environments: Precision and Accuracy of Spectral Mixture Analysis and the Normalized Difference Vegetation Index. *Remote Sensing of Environment*, 73 (1), 87–102.



## Appendices

---

- Engdahl, M., Minchella, A., Marinkovic, P., Veci, L., and Lu, J., 2012. NEST: An esa open source Toolbox for scientific exploitation of SAR data. *Geoscience and Remote Sensing Symposium (IGARSS), 2012 IEEE International*.
- Enyong, L.A., Debrah, S.K., and Bationo, A., 1999. Farmers' perceptions and attitudes towards introduced soil-fertility enhancing technologies in western Africa. *Nutrient Cycling in Agroecosystems*, 53 (2), 177–187.
- Eva, H. and Lambin, E.F., 1998. Remote Sensing of Biomass Burning in Tropical Regions. *Remote Sensing of Environment*, 64 (3), 292–315.
- Ezeh, A.C., Bongaarts, J., and Mberu, B., 2012. Global population trends and policy options. *Lancet*, 380 (9837), 142–8.
- FAO /GIEWS, 1996. *Global Watch*.
- FAO and University of Ibada, 1982. *Recommendations arising from the Workshop on Shifting Cultivation and Extension*. Rome: Food and Agricultural Organization.
- Farr, T.G. and Kobrick, M., 2000. Shuttle radar topography mission produces a wealth of data. *Eos, Transactions American Geophysical Union*, 81 (48), 583–585.
- Ferrazzoli, P., Paloscia, S., Pampaloni, P., Schiavon, G., Sigismondi, S., and Solimini, D., 1997. The potential of multifrequency polarimetric SAR in assessing agricultural and arboreous biomass. *Geoscience and Remote Sensing, IEEE Transactions on*.
- Flitcroft, I.D., Milford, J.R., and Dugdale, G., 1989. Relating Point to Area Average Rainfall in Semiarid West Africa and the Implications for Rainfall Estimates Derived from Satellite Data. *Journal of Applied Meteorology*, 28 (4), 252–266.
- Foerster, S., Kaden, K., Foerster, M., and Itzerott, S., 2012. Crop type mapping using spectral–temporal profiles and phenological information. *Computers and Electronics in Agriculture*, 89, 30–40.
- Foley, J. a, Defries, R., Asner, G.P., Barford, C., Bonan, G., Carpenter, S.R., Chapin, F.S., Coe, M.T., Daily, G.C., Gibbs, H.K., Helkowski, J.H., Holloway, T., Howard, E. a, Kucharik, C.J., Monfreda, C., Patz, J. a, Prentice, I.C., Ramankutty, N., and Snyder, P.K., 2005. Global consequences of land use. *Science (New York, N.Y.)*, 309 (5734), 570–4.
- Foley, J. a, Ramankutty, N., Brauman, K. a, Cassidy, E.S., Gerber, J.S., Johnston, M., Mueller, N.D., O'Connell, C., Ray, D.K., West, P.C., Balzer, C., Bennett, E.M., Carpenter, S.R., Hill, J., Monfreda, C., Polasky, S., Rockström, J., Sheehan, J., Siebert, S., Tilman, D., and Zaks, D.P.M., 2011. Solutions for a cultivated planet. *Nature*, 478 (7369), 337–42.
- Foody, G.M., 1995. Land cover classification by an artificial neural network with ancillary information. *International Journal of Geographical Information Systems*, 9 (5), 527–542.
- Foody, G.M., 2004a. Thematic Map Comparison. *Photogrammetric Engineering & Remote Sensing*, 70 (5), 627–633.

## Appendices

---

- Foody, G.M., 2004b. Thematic Map Comparison. *Photogrammetric Engineering & Remote Sensing*, 70 (5), 627–633.
- Forkuor, G. and Cofie, O., 2011. Dynamics of land-use and land-cover change in Freetown, Sierra Leone and its effects on urban and peri-urban agriculture – a remote sensing approach. *International Journal of Remote Sensing*, 32 (4), 1017–1037.
- Forkuor, G., Conrad, C., Landmann, T., and Thiel, M., 2013. Improving agricultural land use mapping in West Africa using multi-temporal Landsat and RapidEye data. In: E. Borg, H. Daedelow, and R. Johnson, eds. *From the Basics to the Service*. Berlin: GITO mbH Verlag, 57–72.
- Forkuor, G., Conrad, C., Thiel, M., Ullmann, T., and Zoungrana, E., 2014. Integration of Optical and Synthetic Aperture Radar Imagery for Improving Crop Mapping in Northwestern Benin, West Africa. *Remote Sensing*, 6 (7), 6472–6499.
- Fraser, R.H., Hall, R.J., Landry, R., Lynham, T., Raymond, D., Lee, B., and Li, Z., 2004. Validation and Calibration of Canada-Wide Coarse-Resolution Satellite Burned-Area Maps. *Photogrammetric Engineering & Remote Sensing*, 70 (4), 451–460.
- Friedl, M.A. and Brodley, C.E., 1997. Decision tree classification of land cover from remotely sensed data. *Remote Sensing of Environment*, 61 (3), 399–409.
- Friedl, M.A., McIver, D.K., Hodges, J.C.F., Zhang, X.Y., Muchoney, D., Strahler, A.H., Woodcock, C.E., Gopal, S., Schneider, A., Cooper, A., Baccini, A., Gao, F., and Schaaf, C., 2002. Global land cover mapping from MODIS: algorithms and early results. *Remote Sensing of Environment*, 83 (1–2), 287–302.
- Friedl, M.A., Sulla-Menashe, D., Tan, B., Schneider, A., Ramankutty, N., Sibley, A., and Huang, X., 2010. MODIS Collection 5 global land cover: Algorithm refinements and characterization of new datasets. *Remote Sensing of Environment*, 114 (1), 168–182.
- Friedlingstein, P., Houghton, R.A., Marland, G., Hackler, J., Boden, T.A., Conway, T.J., Canadell, J.G., Raupach, M.R., Ciais, P., and Le Quere, C., 2010. Update on CO2 emissions. *Nature Geosci*, 3 (12), 811–812.
- Friesen, J., 2002. Spatio-temporal Rainfall Patterns in Northern Ghana. Universität Bonn.
- Fritz, S., Massart, M., Savin, I., Gallego, J., and Rembold, F., 2008. The use of MODIS data to derive acreage estimations for larger fields: A case study in the south-western Rostov region of Russia. *International Journal of Applied Earth Observation and Geoinformation*, 10 (4), 453–466.
- Fritz, S., See, L., and Rembold, F., 2010. Comparison of global and regional land cover maps with statistical information for the agricultural domain in Africa. *International Journal of Remote Sensing*, 31 (9), 2237–2256.
- Frizzelle, B.G. and Moody, A., 2001. Mapping Continuous Distributions of Land Cover: A Comparison of Maximum-Likelihood Estimation and Artificial Neural Networks. *Photogrammetric engineering and remote sensing*, 67 (6), 693–705.

## Appendices

---

- GALLEGO, F.J., DELINCE, J., and RUEDA, C., 1993. Crop area estimates through remote sensing: stability of the regression correction. *International Journal of Remote Sensing*, 14 (18), 3433–3445.
- Gao, F., Masek, J., Schwaller, M., and Hall, F., 2006. On the blending of the Landsat and MODIS surface reflectance: predicting daily Landsat surface reflectance. *Geoscience and Remote Sensing, IEEE Transactions on*.
- Gauthier, Y., Bernier, M., and Fortin, J.-P., 1998. Aspect and incidence angle sensitivity in ERS-1 SAR data. *International Journal of Remote Sensing*, 19 (10), 2001–2006.
- Genesio, L., Bacci, M., Baron, C., Diarra, B., Di Vecchia, a., Alhassane, a., Hassane, I., Ndiaye, M., Philippon, N., Tarchiani, V., and Traoré, S., 2011. Early warning systems for food security in West Africa: evolution, achievements and challenges. *Atmospheric Science Letters*, 12 (1), 142–148.
- Genuer, R., Poggi, J.-M., and Tuleau-Malot, C., 2010. Variable selection using random forests. *Pattern Recognition Letters*, 31 (14), 2225–2236.
- GERSTL, S.A.W., 1990. Physics concepts of optical and radar reflectance signatures A summary review. *International Journal of Remote Sensing*, 11 (7), 1109–1117.
- Gessner, U., Machwitz, M., Conrad, C., and Dech, S., 2013. Estimating the fractional cover of growth forms and bare surface in savannas. A multi-resolution approach based on regression tree ensembles. *Remote Sensing of Environment*, 129 (0), 90–102.
- Ghana Statistical Service, 2005. *2000 Population and Housing Census: Analysis of District Data and Implications for Planning Upper East Region*. Accra: Ghana Statistical Service.
- Ghana Statistical Service, 2007. *Patterns and Trends of Poverty in Ghana: 1991–2006*. Accra: Ghana Statistical Service.
- Ghana Statistical Service, 2012. *2010 POPULATION & HOUSING CENSUS SUMMARY REPORT OF FINAL RESULTS*. Accra: Ghana Statistical Service.
- Gibbs, H.K., Ruesch, A.S., Achard, F., Clayton, M.K., Holmgren, P., Ramankutty, N., and Foley, J.A., 2010. Tropical forests were the primary sources of new agricultural land in the 1980s and 1990s. *Proceedings of the National Academy of Sciences of the United States of America*, 107 (38), 1–6.
- Gilruth, P.T., Hutchinson, C.F., and Barry, B., 1990. Assessing deforestation in the Guinea Highlands of West Africa using remote sensing. *Photogrammetric engineering and remote sensing*, 56 (10), 1375–1382.
- Giri, C.P., 2012. *Remote Sensing of Land Use and Land Cover: Principles and Applications*. Boca Raton, Florida: CRC Press Inc.
- Gislason, P.O., Benediktsson, J.A., and Sveinsson, J.R., 2006. Random Forests for land cover classification. *Pattern Recognition Letters*, 27 (4), 294–300.

## Appendices

---

- Gong, P. and Howarth, P., 1990. The Use of Structural Information for Improving Land Cover Classification Accuracies at the Rural-Urban Fringe. *Photogrammetric engineering and remote sensing*, 56 (1), 67–73.
- Gordon, L.J., Finlayson, C.M., and Falkenmark, M., 2010. Managing water in agriculture for food production and other ecosystem services. *Agricultural Water Management*, 97 (4), 512–519.
- Di Gregorio, A.D. and Jansen, L., 2005. *Land Cover Classification System, Classification Concepts and User Manual, Software Version 2: Environmental and Natural Resources Series 8*. Rome: Food and Agricultural Organization.
- De Groote, H. and Traoré, O., 2005. The cost of accuracy in crop area estimation. *Agricultural Systems*, 84 (1), 21–38.
- Guissard, A., 1994. Mueller and Kennaugh matrices in radar polarimetry. *Geoscience and Remote Sensing, IEEE Transactions on*.
- Gumma, M., Pyla, K., Thenkabail, P., Reddi, V., Naresh, G., Mohammed, I., and Rafi, I., 2014. Crop Dominance Mapping with IRS-P6 and MODIS 250-m Time Series Data. *Agriculture*, 4 (2), 113–131.
- Gyau-Boakye, P. and Tumbulto, J.W., 2006. Comparison of rainfall and runoff in the humid south-western and the semiarid northern savannah zone in Ghana. *African Journal of Science and Technology*, 7 (1), 64–72.
- Haack, B. and Rafter, A., 2010. Regression estimation techniques with remote sensing: a review and case study. *Geocarto International*, 25 (1), 71–82.
- Haack, B.N., 2007. Comparison of Land Use/Cover Mapping with Varied Radar Incident Angles and Seasons. *GIScience and Remote Sensing*, 44, 1–15.
- Hannerz, F. and Lotsch, A., 2008. Assessment of remotely sensed and statistical inventories of African agricultural fields. *International Journal of Remote Sensing*, 29 (13), 3787–3804.
- Hansen, M., Dubayah, R., and Defries, R., 1996. Classification trees: an alternative to traditional land cover classifiers. *International Journal of Remote Sensing*, 17 (5), 1075–1081.
- Hansen, M., DeFries, R., Townshend, J.R., Sohlberg, R., Dimiceli, C., and Carroll, M., 2002. Towards an operational MODIS continuous field of percent tree cover algorithm: examples using AVHRR and MODIS data. *Remote Sensing of Environment*, 83, 303–319.
- Hansen, M.C. and DeFries, R.S., 2004. Detecting Long-term Global Forest Change Using Continuous Fields of Tree-Cover Maps from 8-km Advanced Very High Resolution Radiometer (AVHRR) Data for the Years 1982–1999. *Ecosystems*, 7 (7), 695–716.
- Hansen, M.C., DeFries, R.S., Townshend, J.R.G., Marufu, L., and Sohlberg, R., 2002. Development of a MODIS tree cover validation data set for Western Province, Zambia. *Remote Sensing of Environment*, 83 (1-2), 320–335.
- Hassan, R.M., 1996. Planting strategies of maize farmers in Kenya: a simultaneous equations analysis in the presence of discrete dependent variables. *Agricultural Economics*, 15 (2), 137–149.

## Appendices

---

- Hayward, D. and Oguntoyinbo, J., 1987. *Climatology of West Africa*. London: Rowman & Littlefield Publishers.
- Henderson, F.M., Chasan, R., Portolese, J., and Hart, T., 2002. Evaluation of SAR-Optical Imagery Synthesis Techniques in a Complex Coastal Ecosystem. *Photogrammetric engineering and remote sensing*, 68, 839–846.
- Henson, B.. and Tomkins, B., 2011. *A Sociolinguistic Survey of the Biali Language Area: SIL Electronic Survey Report, 2011-011*. Dallas, TX, USA.
- Herold, M., Mayaux, P., Woodcock, C.E., Baccini, A., and Schmullius, C., 2008. Some challenges in global land cover mapping: An assessment of agreement and accuracy in existing 1 km datasets. *Remote Sensing of Environment*, 112 (5), 2538–2556.
- Herrmann, S.M., Anyamba, A., and Tucker, C.J., 2005. Recent trends in vegetation dynamics in the African Sahel and their relationship to climate. *Global Environmental Change*, 15 (4), 394–404.
- Heubes, J., Schmidt, M., Stuch, B., García Márquez, J.R., Wittig, R., Zizka, G., Thiombiano, A., Sinsin, B., Schaldach, R., and Hahn, K., 2013. The projected impact of climate and land use change on plant diversity: An example from West Africa. *Journal of Arid Environments*, 96, 48–54.
- Hideto, F., Muralikrishna, G., Prasad, T., and Regassa, N., 2011. Suitability Evaluation for Lowland Rice in Inland Valleys in West Africa. *Transactions of The Japanese Society of Irrigation, Drainage and Rural Engineering, Volume 78, Issue 4, pp. 281-289 (2011).*, 78, 281–289.
- Hilker, T., Wulder, M.A., Coops, N.C., Linke, J., McDermid, G., Masek, J.G., Gao, F., and White, J.C., 2009. A new data fusion model for high spatial- and temporal-resolution mapping of forest disturbance based on Landsat and MODIS. *Remote Sensing of Environment*, 113 (8), 1613–1627.
- Hong, G., Zhang, A., Zhou, F., and Brisco, B., 2014. Integration of optical and synthetic aperture radar (SAR) images to differentiate grassland and alfalfa in Prairie area. *International Journal of Applied Earth Observation and Geoinformation*, 28, 12–19.
- Huang, C., Davis, L.S., and Townshend, J.R.G., 2002. An assessment of support vector machines for land cover classification. *International Journal of Remote Sensing*, 23 (4), 725–749.
- Huete, A.R., 1988. A soil-adjusted vegetation index (SAVI). *Remote Sensing of Environment*, 25 (3), 295–309.
- Husak, G.J., Marshall, M.T., Michaelsen, J., Pedreros, D., Funk, C., and Galu, G., 2008. Crop area estimation using high and medium resolution satellite imagery in areas with complex topography. *Journal of Geophysical Research: Atmospheres*, 113 (D14), n/a–n/a.
- Hutchinson, C.F., 1982. Techniques for combining Landsat and Ancillary Data for Digital Classification Improvement. *Photogrammetric engineering and remote sensing*, 48 (1), 123–130.
- Hutchinson, C.F., 1991. Uses of satellite data for famine early warning in sub-Saharan Africa. *International Journal of Remote Sensing*, 12 (6), 1405–1421.

## Appendices

---

- Ibrahim, B., Karambiri, H., Polcher, J., Yacouba, H., and Ribstein, P., 2014. Changes in rainfall regime over Burkina Faso under the climate change conditions simulated by 5 regional climate models. *Climate Dynamics*, 42 (5-6), 1363–1381.
- Igue, A.M., Floquet, A., and Stahr, K., 2000. Land use and farming systems in Benin. In: F. Graef, P. Lawrence, and M. von Oppen, eds. *Adapted Farming in West Africa: Issues, Potentials and Perspectives*. Stuttgart, Germany: Verlag Ulrich E. Grauer, 227–238.
- Infoterra, 2008. Radiometric Calibration of TerraSAR-X Data: Beat Nought and Sigma Nought Coefficient Calculation; TSXX-ITD-TN-0049 [online]. Available from: file:///C:/Users/ [Accessed 14 Mar 2014].
- Ingram, K.T., Roncoli, M.C., and Kirshen, P.H., 2002. Opportunities and constraints for farmers of west Africa to use seasonal precipitation forecasts with Burkina Faso as a case study. *Agricultural Systems*, 74 (3), 331–349.
- INSD, 2007. *Résultats préliminaires du recensement général de la population et de l'habitat de 2006*. Ouagadougou, Burkina Faso: Institut National des Statistiques et de la Demographie (INSD), Direction de la Demographie.
- Institut National de la Statistique et de l'Analyse Economique, 2004. *Cashier des villages et quartiers de ville Département de l'ATACORA*. Cotonou: Ministère Chargé du Plan, de La Prospective et du Développement, Direction des Etudes Demographiques.
- International Food Policy Research Institute, 2006. *Regional Strategic Alternatives for Agriculture-led Growth and Poverty Reduction in West Africa*.
- INTERNATIONALTELECOMMUNICATIONUNION, 2007. Telecommunications/ICT Markets and Trends in Africa [online]. Available from: [http://www.itu.int/ITU-D/ict/statistics/material/af\\_report07.pdf](http://www.itu.int/ITU-D/ict/statistics/material/af_report07.pdf) [Accessed 14 Jun 2014].
- Irish, R. and Scaramuzza, P., 2005. SLC-Off Gap Filled Product Generation. [online]. Available from: [http://igett.delmar.edu/Resources/Remote Sensing Technology Training/SLC-off Gap](http://igett.delmar.edu/Resources/Remote%20Sensing%20Technology%20Training/SLC-off%20Gap) [Accessed 24 Jun 2014].
- ISSER, 2008. *The state of the Ghanaian economy in 2008*. Accra: Institute of Statistical, Social and Economic Research.
- Jakubauskas, M.E., Legates, D.R., and Kastens, J.H., 2002. Crop identification using harmonic analysis of time-series AVHRR NDVI data. *Computers and Electronics in Agriculture*, 37 (1–3), 127–139.
- Jalloh, A., Nelson, G.C., Thomas, T.S., and Roy-macauley, H., 2013. *West African Agriculture and Climate Change: A COMPREHENSIVE ANALYSIS*.
- Jensen, J., 1996. *Introductory digital image processing: a remote sensing perspective*. Upper Saddle River, USA: Prentice-Hall Inc.
- JEWELL, N., 1989. An evaluation of multi-date SPOT data for agriculture and land use mapping in the United Kingdom. *International Journal of Remote Sensing*, 10 (6), 939–951.

## Appendices

---

- Jia, K., Li, Q., Tian, Y., Wu, B., Zhang, F., and Meng, J., 2012. Crop classification using multi-configuration SAR data in the North China Plain. *International Journal of Remote Sensing*, 33 (1), 170–183.
- Jones, P. and Thornton, P., 2003. The potential impacts of climate change on maize production in Africa and Latin America in 2055. *Global Environmental Change*, 13 (1), 51–59.
- Jönsson, A.M., Eklundh, L., Hellström, M., Barring, L., and Jönsson, P., 2010. Annual changes in MODIS vegetation indices of Swedish coniferous forests in relation to snow dynamics and tree phenology. *Remote Sensing of Environment*, 114 (11), 2719–2730.
- Ju, J. and Roy, D.P., 2008. The availability of cloud-free Landsat ETM+ data over the conterminous United States and globally. *Remote Sensing of Environment*, 112 (3), 1196–1211.
- Jung, M., Henkel, K., Herold, M., and Churkina, G., 2006. Exploiting synergies of global land cover products for carbon cycle modeling. *Remote Sensing of Environment*, 101 (4), 534–553.
- JUSTICE, C.O., TOWNSHEND, J.R.G., HOLBEN, B.N., and TUCKER, C.J., 1985. Analysis of the phenology of global vegetation using meteorological satellite data. *International Journal of Remote Sensing*, 6 (8), 1271–1318.
- Kamara, A.Y., Ekeleme, F., Chikoye, D., and Omoigui, L.O., 2009. Planting Date and Cultivar Effects on Grain Yield in Dryland Corn Production All rights reserved. No part of this periodical may be reproduced or transmitted in any form or by any means, electronic or mechanical, including photocopying, recording, or any .
- Kanchebe, E., 2010. Local Knowledge and Livelihood Sustainability under Environmental Change in Northern Ghana. University of Bonn.
- Karbo, N. and Agyare, W.A., 2002. Crop-livestock systems in Northern Ghana. In: G. Tarawali and P. Hiernaux, eds. *Improving crop-livestock systems in the dry savannas of West and Central Africa. Reports from the workshop on crop-livestock systems in the dry savannas of West and Central Africa*. Ibadan: IITA.
- Kolavalli, S., Robinson, E., Diao, X., Alpuerto, V., Folledo, R., Slavova, M., Ngeleza, G., and Asante, F., 2012. *Economic Transformation in Ghana: Where Will the Path Lead?* Washington DC, No. 01161.
- Kontoes, C., Wilkinson, G.G., Burrill, A., Goffredo, S., and Mégier, J., 1993. An experimental system for the integration of GIS data in knowledge-based image analysis for remote sensing of agriculture. *International Journal of Geographical Information Systems*, 7 (3), 247–262.
- Koppe, W., Gnyp, M.L., Hütt, C., Yao, Y., Miao, Y., Chen, X., and Bareth, G., 2013. Rice monitoring with multi-temporal and dual-polarimetric TerraSAR-X data. *International Journal of Applied Earth Observation and Geoinformation*, 21, 568–576.
- Kranjac Brisavljevic, G. and Blench, R., 1999. *Rethinking Natural Resource degradation in Semi-Arid Sub-Saharan Africa: The Case of Semi-Arid Ghana*. London: Overseas Development Institute and Faculty of Agriculture, UDS. Tamale.Ghana.

## Appendices

---

- Kurosu, T., Fujita, M., and Chiba, K., 1997. The identification of rice fields using multi-temporal ERS-1 C band SAR data. *International Journal of Remote Sensing*, 18 (14), 2953–2965.
- L'HÔTE, Y., MAHÉ, G.I.L., SOMÉ, B., and TRIBOULET, J.P., 2002. Analysis of a Sahelian annual rainfall index from 1896 to 2000; the drought continues. *Hydrological Sciences Journal*, 47 (4), 563–572.
- Lacombe, G., McCartney, M., and Forkuor, G., 2012. Drying climate in Ghana over the period 1960–2005: evidence from the resampling-based Mann-Kendall test at local and regional levels. *Hydrological Sciences Journal*.
- Lambin, E.F., Geist, H.J., and Lepers, E., 2003. Dynamics of Land Use and Land-Cover Change in Tropical Regions. *Annual Review of Environment and Resources*, 28 (1), 205–241.
- Lambin, E.F. and Meyfroidt, P., 2011. Global land use change, economic globalization, and the looming land scarcity. *Proceedings of the National Academy of Sciences of the United States of America*, 108, 3465–3472.
- Lambin, E.F., Turner, B.L., Geist, H.J., Agbola, S.B., Angelsen, A., Bruce, J.W., Coomes, O.T., Dirzo, R., Fischer, G., Folke, C., George, P.S., Homewood, K., Imbernon, J., Leemans, R., Li, X., Moran, E.F., Mortimore, M., Ramakrishnan, P.S., Richards, J.F., Skånes, H., Steffen, W., Stone, G.D., Svedin, U., Veldkamp, T. a., Vogel, C., and Xu, J., 2001. The causes of land-use and land-cover change: moving beyond the myths. *Global Environmental Change*, 11 (4), 261–269.
- Laube, W., 2007. *Changing Natural Resource Regimes in Northern Ghana. Actors, Structure and Institutions*. Münster: LIT Verlag.
- Laudien, R., Pofagi, M., and Roehrig, J., 2010. Development and implementation of an interactive Spatial Decision Support System for decision makers in Benin to evaluate agricultural land resources—Case study: AGROLAND. *International Journal of Applied Earth Observation and Geoinformation*, 12, Supple (0), S38–S44.
- Laux, P., Kunstmann, H., and Bárdossy, A., 2008. Predicting the regional onset of the rainy season in West Africa. *International Journal of Climatology*, 28 (3), 329–342.
- Lavigne-Delville, P., Toulmin, C., Colin, J.P., and Chaveau, J.P., 2001. *Securing secondary rights to land in West Africa*. London: IIED, No. 107.
- De Leeuw, J., Jia, H., Yang, L., Liu, X., Schmidt, K., and Skidmore, A.K., 2006a. Comparing accuracy assessments to infer superiority of image classification methods. *International Journal of Remote Sensing*, 27 (1), 223–232.
- De Leeuw, J., Jia, H., Yang, L., Liu, X., Schmidt, K., and Skidmore, A.K., 2006b. Comparing accuracy assessments to infer superiority of image classification methods. *International Journal of Remote Sensing*, 27 (1), 223–232.
- Leisinger, K.M., Schmitt, K., and ISNAR (eds), 1995. *Survival in the Sahel: An ecological and developmental challenge*. The Hague: International Service for National Agricultural Research (ISNAR).



## Appendices

---

- Leroux, M., 2001. *The Meteorology and Climate of Tropical Africa*. London: Springer – Praxis books in environmental sciences.
- Levinson, D.H. and Lawrimore, J.H., 2008. State of the Climate in 2007. *Bulletin of the American Meteorological Society*, 89 (7), S1–S179.
- Li, K.Y., Coe, M.T., Ramankutty, N., and Jong, R. De, 2007. Modeling the hydrological impact of land-use change in West Africa. *Journal of Hydrology*, 337 (3-4), 258–268.
- Liaw, A., 2012. Random Forest Package [online]. Available from: <http://cran.r-project.org/web/packages/randomForest/randomForest.pdf> [Accessed 11 Jul 2014].
- Liaw, A. and Wiener, M., 2002. Classification and regression by random forest. *R News*, 2 (3), 18–22.
- Lillesand, T.M., Kiefer, R.W., and Chipman, J.W., 2004. *Remote sensing and image interpretation*. Chichester, UK: John Wiley & Sons Ltd.
- Lippmann, R.P., 1987. An introduction to computing with neural nets. *ASSP Magazine, IEEE*.
- Liu, D. and Xia, F., 2010. Assessing object-based classification: advantages and limitations. *Remote Sensing Letters*, 1 (4), 187–194.
- Lobell, D.B. and Asner, G.P., 2004. Cropland distributions from temporal unmixing of MODIS data. *Remote Sensing of Environment*, 93 (3), 412–422.
- Lobo, a., Chic, O., and Casterad, a., 1996. Classification of Mediterranean crops with multisensor data: per-pixel versus per-object statistics and image segmentation. *International Journal of Remote Sensing*, 17 (12), 2385–2400.
- LOBO, A., CHIC, O., and CASTERAD, A., 1996. Classification of Mediterranean crops with multisensor data: per-pixel versus per-object statistics and image segmentation. *International Journal of Remote Sensing*, 17 (12), 2385–2400.
- Lopez-Sanchez, J.M., Ballester-Berman, J.D., and Hajnsek, I., 2011. First Results of Rice Monitoring Practices in Spain by Means of Time Series of TerraSAR-X Dual-Pol Images. *Selected Topics in Applied Earth Observations and Remote Sensing, IEEE Journal of*.
- Macelloni, G., Paloscia, S., Pampaloni, P., Marliani, F., and Gai, M., 2001. The relationship between the backscattering coefficient and the biomass of narrow and broad leaf crops. *Geoscience and Remote Sensing, IEEE Transactions on*.
- Marshall, G.J., Dowdeswell, J.A., and Rees, W.G., 1994. The spatial and temporal effect of cloud cover on the acquisition of high quality landsat imagery in the European Arctic sector. *Remote Sensing of Environment*, 50 (2), 149–160.
- Martin, N., 2006. *Development of a water balance for the Atankwidi catchment, West Africa – A case study of groundwater recharge in a semi-arid climate*. Göttingen, Germany: Cuvillier Verlag.
- Marzano, F.S., Mori, S., Chini, M., Pulvirenti, L., Pierdicca, N., Montopoli, M., and Weinman, J., 2011. Potential of High-resolution Detection and Retrieval of Precipitation Fields from X-band

## Appendices

---

- Spaceborne Synthetic Aperture Radar over land. *Hydrology and Earth System Sciences*, 15, 859–875.
- MASON, D.C., CORR, D.G., CROSS, A., HOGG, D.C., LAWRENCE, D.H., PETROU, M., and TAILOR, A.M., 1988. The use of digital map data in the segmentation and classification of remotely-sensed images. *International Journal of Geographical Information Systems*, 2 (3), 195–215.
- Mather, P.M., 1987. *Computer Processing of Remotely Sensed Images*. Chichester: John Wiley & Sons Ltd.
- Mather, P.M., 2004. *Computer Processing of Remotely Sensed Images: An Introduction*. West Sussex, England: John Willey and Sons Ltd.
- Maxwell, S.K., Schmidt, G.L., and Storey, J.C., 2007. A multi-scale segmentation approach to filling gaps in Landsat ETM+ SLC-off images. *International Journal of Remote Sensing*, 28 (23), 5339–5356.
- Mayaux, P., Bartholomé, E., Fritz, S., and Belward, A., 2004. A new land-cover map of Africa for the year 2000. *Journal of Biogeography*, 31 (6), 861–877.
- Mayaux, P., Holmgren, P., Achard, F., Eva, H., Stibig, H.-J., and Branthomme, A., 2005. Tropical forest cover change in the 1990s and options for future monitoring. *Philosophical Transactions of the Royal Society B: Biological Sciences*, 360 (1454), 373–384.
- McCLOY, K.R., SMITH, F.R., and ROBINSON, M.R., 1987. Monitoring rice areas using LANDSAT MSS data. *International Journal of Remote Sensing*, 8 (5), 741–749.
- McNairn, H., Champagne, C., Shang, J., Holmstrom, D., and Reichert, G., 2009. Integration of optical and Synthetic Aperture Radar (SAR) imagery for delivering operational annual crop inventories. *ISPRS Journal of Photogrammetry and Remote Sensing*, 64 (5), 434–449.
- MINISTRY OF LOCAL GOVERNMENT AND RURAL DEVELOPMENT, 2012. *REPORT OF THE COMMITTEE ON DI STRICT BOUNDARY DISPUTES RELATING TO THE 2010 POPULATION AND HOUSING CENSUS*. Accra.
- Möller, M., Lymburner, L., and Volk, M., 2007. The comparison index: A tool for assessing the accuracy of image segmentation. *International Journal of Applied Earth Observation and Geoinformation*, 9 (3), 311–321.
- Mondal, A., Kundu, S., Chandniha, Surendra Kumar Shukla, R., and Mishra, P., 2012. Comparison of Support Vector Machine and Maximum Likelihood Classification Technique using Satellite Imagery. *International Journal of Remote Sensing and GIS*, 1 (2), 116–123.
- Moody, A. and Woodcock, C., 1994. Scale-dependent errors in the estimation of land-cover proportions—implications for global land-cover datasets. *Photogrammetric engineering and remote sensing*, 60 (5), 585–594.
- Mountrakis, G., Im, J., and Ogole, C., 2011. Support vector machines in remote sensing: A review. *ISPRS Journal of Photogrammetry and Remote Sensing*, 66 (3), 247–259.

## Appendices

---

- Murakami, T., Ogawa, S., Ishitsuka, N., Kumagai, K., and Saito, G., 2001. Crop discrimination with multitemporal SPOT/HRV data in the Saga Plains, Japan. *International Journal of Remote Sensing*, 22 (7), 1335–1348.
- Murthy, C.S., Raju, P. V, and Badrinath, K.V.S., 2003. Classification of wheat crop with multi-temporal images: performance of maximum likelihood and artificial neural networks. *International Journal of Remote Sensing*, 24 (23), 4871–4890.
- Murty, D., Kirschbaum, M.U.F., McMurtrie, R.E., and McGilvray, H., 2002. Does conversion of forest to agricultural land change soil carbon and nitrogen ? a review of the literature. *Global Change Biology*, 8, 105–123.
- Mutsaers, H.J.W., Weber, G.K., Walker, P., and Fischer, N.M., 1997. *A Field Guide for On-Farm Experimentation*. Ibadan: IITA/CT A/ISNAR.
- Myint, S.W., 2006. A New Framework for Effective Urban Land Use and Land Cover Classification: A Wavelet Approach. *GIScience & Remote Sensing*, 43 (2), 155–178.
- Myint, S.W., Gober, P., Brazel, A., Grossman-Clarke, S., and Weng, Q., 2011. Per-pixel vs. object-based classification of urban land cover extraction using high spatial resolution imagery. *Remote Sensing of Environment*, 115 (5), 1145–1161.
- Nations, U., 2011. *World population prospects: the 2010 revision*. New York: United Nations.
- Nelson, R., 1989. Regression and ratio estimators to integrate AVHRR and MSS data. *Remote Sensing of Environment*, 30 (3), 201–216.
- Nicholson, S.E. and Palao, I.M., 1993. A re-evaluation of rainfall variability in the sahel. Part I. Characteristics of rainfall fluctuations. *International Journal of Climatology*, 13 (4), 371–389.
- Nicholson, S.E., Some, B., and Kone, B., 2000. An Analysis of Recent Rainfall Conditions in West Africa, Including the Rainy Seasons of the 1997 El Niño and the 1998 La Niña Years. *Journal of Climate*, 13 (14), 2628–2640.
- Van Niel, T.G. and McVicar, T.R., 2001. *REMOTE SENSING OF RICE-BASED IRRIGATED AGRICULTURE: A REVIEW*. Canberra.
- Niel, T.G. Van and McVicar, T.R., 2003. A simple method to improve field-level rice identification: toward operational monitoring with satellite remote sensing. *Australian Journal of Experimental Agriculture*, 43 (4), 379.
- Van Niel, T.G. and McVicar, T.R., 2004a. Determining temporal windows for crop discrimination with remote sensing: a case study in south-eastern Australia. *Computers and Electronics in Agriculture*, 45 (1-3), 91–108.
- Van Niel, T.G. and McVicar, T.R., 2004b. Determining temporal windows for crop discrimination with remote sensing: a case study in south-eastern Australia. *Computers and Electronics in Agriculture*, 45 (1-3), 91–108.

## Appendices

---

- Nin-Pratt, A., Johnson, M., Magalhaes, E., You, L., Diao, X., and Chamberlin, J., 2011. *Yield Gaps and Potential Agricultural Growth in West and Central Africa*. Washington DC: International Food Policy Research Institute and World Resource Institute.
- Norris, K., Asase, A., Collen, B., Gockowski, J., Mason, J., Phalan, B., and Wade, A., 2010. Biodiversity in a forest-agriculture mosaic – The changing face of West African rainforests. *Biological Conservation*, 143 (10), 2341–2350.
- Odenweller, J.B. and Johnson, K.I., 1984. Crop identification using Landsat temporal-spectral profiles. *Remote Sensing of Environment*, 14 (1–3), 39–54.
- Oguntunde, P.G., 2004. *No Title Evapotranspiration and complementarity relations in the water balance of the Volta Basin: field measurements and GIS-based regional estimates*. Ecology an. Bonn: Cuvillier Verlag Göttingen.
- Oguntunde, P.G., Friesen, J., van de Giesen, N., and Savenije, H.H.G., 2006. Hydroclimatology of the Volta River Basin in West Africa: Trends and variability from 1901 to 2002. *Physics and Chemistry of the Earth, Parts A/B/C*, 31 (18), 1180–1188.
- Otukei, J.R. and Blaschke, T., 2010. Land cover change assessment using decision trees, support vector machines and maximum likelihood classification algorithms. *International Journal of Applied Earth Observation and Geoinformation*, 12, Supple (0), S27–S31.
- Ouattara, K., Nyberg, G., Ouattara, B., Sédogo, P.M., and Malmer, A., 2011. Performances of Cotton–Maize Rotation System as Affected by Ploughing Frequency and Soil Fertility Management in Burkina Faso. In: A. Bationo, B. Waswa, J.M. Okeyo, F. Maina, and J.M. Kihara, eds. *Innovations as Key to the Green Revolution in Africa SE - 82*. Springer Netherlands, 817–831.
- Ouedraogo, E., 2004. *Soil Quality Improvement for Crop Production in semi-arid West Africa*. Wageningen: Wageningen University.
- Ouédraogo, E., Mando, A., and Zombré, N.P., 2001. Use of compost to improve soil properties and crop productivity under low input agricultural system in West Africa. *Agriculture, Ecosystems & Environment*, 84 (3), 259–266.
- Ouedraogo, I., Tigabu, M., Savadogo, P., Compaore, H., Oden, P.C., and Ouadba, J.M., 2010. LAND COVER CHANGE AND ITS RELATION WITH POPULATION DYNAMICS IN BURKINA FASO , WEST AFRICA. *Land Degradation & Development*, 21, 453–462.
- Owusu, K., 2009. CHANGING RAINFALL CLIMATOLOGY OF WEST AFRICA: IMPLICATIONS FOR RAINFED AGRICULTURE IN GHANA AND WATER SHARING IN THE VOLTA BASIN. UNIVERSITY OF FLORIDA.
- Owusu, K., Waylen, P., and Qiu, Y., 2008. Changing rainfall inputs in the Volta basin: implications for water sharing in Ghana. *GeoJournal*, 71 (4), 201–210.
- Øygaard, R., Vedeld, T., and Aune, J., 1999. *Good Practices in Drylands Management*. 1st ed. As, Norway: Noragric Agricultural University of Norway.
- Ozdogan, M., 2010. The spatial distribution of crop types from MODIS data: Temporal unmixing using Independent Component Analysis. *Remote Sensing of Environment*, 114 (6), 1190–1204.

## Appendices

---

- Ozdogan, M. and Gutman, G., 2008. A new methodology to map irrigated areas using multi-temporal MODIS and ancillary data: An application example in the continental US. *Remote Sensing of Environment*, 112 (9), 3520–3537.
- Paeth, H., Born, K., Podzun, R., and Jacob, D., 2005. Regional dynamical downscaling over West Africa: model evaluation and comparison of wet and dry years. *Meteorologische Zeitschrift*, 14 (3), 349–367.
- Paeth, H., Capo-Chichi, A., and Endlicher, W., 2008. Climate Change and Food Security in Tropical West Africa — A Dynamic-Statistical Modelling Approach. *Erdkunde*, 62 (2), 101–115.
- Paeth, H., Fink, A.H., Pohle, S., Keis, F., Mächel, H., and Samimi, C., 2011. Meteorological characteristics and potential causes of the 2007 flood in sub-Saharan Africa. *International Journal of Climatology*, 31 (13), 1908–1926.
- Pal, M., 2005. Random forest classifier for remote sensing classification. *International Journal of Remote Sensing*, 26 (1), 217–222.
- Pal, M. and Mather, P.M., 2003. An assessment of the effectiveness of decision tree methods for land cover classification. *Remote Sensing of Environment*, 86 (4), 554–565.
- Pal, M. and Mather, P.M., 2005. Support vector machines for classification in remote sensing. *International Journal of Remote Sensing*, 26 (5), 1007–1011.
- Panigrahy, S. and Parihar, J.S., 1992. Role of middle infrared bands of Landsat thematic mapper in determining the classification accuracy of rice. *International Journal of Remote Sensing*, 13 (15), 2943–2949.
- Paola, J.D. and Schowengerdt, R.A., 1995. A review and analysis of backpropagation neural networks for classification of remotely-sensed multi-spectral imagery. *International Journal of Remote Sensing*, 16 (16), 3033–3058.
- Paré, S., Söderberg, U., Sandewall, M., and Ouadba, J.M., 2008. Land use analysis from spatial and field data capture in southern Burkina Faso, West Africa. *Agriculture, Ecosystems & Environment*, 127 (3–4), 277–285.
- Patnaik, C. and Dadhwal, V.K., 1995. Study of crop discrimination by simulated IRS 1C LISS-III data. *Journal of the Indian Society of Remote Sensing*, 23 (4), 195–199.
- Pedley, M.I. and Curran, P.J., 1991. Per-field classification: an example using SPOT HRV imagery. *International Journal of Remote Sensing*, 12 (11), 2181–2192.
- Peña-Barragán, J.M., Ngugi, M.K., Plant, R.E., and Six, J., 2011. Object-based crop identification using multiple vegetation indices, textural features and crop phenology. *Remote Sensing of Environment*, 115 (6), 1301–1316.
- Petropoulos, G.P., Kontoes, C.C., and Keramitsoglou, I., 2012. Land cover mapping with emphasis to burnt area delineation using co-orbital ALI and Landsat TM imagery. *International Journal of Applied Earth Observation and Geoinformation*, 18 (0), 344–355.

## Appendices

---

- Platteau, J.-P., 1996. The Evolutionary Theory of Land Rights as Applied to Sub-Saharan Africa: A Critical Assessment. *Development and Change*, 27 (1), 29–86.
- Power, A.G., 2010. Ecosystem services and agriculture: tradeoffs and synergies. *Philosophical transactions of the Royal Society of London. Series B, Biological sciences*, 365 (1554), 2959–71.
- Press, W.H., Teukolsky, S.A., Vetterling, W.T., and Flannery, B.P., 2007. *Numerical Recipes: The art of scientific computing*. Third. Cambridge: Cambridge University Press.
- Pringle, M.J., Denham, R.J., and Devadas, R., 2012. Identification of cropping activity in central and southern Queensland, Australia, with the aid of MODIS MOD13Q1 imagery. *International Journal of Applied Earth Observation and Geoinformation*, 19 (0), 276–285.
- QUARMBY, N.A., MILNES, M., HINDLE, T.L., and SILLEOS, N., 1993. The use of multi-temporal NDVI measurements from AVHRR data for crop yield estimation and prediction. *International Journal of Remote Sensing*, 14 (2), 199–210.
- QUARMBY, N.A., TOWNSHEND, J.R.G., SETTLE, J.J., WHITE, K.H., MILNES, M., HINDLE, T.L., and SILLEOS, N., 1992. Linear mixture modelling applied to AVHRR data for crop area estimation. *International Journal of Remote Sensing*, 13 (3), 415–425.
- Ramankutty, N., 2004. Croplands in West Africa: A Geographically Explicit Dataset for Use in Models. *Earth Interactions*, 8 (23), 1–22.
- Ramankutty, N., Evan, A.T., Monfreda, C., and Foley, J. a., 2008. Farming the planet: 1. Geographic distribution of global agricultural lands in the year 2000. *Global Biogeochemical Cycles*, 22 (1), n/a–n/a.
- Ramankutty, N. and Foley, J. a, 1999. Estimating historical changes in global land cover: Croplands from 1700 to 1992. *Global Biogeochemical Cycles*, 13 (4), 997–1027.
- Ramankutty, N. and Foley, J.A., 1998. Characterizing patterns of global land use: An analysis of global croplands data. *Global Biogeochemical Cycles*, 12 (4), 667–685.
- Rao, K.Y., Stephen, M.J., and Phanindra, D.S., 2012. Classification Based Image Segmentation Approach. *International Journal of Computer Science and Technology*, 3 (1), 658–660.
- Raynaut, C., 2001. Societies and nature in the Sahel: ecological diversity and social dynamics. *Global Environmental Change*, 11 (1), 9–18.
- Redo, D.J. and Millington, A.C., 2011. A hybrid approach to mapping land-use modification and land-cover transition from MODIS time-series data: A case study from the Bolivian seasonal tropics. *Remote Sensing of Environment*, 115 (2), 353–372.
- Richards, J.A., 1993. *Remote Sensing Digital Image Analysis. An Introduction*. Berlin: Springer-Verlag.
- Richter, R. and Schläpfer, D., 2012. *Atmospheric/Topographic Correction for Satellite Imagery: ATCOR-2/3 User Guide*. Wil, Switzerland: ReSe Applications Schläpfer.
- Van Rijsbergen, C., 1979. *Information Retrieval*. 2nd ed. London: Butterworths.

## Appendices

---

- Roberts, D.A., Green, R.O., and Adams, J.B., 1997. Temporal and spatial patterns in vegetation and atmospheric properties from AVIRIS. *Remote Sensing of Environment*, 62 (3), 223–240.
- Rodenburg, J., 2013. Inland Valleys: Africa's Future Food baskets. In: M.C.S. Wopereis, D.E. Johnson, N. Ahmadi, E. Tollens, and A. Jalloh, eds. *Realizing Africa's Rice Promise*. Oxfordshire: CABI, 276–293.
- Rodenburg, J., Zwart, S.J., Kiepe, P., Narteh, L.T., Dogbe, W., and Wopereis, M.C.S., 2014. Sustainable rice production in African inland valleys: Seizing regional potentials through local approaches. *Agricultural Systems*, 123, 1–11.
- Rodriguez-Galiano, V.F., Ghimire, B., Rogan, J., Chica-Olmo, M., and Rigol-Sanchez, J.P., 2012. An assessment of the effectiveness of a random forest classifier for land-cover classification. *ISPRS Journal of Photogrammetry and Remote Sensing*, 67 (0), 93–104.
- Rosenthal, W.D. and Blanchard, B.J., 1984. Active microwave responses: An aid in improved crop classification. *Photogrammetric engineering and remote sensing*, 50 (4), 461–468.
- Roy, D.P., Ju, J., Mbow, C., Frost, P., and Loveland, T., 2010. Accessing free Landsat data via the Internet: Africa's challenge. *Remote Sensing Letters*, 1 (2), 111–117.
- Ruelland, D., Levavasseur, F., and Tribotté, A., 2010. Patterns and dynamics of land-cover changes since the 1960s over three experimental areas in Mali. *International Journal of Applied Earth Observation and Geoinformation*, 12, S11–S17.
- Saidou, A., Kossou, D., Acakpo, C., Richards, P., and Kuyper, T., 2012. Effects of farmers' practices of fertilizer application and land use types on subsequent maize yield and nutrient uptake in central Benin. *International Journal of Biological and Chemical Sciences*, 6 (1), 365–378.
- Sakamoto, T., Yokozawa, M., Toritani, H., Shibayama, M., Ishitsuka, N., and Ohno, H., 2005. A crop phenology detection method using time-series MODIS data. *Remote Sensing of Environment*, 96 (3–4), 366–374.
- Sandau, R., 2010. Status and trends of small satellite missions for Earth observation. *Acta Astronautica*, 66 (1–2), 1–12.
- Sandwidi, J.P., 2007. Groundwater potential to supply population demand within the Kompienga dam basin in Burkina Faso. University of Bonn.
- Sanfo, S., 2010. Politiques publiques agricoles et lutte contre la pauvreté au Burkina Faso: le cas de la région du Plateau Central. Université Paris 1 Panthéon-Sorbonne.
- Sanga-Ngoie, K., Iizuka, K., and Kobayashi, S., 2012. Estimating CO<sub>2</sub> Sequestration by Forests in Oita Prefecture, Japan, by Combining LANDSAT ETM+ and ALOS Satellite Remote Sensing Data. *Remote Sensing*, 4 (12), 3544–3570.
- Sarpong, G.A., 2006. *IMPROVING TENURE SECURITY FOR THE RURAL POOR GHANA – COUNTRY CASE STUDY*. Rome: Food and Agricultural Organization.
- Schapiro, R.E., Freund, Y., Bartlett, P., and Lee, W.S., 1998. Boosting the Margin: A New Explanation for the Effectiveness of Voting Methods. *The Annals of Statistics*, 26 (5), 1651–1686.

## Appendices

---

- Schmengler, A., 2011. Modeling soil erosion and reservoir sedimentation at hillslope and catchment scale in semi-arid Burkina Faso. Universität Bonn.
- Schmidt, M., Klein, D., Conrad, C., Dech, S., and Paeth, H., 2014. On the relationship between vegetation and climate in tropical and northern Africa. *Theoretical and Applied Climatology*, 115 (1-2), 341–353.
- Schmitt, A., Hogg, A., Roth, A., and Duffe, J., 2012. Shoreline classification using dual-polarized TerraSAR-X images. In: *Synthetic Aperture Radar, EUSAR 9th European Conference, 23–26 April 2012*. Nuremberg, Germany, 239–242.
- Schraven, B., 2010. Irrigate or migrate? Local livelihood adaptation in Northern Ghana in response to ecological changes and economic challenges. Universität Bonn.
- Schuster, C., Förster, M., and Kleinschmit, B., 2012. Testing the red edge channel for improving land-use classifications based on high-resolution multi-spectral satellite data. *International Journal of Remote Sensing*, 33 (17), 5583–5599.
- Seto, K.C. and Kaufmann, R.K., 2003. Modeling the Drivers of Urban Land Use Change in the Pearl River Delta, China: Integrating Remote Sensing with Socioeconomic Data. *Land economics*, 79 (1), 106–121.
- Shang, J., McNairn, H., Champagne, C., and Jiao, X., 2009. Application of Multi-Frequency Synthetic Aperture Radar (SAR) in Crop Classification. In: G. Jedlovec, ed. *Advances in Geoscience and Remote Sensing*. InTech, 557–569.
- Sheoran, A. and Haack, B., 2013. Classification of California agriculture using quad polarization radar data and Landsat Thematic Mapper data. *GIScience & Remote Sensing*, 50 (1), 50–63.
- Sissoko, K., Keulen, H., Verhagen, J., Tekken, V., and Battaglini, A., 2011. Agriculture, livelihoods and climate change in the West African Sahel. *Regional Environmental Change*, 11 (1), 119–125.
- Skriver, H., 2012. Crop Classification by Multitemporal C- and L-Band Single- and Dual-Polarization and Fully Polarimetric SAR. *Geoscience and Remote Sensing, IEEE Transactions on*.
- Smith, G.M. and Fuller, R.M., 2001. An integrated approach to land cover classification: An example in the Island of Jersey. *International Journal of Remote Sensing*, 22 (16), 3123–3142.
- Smith, J.H., Stehman, S. V, Wickham, J.D., and Yang, L., 2003. Effects of landscape characteristics on land-cover class accuracy. *Remote Sensing of Environment*, 84 (3), 342–349.
- Smith, M.O., Ustin, S.L., Adams, J.B., and Gillespie, A.R., 1990a. Vegetation in deserts: II. Environmental influences on regional abundance. *Remote Sensing of Environment*, 31 (1), 27–52.
- Smith, M.O., Ustin, S.L., Adams, J.B., and Gillespie, A.R., 1990b. Vegetation in deserts: I. A regional measure of abundance from multispectral images. *Remote Sensing of Environment*, 31 (1), 1–26.



## Appendices

---

- Soria-Ruiz, J., Fernandez-Ordóñez, Y., and McNairn, H., 2009. Crop monitoring and crop yield using optical and microwave remote sensing. In: P.G.. Ho, ed. *Geoscience and Remote Sensing*. Rijeka, Croatia: InTech, 405–419.
- Sow, P., Adaawen, S.A., and Scheffran, J., 2014. Migration, Social Demands and Environmental Change amongst the Frafra of Northern Ghana and the Biali in Northern Benin. *Sustainability*, 6, 375–398.
- Stancioff, A., Staljanssens, M., and Tappan, G., 1986. *Mapping and Remote Sensing of the Resources of the Republic of Senegal: A Study of the Geology, Hydrology, Soils, Vegetation and Land Use Potentia*. Brookings, South Dakota.
- Storey, J., Scaramuzza, P., Schmidt, G., and Barsi, J., 2005. Landsat 7 Scan Line Corrector-Off Gap-Filled Product Development. In: *Pecora 16 Global Priorities in Land Remote Sensing*. Sioux Falls, South Dakota: American Society for Photogrammetry and Remote Sensing.
- Sultan, B., Roudier, P., Quirion, P., Alhassane, a, Muller, B., Dingkuhn, M., Ciais, P., Guimberteau, M., Traore, S., and Baron, C., 2013. Assessing climate change impacts on sorghum and millet yields in the Sudanian and Sahelian savannas of West Africa. *Environmental Research Letters*, 8 (1), 014040.
- Sylla, M., Coppola, E., Mariotti, L., Giorgi, F., Ruti, P.M., Dell’Aquila, A., and Bi, X., 2010. Multiyear simulation of the African climate using a regional climate model (RegCM3) with the high resolution ERA-interim reanalysis. *Climate Dynamics*, 35 (1), 231–247.
- Taylor, A., Cross, A., Hogg, D.C., and Mason, D.C., 1986. Knowledge-based interpretation of remotely sensed images. *Image and Vision Computing*, 4 (2), 67–83.
- Tappan, G.G. and Cushing, M., 2008. Experiences of Mapping Land Use and Land Cover And Deriving Trends over the Vast West African Region [online]. Available from: <http://www.oosa.unvienna.org/pdf/sap/2008/graz/presentations/05-01.pdf> [Accessed 16 Jun 2014].
- Tappan, G.G., Hadj, A., Wood, E.C., and Lletzow, R.W., 2000. Use of Argon, Corona, and Landsat Imagery to Assess 30 Years of Land Resource Changes in West-Central Senegal. *Photogrammetric engineering and remote sensing*, 66 (6), 727–735.
- Tappan, G.G., Sall, M., Wood, E.C., and Cushing, M., 2004. Ecoregions and land cover trends in Senegal. *Journal of Arid Environments*, 59, 427–462.
- Thenkabail, P.S., 2003. Biophysical and yield information for precision farming from near-real-time and historical Landsat TM images. *International Journal of Remote Sensing*, 24 (14), 2879–2904.
- Thenkabail, P.S., Hanjra, M. a., Dheeravath, V., and Gumma, M., 2010. A Holistic View of Global Croplands and Their Water Use for Ensuring Global Food Security in the 21st Century through Advanced Remote Sensing and Non-remote Sensing Approaches. *Remote Sensing*, 2 (1), 211–261.
- Thenkabail, P.S. and Wu, Z., 2012. An Automated Cropland Classification Algorithm (ACCA) for Tajikistan by Combining Landsat, MODIS, and Secondary Data. *Remote Sensing*, 4 (10), 2890–2918.

## Appendices

---

- Thornton, P.K., Jones, P.G., Alagarswamy, G., and Andresen, J., 2009. Spatial variation of crop yield response to climate change in East Africa. *Global Environmental Change*, 19 (1), 54–65.
- Tolba, M.K. and El-Kholy, O.A., 1992. *The World Environment 1972–1992: Two Decades of Challenge*. London: Chapman and Hall.
- Torres, R., Snoeij, P., Geudtner, D., Bibby, D., Davidson, M., Attema, E., Potin, P., Rommen, B., Floury, N., Brown, M., Traver, I.N., Deghaye, P., Duesmann, B., Rosich, B., Miranda, N., Bruno, C., L'Abbate, M., Croci, R., Pietropaolo, A., Huchler, M., and Rostan, F., 2012. GMES Sentinel-1 mission. *Remote Sensing of Environment*, 120, 9–24.
- Tottrup, C. and Rasmussen, M.S., 2004. Mapping long-term changes in savannah crop productivity in Senegal through trend analysis of time series of remote sensing data. *Agriculture, Ecosystems & Environment*, 103 (3), 545–560.
- Tottrup, C., Rasmussen, M.S., Eklundh, L., and Jönsson, P., 2007. Mapping fractional forest cover across the highlands of mainland Southeast Asia using MODIS data and regression tree modelling. *International Journal of Remote Sensing*, 28 (1), 23–46.
- Townshend, J.R.G., 1981. The spatial resolving power of Earth resources satellites. *Progress in Physical Geography*, 5, 32–55.
- Townshend, J.R.G. and Justice, C.O., 2002. Towards operational monitoring of terrestrial systems by moderate-resolution remote sensing. *Remote Sensing of Environment*, 83 (1–2), 351–359.
- Tran, T. V., Julian, J.P., and de Beurs, K.M., 2014. Land Cover Heterogeneity Effects on Sub-Pixel and Per-Pixel Classifications. *ISPRS International Journal of Geo-Information*, 3, 540–553.
- Tso, B. and Mather, P., 2009. *Classification Methods for Remotely Sensed Data*. 2nd ed. London: CRC Press Inc.
- Tso, B. and Mather, P.M., 1999. Crop discrimination using multi-temporal SAR imagery. *International Journal of Remote Sensing*, 20 (12), 2443–2460.
- Tu, J. V, 1996. Advantages and disadvantages of using artificial neural networks versus logistic regression for predicting medical outcomes. *Journal of Clinical Epidemiology*, 49 (11), 1225–1231.
- Turker, M. and Arikan, M., 2005. Sequential masking classification of multi-temporal Landsat7 ETM+ images for field-based crop mapping in Karacabey, Turkey. *International Journal of Remote Sensing*, 26 (17), 3813–3830.
- Turner, B.L., Skole, D., Sanderson, S., Fischer, G., Fresco, L., and Leemans, R., 1995. *Land-Use and Land-Cover Change Science/Research Plan: IGBP Report No. 35 and HDP Report No. 7*. Stockholm.
- Turner, D.P., Cohen, W.B., Kennedy, R.E., Fassnacht, K.S., and Briggs, J.M., 1999. Relationships between Leaf Area Index and Landsat TM Spectral Vegetation Indices across Three Temperate Zone Sites. *Remote Sensing of Environment*, 70 (1), 52–68.

## Appendices

---

- Turner, M.D. and Congalton, R.G., 1998. Classification of multi-temporal SPOT-XS satellite data for mapping rice fields on a West African floodplain. *International Journal of Remote Sensing*, 19 (1), 21–41.
- Ullmann, T., Schmitt, A., Roth, A., Banks, S., Baumhauer, R., and Dech, S., 2013. Classification of coastal arctic land cover by means of TerraSAR-X dual co-polarized data (HH/VV). In: *Proceedings of the 5th TerraSAR-X Science Team Meeting, 10 - 11.June, 2013*. Munich, Germany: DLR.
- Valentini, R., Arneeth, a., Bombelli, a., Castaldi, S., Cazzolla Gatti, R., Chevallier, F., Ciais, P., Grieco, E., Hartmann, J., Henry, M., Houghton, R. a., Jung, M., Kutsch, W.L., Malhi, Y., Mayorga, E., Merbold, L., Murray-Tortarolo, G., Papale, D., Peylin, P., Poulter, B., Raymond, P. a., Santini, M., Sitch, S., Vaglio Laurin, G., van der Werf, G.R., Williams, C. a., and Scholes, R.J., 2014. A full greenhouse gases budget of Africa: synthesis, uncertainties, and vulnerabilities. *Biogeosciences*, 11 (2), 381–407.
- Vancutsem, C., Marinho, E., Kayitakire, F., See, L., and Fritz, S., 2012. Harmonizing and Combining Existing Land Cover/Land Use Datasets for Cropland Area Monitoring at the African Continental Scale. *Remote Sensing*, 5 (1), 19–41.
- Vapnik, V., 1979. *Estimation of Dependences Based on Empirical Data*. Moscow: Nuaka.
- Verbeiren, S., Eerens, H., Piccard, I., Bauwens, I., and Van Orshoven, J., 2008. Sub-pixel classification of SPOT-VEGETATION time series for the assessment of regional crop areas in Belgium. *International Journal of Applied Earth Observation and Geoinformation*, 10 (4), 486–497.
- Vintrou, E., Desbrosse, A., Bégué, A., Traoré, S., Baron, C., and Lo Seen, D., 2012. Crop area mapping in West Africa using landscape stratification of MODIS time series and comparison with existing global land products. *International Journal of Applied Earth Observation and Geoinformation*, 14 (1), 83–93.
- Vittek, M., Brink, A., Donnay, F., Simonetti, D., and Desclée, B., 2014. Land Cover Change Monitoring Using Landsat MSS/TM Satellite Image Data over West Africa between 1975 and 1990. *Remote Sensing*, 6 (1), 658–676.
- Vrieling, A., Beurs, K., and Brown, M., 2011. Variability of African farming systems from phenological analysis of NDVI time series. *Climatic Change*, 109 (3-4), 455–477.
- Walker, H.O., 1962. Weather and Climate. In: J.G. Wills, ed. *Agriculture and land-use in Ghana*. London: Oxford University Press, 51–61.
- Wang, F., 1990. Fuzzy supervised classification of remote sensing images. *Geoscience and Remote Sensing, IEEE Transactions on*.
- Wang, X., Gi, L., and Li, X., 2012. Evaluation of filters for ENVISAT ASAR speckle suppression in pasture area. In: *Proceedings of the ISPRS Annals of the XXII ISPRS Congress—Photogrammetry, Remote Sensing and Spatial Information Sciences*. Melbourne, 341–346.
- Wardlow, B.D. and Egbert, S.L., 2008. Large-area crop mapping using time-series MODIS 250 m NDVI data: An assessment for the U.S. Central Great Plains. *Remote Sensing of Environment*, 112 (3), 1096–1116.

## Appendices

---

- Wardlow, B.D., Egbert, S.L., and Kastens, J.H., 2007. Analysis of time-series MODIS 250 m vegetation index data for crop classification in the U.S. Central Great Plains. *Remote Sensing of Environment*, 108 (3), 290–310.
- Wardlow, B.D., Kastens, J.H., and Egbert, S.L., 2006. Using USDA Crop Progress Data for the Evaluation of Greenup Onset Date Calculated from MODIS 250-Meter Data. *Photogrammetric engineering and remote sensing*, 72 (11), 1225–1234.
- Waske, B., 2014. Synergies from SAR-Optical Data Fusion for LULC Mapping. In: I. Manakos and M. Braun, eds. *Land Use and Land Cover Mapping in Europe SE - 11*. Springer Netherlands, 179–191.
- Waske, B. and Braun, M., 2009. Classifier ensembles for land cover mapping using multitemporal SAR imagery. *ISPRS Journal of Photogrammetry and Remote Sensing*, 64 (5), 450–457.
- Watanachaturaporn, P., Arora, M.K., and Varshney, P.K., 2008. Multisource Classification Using Support Vector Machines: An Empirical Comparison with Decision Tree and Neural Network Classifiers. *Photogrammetric engineering and remote sensing*, 74 (2), 239–246.
- Watts, J.D., Powell, S.L., Lawrence, R.L., and Hilker, T., 2011. Improved classification of conservation tillage adoption using high temporal and synthetic satellite imagery. *Remote Sensing of Environment*, 115 (1), 66–75.
- Weldeab, S., Lea, D.W., Schneider, R.R., and Andersen, N., 2007. 155,000 Years of West African Monsoon and Ocean Thermal Evolution. *Science*, 316 (5829), 1303–1307.
- Wellens, J., Midekor, A., Traore, F., and Tychon, B., 2013. An easy and low-cost method for preprocessing and matching small-scale amateur aerial photography for assessing agricultural land use in Burkina Faso. *International Journal of Applied Earth Observation and Geoinformation*, 23 (0), 273–278.
- Willmott, C.J. and Matsuura, K., 2005. Advantages of the mean absolute error (MAE) over the root mean square error (RMSE) in assessing average model performance. *CLIMATE RESEARCH*, 30, 79–82.
- De Wit, A.J.W. and Clevers, J.G.P.W., 2004. Efficiency and accuracy of per-field classification for operational crop mapping. *International Journal of Remote Sensing*, 25 (20), 4091–4112.
- Wood, E.C., Tappan, G.G., and Hadj, A., 2004. Understanding the drivers of agricultural land use change in south-central Senegal. *Journal of Arid Environments*, 59 (3), 565–582.
- Wood, S., Sebastian, K., and Scherr, S.J., 2000. *Pilot analysis of global ecosystems: Agroecosystems*. Washington DC: International Food Policy Research Institute and World Resource Institute.
- Wouterse, F. and Taylor, J.E., 2008. Migration and Income Diversification:: Evidence from Burkina Faso. *World Development*, 36 (4), 625–640.
- WRB, 2006. *World reference base for soil resources 2006 A framework for international classification, correlation and communication*. 2006th ed. Rome: Food and Agricultural Organization.

## Appendices

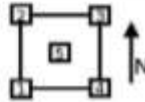
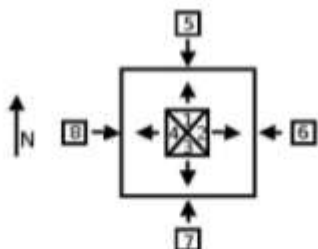
---

- Wright, J.B., Hastings, D.A., Jones, W.B., and Williams, H.R., 1985. *Geology and mineral resources of West Africa*. London: Allen & Unwin.
- Wu, B. and Li, Q., 2012. Crop planting and type proportion method for crop acreage estimation of complex agricultural landscapes. *International Journal of Applied Earth Observation and Geoinformation*, 16 (0), 101–112.
- Wu, Z., Thenkabail, P.S., and Verdin, J.P., 2014. Automated Cropland Classification Algorithm (ACCA) for California Using Multi-sensor Remote Sensing. *Photogrammetric Engineering & Remote Sensing*, 80 (1), 81–90.
- Wulder, M.A., White, J.C., Masek, J.G., Dwyer, J., and Roy, D.P., 2011. Continuity of Landsat observations: Short term considerations. *Remote Sensing of Environment*, 115 (2), 747–751.
- Xiao, X., Boles, S., Frohling, S., Salas, W., Moore, B., Li, C., He, L., and Zhao, R., 2002. Landscape-scale characterization of cropland in China using Vegetation and Landsat TM images. *International Journal of Remote Sensing*, 23 (18), 3579–3594.
- Xiao, X., Liu, J., Zhuang, D., Frohling, S., Boles, S., Xu, B., Liu, M., Salas, W.I., Moore, B., and Li, C., 2003. Uncertainties in estimates of cropland area in China: a comparison between an AVHRR-derived dataset and a Landsat TM-derived dataset. *Global and Planetary Change*, 37 (3), 297–306.
- Yan, G., Mas, J. -F., Maathuis, B.H.P., Xiangmin, Z., and Van Dijk, P.M., 2006. Comparison of pixel-based and object-oriented image classification approaches—a case study in a coal fire area, Wuda, Inner Mongolia, China. *International Journal of Remote Sensing*, 27 (18), 4039–4055.
- Yilma, T., 2006. *Modeling farm irrigation decisions under rainfall risk in the Whit Volta Basin of Ghana. A tool for policy analysis at the farm-household level*. Göttingen: University of Göttingen.
- Yuyun, B.I. and Zheng, Z.Y., 2000. Actual changes of cultivated area since the founding of the new China. *Resources Science*, 22 (2), 8–12.
- Zeng, C., Shen, H., and Zhang, L., 2013. Recovering missing pixels for Landsat ETM+ SLC-off imagery using multi-temporal regression analysis and a regularization method. *Remote Sensing of Environment*, 131 (0), 182–194.
- Zhang, Y., Wang, C., Wu, J., Qi, J., and Salas, W.A., 2009. Mapping paddy rice with multitemporal ALOS/PALSAR imagery in southeast China. *International Journal of Remote Sensing*, 30 (23), 6301–6315.
- Zhou, W., Cadenasso, M., Schwarz, K., and Pickett, S., 2014. Quantifying Spatial Heterogeneity in Urban Landscapes: Integrating Visual Interpretation and Object-Based Classification. *Remote Sensing*, 6 (4), 3369–3386.
- Zougmore, R., 2003. Integrated water and nutrient management for sorghum production in semiarid Burkina Faso. Wageningen University.

## Appendices

## Appendices

### Appendix A: Adapted Land Cover Classification System Questionnaire

ANNEX 1: FIELD VERIFICATION FORM		<i>Mitcovar Project</i>																											
<b>A. GENERAL INFORMATION</b>																													
RELEVÉE N°	<div style="border: 1px solid black; height: 100%;"></div>	FIELD SAMPLE COORDINATES	<table border="1" style="width: 100%;"><tr><td style="width: 50%;">N or S</td><td style="width: 50%;">East</td></tr><tr><td> </td><td> </td></tr></table>			N or S	East																						
N or S		East																											
AREA NAME																													
LOCATION																													
OBSERVER																													
DATE																													
TIME		ACCESSIBILITY	<table border="1" style="width: 100%;"><tr><td><input type="checkbox"/></td><td>Very Good</td></tr><tr><td><input type="checkbox"/></td><td>Good</td></tr><tr><td><input type="checkbox"/></td><td>Medium</td></tr><tr><td><input type="checkbox"/></td><td>Bad</td></tr></table>			<input type="checkbox"/>	Very Good	<input type="checkbox"/>	Good	<input type="checkbox"/>	Medium	<input type="checkbox"/>	Bad																
<input type="checkbox"/>	Very Good																												
<input type="checkbox"/>	Good																												
<input type="checkbox"/>	Medium																												
<input type="checkbox"/>	Bad																												
RELEVÉE SIZE	(in m <sup>2</sup> or ha)																												
COORDINATES	<table border="1" style="width: 100%;"><tr><td style="width: 50%;">N or S</td><td style="width: 50%;">East</td></tr><tr><td> </td><td> </td></tr><tr><td> </td><td> </td></tr><tr><td> </td><td> </td></tr></table>	N or S	East							<table border="1" style="width: 100%;"><tr><th>LAT/LONG</th><th>UTM</th><th>GPS</th><th>Topo Map</th></tr><tr><td><input type="checkbox"/></td><td><input type="checkbox"/></td><td><input type="checkbox"/></td><td><input type="checkbox"/></td></tr><tr><td><input type="checkbox"/></td><td><input type="checkbox"/></td><td><input type="checkbox"/></td><td><input type="checkbox"/></td></tr><tr><td><input type="checkbox"/></td><td><input type="checkbox"/></td><td><input type="checkbox"/></td><td><input type="checkbox"/></td></tr></table>	LAT/LONG	UTM	GPS	Topo Map	<input type="checkbox"/>	<input type="checkbox"/>	<input type="checkbox"/>	<input type="checkbox"/>	<input type="checkbox"/>	<input type="checkbox"/>	<input type="checkbox"/>	<input type="checkbox"/>	<input type="checkbox"/>	<input type="checkbox"/>	<input type="checkbox"/>	<input type="checkbox"/>			
N or S	East																												
LAT/LONG	UTM	GPS	Topo Map																										
<input type="checkbox"/>	<input type="checkbox"/>	<input type="checkbox"/>	<input type="checkbox"/>																										
<input type="checkbox"/>	<input type="checkbox"/>	<input type="checkbox"/>	<input type="checkbox"/>																										
<input type="checkbox"/>	<input type="checkbox"/>	<input type="checkbox"/>	<input type="checkbox"/>																										
On the spot			Observing the spot from a distance																										
Indicate Relative Position of Coordinates				Distance from viewpoint to observed point <input style="width: 50px;" type="text"/> (m)																									
				The bearing of the observed point: <input style="width: 50px;" type="text"/> (°)																									
FIELD PHOTOGRAPHS																													
		Relative Position of photograph																											
		<table border="1" style="width: 100%;"><tr><td style="width: 50%;">Film Roll N°</td><td style="width: 50%;"> </td></tr><tr><td>Photo Shot N°</td><td>Position</td></tr><tr><td> </td><td> </td></tr><tr><td> </td><td> </td></tr><tr><td> </td><td> </td></tr><tr><td> </td><td> </td></tr><tr><td> </td><td> </td></tr><tr><td> </td><td> </td></tr></table>				Film Roll N°		Photo Shot N°	Position																				
Film Roll N°																													
Photo Shot N°	Position																												
GENERAL LANDFORM																													
Slope	<table border="1" style="width: 100%;"><tr><td><input type="checkbox"/></td><td>Flat to Gently Sloping Terrain ( 0 - 7 % )</td></tr><tr><td><input type="checkbox"/></td><td>Gently Sloping to Moderately Sloping ( 8 - 30 % )</td></tr><tr><td><input type="checkbox"/></td><td>Sloping to Moderately Steep, Undulating to Rolling terrain ( 14 - 20 % )</td></tr><tr><td><input type="checkbox"/></td><td>Steep to Very steep, Rolling to Hilly Terrain ( 21 - 55 % )</td></tr><tr><td><input type="checkbox"/></td><td>Extremely Steep Terrain, Steeply Dissected Hilly and Mountainous Terrain ( 56 - 140 % )</td></tr></table>					<input type="checkbox"/>	Flat to Gently Sloping Terrain ( 0 - 7 % )	<input type="checkbox"/>	Gently Sloping to Moderately Sloping ( 8 - 30 % )	<input type="checkbox"/>	Sloping to Moderately Steep, Undulating to Rolling terrain ( 14 - 20 % )	<input type="checkbox"/>	Steep to Very steep, Rolling to Hilly Terrain ( 21 - 55 % )	<input type="checkbox"/>	Extremely Steep Terrain, Steeply Dissected Hilly and Mountainous Terrain ( 56 - 140 % )														
<input type="checkbox"/>	Flat to Gently Sloping Terrain ( 0 - 7 % )																												
<input type="checkbox"/>	Gently Sloping to Moderately Sloping ( 8 - 30 % )																												
<input type="checkbox"/>	Sloping to Moderately Steep, Undulating to Rolling terrain ( 14 - 20 % )																												
<input type="checkbox"/>	Steep to Very steep, Rolling to Hilly Terrain ( 21 - 55 % )																												
<input type="checkbox"/>	Extremely Steep Terrain, Steeply Dissected Hilly and Mountainous Terrain ( 56 - 140 % )																												

## Appendices

### B. GENERAL LAND COVER INFORMATION

#### LAND COVER

- General Land Cover Type  
Relevee Site

A.  Vegetated  Non-Vegetated

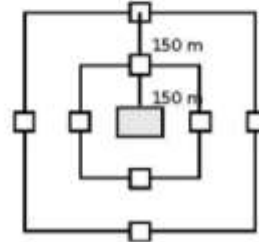
B.  Terrestrial  Aquatic or Regularly Flooded Land  
(Including WADY Areas)

- Specific Land Cover Type

	Single Major Land Cover Aspect	Two Mixed Major Land Cover Aspects	
		Most Important	Second
Cultivated	<input type="checkbox"/>	<input type="checkbox"/>	<input type="checkbox"/>
Natural / Semi-Natural	<input type="checkbox"/>	<input type="checkbox"/>	<input type="checkbox"/>
Built Up	<input type="checkbox"/>	<input type="checkbox"/>	<input type="checkbox"/>
Bare	<input type="checkbox"/>	<input type="checkbox"/>	<input type="checkbox"/>
Artificial Water Body	<input type="checkbox"/>	<input type="checkbox"/>	<input type="checkbox"/>
Inland Water	<input type="checkbox"/>	<input type="checkbox"/>	<input type="checkbox"/>

#### AREA LANDCOVER HOMOGENITY ( Applicable if on spot )

Land Cover Homogeneous for more than 300 m  
around the sample area :  Yes  
 No



### C: SPECIFIC LAND COVER INFORMATION

#### NATURAL AND SEMI-NATURAL VEGETATION

	Level	Cover	Height	Leaf Type			Leaf Phenology	
				Broad	Needle	Aphyllous	Evergreen	Deciduous
<b>WOODY</b>				<input type="checkbox"/>	<input type="checkbox"/>	<input type="checkbox"/>	<input type="checkbox"/>	<input type="checkbox"/>
Trees	1			<input type="checkbox"/>	<input type="checkbox"/>	<input type="checkbox"/>	<input type="checkbox"/>	<input type="checkbox"/>
	2			<input type="checkbox"/>	<input type="checkbox"/>	<input type="checkbox"/>	<input type="checkbox"/>	<input type="checkbox"/>
	3			<input type="checkbox"/>	<input type="checkbox"/>	<input type="checkbox"/>	<input type="checkbox"/>	<input type="checkbox"/>
Shrubs	1			<input type="checkbox"/>	<input type="checkbox"/>	<input type="checkbox"/>	<input type="checkbox"/>	<input type="checkbox"/>
	2			<input type="checkbox"/>	<input type="checkbox"/>	<input type="checkbox"/>	<input type="checkbox"/>	<input type="checkbox"/>
<b>HERBACEOUS</b>								
Graminoids								
Forbs								

Cover Estimation of vegetation

Visual

Instrumental

Other

## Appendices

### D: CULTIVATED TERRESTRIAL AREA AND MANAGED LAND

**Average Field Size**  ( m<sup>2</sup> or ha )

**Field Distribution**

<input type="checkbox"/>	Bordering Fields	
<input type="checkbox"/>	Distance between fields	< average field size
<input type="checkbox"/>		= 1 to 3 X average field size
<input type="checkbox"/>		= 3 to 9 X average field size
<input type="checkbox"/>		> 9 X average field size

**Cultivated Crops**      1. \_\_\_\_\_ 2. \_\_\_\_\_ 3. \_\_\_\_\_  
    4. \_\_\_\_\_ 5. \_\_\_\_\_ 6. \_\_\_\_\_

**Cropping calendar – land preparation, planting, growing and harvesting period**

Crop	S	O	N	D	Ja	Fe	Mr	Ap	M	Jn	Jul	Au

**Cropping System**    Rotational cropping     Relay cropping     Inter-cropping

### ATTRIBUTES

**When did the farmer/his ancestors cultivate the plot for the first time?** \_\_\_\_\_

**What has been the sequence of crops and fallow in the last ten years?**

2002: \_\_\_\_\_      2003: \_\_\_\_\_      2004: \_\_\_\_\_  
 2005: \_\_\_\_\_      2006: \_\_\_\_\_      2007: \_\_\_\_\_  
 2008: \_\_\_\_\_      2009: \_\_\_\_\_      2010: \_\_\_\_\_  
 2011: \_\_\_\_\_      2012: \_\_\_\_\_

**Which kind of fertilizer do you apply to each crop and what quantity?**

Crop 1: \_\_\_\_\_      Crop 2: \_\_\_\_\_      Crop 3: \_\_\_\_\_  
 Crop 4: \_\_\_\_\_      Crop 5: \_\_\_\_\_      Crop 6: \_\_\_\_\_

**Which crops are affected by pest and diseases?** \_\_\_\_\_

**Do weeds (in particular Striga) affect crop yields?**    Yes     No

**Quantity Harvested - historical**

Crops	$\rightarrow$						
Harvest bags/plot	Last 2 Yrs						
	5 Yrs Ago						
	10 Yrs Ago						



## Appendices

### Appendix B: Confusion matrices for watershed scale crop classifications

#### One-time classification in Veja using RapidEye and TerraSAR-X images

Overall Accuracy = 80.0%; Kappa=0.72

	Class	Cereals	Maize	Legumes	Rice	Total	Prod. Acc	User. Acc	F1 score
Reference	Cereals	803	22	102	73	1000	80.3	86.0	0.83
	Maize	51	185	76	122	434	42.6	59.1	0.50
	Legumes	8	38	920	34	1000	92.0	82.2	0.87
	Rice	72	68	21	839	1000	83.9	78.6	0.81

#### One-time classification in Veja using only RapidEye images

Overall Accuracy = 69.8%; Kappa = 0.58

	Class	Cereals	Maize	Legumes	Rice	Total	Prod. Acc	User. Acc	F1 score
Reference	Cereals	753	30	182	35	1000	75.3	79.3	0.77
	Maize	59	62	169	144	434	14.3	22.6	0.18
	Legumes	23	164	788	25	1000	78.8	65.1	0.71
	Rice	115	18	72	795	1000	79.5	79.6	0.80

#### Sequential masking classification in Veja using only RapidEye images

Overall Accuracy=71.1%; Kappa = 0.60

	Class	Cereals	Maize	Legumes	Rice	Total	Prod. Acc	User. Acc	F1 score
Reference	Cereals	696	85	182	37	1000	69.6	85.82	0.77
	Maize	39	51	175	169	434	11.75	16.45	0.14
	Legumes	5	123	848	24	1000	84.8	68.61	0.76
	Rice	71	51	31	847	1000	84.7	78.64	0.82

#### One-time classification in Dano using RapidEye and TerraSAR-X images

Overall Accuracy = 69.5%; Kappa = 0.59

	Class	Cotton	Maize	Cereals	Rice	Total	Prod. Acc	User. Acc	F1 score
Reference	Cotton	766	73	151	10	1000	76.6	75.5	0.76
	Maize	207	442	175	176	1000	44.2	61.1	0.51
	Cereals	11	66	834	89	1000	83.4	66.7	0.74
	Rice	30	142	90	738	1000	73.8	72.9	0.73

## Appendices

### One-time classification in Dano using only RapidEye images

Overall Accuracy= 55.4%; Kappa = 0.41

	Class	Cotton	Maize	Cereals	Rice	Total	Prod. Acc	User. Acc	F1 score
Reference	Cotton	529	204	226	41	1000	52.9	63.6	0.58
	Maize	116	217	478	189	1000	47.8	43.5	0.46
	Cereals	106	602	194	98	1000	60.2	53.1	0.56
	Rice	81	111	200	608	1000	60.8	65.0	0.63

### Sequential masking classification in Dano using only RapidEye images

Overall Accuracy = 64.0%; Kappa = 0.52)

	Class	Cotton	Maize	Cereals	Rice	Total	Prod. Acc	User. Acc	F1 score
Reference	Cotton	479	218	288	15	1000	47.9	60.9	0.54
	Maize	148	554	205	93	1000	55.4	51.9	0.54
	Cereals	69	187	744	0	1000	74.4	59.3	0.66
	Rice	91	108	18	783	1000	78.3	87.9	0.83

### One-time classification in Dassari using RapidEye + TerraSAR-X images

Overall Accuracy = 52.0%; Kappa = 0.44

	Class	Cotton	Maize	Cereals	Rice	Yam	Total	Prod. Acc	User. Acc	F1 score
Reference	Cotton	662	94	244	0	0	1000	66.2	71.6	0.69
	Maize	149	525	286	30	10	1000	52.5	56.9	0.55
	Cereals	105	178	592	117	8	1000	59.2	38.4	0.47
	Rice	0	47	253	602	98	1000	60.2	53.8	0.57
	Yam	9	79	165	370	377	1000	37.7	76.5	0.51

Dassari: One-time, optical only; Overall=50.8; 0.39

	Class	Cotton	Maize	Cereals	Rice	Yam	Total	Prod. Acc	User. Acc	F1 score
Reference	Cotton	670	124	206	0	0	1000	67.0	69.4	0.68
	Maize	177	446	343	4	30	1000	44.6	46.4	0.45
	Cereals	111	192	517	125	55	1000	51.7	39.4	0.45
	Rice	1	107	59	506	327	1000	50.6	53.5	0.52
	Yam	6	93	187	311	403	1000	40.3	49.5	0.44

## Appendices

---

### Sequential masking classification in Dassari using only RapidEye images

Overall Accuracy = 56.5%; Kappa=0.46

---

	Class	Cotton	Maize	Cereals	Rice	Yam	Total	Prod. Acc	User. Acc	F1 score
Reference	Cotton	701	164	135	0	0	1000	70.1	66.5	0.68
	Maize	232	436	268	35	29	1000	43.6	50.8	0.47
	Cereals	116	164	501	151	68	1000	50.1	43.2	0.46
	Rice	0	26	34	781	159	1000	78.1	61.8	0.69
	Yam	5	69	223	296	407	1000	40.7	61.4	0.49

---

## Appendices

### Appendix C: Confusion matrices for watershed scale cropland classifications using Landsat data

#### Dano watershed

Year 2002; Overall Accuracy = 90.0%; Kappa = 0.875

	Class	Cropland	Mixed Veg.	Forest	Artificial Surf.	Water	Total	Prod. Acc	User. Acc	F1 score
Reference	Cropland	895	3	0	102	0	1000	89.4	89.5	0.89
	Mixed Veg	33	778	188	0	1	1000	77.8	88.3	0.83
	Forest	36	97	867	0	0	1000	86.7	82.2	0.84
	Artificial Surf	36	3	0	961	0	1000	96.1	90.4	0.93
	Water	0	0	0	0	1000	1000	100.0	99.9	1.00

Year 2005; Overall Accuracy = 90.9%; Kappa = 0.89

	Class	Cropland	Mixed Veg.	Forest	Artificial Surf.	Water	Total	Prod. Acc	User. Acc	F1 score
Reference	Cropland	906	12	2	80	0	1000	90.6	93.9	0.92
	Mixed Veg	28	792	179	1	0	1000	79.2	85.4	0.82
	Forest	2	123	875	0	0	1000	87.5	82.9	0.85
	Artificial Surf	29	0	0	971	0	1000	97.1	92.3	0.95
	Water	0	0	0	0	1000	1000	100.0	100.0	1.00

Year 2006; Overall Accuracy = 90.5%; Kappa = 0.88

	Class	Cropland	Mixed Veg.	Forest	Artificial Surf.	Water	Total	Prod. Acc	User. Acc	F1 score
Reference	Cropland	953	16	0	31	0	1000	95.3	94.0	0.95
	Mixed Veg	8	962	30	0	0	1000	96.2	73.1	0.83
	Forest	2	336	659	0	0	997	66.1	95.7	0.78
	Artificial Surf	51	2	0	947	0	1000	94.7	96.8	0.96
	Water	0	0	0	0	1000	1000	100.0	100.0	1.00

Year 2007; Overall Accuracy = 89.3%; Kappa = 0.87

	Class	Cropland	Mixed Veg.	Forest	Artificial Surf.	Water	Total	Prod. Acc	User. Acc	F1 score
Reference	Cropland	919	16	1	63	1	1000	91.9	92.3	0.92
	Mixed Veg	39	831	122	8	0	1000	83.1	75.8	0.79
	Forest	1	247	752	0	0	1000	75.2	85.9	0.80
	Artificial Surf	37	2	0	961	0	1000	96.1	93.1	0.95
	Water	0	0	0	0	1000	1000	100.0	99.9	1.00

## Appendices

**Year 2008;** Overall Accuracy = 97.8%; Kappa = 0.97

	Class	Cropland	Mixed Veg.	Forest	Artificial Surf.	Water	Total	Prod. Acc	User. Acc	F1 score
<b>Reference</b>	<b>Cropland</b>	994	2	2	2	0	1000	99.4	97.5	0.98
	<b>Mixed Veg</b>	14	922	53	0	0	989	92.2	98.3	0.95
	<b>Forest</b>	2	14	984	0	0	1000	98.4	94.7	0.97
	<b>Artificial Surf</b>	10	0	0	990	0	1000	99.0	99.8	0.99
	<b>Water</b>	0	0	0	0	1000	1000	100.0	100.0	1.00

**Year 2010;** Overall Accuracy= 92.6%; Kappa = 0.91

	Class	Cropland	Mixed Veg.	Forest	Artificial Surf.	Water	Total	Prod. Acc	User. Acc	F1 score
<b>Reference</b>	<b>Cropland</b>	935	8	0	57	0	1000	93.5	92.9	0.93
	<b>Mixed Veg</b>	35	810	125	30	0	1000	81.0	90.4	0.85
	<b>Forest</b>	1	77	922	0	0	1000	92.2	88.1	0.90
	<b>Artificial Surf</b>	35	1	0	964	0	1000	96.4	91.7	0.94
	<b>Water</b>	0	0	0	0	1000	1000	100.0	100.0	1.00

**Year 2011;** Overall Accuracy = 94.8%; Kappa = 0.94

	Class	Cropland	Mixed Veg.	Forest	Artificial Surf.	Water	Total	Prod. Acc	User. Acc	F1 score
<b>Reference</b>	<b>Cropland</b>	964	5	0	31	0	1000	96.4	89.3	0.93
	<b>Mixed Veg</b>	61	897	41	1	0	1000	89.7	92.9	0.91
	<b>Forest</b>	14	64	922	0	0	1000	92.2	95.7	0.94
	<b>Artificial Surf</b>	41	0	0	959	0	1000	95.9	96.8	0.96
	<b>Water</b>	0	0	0	0	1000	1000	100.0	100.0	1.00

**Year 2013;** Overall Accuracy = 89.8%; Kappa=0.87

	Class	Cropland	Mixed Veg.	Forest	Artificial Surf.	Water	Total	Prod. Acc	User. Acc	F1 score
<b>Reference</b>	<b>Cropland</b>	925	12	0	63	0	1000	92.5	87.0	0.90
	<b>Mixed Veg</b>	76	861	58	5	0	1000	86.1	77.7	0.82
	<b>Forest</b>	10	235	755	0	0	1000	75.5	92.9	0.83
	<b>Artificial Surf</b>	52	0	0	948	0	1000	94.8	93.3	0.94
	<b>Water</b>	0	0	0	0	1000	1000	100.0	100.0	1.00

## Appendices

### Veja watershed

Year 2002; Overall Accuracy = 88.5%; Kappa=0.86

	Class	Cropland	Mixed Veg.	Forest	Artificial Surf.	Water	Total	Prod. Acc	User. Acc	F1 score
Reference	Cropland	871	84	24	21	0	1000	87.1	95.1	0.91
	Mixed Veg	25	812	155	8	0	1000	81.2	71.6	0.76
	Forest	0	207	793	0	0	1000	79.3	81.4	0.80
	Artificial Surf	20	24	2	954	0	1000	95.4	97.1	0.96
	Water	0	7	0	0	993	1000	99.3	100.0	1.00

Year 2005; Overall Accuracy = 88.5%; Kappa=0.86

	Class	Cropland	Mixed Veg.	Forest	Artificial Surf.	Water	Total	Prod. Acc	User. Acc	F1 score
Reference	Cropland	961	28	2	9	0	1000	96.1	94.6	0.95
	Mixed Veg	48	772	172	8	0	1000	77.2	70.8	0.74
	Forest	0	274	726	0	0	1000	72.6	80.7	0.76
	Artificial Surf	7	17	0	967	9	1000	96.7	98.3	0.97
	Water	0	0	0	0	1000	1000	100.0	99.1	1.00

Year 2006; Overall Accuracy =; Kappa=

	Class	Cropland	Mixed Veg.	Forest	Artificial Surf.	Water	Total	Prod. Acc	User. Acc	F1 score
Reference	Cropland	859	65	7	6	0	937	91.68	93.47	0.93
	Mixed Veg	38	724	162	0	0	924	78.35	67.92	0.73
	Forest	0	260	618	0	0	878	70.39	77.83	0.74
	Artificial Surf	22	12	7	959	0	1000	95.9	99.38	0.98
	Water	0	5	0	0	995	1000	99.5	100	1.00

Year 2007; Overall Accuracy = 87.3%; Kappa=0.84

	Class	Cropland	Mixed Veg.	Forest	Artificial Surf.	Water	Total	Prod. Acc	User. Acc	F1 score
Reference	Cropland	959	28	4	9	0	1000	95.9	88.6	0.92
	Mixed Veg	120	739	137	4	0	1000	73.9	67.6	0.71
	Forest	0	288	712	0	0	1000	71.2	83.5	0.77
	Artificial Surf	4	39	0	956	1	1000	95.6	98.7	0.97
	Water	0	0	0	0	1000	1000	100.0	99.9	1.00

## Appendices

**Year 2008;** Overall Accuracy = 92.9%; Kappa=0.91

	Class	Cropland	Mixed Veg.	Forest	Artificial Surf.	Water	Total	Prod. Acc	User. Acc	F1 score
Reference	Cropland	963	25	0	12	0	1000	96.3	97.4	0.97
	Mixed Veg	23	786	184	7	0	1000	78.6	86.2	0.82
	Forest	2	100	898	0	0	1000	89.8	83.0	0.86
	Artificial Surf	1	1	0	998	0	1000	99.8	98.1	0.99
	Water	0	0	0	0	1000	1000	100.0	100.0	1.00

**Year 2010;** Overall Accuracy = ; Kappa=

	Class	Cropland	Mixed Veg.	Forest	Artificial Surf.	Water	Total	Prod. Acc	User. Acc	F1 score
Reference	Cropland	912	57	1	2	0	972	93.83	96.41	0.95
	Mixed Veg	16	748	167	5	0	936	79.91	71.24	0.75
	Forest	0	212	704	0	0	916	76.86	80.18	0.78
	Artificial Surf	18	23	6	953	0	1000	95.3	99.27	0.97
	Water	0	10	0	0	990	1000	99	100	0.99

**Year 2011;** Overall Accuracy = 85.0%; Kappa=0.81

	Class	Cropland	Mixed Veg.	Forest	Artificial Surf.	Water	Total	Prod. Acc	User. Acc	F1 score
Reference	Cropland	844	145	1	8	2	1000	84.4	89.2	0.87
	Mixed Veg	66	820	106	0	8	1000	82.0	61.0	0.70
	Forest	0	343	657	0	0	1000	65.7	86.0	0.74
	Artificial Surf	36	33	0	930	1	1000	93.0	99.2	0.96
	Water	0	3	0	0	997	1000	99.7	98.9	0.99

**Year 2013;** Overall Accuracy = 90.6%; Kappa=0.88

	Class	Cropland	Mixed Veg.	Forest	Artificial Surf.	Water	Total	Prod. Acc	User. Acc	F1 score
Reference	Cropland	958	28	1	13	0	1000	95.8	97.76	0.97
	Mixed Veg	21	898	68	13	0	1000	89.8	71.73	0.80
	Forest	0	322	678	0	0	1000	67.8	90.76	0.78
	Artificial Surf	1	2	0	997	0	1000	99.7	97.46	0.99
	Water	0	2	0	0	998	1000	99.8	100	1.00